Ph. D. School "High Mechanics and Automotive Design and Technology" - Cycle XXIII

Dean: prof. ing. A. Strozzi – Course coordinator: prof. ing. G.S. Barozzi

Optimally reduced reaction mechanisms for Internal Combustion Engines running on biofuels

Federico Perini

Dipartimento di Ingegneria Meccanica e Civile

Università di Modena e Reggio Emilia

A thesis submitted for the degree of

PhilosophiæDoctor (PhD)

Academic Tutor: **prof. ing. Giuseppe Cantore**

Co-Tutor: **prof. ing. Paolo Tartarini**

April 4th, 2011

Ph.D. School "High Mechanics and Automotive Design and Technology"
Cycle XXIII

Academic Tutor: **prof. ing. Giuseppe Cantore**
Co-Tutor: **prof. ing. Paolo Tartarini**

Chair of the Ph.D. School: **prof. ing. Antonio Strozzi**
Chair of the Ph.D. Course: **prof. ing. Giovanni Sebastiano Barozzi**

1. Reviewer: **prof. ing. Giovanni Sebastiano Barozzi**
Università di Modena e Reggio Emilia

2. Reviewer: **prof. ing. Maria Pia Pedeferri**
Politecnico di Milano

3. Reviewer: **prof. ing. Giovanni Molari**
Università di Bologna

Day of the defense: April 4th, 2011

Signature from head of PhD committee:

sempre fortissimo, e con strepito

F. Liszt

Abstract

Research for new combustion concepts for internal combustion engines has been made possible in recent years by the adoption of CFD codes which are capable of computing complete reaction mechanisms, as current pollutant regulations are leading to an increasing need for accurate predictions of the spatial distribution and time evolution of species within the combustion chamber. However, the adoption of full or detailed reaction mechanisms in multi-dimensional studies is still too computationally demanding, and the development of accurate reduced mechanisms is of fundamental importance for mantaining the predictive capabilities of the simulations. In this context, research is urged by the need for finding adequate substitutes to petroleum-based fuels for the transportation sector of the near future. Biofuels, such as bioethanol, biobutanol, biodiesel currently seem to be suitable for gradually being introduced as additives to traditional hydrocarbon fuels, and then to fully substitute them, to contribute to a viable and environmentally sustainable alternative to oil. The present work introduces a novel approach for the automatic development of reduced reaction mechanisms for biofuels' combustion, with the aim of generating reaction mechanisms which can be efficiently adopted for engine simulations with detailed chemistry.

First of all, efforts have been devoted to the development of a new computer code for the computationally efficient solution of detailed chemistry in the simulation of combustion systems. The software has been coded as a package for the estimation of finite-rate chemical kinetics in zero dimensional batch reactors and internal combustion engines. All the routines have been developed in a fully vectorized fashion, for maximum computational efficiency. The performance of the code has been compared adopting different ODE solvers, showing robustness and computational efficiency. Finally, the code has been coupled with KIVA-4, well-known CFD tool for the simulation of internal combustion

engines, and parallelised adopting a shared memory paradigm.
Performance of the solution of the chemistry ODE system has then been improved through the study of a novel explicit ODE solver, exploiting time scale separation. The solution of the reacting environment is carried out according to the assumption that, if the time integration interval is small enough, a linear analysis can yield accurate predictions of the characteristic times of each species, and thus the evolution of each of them can be stopped after its estimated expiration time. This method thus significantly reduces the stiffness of the ODE system, and allows a significant reduction in total computational times, if compared to the more commonly used implicit integration approach, which cannot exploit its potential if bounded by strict integration timesteps (as happening during CFD simulations, where the fluid-dynamic timestep usually rules over the chemistry source terms).
Once that all the numerical tools have been validated and tested, the mechanism reduction procedure has been set up as an iterative algorithm, with the aim of gradually reducing the number of species involved in the mechanism, while still mantaining its predictiveness in terms of not only ignition delay times, but also the time evolution of important species. In particular, a global error function is defined taking into account a set of ignition delay calculations at different, engine-relevant, initial mixture compositions, temperatures and pressures. The choice of the species to be deleted is performed exploiting the element flux analysis method; when a global error function of the reduced mechanism exceeds the required accuracy, the collision frequencies and activation energies of selected reactions are corrected by means of a GA-based code. The results show that significantly smaller, accurate reaction mechanisms can be automatically generated and applicated to internal combustion engine simulations. Further research needs to be devoted to the development of skeletal, multi-component reaction mechanisms for allowing new combustion concepts such as multi-fuel combustion and reactivity-controlled combustion to be explored.

Sommario

Lo studio della combustione dei biocombustibili, come bioetanolo, biobutanolo, biodiesel, sta prendendo sempre maggior terreno nell'ambito della ricerca in campo energetico grazie alle aspettative che tali combustibili suscitano quali possibili alternative all'utilizzo di combustibili derivati dal petrolio, nel medio-lungo termine, per alimentare il sistema dei trasporti. In particolare, alcune previsioni stimano che la richiesta energetica mondiale crescerà del 50% circa entro il 2025, e dunque non sembra attuabile la possibilità di sostituire il petrolio con un'unica fonte di approvvigionamento energetico, quanto piuttosto appare necessario che si debba sviluppare una nuova infrastruttura energetica che preveda l'impiego di un portafoglio di fonti differenziate ed, ove possibile, ecosostenibili a seconda dell'ambito di applicazione. Per quanto riguarda l'impiego dei biocombustibili sono già presenti ed in vigore normative presso l'Unione Europea e gli Stati Uniti d'America, volte alla graduale integrazione, ed alla progressiva sostituzione del petrolio con combustibili bioderivati nel settore dei trasporti. Questo appare uno dei pochi casi verificatisi in cui sia stato l'impulso normativo a dare urgenza alla ricerca, che – nell'ambito – era poco sviluppata sino a pochi anni fa, e che sta solo ora raggiungendo gradi di accuratezza e di accettabilità delle previsioni che consentano lo sviluppo di nuovi, e più puliti, sistemi ottimizzati per la combustione con biocombustibili. Si tratta infatti di combustibili il cui impiego è stato sinora volto alla parziale sostituzione dei più comuni idrocarburi derivati dal petrolio, al fine di non intaccare il parco veicolistico circolante, e consentendo a motori progettati per il funzionamento con combustibili tradizionali di continuare a funzionare regolarmente. Gli sviluppi più recenti della ricerca in questo campo, tuttavia, sono volti in particolare ad uno studio dettagliato delle caratteristiche di reattività dei sistemi che prevedano l'impiego di biocombustibili: si tratta infatti di composti che non possono essere identificati attraverso una specie chimica singola (così come

era invece possibile per i combustibili tradizionali, mediante la selezione di specie di riferimento quali l'iso-ottano e l'n-ettano per la definizione della reattività e delle caratteristiche di autoaccensione), ma debbono essere rappresentati tramite una 'ricetta' di specie, spesso in termini di gruppi funzionali (esteri, eteri, acidi grassi, etc.). Questo si rende necessario non solo a causa della variabilità in composizione che tali combustibili presentano alla fonte, ma anche stante il fatto che le dimensioni delle molecole che li compongono richiedono che previsioni di combustione adeguate debbano includere tutti i gruppi di specie di dimensioni via via inferiori, fino ai composti più semplici e caratteristici dei prodotti della combustione. Per questo motivo, sono stati realizzati negli ultimi anni (dal 2005 circa in avanti) meccanismi di reazione per biocombustibili che prevedono la presenza di centinaia di specie e di migliaia di reazioni; gli ultimi esempi disponibili in letteratura mostrano come un tipico meccanismo di reazione per il bio-diesel sia solitamente composto da circa 2-3000 specie e da circa 10000 reazioni. L'importanza che lo sviluppo di simili meccanismi di cinetica chimica riveste nell'ambito della ricerca non risiede unicamente nella necessità di prevedere in modo sufficientemente accurato le caratteristiche termiche globali relative alla combustione di una miscela combustibile-comburente, ma soprattutto nella capacità previsionale locale che il meccanismo ha per lo studio della reattività della miscela e per la conoscenza della formazione delle specie intermedie, di fondamentale importanza per la previsione delle emissioni inquinanti in atmosfera.

La disponibilità di questo genere di strumenti dettagliati ha recentemente consentito, mediante l'applicazione di solutori per la simulazione di sistemi di reazioni chimiche a codici di simulazione fluidodinamica tridimensionale, una ricerca sempre più avanzata di nuovi concetti di combustione, da applicarsi a sistemi di interesse pratico industriale quali i motori a combustione interna. Per esempio, recentemente sono in corso di studio nuove modalità per l'espletamento della combustione della miscela per accensione spontanea, quali l'HCCI (homogeneous-charge compression ignition, o accensione per compressione di una carica premiscelata), o la cosiddetta RCCI (Reactivity-controlled compression ignition, od accensione per compressione controllata dalla reattività

della miscela). A differenziare principalmente queste nuove modalità di combustione è il fatto che lo sviluppo della combustione all'interno del cilindro, anziché essere governata dalla propagazione di un fronte di fiamma – quale avviene nei motori ad accensione spontanea –, a sua volta influenzato dalla presenza di un campo di microturbolenza in camera, oppure dalla miscelazione locale del combustibile con la carica fresca grazie a moti organizzati macroscopici, è invece *kinetically-controlled*, ossia controllata prevalentemente dalla cinetica chimica del sistema reagente che la carica fresca (eventualmente in presenza anche di una frazione di gas combusti) costituisce quando miscelata con il vapore di combustibile. In particolare, appare possibile sfruttare la diversa reattività che diversi combustibili posseggono (come, ad esempio, benzina ed etanolo da un lato, caratterizzati da una elevata resistenza alla autoaccensione, oppure gasolio e biodiesel dall'altro, caratterizzati al contrario da una facile accendibilità per semplice compressione), per caratterizzare diversamente la carica interna al cilindro al variare delle condizioni di carico e di regime di rotazione, mediante la loro iniezione combinata, anche in tempi diversi, e secondo differenti rapporti di massa. Le attività di modellazione di motori che sfruttano così complessi concetti di combustione, che – secondo quanto riportato in letteratura – consentono efficienze indicate di esercizio nell'ordine del 60% circa, non possono prescindere dallo sfruttamento di meccanismi di cinetica chimica ridotti, e sviluppati specificamente per il caso in esame. Se una simulazione motore tradizionale, con un meccanismo di cinetica chimica ridotto, impiega attualmente un tempo nell'ordine delle decine di ore su di una macchina monoprocessore, il tempo di calcolo potrebbe lievitare fino a 3-4 ordini di grandezza qualora fossero impiegati meccanismi di reazione dettagliati, che hanno dimensioni in termini di numero di reazioni e di specie considerate maggiori per uno-due ordini di grandezza. Se, a questo proposito, si volessero considerare le specie caratteristiche costituenti i principali biocombustibili, i costi computazionali lieviterebbero ulteriormente, il che rende inattuabile – correntemente – questa possibilità.

Per tutti questi motivi, oggetto principale della presente Tesi è stato lo studio della riduzione dei meccanismi di cinetica chimica, con l'obiettivo di una loro

destinazione computazionalmente efficiente ed accurata nella simulazione di motori a combustione interna alimentati con biocombustibili. In particolare, sono attualmente in corso di sviluppo numerose metodologie per la riduzione di meccanismi di cinetica chimica, le quali è possibile raggruppare all'interno di due categorie. Una prima classe di metodi prevede la riduzione del meccanismo 'al volo', ovvero viene considerato per la simulazione un meccanismo di reazione dettagliato, il quale viene poi ridotto ad ogni passo di integrazione temporale della simulazione CFD mediante la selezione di un sottoinsieme di specie e di reazioni che rispetti determinati requisiti complessivi di accuratezza. Questa tipologia di metodi consente una buona riduzione dei tempi complessivi di calcolo, specialmente in corrispondenza delle condizioni operative nelle quali il sistema è caratterizzato da una reattività lenta e da reazioni vicine alle condizioni di equilibrio. Una seconda classe di metodologie prevede invece la messa a punto di tecniche per lo sviluppo di meccanismi di cinetica chimica ridotti in senso proprio (denominati come *skeletal*, in linguaggio anglosassone), i quali posseggono un numero ridotto di reazioni e di specie, le quali però rimangono invariate nel corso della simulazione e sono valide per tutte le condizioni operative. Tra le metodologie più comunemente adoperate per questo tipo di riduzione vi sono a tutt'oggi in primis il senso e l'esperienza chimica del ricercatore, che provvede ad eliminare le reazioni meno importanti secondo analisi di sensibilità che egli stesso va a svolgere simulando condizioni di reazione prefissate; sono stati sviluppati più recentemente metodi più sistematici che prevedono il collassamento degli isomeri all'interno di specie uniche, o la taratura dei coefficienti di reazione per considerare nelle reazioni sopravvissute i contributi dei percorsi reattivi eventualmente eliminati.

Lo sviluppo del presente lavoro è stato reso possibile dallo svolgimento di una fase preliminare di studio, e di realizzazione, delle metodologie successivamente utilizzate per stabilire una procedura di riduzione univoca e computazionalmente efficiente. In particolare, la prima parte delle attività di ricerca è stata dedicata alla realizzazione di codici di calcolo più computazionalmente efficienti, ed adatti all'impiego su di infrastrutture per il calcolo parallelo, rispetto a quelli correntemente utilizzati. Infatti, per lo studio della cinetica di combustione in sistemi reattivi standard (quali, ad esempio, reattori adiabatici, fiamme

laminari premiscelate, *rapid compression machines*), quali quelli comunemente utilizzati per validare sperimentalmente i meccanismi di cinetica chimica, CHEMKIN è il pacchetto più utilizzato nell'ambito della ricerca, in quanto esso ha costituito uno standard mondiale fino a partire dagli anni '90, e tuttora la bibliografia relativa ai meccanismi di cinetica chimica quasi esclusivamente propone librerie in formato CHEMKIN. Tuttavia, il pacchetto CHEMKIN disponibile accademicamente, ed ancora ampiamente utilizzato anche nel caso di accoppiamento con codici CFD, sfrutta concetti di programmazione ora obsoleti, che portano a tempi di calcolo significativi allorquando si considerino set di simulazioni di grandi dimensioni, quali quelli nei quali appunto si può incorrere nel corso di una simulazione fluidodinamica tridimensionale, oppure anche nel caso di ottimizzazione secondo algoritmi genetici. Per queste ragioni, si è studiato e messo a punto un nuovo codice per il calcolo di sistemi chimici reagenti, basato su di un approccio completamente vettorizzato. L'impiego di matrici, vettori e maschere logiche in luogo dei più comuni cicli iterativi ha consentito innanzitutto un più efficace approccio alla programmazione, e quindi un codice finale più facilmente leggibile e più adatto ad accogliere eventuali modifiche nella struttura del meccanismo di combustione. In secondo luogo, si è potuto appurare come l'approccio matriciale abbia consentito, dopo una serie di validazioni e di raffronto con altri codici, una riduzione dei tempi di calcolo rispetto al pacchetto CHEMKIN originale di quasi un ordine di grandezza.

A seguito della completa validazione del codice di calcolo realizzato, esso è stato accoppiato a KIVA-4, standard di riferimento per la simulazione fluidodinamica dei motori a combustione interna. L'accoppiamento ha consentito di dotare il codice degli strumenti necessari al calcolo della cinetica chimica dettagliata, che recentemente si è resa necessaria per consentire simulazioni efficienti di combustione, che siano in grado di prevedere non solo le prestazioni medie del motore, ma anche la formazione locale delle emissioni inquinanti e le caratteristiche istantanee di reattività della miscela aria – combustibile. La fase di programmazione è stata successivamente arricchita dall'implementazione, nel codice, di OpenMP, un paradigma per il calcolo parallelo su sistemi a memoria condivisa. Questo linguaggio si colloca attualmente all'avanguardia del calcolo

parallelo, in quanto lo sfruttamento delle medesime aree di memoria da parte di tutti i processi che sono eseguiti in parallelo consente una efficienza della parallelizzazione quasi unitaria, grazie alla possibilità di evitare la moltiplicazione delle informazioni contenute in memoria, come accade secondo i tradizionali sistemi che sfruttano l'interfaccia a passaggio di informazioni (MPI, *message-passing interface*). Tra i limiti di questo approccio, vi è la impossibilità del codice di girare contemporaneamente su un macchine distinte, e tuttavia questo problema appare trascurabile, se si considera che una tipica simulazione di motore a combustione interna, in cui la combustione sia calcolata secondo cinetica chimica dettagliata, difficilmente è effettuata su più di 4 processori contemporaneamente, mentre le odierne macchine a memoria condivisa solitamente posseggono tra gli 8 ed i 16 processori.

Come spesso accade nell'ambito della ricerca, la soluzione di un problema può porre nuovi problemi da risolvere. In questo caso, si è potuto osservare che le simulazioni di combustione, per le quali il sistema di equazioni differenziali ordinarie era risolto con il solutore VODE, riferimento nell'ambito dei sistemi caratterizzati da una molteplicità di scale temporali e da un alto grado di *stiffness*, non erano computazionalmente sufficientemente efficaci. Infatti, tra le potenzialità di solutori quali VODE vi è quella di consentire, pur in presenza di sistemi la cui risoluzione esplicita richiederebbe passi di integrazione minimi, anche dell'ordine di $10^{-13} - 10^{-15} s$, con conseguenti tempi di calcolo inaccettabili, passi di integrazione molto grandi rispetto allo spettro dello Jacobiano del sistema. Tuttavia, l'accoppiamento della cinetica chimica a simulazioni fluidodinamiche motore prevede che il passo di integrazione relativo al calcolo della variazione in concentrazione delle specie nella singola cella della griglia computazionale sia governato da altri fenomeni, quali il campo di moto, lo spettro di turbolenza, i fenomeni dinamici e di evaporazione delle particelle in fase liquida. Per questi motivi, l'integrazione implicita del sistema di equazioni differenziali della cinetica chimica appare impropria, dal momento che buona parte del tempo di calcolo viene dedicato alla stima numerica dello Jacobiano del sistema, e che tuttavia i timestep massimi sono vincolati.
Per questi motivi, si è sviluppato ex-novo un solutore esplicito di sistemi di

equazioni differenziali ordinarie, che si basa sulla stima e sulla separazione delle scale temporali caratteristiche delle specie chimiche, con specifico riguardo al caso dell'accoppiamento della cinetica chimica in simulazioni CFD di motori a combustione interna. Il principio alla base del solutore risiede in concetto già utilizzato in passato, in particolare per simulazioni chimiche in atmosfera, e solo recentissimamente ritrovato in letteratura per simulazioni DNS bidimensionali di fiamme turbolente. Si tratta infatti di assumere che gli intervalli di integrazione ai quali il solutore deve rispondere per ragioni inerenti la fluidodinamica, siano sufficientemente ravvicinati da poter assumere che la linearizzazione del sistema possa dare buone stime dei tempi caratteristici istantanei delle specie ivi contenute. In buona sostanza, i tempi corrispondenti agli intervalli di integrazione fissati dalla fluidodinamica agiscono come istanti di campionamento dei tempi caratteristici delle specie. Secondo questa stima, l'integrazione viene portata avanti per ciascuna specie solo fino ad un tempo pari all'ordine di grandezza corrispondente alla propria costante di tempo caratteristica, cosicché, per tempi avanzati, le specie caratterizzate dalle costanti temporali più basse, che creano *stiffness* nel sistema, vengano di fatto congelate, consentendo quindi al sistema di procedere secondo passi di integrazione maggiori, caratteristici delle specie che sono ancora attive.

L'efficacia di questo solutore è stata verificata incrociando matrici di simulazioni per due diversi meccanismi di cinetica chimica, rilevanti nell'ambito delle simulazioni motore, e relativi alla combustione dell'etanolo e dell' n-ettano. Le matrici di simulazioni hanno riguardato l'assunzione di intervalli di campionamento differenti (da $10^{-5}s$ a $10^{-8}s$) e di diversi valori di soglie per la valutazione delle reazioni all'equilibrio. I risultati di queste simulazioni sono poi stati utilizzati per la costruzione di scenari di merito, ricostruiti secondo la tecnica del kriging ordinario per la costruzione di superfici di risposta. Dall'analisi degli scenari è risultato evidente come le simulazioni effettuate tramite il solutore TSS (*time scale separation*) hanno consentito fattori di accelerazione del calcolo, rispetto al solutore VODE, nell'ordine delle unità, fino alle decine in corrispondenza dei valori di intervalli di campionamento più bassi, sempre con un ottimo grado di accuratezza della soluzione.

Viste l'efficacia e l'accuratezza del solutore TSS, esso è stato successivamente

accoppiato, in sostituzione di VODE, al codice KIVA-4, e valutato sulla base di un numero di simulazioni motore che comprendesse sia il caso di accensione HCCI dovuta interamente alla cinetica chimica, che il caso più complesso della combustione diesel per iniezione diretta in camera di combustibile. Dalle analisi è stato possibile osservare come, a fronte di un'ottima corrispondenza dei risultati delle simulazioni riguardo ai medesimi casi quando calcolati con VODE, i tempi complessivi di calcolo sono risultati particolarmente ridotti, fino ad un massimo del 60% circa nel caso della combustione HCCI. Questa configurazione del codice si presta dunque in modo particolarmente efficace all'effettuazione di analisi dettagliate, che prevedano l'impiego di meccanismi di reazione, anche quando molti casi di calcolo debbano essere previsti, come per esempio nel caso della ottimizzazione motore tramite algoritmi genetici. Essa inoltre potrà essere in futuro ancora ulteriormente migliorata tramite la possibilità di introdurre metodologie volte al raggruppamento delle celle di calcolo in *clusters* caratterizzati da condizioni simili di reattività, nonché alla riduzione 'al volo' del meccanismo di cinetica chimica per una ulteriore e più estrema riduzione del tempo di calcolo.

Al termine della fase di sviluppo e di validazione degli strumenti di calcolo da dedicare all'obiettivo principale della tesi, sono state analizzate in parallelo le due classi di metodologie da destinarsi allo sviluppo di un codice automatico per la realizzazione di meccanismi di cinetica chimica di tipo *skeletal*.
In primo luogo, si sono valutate le metodologie disponibili in letteratura per la riduzione dei meccanismi per selezione di sottoinsiemi di specie e di reazioni. Molte sono in questo ambito le metodologie disponibili che si basino su assunzioni di carattere analitico, anche se molte di esse sono state sviluppate per l'applicazione 'al volo', al fine di ridurre il costo computazionale istantaneo della soluzione. Molti di questi metodi richiedono pertanto un certo sovrapprezzo computazionale, che viene però assorbito dal guadagno conseguente alla riduzione del meccanismo. Non essendo disponibile una metodologia univoca per la riduzione complessiva di un meccanismo, si è proceduto a sviluppare una procedura nuova, che combinasse le possibilità di riduzione delle metodologie sviluppate per la condizione operativa istantanea con la necessità di

realizzare un meccanismo ridotto con uno spazio di validità il più ampio possibile. Per questo scopo è stata identificata la metodologia dell'analisi a flusso di elementi (EF). Secondo questa teoria, la reattività istntanea tra tutte le possibili coppie ordinate di specie nel meccanismo è quantificata secondo un approccio che le modella come sorgenti o pozzi di flussi di atomi degli elementi costitutivi. In questo modo, è possibile valutare le specie istantaneamente più reattive quali quelle che partecipino al flusso totale di atomi oltre una certa determinata soglia. Il variare del valore della soglia determina quindi un indice per selezionare sottoinsiemi di specie e di reazioni più o meno contratti. Al fine di considerare la applicazione di questa metodologia per la riduzione di un meccanismo secondo un ampio spettro di validità, si è messo a punto un approccio di tipo integrale.
In particolare, è stato identificato un set di simulazioni di accensione all'interno di un reattore adiabatico a pressione costante, che fossero di rilevanza per il meccanismo in esame. Dal momento che il campo di applicabilità finale era relativo a motori a combustione interna, si è identificata quale miscela reagente quella del combustibile in aria secca, a vari livelli di dosatura – da molto magra a molto ricca. Queste simulazioni sono state moltiplicate poi cartesianamente per un set di differenti temperature iniziali di riferimento, e per un set di differenti pressioni iniziali. In questo modo, si è determinato un insieme di soluzioni che, complessivamente, ricopriva un buon numero di condizioni di reattività del sistema, simili a quelle esperibili all'interno di un motore a combustione interna. Per ciascuna di tali simulazioni, il tempo complessivo di integrazione dell'evoluzione del reattore è stato imposto pari a 1.5 volte il tempo necessario all'autoaccensione della miscela, inteso come il tempo necessario affinché si verificasse, all'interno del reattore, un incremento di temperatura pari a 200 K.
L'analisi a flusso di elementi per la stima del sottoinsieme di specie da ottenersi, per ciascun valore di soglia, è stata dunque effettuata a ciascun passo di integrazione e per ciascuno dei casi, cosicché i risultati potessero essere integrati e mediati su tutto il range di validità desiderato per il meccanismo.

Nel momento in cui è creato un meccanismo di combustione ridotto, è necessario valutarne le prestazioni e quantificarne l'efficacia in confronto ad un

riferimento. Per la massima accuratezza, si è scelto di assumere due riferimenti per la accuratezza del meccanismo. In primis, si è ritenuto di confrontare le prestazioni del meccanismo ridotto con quelle del meccanismo dettagliato complessivo, cosicché potessero essere valutati non solo dati medi o complessivi, ma le variazioni istantanee nelle concentrazioni delle specie più importanti, nonché lo stato termico istantaneo del reattore. Per fare ciò, si è sviluppata una funzione di merito che comparasse lo specifico meccanismo di combustione ridotto, campionando le concentrazioni delle specie e la temperatura del sistema su un numero molto elevato di punti di valutazione, e su tutto il set di simulazioni che definisce il range di validità del meccanismo. Nel momento in cui ad un determinato meccanismo iniziale corrisponde univocamente un valore della funzione di merito, è possibile impostare il problema della generazione di un meccanismo di combustione ridotto come un problema di ottimizzazione. A questo proposito, molti sono gli approcci all'ottimizzazione di meccanismi di reazione presenti in bibliografia, ciascuno dei quali è stato messo a punto per ottenere un determinato scopo. In questo caso, l'obiettivo era quello di ottenere un meccanismo ridotto che fosse di buona validità ad un range di condizioni termochimiche ampio il più possibile, e quindi le reazioni sopravvissute rispetto al meccanismo dettagliato originale dovevano in qualche modo considerare i contributi eliminati tramite la cancellazione delle reazioni e delle specie meno importanti. Per queste ragioni, si è demandata la fase di riduzione del meccanismo unicamente al procedimento della analisi a flusso di elementi, e si è invece impostato un successivo problema di ottimizzazione al fine di calibrare le costanti di reazione delle reazioni presenti nel sistema, perché esse potessero supplire al numero di reazioni e di specie cancellate.

Va infatti ricordato che molte delle reazioni incluse nei meccanismi di combusitone per combustibili realistici riguardano specie per le quali è molto difficile che siano disponibili in letteratura riscontri sperimentali, od anche calcoli teorici. Si è quindi ritenuto di sfruttare le inevitabili bande di incertezza sperimentale di tali reazioni come agi per una eventuale ottimizzazione del meccanismo, senza tuttavia modificare le reazioni per le quali i dati sono più certi, come quelle relative ai sistemi reattivi di base idrogeno-ossigeno e carbonio-ossigeno.

Dal momento che una simile ottimizzazione coinvolge un numero molto elevato di variabili, che può essere nell'ordine delle migliaia se la dimensione del meccanismo ridotto è simile a quella del meccanismo dettagliato, e che il conseguente spazio delle soluzioni possibili è di difficile gestione, si è ritrovato nella ottimizzazione mediante algoritmi genetici il metodo ottimale per espletare tali attività. Si è dunque innanzitutto realizzato un codice di ottimizzazione multipattaforma, il quale è stato confrontato e validato nell'applicazione ad un caso di interesse meccanico. Successivamente, il codice è stato personalizzato per l'inserimento all'interno di una procedura unica di generazione di meccanismi di combustione ridotti. In particolare, la fase di ottimizzazione delle costanti di reazione è vista come parte integrante di una procedura graduale, che prevede la riduzione passo-passo di un certo numero di specie e di reazioni dal meccanismo dettagliato, e la conseguente ottimizzazione ad ogni iterazione delle costanti di reazione relative al sottoinsieme sopravvissuto, al fine di mantenere nel modo più efficace la accuratezza del meccanismo ridotto anche man mano che le sue dimensioni vengono contratte, così da ottenere un costo computazionale complessivo inferiore rispetto a quello che si avrebbe nel caso fosse effettuata una riduzione unica fino alle dimensioni desiderate, ed una conseguente unica ottimizzazione a partire da un meccanismo che – di dimensioni molto differenti dal meccanismo originale – mostri risultati parecchio lontani da esso.

La seconda opportunità di valutazione delle prestazioni di un meccanismo ridotto è quella del raffronto con dati di carattere sperimentale. In questo caso, si è ritenuto un valido esempio quello di utilizzare per il raffronto i dati relativi ai tempi di autoaccensione di miscele combustibile – comburente diluite in argon od azoto. Le simulazioni vengono effettuate considerando le medesime condizioni iniziali rispetto a quelle indicate nelle pubblicazioni che presentano i risultati, che corrispondono alle condizioni termodinamiche seguenti l'impatto di un'onda incidente all'interno di un dispositivo per esperire il colpo d'ariete (*shock-tube*). L'accuratezza del modello previsionale è poi quantificata sulla base dello scarto quadratico medio complessivo sull'intero set di dati.

La procedura iterativa complessiva per la generazione del meccanismo ridotto è stata schematizzata sotto forma di un algoritmo. In particolare, essa comincia calcolando le simulazioni di accensione mediante il meccanismo dettagliato, e determinando quindi un set di risultati di riferimento alle tolleranze di integrazione standard (RTOL = 10^{-4},ATOL = 10^{-13}). Successivamente, prende avvio la fase di riduzione/ottimizzazione del meccanismo: ad ogni iterazione il valore di soglia per l'analisi a flusso di elementi è abbassato, così da considerare quale meccanismo ridotto candidato un sottoinsieme sempre più contenuto di specie e reazioni. Una volta che è stato determinato il nuovo meccanismo ridotto per sottrazione delle specie e delle reazioni oltre soglia, è valutato il corrispondente valore della funzione di merito. Qualora detto valore risulti essere inferiore ad un valore limite adottato inizialmente, le costanti di reazione relative alle reazioni che includano unicamente le specie per le quali sussiste incertezza sperimentale vengono ottimizzate secondo la procedura genetica. La procedura viene reiterata finché non accada che il valore di merito del meccanismo rimanga inferiore alla soglia di sufficienza anche a seguito dell'ottimizzazione genetica dei parametri di reazione. In questo caso, l'algoritmo interrompe la fase iterativa ed avvia un'ultima ottimizzazione che prevede il confronto numerico-sperimentale in termini di tempi di autoaccensione.

Al fine di testare e validare la metodologia così inndividuata, sono stati generati tre meccanismi ridotti di combustione relativi all'etanolo, al metil-butanoato ed al metil-decanoato. Queste ultime due molecole sono, in particolare, tra gli esteri di metile più comunemente derivabili dalla transesterificazione degli acidi grassi contenuti negli oli vegetali con il metanolo. Dalla verifica in confronto con le prestazioni dei relativi meccanismi dettagliati, e con le misurazioni sperimentali, si verifica come questi meccanismi, pur considerevolmente ridotti rispetto agli originali, garantiscano risultati accurati ed affidabili, e quindi si rendano particolarmente adatti per simulazioni motore.

La conclusione del presente lavoro di Tesi ha indicato anche alcune direzioni sulle quali concentrare le prossime ricerche. In primo luogo, il miglioramento ulteriore delle prestazioni di codici CFD di simulazione motore che introducano

meccanismi di cinetica chimica dettagliata, per esempio mediante il raggruppamento delle celle della griglia computazionale che posseggano condizioni di reattività simili; in secondo luogo, la realizzazione di meccanismi ridotti di tipo multi-componente, che consentano l'analisi e lo studio di motori a combustione interna basati sulla combustione a reattività variabile.

Acknowledgements

I first of all would like to express my sincere gratitude to my academic supervisor, Prof. Giuseppe Cantore, for the freedom he left me in exploring and in finding out the research topics I have studied, for his suggestions and teachings, and for his never-ending support and trust in my work. Thank you: it has truly been a privilege.

I also gratefully thank Prof. Rolf D. Reitz, of the University of Wisconsin–Madison: without his help perhaps this Thesis would never have come to light. I can't forget all of the encouragements and the pieces of advice during my stay in Madison, neither the fantastic months spent at the Engine Research Center.

I'm grateful to Prof. Paolo Tartarini: now I can understand how such an experience can change everyone's life, and to Prof. Gian Marco Bianchi too, for having made my trip to the U.S.A. possible. I also thank a lot my colleagues at the University of Modena, and in particular Federico, Fabrizio, Fabio, Marcello; together with Gokul, Jessica, Won-Geun, Youngchul and all the colleagues at the ERC. I'd like to spend a word for Livio Laurora: without his technical support and passion many of the computer issues I've faced wouldn't have been solved. I can't forget about the 'Lab Gentili' group of the University of Pisa: special thanks go to Ettore and Riccardo, colleagues and friends; I have appreciated every bit of help along the way, be it Fortran code or a cup of coffee.

I cannot forget to thank Fays and all the friends who made me feel at home in Madison; there is nothing else as friday lunches at Med Cafe. I hope to see everybody soon, maybe in front of 'my' awesome Akin's plate.

Finally, there are no words to thank my family, your support helped me more than you can imagine, my friends, and Barbara, for – well – more or less about everything...

Contents

List of Figures

List of Tables

Glossary

BSFC Brake specific fuel consumption; measure of the fuel consumption of an internal combustion engine when running at the dynamometer bench, at a specified load defined by the brake torque and engine rotational speed

CFR Cooperative Fuel Research; acronym defining a standard engine model initially developed for conducting ignition studies on fuels

EE Explicit Euler. Explicit integration method for ODE systems. Characterized by easy and robust implementation, stability constraint requires small integration timesteps.

EGR Exhaust Gas Recirculation; technique for introducing exhaust gases into the combustion chamber, in order to add an inert heat capacity, thus lowering the combustion temperatures and decreasing pollutant formation

FAME Fatty-acid methyl esters: defines a class of methyl esters usually formed from an alkali catalyzed reaction between fats or fatty acids and methanol. Most molecules in biodiesel fuels are FAMEs obtained through transesterification of vegetable oils.

HCCI Homogeneous-Charge Compression Ignition; kinetically-controlled engine operation which features compression ignition of a premixed homogeneous charge

ICE Internal Combustion Engine

IVP Initial value problem. It is a 1st order ODE system plus an initial system condition.

MB Methyl-butanoate or Methyl-butyrate ($C_5H_{10}O_2$): it is the methyl ester of butyric acid. It is used as a surrogate fuel for biodiesel.

MD Methyl-decanoate ($C_{11}H_{22}O_2$): it is the methyl ester of decanoic acid. It is a candidate surrogate for biodiesel fuel.

ODE Ordinary Differential Equation. It is a relation that contains a unique independent variable, and one or more derivatives with respect to it. A system of ordinary differential equations is an ODE where the unknown function is a vector-valued function.

RKF45 Runge-Kutta-Fehlberg method. The term refers to a class of Runge-Kutta solvers with overall $O(h^5)$ accuracy order, where the 5^{th} order integration is based on the same coefficients of the 4^{th} order integration, so that no further computational evaluation of the ODE system is needed.

TSS Time scale separation: methodology which aims at separating the timescales of the variables in stiff IVPs, and freezing during the integration the variables whose evolution is already over, for reducing the stiffness of the ODE system.

1 Introduction

1.1 Motivation and challenges

Many are the frontiers of energy that are currently advancing and that still need lots of research efforts from people around the World, in order to move society towards a more sustainable and environmentally friendly development. Combustion is the first technological discovery of the mankind, and its use, after 4 000 centuries, still accounts for more than 90% the total worldwide energy conversion. Thus, every improvement in combustion science can lead to significant positive effects, that can have an impact on the widest possible horizon. In particular, combustion technology for internal combustion engines is perhaps among the most advanced and widely available technologies for energy conversion: current development in the field of new combustion concepts, adoption of multi-component fuels with variable reactivity, etc. show that this field is unproperly addressed as a 'mature' technology, which can be treated as a black-box and only improved through the adoption of sophisticated control electronics. Instead, recent research results are showing that impressive improvements in energetic efficiency and cleanliness of the combustion products can be achieved by addressing the combustion phenomenology more than adding more complex control systems to the engine. What is more exciting is that all of these recent advancements always show strong and mutual influences among phenomena related to different disciplines, such as fluid mechanics, chemistry, physics, statistics, and that the degree of analytic insight into these phenomena is so deep that many standard approaches to physical problems are becoming obsolete. For example, it is interesting to consider that most of the last three centuries, in science, have been devoted to finding description of real phenomena according to the continuum assumption, and that since G. W. von Leibniz (1646 - 1716) many of the laws which rule over classical physics and chemistry are thus written in dif-

Figure 1.1: Interaction of multiple disciplines in combustion: L. Boltzmann among his staff and foreign students at the Physics Institute of the University of Graz, summer semester 1887.

ferential form. However, all of the computer methods which have been developed since the 1950's rely on the subdivision of the physical domain into a number of finite volumes, within which the physical and thermodynamical properties are assumed to be constant and average, bringing to the discretization of the problem into a huge number of simple problems, so that the true solution of the differential problem formulation is not reachable anymore. Next, also this approach for the description of complex phenomena is becoming obsolete, as knowledge is needed on the behaviour of nature at such small scales that any accurate subdivision of the physical domain would need an excessive number of subdivisions. Thus, the concepts of statistics and of statistical averaging, which go back to Ludwig Boltzmann (1844 - 1906) and his classical theory of statistical mechanics, are becoming necessary for the accurate description of turbulence and of turbulence – flame interaction.

Among all of these issues, research is looking for viable alternatives to substitute oil as the major energy supply for the industrial society. And in particular, a lot of efforts are currently being spent towards the study of combustion of biofuels (ethanol and biodiesel

more than any other one), as they seem to be among the most promising alternatives to oil-derived fuels, at least for the transportation field. It is still challenging to predict combustion characteristics of these fuels, as there is a great variance in their composition, and what is even more challenging is that they are made up of such large molecules that no experimental data of reactions involving them are available in the literature, and each of those molecules also presents a number of isomers, which makes the task more difficult.
In this context, the development of detailed reaction mechanisms for coupled fluid dynamics - combustion simulations has become fundamental, but the species contained in biofuels require sets of reactions of the order of thousands in order to achieve acceptable results. This is a big problem, as simulations (for example, of internal combustion engines) require domains made up of millions up to tenths millions cells, and that chemistry needs to be solved within each of the cell and at each time instant of the simulation. For all of these reasons, I've tried to challenge this problem aiming at establishing a new, affordable procedure for the automatic reduction of reaction mechanisms, and to generate accurate and reliable skeletal reaction mechanisms for the combustion of biofuels. As acknowledged, times needed for the solution of chemistry through computational simulations scale with n^3, n being the number of reactions included in the mechanism. So, the generation of a skeletal mechanism made up of hundreds reactions instead than thousands can lead to reduced computational times by two orders of magnitude.
The development of this task has been anticipated by the study, the development and the implementation of a number of numerical tools for the efficient simulation of reacting systems and of internal combustion engines exploiting detailed reaction mechanisms, on serial and distributed systems. Then, the principles of evolutionary optimization and of element flux analysis in chemistry have been coupled in order to establish a robust algorithm for mechanism reduction and optimization. Finally, the procedure has been applied to the biofuels of interest, showing that the procedure is able to get skeletal mechanisms of significantly smaller size, though keeping excellent degrees of accuracy.

1.2 Background for biofuels research

Interest in biofuels, such as bio-ethanol, bio-butanol, biodiesel is currently reaching wide audiences due to the perspectives these fuels arise in the long-term, as alternatives, and possible substitutes, for nowadays' petroleum-based transportation system. The global energy demand is expected to grow by about 50% by 2025, the major part of this increase coming from rapidly emerging countries, thus urging the need for finding alternative energy sources (12; 13). Hence, research in biofuels combustion has to be seen in the context of a future outlook which points out a concurrent progressive reduction in the extraction of petroleum and in the production of petroleum-based energy carriers, together with a burgeoning request for cheap and environmentally sustainable fuels. National and multinational institutions have already started to take up the path of building a sustainable industrial society; in the field of transportation fuels, ethanol and biodiesel are currently adopted as additives to petroleum-based gasoline and diesel fuels. In particular, the European Union Directive 2003/30/EC calls for dependence on oil, estimated to be at 98% for road transportation, to be reduced, and targets at least 5.75% of the total transport fuels market in the European Union to be derived from biomass by the end of 2010; similarly, the U.S. Department of Energy has targeted 30% of the total liquid petroleum-based fuels for transportation to be substituted through biofuels, and 25% of the total industrial organic chemicals to be substituted by biomass-derived chemicals by 2025 (14; 15).

It is acknowledged that, among biofuels, ethanol and biodiesel represent viable alternatives to fossil fuels because they provide a net energy gain – when considering their whole life-cycle from plant growth to production to combustion within internal combustion engines –, they have positive environmental effects, they are economically competitive and can be produced in suitable quantities without affecting food supplies (16). In particular, ethanol produced from corn grain cultivations is reported to provide about 25% more energy then what is required for its production; the net energy balance for soybeans-derived biodiesel instead adds up to about 93%. Furthermore, the whole production and combustion cycles for these fuels feature significant reductions in greenhouse gas emissions, which range from 12% (ethanol) to 41% (biodiesel) with respect to petroleum.

Besides the global aspects, which place biofuels in the framework of social, political and economical actions, in order to make these fuels real alternatives to fossil energy sources,

huge efforts are still needed with respect to the study of their combustion chemistry, which still has to be completely understood (17).

1.2.1 Combustion chemistry of biofuels.

Since the discovery of fire, combustion is the first technology of the mankind, as it is still acknowledged to take part into about 90% of the energy processes worldwide (18). However, due to its complexity in involving multiple disciplines, such as chemistry, thermo- and fluid-dynamics, and in presenting a wide range of physical timescales, combustion chemistry is gaining only from the recent years quantitative predictive capabilities. To this respect, computer models which accurately describe complete reaction sequences, and which are properly validated against experiments in shock-tubes, flow reactors, jet-stirred reactors, rapid compression machines or other practical combustion systems, need to include thousands of species and elementary reactions (17). In order to properly model and simulate the physical behaviour of reacting systems, deep knowledge is needed also for considering the interaction that chemistry has with fluid mechanics, and with turbulence in particular: an insight into the challenges of current research in combustion chemistry can be found in a series of papers written for celebrating the 50th anniversary of the Combustion Institute (19; 20; 21; 22).

As far as biofuels are concerned, a high degree of heterogeneity in composition needs to be considered when analysing their combustion characteristics, as processes for deriving fuels from biomass are still under research, and many strategies for producing fuel molecules are possible from plant matters. So, accurate prediction of the combustion behaviour of biofuel strongly depends on the development of rich reaction mechanisms, which contain proper species, reactions, rate coefficients, together with appropriate estimation of thermochemical properties, also for intermediate species. All of these issues are nowadays solved for common hydrocarbon fuels, as research in that field is active since almost one century, but there is still significant lack of information for many species involved in functional groups present in biofuel molecules.

The current research focuses on alternatives to typical hydrocarbon fuels for internal combustion engines, i.e. gasoline and diesel fuels. Biofuels used to replace them are typically liquid, oxygenated hydrocarbons produced from many biomass sources, such as wastes and plant matter (17); thus, combustion properties are of fundamental importance not only for

heat release and performance when burnt within practical combustion systems, but especially for predicting pollutant emissions. Ethanol and Biodiesel, two candidates for substituting gasoline and diesel fuels respectively, have been considered in the present research.

1.2.1.1 Ethanol

Ethanol (C_2H_5OH) has been widely adopted as a fuel for internal combustion engines. In the past, it was expected to fuel the Fort Model T car, before being superseded by the 'new' gasoline fuel (23). Nowadays, the adoption of Ethanol as a fuel in engines mainly occurs in Brazil (as 'alcohol'), and in USA, Canada and India as an additive to gasoline, thanks to its better combustion properties such as higher octane rating, lower harmful emissions and toxicity. Worldwide Ethanol production analyses (1) have shown that the USA and Brasil produced Ethanol in the amount of about 65 Million cubic meters, accounting for about 86% the total world production. As mentioned, in these two countries policies for promoting Ethanol as a fuel are strong: in Brazil, its production from sugar cane has a long tradition, and actually most of the cars sold in the country are fuel-flexible, i.e. are capable of self-adapting their operation parameters according to the actual gasoline-ethanol blending in the fuel tank. In Europe, the Renewable Energy Directive (2009/28/EC) (24) introduced in 2009 mandatory use of renewable energy in the transportation sector, and Member States have presented a National Renewable Energy Action Plans about how they will achieve their targets in 2020.

Production of Ethanol can be made from renewable resources, such as crops and waste products (paper, trees, grass, etc.). These features make ethanol the most interesting possible candidate in substituting gasoline as a fuel for spark ignited engines, and a number of recent studies is also showing the potential of mixtures of ethanol and air to be mixed with diesel fuel within CI engines, too (25). A number of experimental and modelling studies on Ethanol combustion, started from the early 90's (4; 26; 27; 28; 29; 30), have been presented. In particular, experimental validations featured wide ranges of temperatures and pressures in various experimental apparatus, such as shock-tubes, flames, and reactors. From these analyses it has been seen that the combustion of ethanol, such as that involving oxygenated hydrocarbons, tends to reduce PAHs and soot precursors presence, as they show lower peak mole fractions of C_2H_2, C_3H_3 and benzene in fuel-rich flames than similar non-oxygenated hydrocarbons; however, a tendency has been shown to increase aldehyde concentrations.

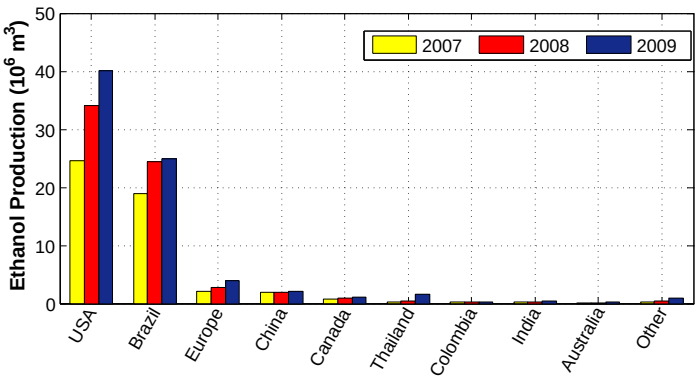

Figure 1.2: World Ethanol fuel production, 2007-2009. (1)

Overall, this fuel has been acknowledged to present a number of positive aspects for its combustion within internal combustion engines.

1.2.1.2 Biodiesel

The first Diesel engine, by Rudolph Diesel, has been reported to run on peanut oil during the world exhibition held in Paris in 1900. Dr. Diesel was later (1912) reported to state "The use of vegetable oils for engine fuels may seem insignificant today. But such oils may become in course of time as important as petroleum and the coal tar products of the present time" (23). However, the adoption of common vegetable oils in diesel engines can lead to operation problems such as coking, low viscosity and poor mixture ignition. Nowadays, biodiesel fuels mainly consist of methyl and ethyl esters. These compounds are derived from fatty acids recovered from plants, such as soy beans, rapeseed, palms, olives, sunflowers, etc., and are blended to oil-based diesel fuel in automotive engines, leading to a decrease in unburned hydrocarbons and particulate emissions.

The combustion of methyl and ethyl esters is thus under deep research, as the variety of compounds which can be used for simulating biodiesel combustion leads to a variety of cases and different behaviours. For this reason, submodels are being developed for 'simpler' molecules, such as methyl butanoate and methyl decanoate (10; 31; 32; 33; 34; 35; 36; 37), which however are still challenging. As a matter of fact, the development of these kinetic mechanisms for the oxidation of esters is of fundamental importance for understanging the properties of biodiesel components when burnt into diesel engines. Insight into the differ-

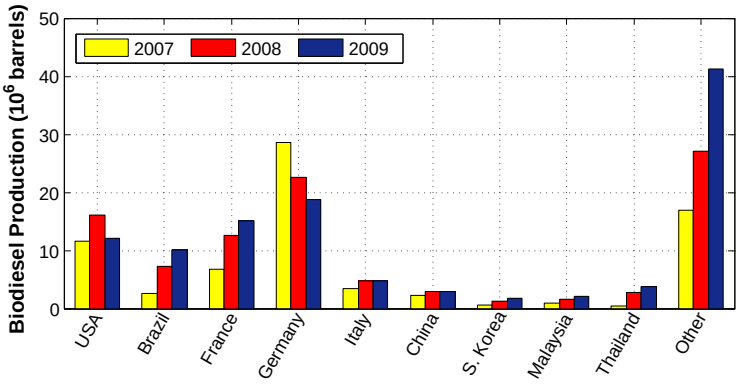

Figure 1.3: World Biodiesel fuel production, 2007-2009. (2)

ent families of esthers has shown that ignition timings can be very different (38), thus, predictive modeling studies for these esthers are needed for building of comprehensive mechanisms for typical biodiesel, which usually contains more than one esther type. Thus, the predictive capability of kinetic models for biodiesels can be limited to the local sample, as fuel produced in each plant offers a different composition.

1.2.2 Biofuels in internal combustion engines.

While research is spending a lot of efforts for developing chemically complete, and reliable kinetic models for the oxidation of biofuels, in parallel these same biofuels are currently adopted as either additives or substitutes to petroleum-based fuels in internal combustion engines, as the transportation sector is the most important consumer of fossil fuels (23). Promotion in the use of biofuels for internal combustion engines has been made in many industrial countries for their environmental benefits, plus their limited impact on current engine technologies and transportation infrastructures. As a matter of fact, alternative liquid biofuels don't require perhaps any modification to the existing engine hardware, as they can be stored in the same fuel tanks as petroleum-based fuels; furthermore, their different physical and chemical properties can be accounted for through a proper calibration of the engine central processing unit. Finally, they require no additional costs with respect to routine manteinance, equipment wear and lubricating oil life.

As far as *Ethanol* is concerned, it has been known as a viable fuel for internal combustion engines since early Twentieth Century, as it had been expected that Ford Model T would have

been fueled with ethanol itself. However, transportation during almost the whole century happened to rely on petroleum-based fuels, and interest in ethanol has emerged again since the last decades. As other alcohol fuels, ethanol owns similar physical properties and emission characteristics as other petroleum fuels, thus it can be adopdet directly in a spark ignited engine, or even in compression ignition engines, if blended with diesel fuel (23). Some vehicle modifications are needed in comparison with gasoline fueling, because the stoichiometric air-fuel ratio is lower, and higher heat of vaporization leads to the need for appropriate heating during the intake stroke. Then, the increased octane rating allows higher engine compression ratios to be reached. However, corrosive features of ethanol prompt the need for specific material coatings over the whole fuel circuit. From the emissions point of view, it has been acknowledged that atmospheric carbon dioxide levels over the whole ethanol lifecycle can be slightly reduced, as the growth of plants for the production of ethanol can remove the CO_2 introduced into the atmosphere through ethanol combustion in engines. Also carbon monoxide emissions are reduced, as the ethanol molecule contains an oxygen atom, and combustion is more complete; average reductions in comparison to gasoline have been reported to add up to 30% circa. However, stoichiometric engine operation with ethanol can increase noxious emissions, and an amount of aldehydes is released during combustion. These drawbacks can however be reduced through a leaner engine operation.

As far as *biodiesel* is concerned, its production from vegetable oils has many advantages in comparison with conventional, petroleum-based diesel fuel. First of all, it is produced from renewable sources, so that the problem of crude oil prices and fossil oil resources can be avoided; then, its combustion can provide lower pollutant emissions, and it is economically competitive with common diesel oil. However, for its adoption into internal combustion engines, some modifications to the fuel injection system are needed. As a matter of fact, vegetable oils own similar thermophysical properties as mineral diesel fuel; however, they have greater average viscosity, and, for this reason, the fuel spray evolution within the combustion chamber is pretty different. The fuel jet behaves much more as a liquid column, thus resulting in poorer mixing and combustion, together with massive impingement against the cylinder walls and piston bowl. This inefficient mixing is reported to lead to incomplete combustion loss of engine power and fuel economy, also resulting in long-term problems such as formation of carbon deposits, injector coking, piston ring sticking and lubrication oil degradation. For these reasons, the best way to use vegetable oils for feeding internal combustion engines is treating them and converting them into biodiesel. Biodiesel

is thus the product of transesterification of vegetable oils: during this process, the reaction of fatty acids and oils with alcohols produces esthers and glycerol. As a result, the biodiesel produced has similar viscosity to the diesel fuel, and it is miscible with it in any proportion. When injected into an internal combustion engine, it shows similar performances than those allowed by standard diesel injection; some variations are observed depending on the source. An average reduction in maximum power output can be observed, together with a reduction in both carbon monoxide and noxious emissions. Furthermore, higher thermal efficiencies, lower BSFC values and higher exhaust temperatures have been observed for all biodiesel blends. Overall, biodiesel appears to be a suitable and economically viable alternative to petroleum-based diesel fuel for internal combustion engines, even if its molecular complexity and process variability is urging the need for a deep research in all of its representative compounds.

1.3 Background for reaction mechanism reduction

As analysed in the previous paragraph, research for combustion of biofuels is driving chemical kinetics studies to develop reaction mechanisms of huge sizes, also for the fuel subspecies which need to be collected and coupled in order to have an idea on how a 'biofuel', i.e. a blend of oxygenated hydrocarbons and alcohols, behaved during combustion. As a matter of fact, Figure 1.4 shows a comparison in mechanism size for most reaction mechanisms recently developed which involve biofuels or biofuel subspecies; detailed data are reported in Table 1.1. From them, it is clear that mechanisms of such dimensions aren't suitable for coupling with multidimensional CFD simulations, due to an excessive computational demand when solved in each cell of the computational grid, and due to excessive chemical stiffness due to the presence of thousands of species whose characteristic time scales can span more than ten orders of magnitude; and thus strategies need to be adopted for reducing, either dynamically or *a priori*, their size, thus allowing them to be suitable for simulation of practical combustion systems running on biofuels. However, mechanisms which are too simplified usually either suffer lack of validity at many reactor conditions, thus being useful only for reduced ranges of temperatures, pressures, and mixture equivalence ratios, or can show non-physical combustion behaviours when adopted for simulating cases which incorporate kinetics, mass diffusion and transport (39).

For all of these reasons, many methodologies have been developed in recen years for addressing the issues of computational simulation of practical combustion systems. As most fields in which research is very active, these methodologies can, for the sake of simplicity, be grouped into homogeneous cathegories. In particular, a first class of methods involves the development of 'skeletal' reduced mechanisms: the definition of skeletal mechanisms meaning that a unique mechanism is generated which includes only the most important reaction pathways, and thus can be obtained from a full, detailed mechanism through elimination of the less important species and reactions. In particular, techniques involving the selection of 'important' species or reaction sets can be summed up within the following types:

- `sensitivity analysis` (48; 49; 50): according to this widely adopted methodology, the modeler firstly chooses the important species, such as the initial reactants and the main expected products; then, redundant species are identified through Jacobian analysis: indeed, elements in the normalized Jacobian matrix represent the fractional

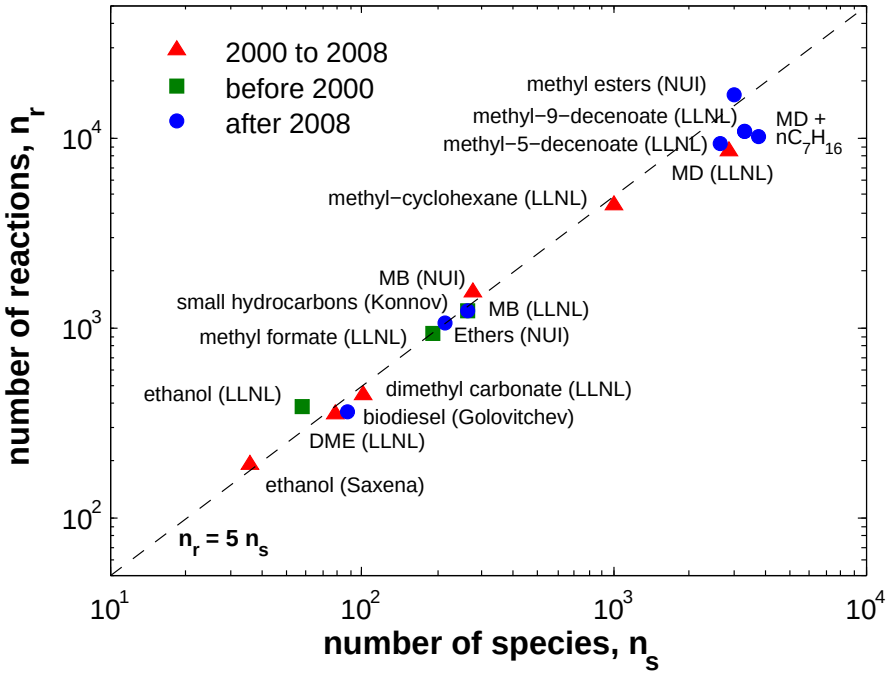

Figure 1.4: Overview of sizes of reaction mechanisms for the oxidation of biofuels.

change in the rate of production of a species i due to a change in concentration C_j. It is thus possible to identify species whose changes contribute for changes in the important species set, and delete them. A similar analysis can be conducted considering the effects of each of the reactions in the system over the same selected set of species.

- `principal component analysis (PCA)` (51; 52; 53; 54; 55): this kind of analysis aims to provide a minimum reaction set based on a sensitivity analysis at selected time steps or grid points. In particular, the sensitivity matrix is built and then diagonalized, to obtain its eigenvalues and eigenvectors, which are linked to an estimation of a response function, i.e. they quantify the variation in the dependent variables brought by variations in the reaction rates; then, eigenvalues are sorted and selected according to a cut-off value estimated by the user; for each of the eigenvectors whose related eigenvalues are survived, only the components which include the necessary reactions for simulating combustion within a requested precision value are retained. This method however introduces some computational burden due to systematic eval-

Ref.	Authors	Year	species	nr	ns
(4)	Marinov	1999	C_2H_5OH	383	58
(32)	Herbinet et al.	2010	$MD + nC_7H_{16}$	10208	3787
(32)	Herbinet et al.	2010	$MD + nC_7H_{16}$ + methyl – 9 – decen.	10806	3299
(40)	Pitz et al.	2007	methyl – cyclohexane	4418	1010
(41)	Fisher et al.	2000	MB	1219	264
(41)	Fisher et al.	2000	methylformate	925	193
(31)	Herbinet et al.	2008	MD	8555	2878
(32)	Herbinet et al.	2010	methyl – 5 – decenoate	9247	2649
(32)	Herbinet et al.	2010	methyl – 9 – decenoate	10753	3298
(42)	Glaude et al.	2004	dimethyl – carbonate	442	102
(43)	Fischer et al.	2001	DME	351	79
(29)	Saxena et al.	2007	C_2H_5OH	192	36
(44)	Konnov	2009	C_2H_5OH	1231	265
(45)	Golovitchev et al.	2009	Rapeseedbiodiesel	363	88
(10)	Dooley et al.	2008	MB	1549	275
(46)	Yasunaga et al.	2010	Ethers	1051	214
(47)	Naik et al.	2011	methyloleate + methylstearate	17000	3000

Table 1.1: Overview of reaction mechanisms for the oxidation of biofuels.

uation of the system Jacobian and to matrix diagonalization.

- `computational singular perturbation (CSP)` (56; 57; 58; 59; 60; 61): this approach has been widely adopted in the past for both generating skeletal mechanisms, and for producing reduced kinetics models. The methodology consists of an 'exact' algorithm for groupung elementary reactions in combustion mechanisms into separate sets, characterized by the same time scale. According to this algorithm, terms representing fast reaction groups are discarded when they are already exhausted. Thus, a simplified version of the combustion system can be achieved as a function of time, at each integration step.

- `optimization methods` (62; 63; 64; 65; 66; 67; 68; 69; 70): many examples are available in the literature which adopt a variety of optimization methods for finding optimal reduced sets of species and reactions. Among these methodologies, many examples are covered by the adoption of genetic algorithm techniques: these methods,

which exploit the principles of natural selection and evolution, rely on binary representations of 'chromosomes' which well suit the mechanism reduction procedure, when posed as an optimization problem. As a matter of fact, presence or absence of a certain species or reaction can be modeled as the binary instance of a particular allele (either `0` or `1`), and the chromosome thus easily identifies a reduced mechanism in tems of either species or reactions.

- `element flux analysis (EF)` (71; 72; 73; 74; 75; 76): this methodology features the selection of an important subset of species in a reaction mechanism analysing the fluzes of elements which instantly occur among all the possible couples of species, which are seen as source/sink pairs. Estimation of the fluxes of elements is achieved through rates of progress variable of the reactions, so that almost no further computational burden is required more than the simple evaluation of the chemistry ODE system. For this reason, the methodology has been adopted for both on-the-fly reduction of reaction mechanisms during combustion computations, and for the generation of skeletal mechanisms.

- `direct relation graph (DRG)` (77; 78; 79; 80; 81; 82): this methodology has been developed recently and has found many applications for both skeletal mechanism generation and on-the-fly reduction, and it has been shown to be particularly efficient for large reaction mechanisms. In particular, grouping and relationships among the species are achieved through construction of a graph in which vertexes are the species, and paths across the vertices quantify the dependence of each other species. So, in this approach some major species are defined as an input, and all the related species (over a pathwise cutoff value) are retained, because the link between two species conceives that the change in the first one affects the other one in a non negligible way. Many variants of the DRG method have been proposed, differing each other by the way in which the links among the species are computed. The most common approach considers the net reaction rate of the reactions which involve the recipient species.

A second major category involves time scale analysis and stiffness reduction: in particular, these methodologies are devoted to identifying and separating fast and slow reaction modes, thus allowing to treat quasi-steady-state (QSS) species and partial equilibrium (PE)

according to algebraic relationships which simplify the solution of the chemistry ODE system. Again, some subtypes can be identified:

- Quasi steady-state approximation (QSSA) and partial equilibrium approximation (PEA) (83; 84): these methodologies have been developed many years ago, and nevertheless provide simple and accurate estimations, and they have been widely adopted for the generation of reduced reaction mechanisms.

- Rate-controlled constrained equilibrium (RCCE) (85; 86; 87; 88; 89; 90; 91; 92): this approach assumes that the reacting system, during time intervals in the order of magnitude of the characteristic time scales of the fast reactions, develops an equilibrium state which is characterized by a minimum in free energy, subject to the a set of rate-controlled constraints which do not depend on the fast reactions. This procedure however relies on experimental knowledge on fast and slow reactions, and thus requires the scientist's efforts.

- intrinsic low-dimensional manifolds (ILDM) (93; 94; 95; 96): this methodology, similarly to CSP, is devoted to identifying and decoupling fast and slow species through Jacobian analysis. Its main avantage, in comparison with the previous methodologies, is that the analysis is performed without need for any user's input but the desired manifold dimension. The technique exploits the concepts of system dynamics, aiming at finding low-dimensional manifolds, which represent a simplified description of the system's behaviour within the states space. Again, the dimension reduction is made identifying the fast timescales as those which already have reached equilibrium conditions.

- As seen in the previous paragraph, also CSP can be seen as a methodology for the selection of slow and fast reaction modes; this methodology is however scarcely used in this context as repeated Jacobian evaluations usually lead to high computation times, so that *a priori* data tabulation is needed for allowing efficient coupling with codes for the simulation of practical combustion systems.

These two categories don't consider a number of other non-conventional methods, which have been proposed recently and which mainly involve theories of computation and of information, such as artificial neural networks, self-organizing maps, graph theory and data tabulation. As with any other topic in which research is very active, also in the numerics

of combustion chemistry any new proposal can lead to a step forward. As a matter of fact, the needs of reduction in computational times for chemistry are strongly urging research not only due to the increasing size of reaction mechanisms, but also due to the increasing computational efforts which more accurate CFD methodologies, such as LES, need in comparison with more traditional – but also less accurate – approaches do require. In the following paragraph, the context for numerical simulation of internal combustion engines, which is in the final aims of the present work, is presented.

1.4 Background for numerical simulation of reacting systems

The use of computer models and of numerical simulation as tools for research on renewable fuel systems in internal combustion engines is now mandatory, as the expensiveness of experimental campaigns makes it difficult to explore the behaviour of new combustion concepts. Furthermore, as computing capabilities are rapidly increasing, and numerical and computational methods are constantly improved, the use of numerical simulation is not confined anymore to laboratories and huge computer systems, but is gradually becoming a design tool available to most scientists and engineers. So, in this paragraph the bases of numerical simulation of reacting flows are presented.
First of all, the definition of *computer model* needs attention, as thus general term it is usually adopted as a synonym for *computer simulation* of any nature. A *model* is the representation of a physical phenomenon by means of either formulas, or quantitative relations, collections of empirical data, equations. So, the objective of modelling is to represent some interesting features of a physical system more than trying to produce an exact copy of the system itself. This is particularly true in combustion science, where most phenomena are much more complex than how usually considered, as they involve turbulence, presence of two phases, radiation, and extreme thermodynamic and dynamic conditions. So, a model can be of different nature, depending on the features of the physical system it is developed to represent. In particular:

- `Detailed models` are developed to describe the behaviour and the physical properties of a system starting from basic physical assumptions and laws. For this reason, detailed models are usually able to cover limited ranges of problems; on the other hand, they can be used to provide more general – but less rigorous – models with practical constants or other pieces of information. An example of detailed model in combustion chemistry is that of quantum mechanical calculations for establishing the reaction rates of elementary reactions: it is not possible to consider this kind of modeling when simulating combustion of systems involving thousands of species and reactions, however the reliability of the reaction rate constants for most reactions involving complex species, which can scarcely be derived from experimental measurements, is usually provided by their simulation adopting detailed molecular modelling.

- `Phenomenological models` are usually adopted when the phenomena to be modelled involve a variety of different physical aspects, which usually lead to a non negligible number of time scales. In these situations, a detailed modelling approach would bind the computational burden to the smallest scales, thus giving a level of detail which is usually not necessary, when a large scale system is simulated. For these reasons, the adoption of phenomenological models involves the derivation of averaged models for the small scale processes. In this way, formulas are adopted which qualitatively describe the particular physical situation, eventually accepting to introduce some simplifying assumptions, and thus their approximate form requires to be calibrated by adjusting coefficients, to fit data derived from either experiments or more detailed simulations.

- `Empirical models` are usually adopted for simple but effective representations of physical situations, where amounts of data are available from experiments or detailed numerical simulations. Usually these models rely on retrieval of data, mainly stored in tabular form. The most important issue with this kind of problems is that the data array usually cover specific validity ranges, which the empirical models themselves are not able to extrapolate. This is true not only with regards to the physical validity ranges of the parameters considered in the tabulation, but also to the particular physical environment from which the tabulated data come from.

The possibility of developing so many types of models mirrors the possibility of analyzing physical and chemical phenomena from many different points of view. Any numerical simulation model which is developed to describe complex phenomena such as those involving combustion development thus usually combines all the different types of components into a multi-layered environment, where each individual physical process is described according to a particular degree of detail depending on its range of time and space scales.

1.4.1 Computer models and numerical simulation

As the researcher produces models for understanding physical phenomena, *numerical simulation* is the way needed to produce results from them, under particular conditions. In particular, detailed simulation is acknowledged to act as a bridge between theoretical analysis and laboratory experiments, as it allows to tell something new about the physical environment it simulates, under defined and certain geometric, physical, initial band boundary

conditions. This can be useful in combustion systems, as disoveries can be made without needing any further theoretical insight into the problem. From this point of view, numerical simulation is similar to an experiment. As a matter of fact, it reproduces complex interactions among physical phenomena, and – more or less as it happens during real experiments – if there are any unexpected/unwanted effects, for example due to bugs in the program, or to incorrect calibration or choice of the submodels and of the parameters, the results of the simulation may lead to wrong assumptions even if the numbers seem to be quantitatively accurate in the context of the physical problem. To this regard, simulation can take benefits from assuming idealized and simplified problems as much as pssible, in order to limit the unwanted interactions due to geometric complications, wall boundary effects, etc.

One of the most important features of simulation, which cannot easily be represented by theory or by real experiments, is its flexibility in allowing the researcher to isolate the interactions among multiple phenomena. As a matter of fact, numerical simulation allows to analyse and evaluate the effects of single physical phenomena by turning them on or off, or by either changing ther intensity or their functional representation.

All of these positive aspects of numerical simulation however do not consider the cost it has, when it is adopted for calibrating phenomenological models, for testing physical laws, and to calibrate quantitative predictions of physical processes. As a matter of fact, simulating any physical system implies 'integrating' and 'advancing' the equations which define the time evolution of the particular system over a defined time period. This advancement of the simulation is made at finite *timestep*, which monitor the evolution of the system and which are usually smaller than the smallest of the timescales present in the problem. In complex problems such as those involving fluids and combustion, a variety of timescales is usually present, and the integration time steps can be as small as $1.0 \cdot 10^{-13} s$ (97), leading to unacceptably high computational times in case practical combustion systems with characteristic times of the orders of milliseconds up to seconds need to be simulated. For all of these reasons, a good numerical simulation is that which guarantees the best tradeoff between the required degree of accuracy and a suitable computational cost. In this context it is of crucial importance that both the models upon which the simulation relies guarantee the lowest possible computational cost at the required degree of accuracy, and the algorithms for numerical simulation use the most advanced techniques for exploiting modern computer hardware, thus allowing to use time efficiently.

1.4.2 Modelling reactive flow

In this paragraph, the basic time-dependent relationships which define the evolution of gas-phase reactive flows. This set of equations describes the convective fluid flow motion, the chemical reactions among the species, and diffusive transport processes due to heat and molecular diffusion. Even if this finite set of equations virtually can be able to model a huge variety of combustion phenomena, their simulation requires further simplifying assumptions which are problem-dependent, and which will be discussed later in the cases of interest of the present work, such as batch reactor systems and internal combustion engines.

1.4.2.1 Time-dependent conservation equations

The equations which can be adopted for modelling chemically reacting gas flows are conservation equations. The gas mixture is treated as a continuum, and the equations are presented in differential form. In particular, conservation of overall mass density ρ, of individual species mass fractions Y_i, of momentum density $\rho\boldsymbol{v}$, and the total energy density E can be written as:

$$\frac{\partial \rho}{\partial t} = -\nabla\cdot\left(\rho\boldsymbol{v}\right) \tag{1.1}$$

$$\frac{\partial Y_i}{\partial t} = -\nabla\cdot\left(Y_i\boldsymbol{v}\right) - \nabla\cdot Y_i\boldsymbol{v}_{d,i} + \frac{1}{\rho}\dot{\omega}_i W_i \tag{1.2}$$

$$\frac{\partial \rho\boldsymbol{v}}{\partial t} = -\nabla\cdot\left(\rho\boldsymbol{v}\boldsymbol{v}\right) - \nabla\cdot\boldsymbol{P} + \sum_j \rho_j \boldsymbol{a_j} \tag{1.3}$$

$$\frac{\partial E}{\partial t} = -\nabla\cdot\left(E\boldsymbol{v}\right) - \nabla\cdot\left(\boldsymbol{v}\cdot\boldsymbol{P}\right) - \nabla\cdot\left(\dot{\boldsymbol{Q}} + \dot{\boldsymbol{Q}}_{\boldsymbol{r}}\right) + \boldsymbol{v}\cdot\sum_j m_j\boldsymbol{a_j} + \sum_j \boldsymbol{v}_{d,i}\cdot m_j\boldsymbol{a}_j \tag{1.4}$$

In these equations, a number of terms which involves the physical nature of the fluid and its chemical properties are present. In particular, for a continuum, Newton's fluid, the pressure tensor $\boldsymbol{P}$, the heat flux $\dot{\boldsymbol{Q}}$, and the total energy E are defined as:

$$\boldsymbol{P} = p\left(\rho,T\right)\bar{\bar{\boldsymbol{I}}} + \left(\frac{2}{3}\mu - \kappa\right)\left(\nabla\cdot\boldsymbol{v}\right)\bar{\bar{\boldsymbol{I}}} - \mu\left[\left(\nabla\boldsymbol{v}\right) + \left(\nabla\boldsymbol{v}\right)^T\right] \tag{1.5}$$

$$\dot{\boldsymbol{Q}}\left(\rho,T\right) = -\lambda\nabla T + \sum_i \rho Y_i h_i \boldsymbol{v}_{d,i} + p\sum_i K_i\boldsymbol{v}_{d,i} \tag{1.6}$$

$$E = \frac{1}{2}\rho\boldsymbol{v}\cdot\boldsymbol{v} + \rho\bar{u} \tag{1.7}$$

where μ and κ represent shear and bulk mixture viscosities, respectively, λ the thermal conductivity coefficient, and K_i the thermal diffusion cofficient of species i. The net species

production rate ω_i obliges to the laws of chemical kinetics, whose deeper description is reported later on, in Paragraph 2.1. The bulk gas pressure value can then be evaluated according to the thermal equation of state for an ideal gas mixture:

$$p = N\,k_B\,T = \rho\,R_u\,T; \tag{1.8}$$

the external accelerations $\boldsymbol{a_i}$ can – in general – be specific of the species, and can be of various nature, such as electrical, gravitational, etc. Usually, only gravity is present, and in this case all the accelerations are the same: $\boldsymbol{a_i} = \boldsymbol{g}$. Finally, diffusion velocities of the species $\boldsymbol{v}_{d,i}$ can be found inverting the matrix equation:

$$\sum_k \frac{n_i\,n_k}{N^2 D_i,k}\left(\boldsymbol{v}_{d,k} - \boldsymbol{v_d, i}\right) = \boldsymbol{G_i} = \nabla\left(X_i\right) - \left(Y_i - X_i\right)\frac{\nabla p}{p} - K_i\frac{\nabla T}{T}. \tag{1.9}$$

where n_i terms represent the species number densities, in molecules per volume unit, and $N = \sum_i n_i$. The diffusion velocities are also subject to the constraint $\sum_i Y_i\,\boldsymbol{v}_d, i = 0$.

All of these equations serve to describe the time evolution of a reactive gaseous mixture intended as a continuum, where the continuum assumption comes from the statistical averaging over processes involving the small-scale phenomena of the orders of magnitude of particles ($\sim 10^{-10}\,m$). These equations thus 'chunk' the microscopic, molecular processes into a continuum, and thus seem to 'look' at the system only from a macroscopic point of view, thus introducing a lack of resolution in the description of the problem. However, they still represent a microscopic behaviour in case any practival system is to be represented that way: millimeters are as much as 7 orders of magnitude away from their lowest limit validity lengthscale. Furthermore, no possible analytical solution exists for these equations in any practical system configuration, so that time and space over which they need to be evaluated need to be subdivided into finite intervals. This process thus defines discrete variables, which put these equations in a form which is suitable for numerical computation, and where their integral evaluation is performed numerically.

Codes for the simulation of internal combustion engines involve the solution of unsteady-state turbulent fluid dynamics with presence of multiphase flow (due to sprays) and chemistry (due to combustion of the in-cylinder mixture). As a matter of fact, during the recent years, the study of more efficient and environmentally sustainable energy systems has been undergoing intensive research, and the use of computer tools for combustion calculations

has become necessary for both understanding the physics and predicting the behaviour of new combustion concepts (18). In particular, the coupling of computational fluid dynamics (CFD) codes with chemical kinetics has progressively become more important, and now no accurate engine simulation can avoid it, as computers need new combustion strategies to be considered, explored and applied to cases of industrial practice (98; 99; 100). As a result, research on internal combustion engines is one of the fields which more extensively exploits chemical kinetics applied to CFD, since the accurate prediction of chemical kinetics is mandatory for the simulation of the fuel ignition and combustion processes, as well as flame development, turbulence–chemistry interaction and pollutant formation are concerned. One of the most widely adopted codes for computing chemical kinetics is the CHEMKIN package (101) developed at Sandia National Laboratories; there are many evidences in literature showing its effectiveness when coupled to CFD codes for internal combustion engine simulations (102; 103; 104). Recently, the open source Cantera kinetic library (105) is gaining attention due to its object-oriented implementation, and ability to be coupled to codes written in a variety of languages (C++, FORTRAN, Matlab, Python). These codes offer full insight into the chemistry of zero-dimensional and simplified reacting systems, but often imply a huge computational burden when applied to detailed CFD simulations of internal combustion engines, for which the computational grids can add up to millions cells, this being particularly true as wider is the combustion mechanism adopted for the simulations. In fact, it is reported that the computational burden due to chemistry increases as much as n_r^3, the third power of the number of reactions in the mechanism (18). This implies that a simulation that contains a detailed mechanism consisting of 2000 reactions is expected to take 1000 times more time than the same simulation, if considering a skeletal reaction mechanism made up of 200 reactions.

So, though being the use of detailed chemistry essential for the predictive capability of computer models, for example for internal combustion engine simulations (106), however it is still too computationally demanding when chemistry ODE systems need to solve detailed reaction mechanisms. For all of these reasons, not only the size of the reaction mechanism is of crucial importance for the efficient simulation of internal combustion engines running on complex fuels, but also the efficiency of the software which performs the integration of the chemistry ODE system needs to be improved. Hence, a significant part of this Ph. D. thesis has been devoted to the development of a new, vectorized code for combustion chemistry. First of all, the vectorized code architecture adopted is particularly suitable for

mechanism analysis and reduction. Furthermore, an efficient explicit ODE solver for stiff chemistry problems has been developed and tested, exploiting the principle of time scale separation (97). As a matter of fact, some of the most widely adopted algorithms for the solution of stiff ODE systems, such as the DVODE for chemistry, are implicit, and vary the step size very quickly depending on the current stiffness conditions. However, this procedure is not very efficient when coupling this kind of solvers to CFD codes, as the fluid dynamic part of the code rules over the choice of the overall time step (see, for instance, management of the 'big iteration' width in the KIVA code (107)), so, any implicit code needs to be initialised in each cell and per each time step. This means that the implicit solver is not allowed to freely extend the integration timestep, and that a very small initial time step will be adopted when starting each cell integration, thus leading to proportionally higher CPU times. The new solver exploits an explicit Euler integration approach, thus being simple and robust. The stiffness of the ODE system is removed through the deactivation of the species whose characteristic time scales have already expired. This approach allows significantly smaller computation times for the integration of chemistry within CFD codes for engine simulations, and higher parallelisation efficiency due to the absence of huge private working arrays.

1.5 Presentation outline

In Chapter 2, the numerical methods adopted for the simulation internal combustion engines with detailed chemistry are presented. Particular attention is devoted to the explanation of the efforts made for the advancement in numerics for engine simulations with detailed chemistry. In particular, first of all the generalized problem of a chemically reacting environment, described through a finite set of reactions is presented; then, the development of a computationally efficient code for its solution is discussed, and validated through comparison with experimental and numerical data available in the literature for the most important zero-dimensional cases of engine relevance. Then, the numerical and computational details about its implementation are presented and discussed. As a second aspect of the efforts carried on for the solution of reactive systems, the development and validation of an explicit integrator for stiff ODE systems are presented, and its computational performances and accuracy are discussed, in comparison with the DVODE (108), the most widely adopted solver for combustion chemistry within CFD simulations. Finally, coupling of the reaction chemistry code with the internal combustion engine RANS simulation program KIVA-4 (109), and its parallelisation according to a shared memory paradigm are presented, and validated with respect to experimental engine data for cases concerning HCCI and DI diesel combustion modes: the first operation mode is kinetically controlled, and thus mainly relies on the reactivity of the air-fuel mixture; the second is more complex, as it involves a number of other phenomena, such as liquid fuel injection, breakup, evaporation and mixing.

In Chapter 3, a new methodology for the development of optimally reduced reaction mechanisms for internal combustion engine simulations is presented. The methodology is based on a robust algorithmic procedure which features successive reduction and optimization steps: at each of them, a number of species and reactions is removed from the detailed mechanism. This mechanism shrinking leads to the removal of the less important reaction pathways, which however introduce some error. For this reason, a new formulation for an error cost function is presented and discussed with respect to a well established reaction mechanism for ethanol combustion: in this approach, the evaluation of the predictive error made by an arbitrarily reduced reaction mechanism is not made on macroscopic observations, such as the overall ignition delay time, but it is instead made point-by-point over the entire desired validity range of the reduced mechanism. In particular, the validity

range is defined in terms of mixture temperatures, pressures and equivalent ratios, which are evaluated by subdividing this whole space into a set of initial reactor conditions. Then, the comparison between the detailed and the reduced mechanism is made over all these cases, and considering the whole set of species in the reduced mechanism, plus the average system temperature. Furthermore, these parameters are evaluated in terms of root mean squared errors over the entire time history at all cases. This formulation thus allows to consider all the system phenomenology, such as low-temperature combustion, cool flame and main mixture ignition.

As mentioned, at each step the mechanism is to be reduced, by elimination of the less important species and reaction pathways. In order to do this, an implementation of the well established element-flux analysis method (EF) has been coded (71), which analyses the activity among the species – considering them as sources or sinks of element fluxes – quantifying the instantaneous fluxes of carbon and oxygen atoms among them due to the active reactions. Establishing a threshold value, the species which do not contribute enough to the overall system reactivity can thus be deleted from the set. This method has been coupled to the reduction algorithm because of its suitability to a step-by-step, progressive shrinking of the mechanism, as an increasing subset of unimportant species can be monotonically determined through an increase in the overall flux cutoff value. Then, among the new features of the proposed methodology, optimization of the reaction rate parameters of the reduced mechanism has been considered at each reduction step, in order to include the effects of the discarded reactions into the surviving sub-mechanism. Furthermore, in order to preserve the physical soundness of the reaction mechanism, the optimization introduced has been limited to the uncertainty ranges for the reaction rate parameters available in the literature. Since the optimization featured – in general – a huge number of parameters, i.e. at least two or three per reaction, adding up to thousands, when the dimensions of the reduced mechanism are still similar to those of the detailed one, genetic algorithms represented the methodology which best fitted the optimization problem described. So, the development of a GA-based optimizer is presented, together with its validation in comparison with a commercial optimization code. Then, its application to the mechanism reduction and optimization case, together with the development of an appropriate 'fitness' function are reported. Finally, the assembly into a robust algorithmic procedure, including the strategies for the automatic generation of a skeletal mechanism starting from a detailed one are presented.

Chapter 4 finally contains the application of the proposed mechanism reduction and optimization methodology to the two biofuels on which the present research effort is focused: ethanol and biodiesel. If the definition of ethanol is actually straightforward, and similarly its application as a fuel for internal combustion engines, the definition of a chemical recipe for biodiesel cannot be made with ease, as its composition is subject to variability, even if the compounds which it includes are within the class of methyl ethers. So, two of the most important species which can be used as biodiesel surrogates, methyl-butanoate and methyl-decanoate, have been chosen, and mechanism for each of them have been created. Then, the two mechanisms have been merged into a unique set, and optimized for gaining capability to predict mixtures containing these two compounds. For each of the cases, simulations have involved both ignition delays from shock-tube cases, and ignition within internal combustion engines. The reliability of the methodology has been observed from the accuracy shown by all of these mechanisms, which were generated from detailed mechanisms of far different sizes (ranging from about 300 to 10000 reactions).
In conclusion (Chapter 5), the major achievements of the present thesis can be summarized as follows:

- A new methodology for the semi-automatic generation of skeletal reaction mechanism has been achieved.
- Adoption of genetic algorithms can be profitably adopted in reduced mechanism generation not only for binary selection of important/unimportant species, but with results beyond expectations for the calibration of the reaction rate parameters.
- Mechanisms for biofuels relevant to internal combustion engine applications have been developed, allowing computationally efficient, but highly accurate simulations to be carried out exploiting CFD + chemistry coupling.
- The skeletal mechanism proposed for biodiesel is among the first examples of reduced, multicomponent mechanism for biodiesel chemistry.
- A new vectorized representation of combustion chemistry allows computations for reactive systems to be carried out with almost 10× reduction in the overall computational times.

- An efficient, explicit ODE solver exploiting time scale separation allows further reduction in computational times to be achieved when considering CFD + detailed chemistry coupling.

2

Numerical studies

The issues related to numerical simulation are a key factor when dealing with chemically reacting environments, especially because of the stiffness of the kinetics and of the size of the mechanisms which describe the evolution of the species. For these reasons, an important part of the research has been devoted to the development, the validation and the application of codes exploiting numerical schemes which would allow the analyses on the chemistry system for mechanism reduction to be carried out with a high degree of computational efficiency, and to be conducted even on standalone machines. In this chapter, the analytical definition for chemically reacting environments and the numerical setup are reported. Particular focus is made on the development of a vectorized code, which allows a computationally efficient solution of evolving reacting environments to be carried out. Moreover, the application of a new ODE solver which features time-scale separation is discussed. Finally, coupling of the code with the multidimensional CFD code KIVA-4 (109) is presented.

2.1 Problem formulation

In the present work, chemical kinetics of reactive gaseous mixtures are evaluated in a modular way, in order to allow combustion chemistry to be coupled with more complex systems of differential equations. In particular, the structure of chemical kinetics calculations in the code is illustrated in Figure 2.1: three initial inputs are needed, for determining the structure of the chemical environment; then, three different packages are used for computing the thermodynamic properties of gaseous species and mixtures; the rates of progress variable of the reactions in the reaction mechanism and the production rates of the species; the conservation equations which close the ODE system after proper initialisation.

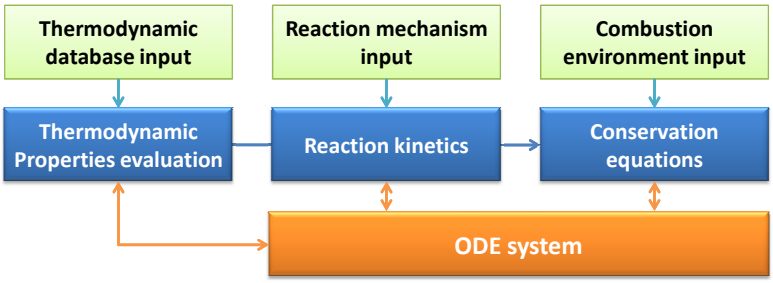

Figure 2.1: Structure of the chemical kinetics calculations for zero-dimensional batch reactors.

The following calculations can be made adopting any generic full reaction mechanism consisting of n_s species and n_r reversible/irreversible reactions.

2.1.1 Evaluation of thermodynamic properties and reaction mechanism definition

The evaluation of thermodynamic properties of gas-phase species and mixtures is of crucial importance for the calculation of combustion development, as species concentrations can vary many orders of magnitude the each others, significantly affecting their own production rates. Even if accurate predictions can derive from a theoretical approach descending from the kinetic theory of gases (110), the most common engineering-oriented approach has been adopted: the tabulation of polynomial coefficients for the interpolation of thermodynamic properties as a function of the system temperature (111; 112). Arrays containing mass- and molar- based properties of the pure species are defined and updated at each change in the system temperature; mixture-averaged properties are instead evaluated as:

$$\begin{aligned} \bar{c_p} &= \mathbf{c_p}^T\mathbf{Y}; \qquad \bar{c_v} = \mathbf{c_v}^T\mathbf{Y}; \\ \bar{h} &= \mathbf{h}^T\mathbf{Y}; \qquad \bar{s} = \mathbf{s}^T\mathbf{Y}; \end{aligned} \tag{2.1}$$

the value for mixture internal energy is also derived on the knowledge of the temperature value of the system: $\bar{u} = \bar{h} - R_m T$; where the average molecular weight of the mixture is evaluated as $\bar{W} = \sum_{i=1}^{n_s} [Y_i / W_i]^{-1}$, and the specific gas constant of the mixture is accordingly computed as $R_m = R_u / \bar{W}$.

A complete reaction mechanism is represented, in the code, by a set of n_r reactions involving a total number n_s of chemical species. Each k-th reaction is expressed as (113):

$$\sum_{i=1}^{n_s} \nu'_{k,i} M_i \rightleftharpoons \sum_{i=1}^{n_s} \nu''_{k,i} M_i. \tag{2.2}$$

The stoichiometric coefficients are stored as matrices $\boldsymbol{\nu}'$ and $\boldsymbol{\nu}''$ of n_r rows and n_s columns. The matrix M contains the labels identifying the names of the chemical species in the mechanism. As this expression is completely general, and can account for both reversible and non-reversible, elementary and non-elementary reactions, some other matrices are needed to the code in order to completely define their behaviour. In particular, the values in matrix **R** ($n_r \times 1$) logically identify reaction reversibility; matrix **Tb** identifies third-body reactions, where third-body molecularities with eventual enhanced efficiencies from some species have to be considered; finally, matrix **Pd** identifies pressure-dependent reactions where two different rate laws are followed at the lower and upper limits of the pressure range, and their interpolation at arbitrary pressure values can be evaluated according to different theories. The implementation of the effects of these reaction categories on the reaction rate are discussed in the following.

2.1.2 Reaction rates

The evolution in species' concentration in combustion systems can be expressed as the sum of the contributions due to the progress of each reaction. In particular, the species production rate array $\dot{\boldsymbol{\omega}}_{\boldsymbol{i}}$ is evaluated as

$$\dot{\boldsymbol{\omega}} = \left(\boldsymbol{\nu}^T \mathbf{q}\right)^T, \tag{2.3}$$

where $\boldsymbol{\nu} = \boldsymbol{\nu}'' - \boldsymbol{\nu}'$ and $\mathbf{q}$ ($n_r \times 1$) represents the rate of progress variable for the reactions. The rate of progress variable is defined as the difference between the forward and backward reaction rates, and is estimated as:

$$\mathbf{q} = \mathbf{k_f} \circ \mathbf{P_f} - \mathbf{k_b} \circ \mathbf{P_b} \tag{2.4}$$

where the symbol $\circ$ represents element-wise matrix multiplication (or Hadamard product), and the productories are stored as $P_{f,k} = \prod_{i=1}^{n_s} C_i^{\nu'_{k,i}}$ and $P_{b,k} = \prod_{i=1}^{n_s} C_i^{\nu''_{k,i}}$. As the computation of the terms $\mathbf{P_f}$ and $\mathbf{P_b}$ is usually the most CPU demanding task when evaluating reaction rate constants, an efficient algorithm has been developed for computing the two

matrices, which involves smaller arrays, and only vectorized operations. A full description of the algorithm is reported, together with pseudo-code implementation, in Appendix B.

The computation of reaction rates relies on the knowledge of reaction rate constants, $\mathbf{k_f}$ and $\mathbf{k_b}$, which is actually straightforward. In our approach, the forward reaction rates are initially evaluated according to the Arrhenius formulation (113) for all the reactions, and then corrections are imposed where needed, in order to match eventual pressure dependence or third-body enhancements. In particular, the forward reaction rate constants array is evaluated as:

$$\mathbf{k_f} = \mathbf{A} \circ T^{\mathbf{b}} \circ \exp\left(-\frac{\mathbf{E}}{R_c T}\right), \tag{2.5}$$

where the arrays **A**, **b** and **E** contain the Arrhenius law coefficients, and the operator exp is intended to apply the exponential function to each element in the matrix. For the reactions which undergo pressure dependence, the values at the high pressure limit are stored.
In particular, as far as pressure-dependent reactions are concerned, common treatment of the pressure dependence has been implemented, featuring computation of the forward reaction rate constants according to either Lindemann's expression (114) or the more evoluted Troe's form (115). As far as three-body reactions are concerned, equation 2.4 is modified in order to take into account the effects due to the presence of third bodies which are needed to activate the reaction. In particular, for each termolecular reaction, an effective molecularity premultiplies the rate-of progress variable:

$$\mathbf{q} = \mathbf{M_{eff}} \circ (\mathbf{k_f} \circ \mathbf{P_f} - \mathbf{k_b} \circ \mathbf{P_b}) . \tag{2.6}$$

The array of effective molecularities $\mathbf{M_{eff}}$ represents, for each reaction, the effective concentration of the third bodies which cause the reaction to activate (113), and it is equal to the sum of the concentrations of the species, each one multiplied by an 'enhancement' coefficient which is generally unity, but can be higher or lower in case some species participate more or less efficiently to the collisions:

$$\mathbf{M_{eff}} = \mathbf{E}^{\mathbf{T}} \mathbf{C}. \tag{2.7}$$

In elementary reactions which do not undergo third body effects, the corresponding column in matrix **E** is set to zeros, and the effective molecularity is set to unity.

Finally, backward rate constants have to be computed for all the reversible reactions. The array $\mathbf{k_b}$ of backward rate constants is evaluated exploiting the relationship occurring beteen forward and reverse rate constants and the equilibrium constant $\mathbf{K_{eq}}$:

$$\mathbf{K_{eq}} = \mathbf{k_f}/\mathbf{k_b} = \left(\frac{p_{atm}}{R_u\,T}\right)^{\sum_{i=1}^{n_s}\boldsymbol{\nu}} \circ \exp\left(-\frac{\mathbf{\Delta G}}{R_u\,T}\right), \tag{2.8}$$

where the sum along the species, i.e. the columns of the matrix $\boldsymbol{\nu}$, turns out an $(n_r \times 1)$ array of the same dimensions as the array $\mathbf{\Delta G}$, and – again – exponent and power operators are to be intended as element-wise. This last array, containing the changes in standard state molar Gibbs free energies between reactants and products, it is computed as:

$$\mathbf{\Delta G} = \mathbf{\Delta H} - T\,\mathbf{\Delta S} = (\boldsymbol{\nu}\mathbf{H})^T - T\,(\boldsymbol{\nu}\mathbf{S})^T. \tag{2.9}$$

Finally, the equilibrium-based calculation of backward reaction rates can eventually be overridden in case any explicit definition of the Arrhenius coefficients for the backward reaction are specified.

2.2 Closure equations

The set of differential equations obtained in Equation 2.3 can be applied to any time-evolving reacting system. However, chemical reactions can be found in a huge variety of engineering systems of various nature, such as batch reactors, testing equipment, and so on. Even internal combustion engines can be modeled as simplified reactors, when operated in HCCI mode: the closed-valve part of the engine cycle can be modeled as a closed thermodynamic environment, whose volume varies according to a specified law, defined by the slider-crank mechanism.

Thus, the chemical kinetics problem needs more closure equations in order to completely describe the physical evolution of any reacting system. In this case, the most important solutions adopted for testing fuels and their applicability to internal combustion engines have been modeled: first of all, simplified, zero dimensional reactors are needed for modelling the ignition of air/fuel or oxygen/fuel dilute mixtures. Ignition delay experiments are usually conducted in shock tubes, where the shock wave introduces an almost instantaneous increase in mixure's temperature and pressure, thus leading to ignition; the ignition process is hence similar to a constant-volume process. Furthermore, it is possible to reconstruct the thermodynamic conditions of the mixture after reflection of the shock wave (see, for instance, the SHOCK program (116)).

The solution of a simplified, zero-dimensional reacting environment requires a set of conservation equations for mass and energy to be solved. Under the assumptions of no mass inflow/outflow, and adiabatic system, the set of conservation equations features, as unknowns, the species mass fractions and the temperature of the reacting environment (117). In particular, mass fractions' evolution is evaluated as follows:

$$\frac{d\mathbf{Y}}{dt} = v\,\dot{\boldsymbol{\omega}} \circ \mathbf{W}. \tag{2.10}$$

As far as the energy conservation equation is concerned, its formulation has been considered specifically for each of the three cases. In particular, for an adiabatic, constant-pressure environment, it is computed as:

$$\frac{dT}{dt} = -\frac{v}{\bar{c}_p}\,\mathbf{H}^{\mathbf{T}}\dot{\boldsymbol{\omega}}_{\mathbf{i}}; \tag{2.11}$$

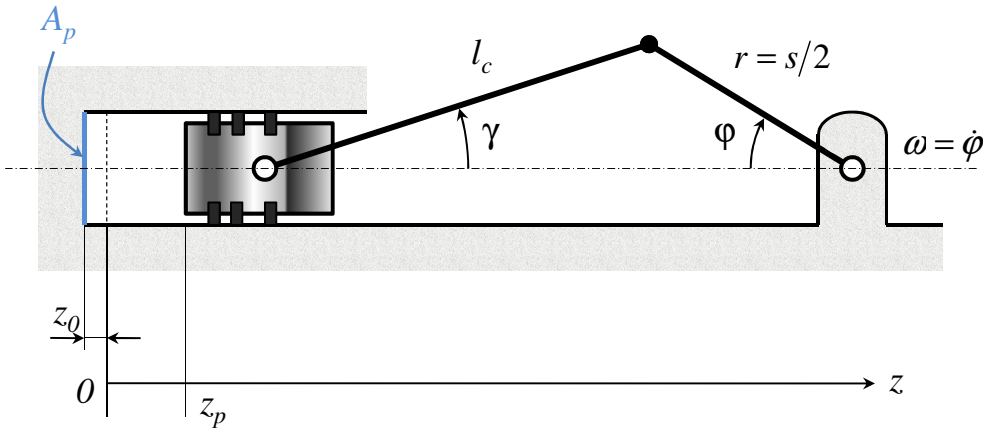

Figure 2.2: Schematic representation of the slider-crank mechanism

for an adiabatic, constant-volume environment, it is instead evaluated as:

$$\frac{dT}{dt} = -\frac{v}{\bar{c}_v}\mathbf{U}^{\mathbf{T}}\dot{\boldsymbol{\omega}}_{\mathbf{i}}. \tag{2.12}$$

When considering a zero-dimensional internal combustion engine, none of the previous assumptions is verified, and the more general relationship for a thermodynamic environment with time-dependent volume estimation has to be adopted:

$$\frac{dT}{dt} = -\frac{v}{\bar{c}_v}\left[\mathbf{U}^{\mathbf{T}}\dot{\boldsymbol{\omega}}_{\mathbf{i}} + \frac{p}{V}\frac{dV}{dt}\right]. \tag{2.13}$$

In this case, the instantaneous in-cylinder volume V and its rate of change dV/dt are evaluated on the knowledge of the dimensions of the slider-crank mechanism (see Figure 2.2 for the definition of the variables):

$$V = (z_0 + z_p)\,A_p = \left[z_0 + l_c\left(1-\cos\gamma\right) + \frac{s}{2}\left(1-\cos\varphi\right)\right]A_p; \tag{2.14}$$

$$\frac{dV}{dt} = v_p\,A_p = \omega\left[\frac{s}{2}\sin\varphi + l_c\sin\gamma\frac{d\gamma}{d\varphi}\right]A_p. \tag{2.15}$$

Homogeneous pressure value is computed evaluating the ideal gas law, where the average mixture thermodynamical properties have been defined as in eq. 2.1.

2.3 An efficient vectorized code implementation

The chemical problem posed in the previous sections is described in terms of matrices, thus allowing code to be tailored for vectorized computations. As a matter of fact, a library of routines has been implemented in both Matlab (118) and FORTRAN 90 (119). The first one is usually acknowledged to have slower performance in terms of computational times than FORTRAN, due to its nature as interpreted language; nevertheless, as its low-level engine is optimized for vectorized computation, it can take advantage of matrix-based operations, and hundreds-times speedup factors can be achieved in comparison with the more common loop-based programming (120). Furthermore, easy handling of matrices can simplify the manipulation of reaction mechanisms, as far as reduction in arbitrary sets of species and reactions can be concerned, for instance when dealing with the definition of new, reduced and optimized combustion mechanisms. Lastly, a huge set of optimisation tools is either embedded in Matlab or available in literature in Matlab format – as, for example, the NSGA-II genetic-algorithm based optimizer developed at Kanpur Genetic Algorithm Laboratory (121).
As far as FORTRAN language is concerned, vectorized programming is allowed as a number of compiler intrinsic functions is available for dealing with matrices and multidimensional arrays (119); furthermore, a number of libraries are available for download (122; 123), which include architecture-optimized routines for basic linear matrix algebra. In the present work, both the code and the libraries have been compiled using the GNU Fortran compiler. In particular, for efficient matrix manipulation, the double-precision BLAS libraries for both full and sparse matrices (124; 125) have been exploited instead than the compiler intrinsic functions, which were found to be more time consuming.

The computational efficiency of the two implementations of the code has been tested with respect to the choice of the ODE solver. In particular, integration for the Matlab library was provided by `ode15s` (126), embedded ODE integrator for stiff problems, and linking routines were developed especially for allowing the solver to estimate the Jacobian matrix in a vectorized fashion. As far as the Fortran implementation was concerned, a set of stiff ODE solvers was chosen and coupled to the code for the comparison: DLSODE (127), DVODE (108), RADAU-5 (128) and ROWMAP (129). The comparisons were made considering three different reaction mechanisms related to internal combustion engine-relevant fuels: the

Fuel	Ref.	n_s	n_r	p_i [bar]	ϕ_i [-]	T_i [K]
CH_4	(3)	53	325	2.0; 20.0	0.5; 1.0; 2.0	750; 1000; 1500
C_2H_5OH	(4)	58	383	2.0; 20.0	0.5; 1.0; 2.0	750; 1000; 1500
$n-C_7H_{16}$	(5)	561	2539	2.0; 20.0	0.5; 1.0; 2.0	750; 1000; 1500

Table 2.1: Detail of the mechanisms and of the initial states considered for the performance evaluation of the code, comparing different implementations and ODE solvers.

GRI-mech for methane combustion (3), and two detailed mechanisms from Lawrence Livermore National Laboratory which model combustion of n-heptane (5) and ethanol (4). For each of the combustion mechanisms, a set of 18 different initial conditions of the constant pressure reacting environment were considered, with the aim of simulating a number of problems with different stiffness. In particular, for each of them, two different operating pressure values, three different air-fuel mixture equivalence ratios, and three initial system temperatures were chosen. The details about the adopted values are reported in Table 2.1. Finally, integration tolerances were set to $\delta_{rel} = 1.0e-4$ and $\delta_{abs} = 1.0e-8$, fixed for each of the solvers.

The tests were run on an Intel i7-860 powered PC, with 6.0GB RAM, under a Windows 7 environment, and they spanned simulated time integrals ranging from $\Delta t = 1.0e-7\,s$ up to $\Delta t = 1.0\,s$. Figures 2.3, 2.4, 2.5 show the performances of the solvers for each of the three mechanisms considered. A further comparison with the performance, on the same machine, of the CHEMKIN-II library, coupled with SENKIN (117), has been included for the first two mechanisms; even if it is acknowledged that this code is significantly slower if compared to any of the newer versions, it has been chosen as a reference because is still widely adopted for coupling chemistry to CFD simulations.

As far as the results from the FORTRAN coded implementations are concerned, the best performance was shown by the DVODE solver: it guaranteed the lowest computing times at almost all the simulated time ranges, being overwhelmed by the ROWMAP only at the shortest simulations. However, the ROWMAP showed CPU time needs much more increasing than any other solver, as the simulated time grew; this led to unacceptably high CPU times needed for the longer simulated Δt values. Interesting performance was shown also by the RADAU5 solver, especially for the lowest Δt values, as it behave similarly to the DVODE,

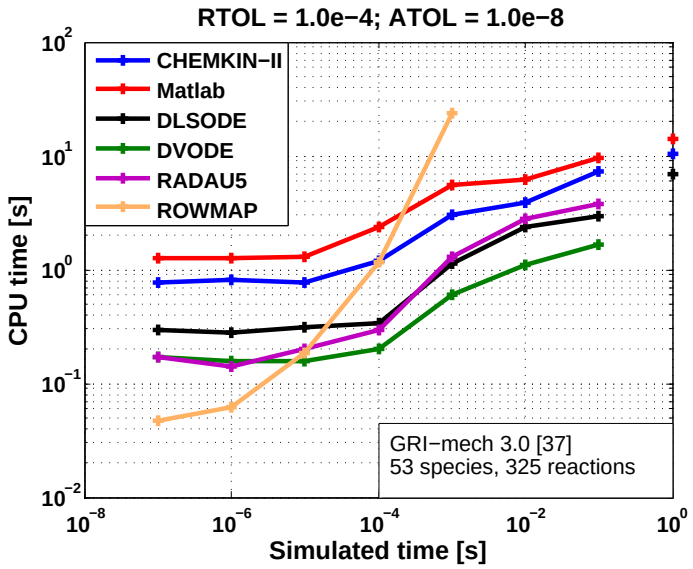

Figure 2.3: Performance comparison among constant pressure simulations of the GRI-mech combustion mechanism (3), using either the CHEMKIN-II package, or the present code, in Matlab language with ode15s solver or Fortran with different solvers (DLSODE, DVODE, RADAU5, ROWMAP). Details on the initialisation in Table 2.1.

although then worsening its computational efficiency at Δt values greater than $1.0e-5$. Finally, the DLSODE showed similar performance as the RADAU5 for most of the simulated time span. From the figures, the performance of the solvers shows to be pretty consistent across the three different combustion mechanisms simulated. Even the huge mechanism for n-Heptane combustion doesn't lead to an enough large ODE system for having the ROWMAP solver show interesting performance.

The comparison with CHEMKIN-II performance shows that the code, when coupled with the DVODE solver, always provides better results in terms of CPU times. An average reduction in the overall CPU time by 67% was reached for the ethanol combustion mechanism, and by 79% for the GRI-mech.

As far as the Matlab code implementation is concerned, higher CPU times were needed; nevertheless, the solver proved to be robust, as none of the computations failed to integrate. Furthermore, the CPU times were always in the same order of magnitude of those required by the CHEMKIN simulations: Matlab required an average 58% (GRI-mech) and 90% (ethanol) more time than the CHEMKIN.

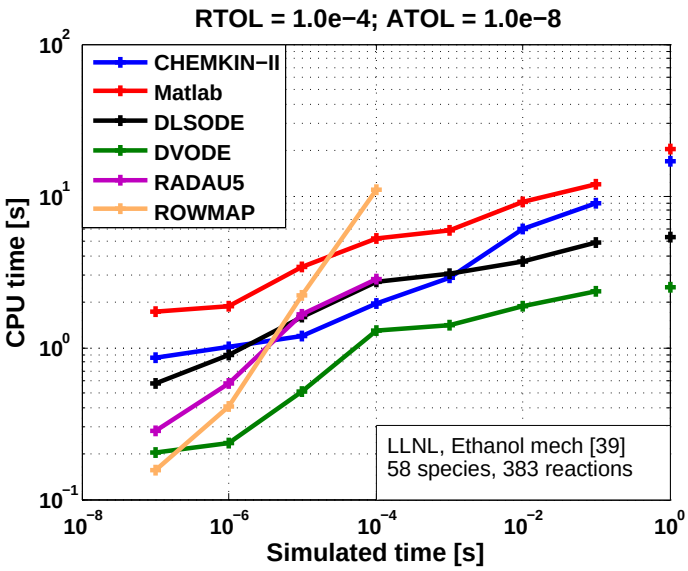

Figure 2.4: Performance comparison among constant pressure simulations of the ethanol combustion mechanism from LLNL (4), using either the CHEMKIN-II package, or the present code, in Matlab language with ode15s solver or Fortran with different solvers (DLSODE, DVODE, RADAU5, ROWMAP). Details on the initialisation in Table 2.1.

Overall, the FORTRAN-coded implementation showed to be suitable for coupling with multidimensional CFD simulations, due to being compiled, easily linkable to any other FORTRAN code, and showing good performance in terms of required CPU times; on the other hand, the Matlab code combines a high degree of flexibility, a reliable and robust solver with a still computationally good performance.

Once the DVODE solver was chosen as the reference one for the FORTRAN computations, in order to analyse the reliability of the results, validations were made on two different test cases: a set of ignition delay calculations in zero-dimensional, constant volume batch reactors; and computation of in-cylinder pressure traces using a zero-dimensional model for HCCI operated internal combustion engines. The details for each of the cases are summed up in the following.

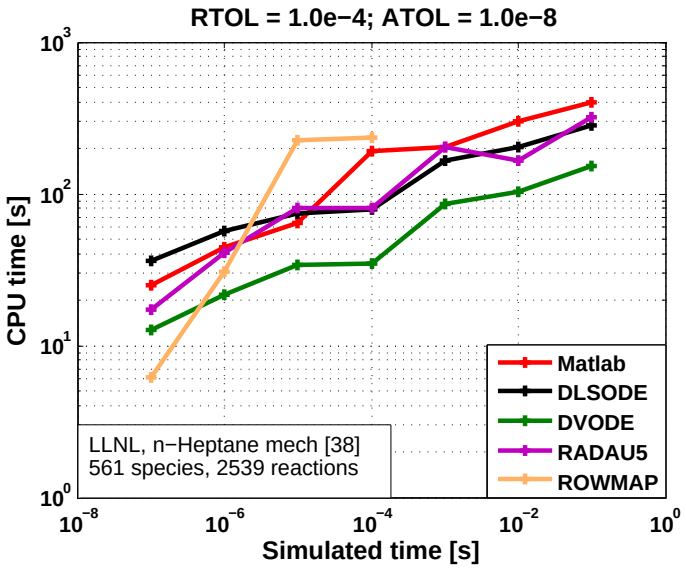

Figure 2.5: Performance comparison among constant pressure simulations of the n-heptane combustion mechanism from LLNL (5), using either the present code, in Matlab language with ode15s solver or Fortran with different solvers (DLSODE, DVODE, RADAU5, ROWMAP). Details on the initialisation in Table 2.1.

2.3.1 Validation: zero-dimensional reactors and ignition delay evaluations.

Ignition delay calculations are the most widely adopted testcase for verifying the accuracy of combustion mechanisms, especially as complex chemistry systems involve thousands of reactions, and kinetic mechanisms involving an even huge number of species and reactions can't usually represent the whole physical complexity of the phenomenon; and for this reason Arrhenius parameters of some key reactions can be tuned for accounting for the lack of resolution. Moreover, ignition of rare-gas diluted mixtures of fuel and oxygen in shock-tube experiments can be pretty thoroughly modeled as adiabatic processes occurring in constant-volume environments. For this reasons, large sets of experimental measurements are available in literature for a variety of fuels; in the present work, the three fuels of the mechanisms considered for the estimation of the computing performance of the code have been chosen as a reference. As far as methane combustion is concerned, detailed experimental data were available also in terms of time evolution of the most important species; it has been reported in figures 2.6, 2.7, 2.8; ignition delay measurements for the remaining fuels are plotted in figures 2.9 to 2.10.

Ignition delay time calculations after the reactor simulations have been considered according to the explicit rule where available; otherwise, ignition has been assumed to occur when a 200K increase in the reactor temperature was reached, initial time being considered the time at which the system is reached by the shock.

More in detail, from the comparison between the present code and the numerical results available in literature, shown in figures 2.6, 2.7, 2.8 at different mixture equivalence ratios, an excellent agreement is observed, as the slight differences noticeable in comparison with the experimental measurements are due to the kinetic mechanism adopted. Figure 2.9 instead shows ignition delay computations for the ethanol combustion mechanism from LLNL (4): both the curve of the ignition delays simulated by the present code, and the numerical results for the same mechanism, reported in (4) show excellent agreement with the experimental data. Finally, figure 2.10 shows the ignition delay times as computed by the present code, simulating the n-Heptane combustion mechanism from LLNL (561 species, 2539 reactions), in comparison with the experimental data from (130). Again, the comparison shows a pretty good agreement.

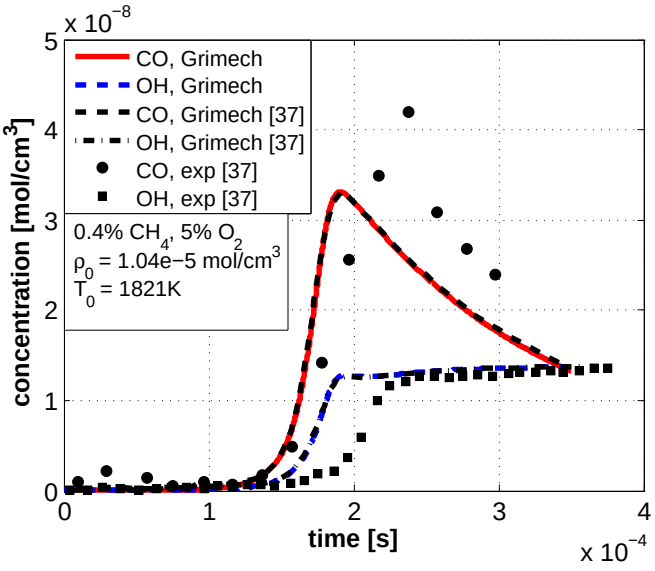

Figure 2.6: Methane combustion: time evolution of CO and OH concentrations as computed by the present code with GRI-mech mechanism, in comparison with experimental data and numerical simulations (3).

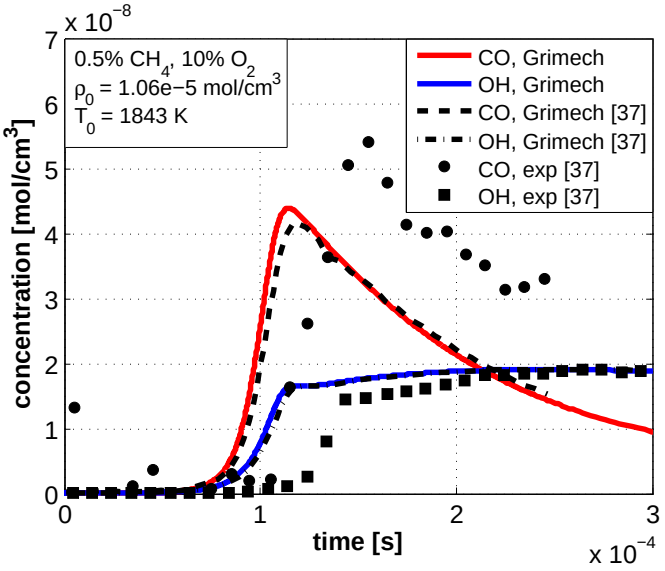

Figure 2.7: Methane combustion: time evolution of CO and OH concentrations as computed by the present code with GRI-mech mechanism, in comparison with experimental data and numerical simulations (3).

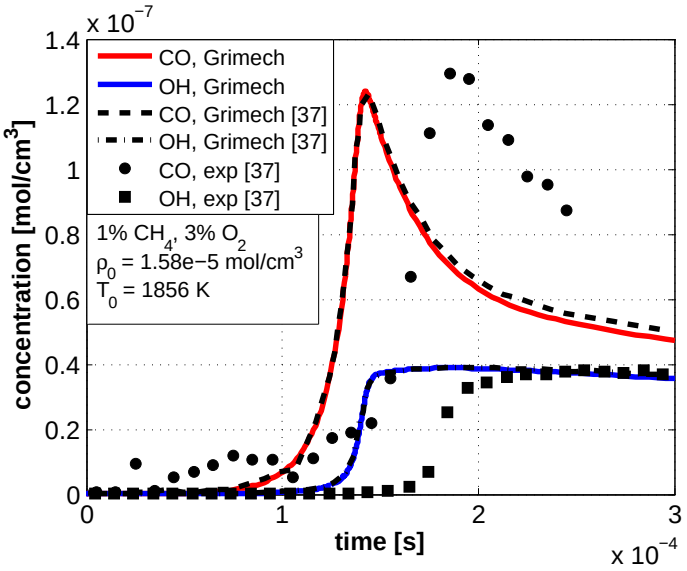

Figure 2.8: Methane combustion: time evolution of CO and OH concentrations as computed by the present code with GRI-mech mechanism, in comparison with experimental data and numerical simulations (3).

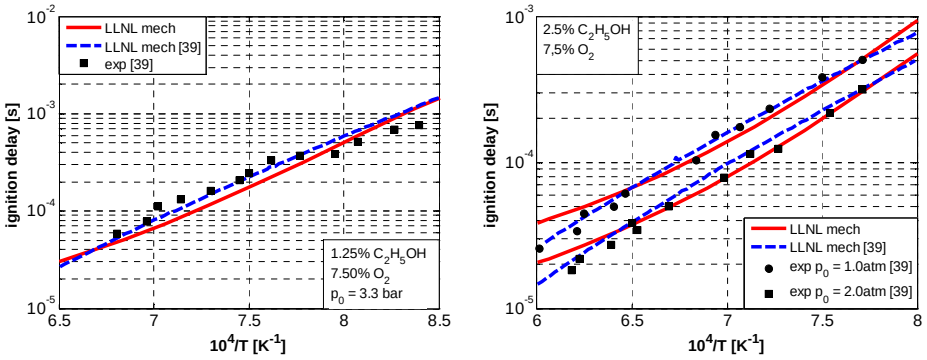

Figure 2.9: Ignition delay measurements and numerical simulations (LLNL ethanol combustion mechanism, (4)) for: left) $1.25\%C_2H_5OH - 7.5\%O_2 - 91.25\%Ar$ mixture with initial pressure $p_0 = 3.3\,bar$; right) $2.5\%C_2H_5OH - 7.5\%O_2 - 90\%Ar$ mixture with initial pressures $p_0 = 1.0\,atm$, $p_0 = 2.0\,atm$.

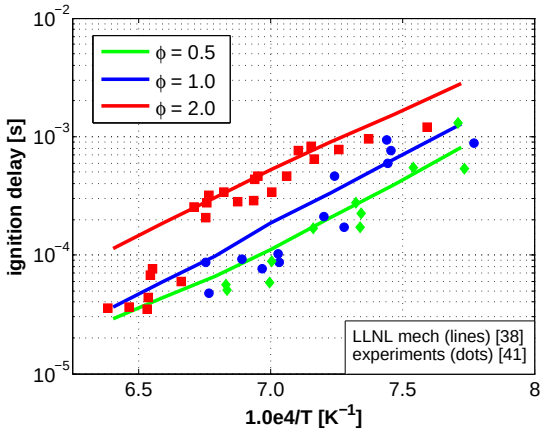

Figure 2.10: Ignition delay measurements and numerical simulations (LLNL n-Heptane combustion mechanism, (5)), for stoichiometric, lean and rich oxygen – n-Heptane mixtures diluted with 98% argon volume fraction, $p_0 = 203 kN/m^2$.

2.3.2 Validation: zero-dimensional ICE model.

A zero-dimensional engine model for simulating HCCI combustion has been implemented: this type of model consists of an adiabatic, zero-dimensional reactor whose volume variation is imposed by the slider-crank mechanism, as previously defined in Eqs. 2.13 to 2.15. Simulations have been run for a CFR engine, running premixed mixtures of n-Heptane and air, and operated in HCCI mode, set up at three different compression ratio values, and compared to experimental curves of average in-cylinder pressure.

From the results, plotted in figure 2.11, the model is able to catch the ignition timings with a high degree of accuracy. The intake charge temperature has been used as a calibration parameter for the case, as simplified modelling of HCCI combustion isn't able to capture phenomena such as wall heat transfer, charge blowby to the crankcase, influcence of the piston-ring crevice volumes, and thus an increase in the initialisation temperature up to 50K is usually accepted (131). In the present case, instead the experimental value reporting an initial charge temperature $T_{IVC} = 313K$ was increased by 50K.

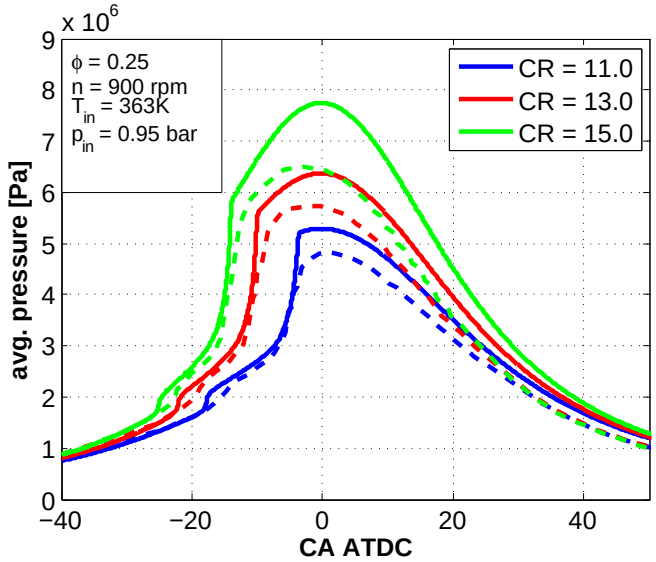

Figure 2.11: Experimental and numerical in-cylinder pressure curves for an HCCI CFR engine (6), at compression ratio values $CR = 11.0, 13.0, 15.0$, equivalence ratio $\phi = 0.25$, engine speed $n = 900rpm$. Experimental vs. zero-dimensional calculation comparison; LLNL n-Heptane combustion mechanism.

2.4 An explicit solver for stiff ODEs through time scale separation

Increasing demand for more efficient combustion system is nowadays driving research in the field of internal combustion engines to adopting CFD simulations coupled with detailed chemistry solvers (39). Among the reasons for this step, there is the need for maximum accuracy in predicting fuel chemistry: many innovative combustion concepts applied to internal combustion engines (such as HCCI, PCCI) rely on combustion chemistry and on the reactivity of the air-fuel mixture more than on mixing, flame development or interaction with the in-cylinder flow field (98; 100). Furthermore, simple, phenomenological models are gradually becoming unadequate for the prediction of pollutant emissions: increasing restrictive regulations require heavy design efforts for matching the requested limits, so that a high degree of accuracy is needed in the modeling and simulation phases, which allow the designers to reduce the need for huge experimental campaigns on engine prototypes. To this regard, a number of computational studies is becoming relevant for analyzing the physical and chemical interactions of the exhaust charge to the after-treatment systems, which act as reacting environments. Finally, emerging alternative fuels, such as ethanol and biodiesels, are often blended with petroleum-based hydrocarbon fuels, and still their combustion behavior is under research. Their composition is usually variable, and predictive combustion mechanisms for them need to be based on robust hydrocarbon chemistry. The effect is that reaction mechanisms, adopted for the prediction of their performances when introduced into internal combustion engines, usually own hundreds to thousands reactions and species, and the option of exploiting skeletal mechanisms, made of only few steps, appears to be ineffective and useless. All of these reasons are thus leading researchers in the field of internal combustion engines to couple their CFD codes with detailed chemistry solvers; the CHEMKIN is one of the most widely adopted because of its standard input format, and of its robustness thanks to the presence of the well established DVODE solver. However, the increase in CPU times due to chemistry is significant, and can add up to more than 90% the overall CPU time during practical engine simulations. Thus, a number of efforts is available in literature directed at reducing the computational time needed for solving the ODE system associated to combustion chemistry. To this regard, two kind of approaches are found. A first group of works are chemistry-based, i.e. are devoted to the development of methodologies for simplifying the reaction mechanisms on-the-fly, thus reducing their size and, accordingly, the overall computation time. These approaches are based on sensitivity and

reactivity analyses on the reaction mechanism. For example, a number of works considers the the Direct Relation Graph (DRG) methodology, which establishes links between the reacting species, and constructs a graph among them. Only the group of species which have sufficient bond strength is retained in the simulation, while the other ones are discarded. This process is usually embedded into the ODE solver and it has been reported to allow significant reductions in total computational time when either simulating batch reactors or practical CFD simulations. Other works rely on Element Flux analysis (EF), a methodology which models the species in the reaction mechanism as sources/sinks for fluxes made by atoms of elements (usually, carbon and oxygen, but also hydrogen is found to be considered). The species to be retained are those which activity as a source/sink for atoms is beyond a fixed cut-off value fixed by the user. The advantage of these methodologies is that they can be executed in real-time during the simulation - as they do not require almost any computational overhead in comparison with the standard ODE integration - and updated at each time integration step, so that every new reduced mechanism subset guarantees the maximum degree of reduction at each instantaneous reactive condition of the system. Other efforts in this class of methods consider both chemical and mathematical analysis strategies, which however often introduce major overhead due to more complex matrix manipulations, thus being in-adequate for coupling with ODE solver, while they are usually exploited when generating skeletal mechanisms, due to their capability to achieve better insight into the mechanism.

A second class of methodologies is instead devoted to improving the numerical aspect of the ODE integration, on the knowledge of the problems which are raised by the need for integrating chemically reacting environments. In particular, it is acknowledged that the non-linearity in the formulation of reaction rate variables, together with the strong degree of stiffness which affects the ODE systems due to the contemporary presence of species whose characteristic time scales eventually spans a time interval ranging more than 10 orders of magnitude, can lead to high computation times for most integration methodologies, where the smallest scales rule over the time-step size needed by the algorithm convergence requirements. For example, an explicit time integration for a chemically reacting environment, proceeding at a time-step of the order of $10^{-13}s$, would need millions of evaluations of the ODE system derivative in order to integrate a limited 10^{-6} s simulation time interval, of the order of usual iteration time-steps during RANS CFD calculations. For these reasons,

implicit solvers relying on variable-coefficient methods, such as the DVODE developed at Lawrence Livermore Laboratories (LLNL), usually have the best performance as they are capable of extending the integration time-step if the fast modes of the ODE system have already got to their asymptotic value. However, among the drawbacks of these methodologies a huge number of evaluations of the Jacobian matrix for the ODE system is needed. This operation can require huge amounts of time, and the Jacobian matrix usually cannot be expressed in sparse format, as the interactions among the species are complex. For instance, pressure-dependent and third-body reactions also involve species which are not directly participating into the reaction, but whose concentrations affect the reaction rate, for example contributing to an external molecularity value. For these reasons, a class of methodologies is available in the literature which, depending on the structure of the problem, act in order to better pose it from a numerical point of view independently from its chemical nature, so that its solution can be computationally as efficient as possible. These techniques include operations for numerically manipulating the system matrices, sorting the reactions and the species, reducing the sparsity of the Jacobian matrix, separating the time scales of the variables (39; 132).

In this framework, some literature is available which studies the development of a class of solvers which exploit the separation of the variables' time scales by actually integrating, over a sample time interval, only the variables whose characteristic timescales still haven't been reached. The related analyses show that this kind of approach can lead to a slight reduction in the total computation analysis if compared to implicit methods for batch reactors, but no evidence has been proven for the methodology when coupled with multidimensional CFD simulations. However, it appears that this class of solvers presents many interesting features, which may lead to advantages also in this case. In particular, in case an approximate estimate of the variables' time scales can be adopted, no computational overhead than the actual evaluation of the ODE system is needed by the method, so that even an explicit solution can be attractive, and the huge amounts of CPU time needed for the estimation of the Jacobian matrix can be avoided. Then, the methodology appears to be suitable for coupling with CFD simulations, as the sample time interval for the evaluation of the variables' time scales can be represented by the integration time step determined by the flow field solver. In this way, one of the major drawbacks of the implicit solvers can be avoided: the tiny dimension of the estimate for the initial timestep, which would be present at each

cell in the computational grid and at each time-step of the flow field solver. In the present work, a study is presented concerning the development and the performance analysis of two explicit ODE solvers, based on time scale separation (TSS), and tailored for coupling detailed combustion chemistry with multidimensional internal combustion engine simulations. In particular, an analytical expression, based on the instantaneous reaction rate variables, has been developed for estimating the time scales of the species in the reacting environment. Then, time scale separation has been coupled with two explicit solvers: a 2^{nd} order improved Euler scheme, and a 5^{th} order Runge-Kutta-Fehlberg explicit solver. The accuracy and the performances of the two solvers have then been studied at zero-dimensional reactors, in comparison with the reference DVODE solver, adopting a vectorized code for combustion chemistry previously developed by the authors. Finally, the solution procedures have been coupled with the KIVA-4 code, in order to assess their improvements to code performance. Overall, better performance improvement with reference to coupling with the DVODE solver was shown by the simple 2^{nd} order Euler solver, while the 5^{th} order RKF scheme showed a slightly better robustness across the reference cases. Finally, thanks to the absence of working spaces, which are needed by the DVODE solver for constructing the numerical evaluation of the Jacobian matrix, both the TSS explicit solvers showed better speedups when parallelizing combustion chemistry in the KIVA code by means of a shared memory paradigm.

In the next paragraphs, the approximate time scale separation analysis is presented for combustion chemistry, together with its coupling with explicit ODE solvers. Then, a detailed comparison is reported showing the accuracy and the efficiency of the solver with respect to the DVODE. Finally, coupling of the codes with KIVA-4 is presented, and their performances are assessed at two reference internal combustion engine configurations, upon which the DVODE solver had already been validated.

2.4.1 Time scale separation (TSS)

The broad range of timescales present in combustion chemistry usually limits the advancement timestep during the integration of the chemistry ODE system, because of the presence of the smallest scales, which act within the system even after that the fastest species have already evolved. The time scale separation approach aims at freezing each species after a reasonably long time interval so that it has completely evolved. In this way, the fastest

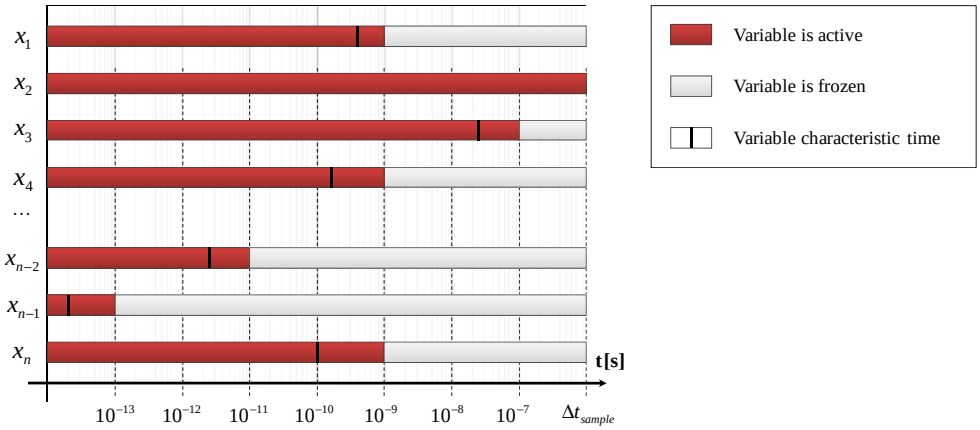

Figure 2.12: Integration exploiting time scale separation

modes are progressively deleted during the time integration, the stiffness of the system is reduced and some constraints to the increase in the timestep are removed (97; 133; 134). Figure 2.12 shows a schematic of this concept: the integration of an arbitrary ODE system made of n variables over a sample time interval, Δt_{sample}, computes the evolution, and thus updates the value of each of them until the end of the integration, at a number of internal integration steps which depend on the method adopted for the integration. Through time scale separation, instead, an initial estimate of the characteristic time of the generic variable is exploited (indicated as black ticks in the graph). These values thus give an indication of the characteristic time scale of the variables, which can be approximated as the nearest next order of magnitude value. Each of the variables is hence integrated and updated only until its own timescale value has been reached (red bars), while its value can be frozen and kept constant after that, and until the end of the whole integration. Obviously, this simplification leads to the introduction of errors into the solution, but it will be shown that it can guarantee good results if a suitable choice of the sampling interval, and a good estimate of the variables' timescales are adopted.

2.4.1.1 Timescales in combustion chemistry

The evolution of a chemically reacting environment, is usually represented throughout a reaction mechanism, which considers n_s species and where n_r reactions describe the effects of the collisions among the molecules, as shown in Equation 2.2, where matrices ν' and ν''

($n_r \times n_s$) contain the stoichiometric coefficients of species in the reactions, and **M** is a matrix containing the names of the species considered by the reaction mechanism. Overall, the change in the species mass fractions can be described in terms of rates of progress variables of the reactions:

$$\frac{\partial \mathbf{Y}}{\partial t} = \frac{1}{\rho}\dot{\omega} \circ \mathbf{W}, \tag{2.16}$$

where the product defined by symbol $\circ$ is intended to be element-wise; matrix **Y** ($1 \times n_s$) indicates the species mass fractions, **W** ($1 \times n_s$) their molecular weights, and the net species production rate array $\dot{\omega}$ ($1 \times n_s$) is evaluated as the difference of the contribution to construction and destruction of species due to forward and backward reactions:

$$\dot{\omega} = \left(\nu^T \mathbf{q}\right)^T, \tag{2.17}$$

$$\mathbf{q} = \mathbf{q_f} - \mathbf{q_b} = \mathbf{M_{eff}} \circ \left(\mathbf{k_f} \circ \prod_{i=1}^{n_s} C_i^{\nu'_{k,i}} - \mathbf{k_b} \circ \prod_{i=1}^{n_s} C_i^{\nu''_{k,i}} \right); \tag{2.18}$$

matrices identified with **q** ($1 \times n_r$) define forward, backward and overall rates of progress variable of the reactions; $\mathbf{k_f}$ and $\mathbf{k_b}$ ($1 \times n_r$) the reaction rate constants and **C** ($1 \times n_s$) the instantaneous species concentrations. $\mathbf{M_{eff}}$ ($1 \times n_r$) contains effective molecularity values at the reactions which undergo third-body effects, while ones are set at elementary reactions.

When analysing a chemically reacting environment, thus, the timescales related to the evolution of the species are directly linked with forward and backward rates of progress variable. Many are the analytical methodologies, developed in the past, for identifying and estimating fast and slow timescales in combustion chemistry, such as Computational Singular Perturbation (CSP) (56; 57), or the Intrinsic Low-Dimensional Manifold (ILDM) (93; 135). However, these exact techniques require computational efforts, and thus are usually adopted for the construction of skeletal and reduced reaction mechanisms, while limited are the efforts reported for their implementation into ODE integration algorithms (136). For this reason, an approach similar to that adopted by Gou et al. (97) has been adopted. In that approach, the characteristic time of each species is estimated descending from the

linearization of the ODE system near the time instant at which it is evaluated. In particular, an approximation of the characteristic time of destruction of the k-th species is adopted:

$$\tau_k = \frac{\partial D_k}{\partial Y_k}, \tag{2.19}$$

where $\mathbf{D} = \left(\nu^T \mathbf{q_b}\right)^T \circ \mathbf{W}/\rho$ represents the species' destruction rate. In the present work, the characteristic time for each species has been determined on the same linearization hypothesis, but a more general final expression has been chosen. In particular, the characteristic time of evolution of the k-th species is computed as (137):

$$\tau_k = -\left[\frac{\partial}{\partial Y_k}\left(\frac{\partial Y_k}{\partial t}\right)\right]^{-1}. \tag{2.20}$$

An analytical derivation of expression 2.20 has been made under the simplifying assumption that third-body effects are not dependent on the k-th species

$$\begin{aligned}\frac{\partial}{\partial Y_k}\left(\frac{\partial Y_k}{\partial t}\right) &= \frac{\partial}{\partial Y_k}\left(\frac{1}{\rho} W_k \sum_{i=1}^{n_r} \nu_{i,j}\left(q_{f,i} - qb, i\right)\right) = \\ &= \frac{\partial}{\partial Y_k}\left\{\frac{1}{\rho} W_k \sum_{i=1}^{n_r}\left[\nu_{i,k}\left(k_{f,i}\prod_{j=1}^{n_s}\left(\frac{\rho Y_j}{W_j}\right)^{\nu'_{i,j}} - k_{b,i}\prod_{j=1}^{n_s}\left(\frac{\rho Y_j}{W_j}\right)^{\nu''_{i,j}}\right)\right]\right\}.\end{aligned} \tag{2.21}$$

After some manipulations, expression 2.21 can finally be summed up into:

$$\begin{aligned}\frac{\partial}{\partial Y_k}\left(\frac{\partial Y_k}{\partial t}\right) &= \frac{1}{\rho} W_k \sum_{i=1}^{n_r}\left[\nu_{i,k}\left(\frac{k_{f,i}}{Y_k}\prod_{j=1}^{n_s}\left(\frac{\rho Y_j}{W_j}\right)^{\nu'_{i,j}} - \frac{k_{b,i}}{Y_k}\prod_{j=1}^{n_s}\left(\frac{\rho Y_j}{W_j}\right)^{\nu''_{i,j}}\right)\right] = \\ &= \frac{1}{\rho}\frac{W_k}{Y_k}\dot{\omega}_k.\end{aligned} \tag{2.22}$$

In conclusion, the simplifying assumption that the third-body effects, which are present in some of the reactions, do not depend on the k-th species, allow the following expression for the characteristic times to be computed, which doesn't need any computational overhead as it only depends on known quantities:

$$\frac{\partial}{\partial \mathbf{Y}} = \frac{1}{\mathbf{Y}} \circ \frac{\partial \mathbf{Y}}{\partial t}. \tag{2.23}$$

Again, the array $1/\mathbf{Y}$ is that containing the reciprocals of the elements of $\mathbf{Y}$. As mentioned, expression 2.23 only gives an estimation of the characteristic time scales of the species,

as it descends from the linearization of the ODE system near the integration time instant, and the behavior of third-body reactions has been considered to affect the characteristic times as any simpler elementary reactions. Furthermore, it is acknowledged (74) that, in presence of species involved in partial equilibrium reactions, the contributions due to forward and reverse reactions are almost equal, and the resulting negligible variation in concentration can lead to the estimation of a very high timescale value. This can significantly affect the ODE system integration, in case the time scale separation is adopted. As a matter of fact, the contributions of reactions which are near equilibrium would lead to significantly high characteristic times in the involved species, thus meaning that they are the more likely to be active during the whole integration time, the more their evolution is close to the end. For this reason, relation 2.20 has been modified in order to limit the increase in characteristic time of the species involved in reactions at equilibrium. Since the actual values of rates of progress variable heavily rely on temperature, a relative threshold in the cumulative rate of progress variable is defined. The contributions of each reaction are firstly sorted in ascending order, and the set of equilibrium reactions is defined as the set of the first k reactions whose overall sum contributes to the total by less than a user-specified threshold, C_τ:

$$\tilde{\mathbf{q}} = \text{sort}\left(\mathbf{q}\right), \tag{2.24}$$

$$k \leftarrow \max\left\{ k = 1,\dots,n_r \ni \sum_{i=1}^{k} \tilde{q}_i \leq C_\tau \cdot \sum\left\{\tilde{\mathbf{q}}\right\} \right\}, \tag{2.25}$$

$$\tilde{\mathbf{q}'} = \begin{cases} \tilde{\mathbf{q}}'\left(k+1:n_r\right) = & \tilde{\mathbf{q}}\left(k+1:n_r\right) \\ \tilde{\mathbf{q}}'\left(1:k\right) = & \left|\tilde{\mathbf{q}_\mathbf{f}}\left(1:k\right)\right| + \left|\tilde{\mathbf{q}_\mathbf{b}}\left(1:k\right)\right| \end{cases} \tag{2.26}$$

So, expliciting equation 2.20, characteristic timescales are finally evaluated as:

$$\tau = \frac{\rho\,\mathbf{Y}}{\mathbf{W} \circ \left(\nu^T \mathbf{q}'\right)^T}, \tag{2.27}$$

where again the division operator is intended as element-wise division. This formulation allows an estimate of the characteristic time scales of the species to be evaluated anytime and in any chemically reacting system. In the following paragraph, its implementation into two explicit ODE integrators is discussed.

2.4.1.2 Explicit integration with time scale separation

As shown in Figure 2.12, owning an the estimate in the variable's time scales allows the stiffness of an ODE system to be reduced by progressively freezing the change in the variables

whose evolution is likely to be over. A number of papers is available in the literature which presents efforts devoted to improving the computational efficiency of the integration of chemistry ODE systems by dynamically freezing some variables/equations (97; 136; 138). In the present work, two explicit solvers for stiff ODE systems with time scale separation have been developed: a first, simpler one, implements the improved Euler's method (IE), with $O(h^2)$ accuracy; the second implements the Runge-Kutta-Fehlberg procedure (RKF45) which allows $O(h^5)$ accuracy order. The choice on the two methods has been motivated by the fact that time scale separation should lead to progressively non-stiff problems, with respect to the instantaneous integration time step, and thus an even simple and computationally inexpensive integrator such as the IE is expected to yield accurate results; however, the RKF45 method should be more reliable, even if at a higher expense.
Both integrators are general, and assume an arbitrary input initial value problem expressed as (139):

$$\frac{\partial \mathbf{y}}{\partial t} = \mathbf{f}\left(t, \mathbf{y}\right), \qquad \mathbf{y}\left(t = t_0\right) = \mathbf{y_0}. \tag{2.28}$$

In the case of chemical kinetics, the ODE system is autonomous, as the evolution of the system $\partial \mathbf{y}/\partial t$ only depends on species concentrations and temperature, and thus it does not rely on time. In presence of time scale separation, however, time dependency is needed for identifying, step by step, the set of active species to update into the solution. Thus, an appropriate estimation of characteristic time scales within the ODE integrator is needed. For this purpose, a procedure as summarized in Figure 2.13 has been developed. The evaluation of time scales is made at fixed and equally spaced time values, which subdivide the total time interval into a number of subcycles. These internal integration steps have been named 'sampling' intervals, as - at each of them - the characteristic time scales of the species are evaluated according to Eq. 2.27. Within each of these intervals, the initial value problem is completely defined, and each evolving species is integrated according to its characteristic time:

$$h_i = 10^{\text{int}\{\log_{10}(\tau_i)+1\}}. \tag{2.29}$$

The relationship thus involves all the species which timescale is at least of one order of magnitude less than the current time, and which are expected to have already completed their time evolution. The procedure shown in Figure 2.13 also shows that, within each sample interval, any ODE integrator may be fit, as the procedure is general, and the advancement in time is ruled by relative and absolute accuracy constraints, which either can be part

of the integrator itself, or can be set through an external routine. In particular, the explicit, second-order IE integrator scheme has been implemented according to (140). The procedure considers that a first, simple Euler integration is performed over the current timestep h:

$$\tilde{\mathbf{y}}(t+h) = \mathbf{y}(t) + h\mathbf{f}\big(t, \mathbf{y}(t)\big); \tag{2.30}$$

then, the first order solution is updated and improved by adopting the trapezoidal rule, through a second evaluation of the ODE function:

$$\mathbf{y}(t+h) = \mathbf{y}(t) + \frac{h}{2}\left[\mathbf{f}\big(t, \mathbf{y}(t)\big) + \mathbf{f}\big(t+h, \tilde{\mathbf{y}}(t+h)\big)\right]. \tag{2.31}$$

The explicit Runge-Kutta algorithm is instead one of the most reliable and less computationally expensive one-step methods, as it gets increased accuracy order on the evaluation of the function $\mathbf{f}$ at many points in the neighborhood of the starting point $\big(t, \mathbf{y}\big)$, instead than evaluating higher-order derivatives. In particular, the Runge-Kutta-Fehlberg variant (RKF-45) (141) yields $O(h^5)$ accuracy:

$$\mathbf{y}(t+h) = \mathbf{y}(t) + h\sum_{i=1}^{s} b_i \mathbf{k_i}, \tag{2.32}$$

with

$$\begin{cases} \mathbf{k_1} = & \mathbf{f}\big(t, \mathbf{y}(t)\big) \\ \mathbf{k_2} = & \mathbf{f}\big(t + c_2 h, \mathbf{y}(t) + a_{21} h\mathbf{k_1}\big) \\ \mathbf{k_3} = & \mathbf{f}\big(t + c_3 h, \mathbf{y}(t) + a_{31} h\mathbf{k_1} + a_{32} h\mathbf{k_2}\big) \\ \vdots & \\ \mathbf{k_{s-1}} = & \mathbf{f}\big(t + c_{s-1} h, \mathbf{y}(t) + a_{s-1,1} h\mathbf{k_1} + a_{s-1,2} h\mathbf{k_2} + \ldots + a_{s-1,s-2} h\mathbf{k_{s-2}}\big) \\ \mathbf{k_s} = & \mathbf{f}\big(t + c_s h, \mathbf{y}(t) + a_{s1} h\mathbf{k_1} + a_{s2} h\mathbf{k_2} + \ldots + a_{s,s-1} h\mathbf{k_{s-1}}\big) \end{cases}$$

where coefficients a_{ij}, b_i, c_i are specific of the RK method adopted. The set of coefficients proper to the RKF-45 solution, is reported in the following. As it can be seen, the main advantage of this method is that coefficients a_{ij} and c_i are common to both the 4^{th}-order and the 5^{th}-order accuracy solutions, thus allowing error control over the 4^{th}-order method to be estimated on the knowledge of the 5^{th} order one, with no need to further evaluations of the ODE system $\mathbf{f}$.

Error estimation and step size control. Having an efficient estimate of the local error is mandatory for the integration of any ODE system, as the knowledge of the global error would be possible only in case the integration would be repeated with different step sizes,

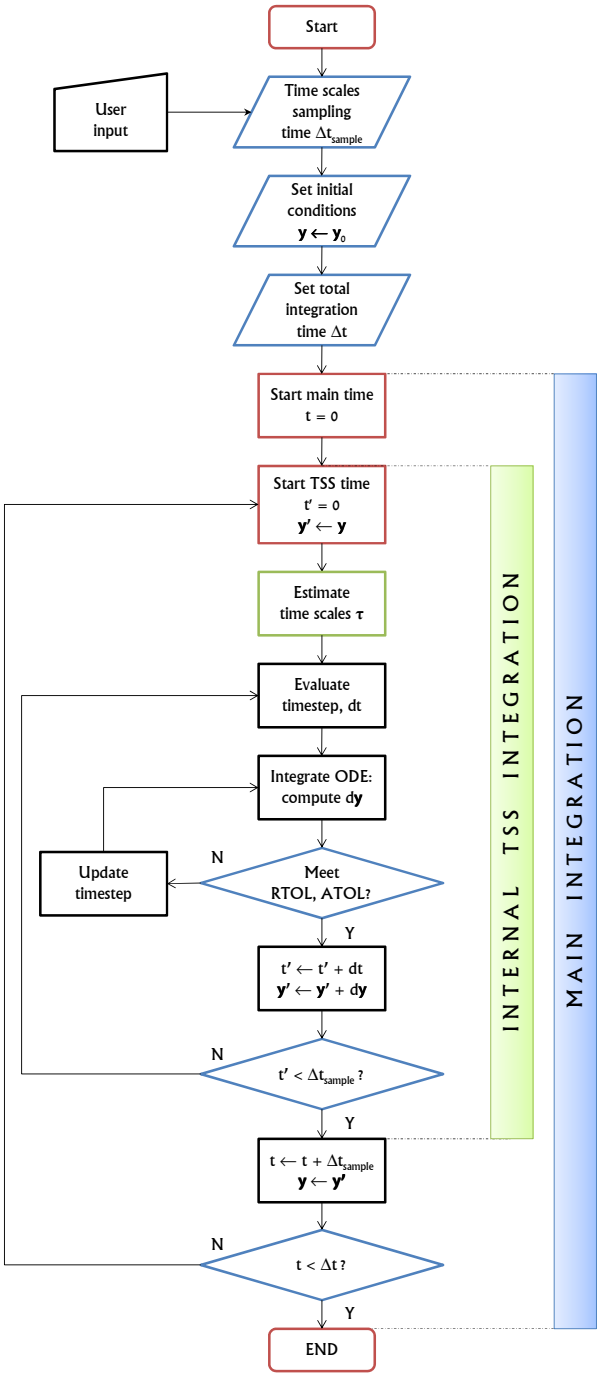

Figure 2.13: Flowchart showing ODE integration through time scale separation method at fixed sampling interval, Δt_{sample}.

c_1						
c_2	a_{21}					
c_3	a_{31}	a_{32}				
c_4	a_{41}	a_{42}	a_{43}			
c_5	a_{51}	a_{52}	a_{53}	a_{54}		
c_6	a_{61}	a_{62}	a_{63}	a_{64}	a_{65}	
	b_1	b_2	b_3	b_4	b_5	b_6
	b'_1	b'_2	b'_3	b'_4	b'_5	b'_6

0						
1/4	1/4					
3/8	3/32	9/32				
12/13	1932/2197	−7200/2197	7296/2197			
1	439/216	−8	3680/513	−845/4104		
1/2	−8/27	2	−3544/2565	1859/4104	−11/40	
	25/216	0	1408/2565	2197/4104	−1/5	0
	16/135	0	6656/12825	28561/56430	−9/50	2/55

Table 2.2: Tables of coefficients of the Runge-Kutta-Fehlberg method.

so that it may be estimated by comparison between the two solutions. As this is not possible when integrating computationally expensive problems, the error control issue is usually addressed by comparison of the same solution, at each integration step, with methods which own different accuracy orders (142). Assuming that the higher-order solution is more accurate, the tentative integration step made by the low-accuracy solver gives an efficient estimate of the local error, and thus can be compared to the relative and absolute accuracy constraints set by the user. In the present work, the local error is estimated according to this rule. In particular, the 2^{nd}-order solution in the IE method and the 5^{th}-order one in the RKF-45 method are considered as the 'exact' solutions ($\mathbf{y}$), to be kept for the next integration timestep, while the lower-order methods produce the relative tentative, error-affected solution ($\tilde{\mathbf{y}}$); so, the estimate of local error array le is computed as follows (143):

$$\mathbf{le}(t+h) = \left|\mathbf{y}(t+h) - \tilde{\mathbf{y}}(t+h)\right|, \tag{2.33}$$

and the accuracy constraint is assumed to be met when the following relationship is verified:

$$eest(t+h) = \sqrt{\frac{1}{n}\sum_{i=1}^{n}\left(\frac{le_i}{tol_i}\right)} < 1, \tag{2.34}$$

where $\mathbf{tol} = RTOL + ATOL \cdot \left|\mathbf{y}(t+h)\right|$ is adopted as an estimator of the overall error tolerance on the current values of the unknowns. The overall error estimator $eest$ is then adopted when computing the tentative size for the next integration step:

$$h' = h \cdot \min\left\{1.5, \max\left(0.1, \frac{0.95}{\sqrt[p+1]{eest}}\right)\right\}, \tag{2.35}$$

where p indicates the accuracy order of the integration method.

2.4.1.3 Accuracy of the TSS solver.

Apart from the error tolerance constraints, which are problem-dependent, accuracy of the time integration depends on the two introduced approximations, without whose the TSS solver reduces to a standard explicit ODE solver. This is of particular importance, as practical I.C. engine simulation usually have larger base timesteps (of the order of 10^{-5} s) during the compression and expansion strokes, while they become pretty smaller (up to about 10^{-8}) when combustion and spray phenomena interact within the combustion chamber. For these reasons, a full validation of the TSS solver has been carried out considering zero-dimensional combustion within constant pressure environment, and compared with the VODE solver in terms of both predicted temperature and species concentration profiles. In order to have an overview of the accuracy of the TSS solver, two mechanisms relevant to internal combustion engine simulations have been considered: the ERC n-Heptane mechanism, consisting of 29 species and 59 reactions (144), and a reduced Ethanol combustion mechanism, consisting of 30 species and 155 reactions, derived from the detailed one developed at LLNL (4). For each of the two mechanisms, a matrix of simulations, with different initial conditions and integration time intervals has been setup.

As mentioned, the accuracy of the TSS solver depends on two parameters: the choice of the sampling timestep for the evaluation of the species characteristic timescales, and the threshold for the reaction equilibrium assumption. As the interaction between these two sources of error is expected to be nonlinear, and their ranges cover different orders of magnitude, a rigorous procedure has been developed. In particular, a merit function has been

developed in order to compare the TSS solution with the VODE solver, at the same tolerance constraints (RTOL = 1.0e-4, ATOL = 1.0e-13):

$$f\left(\Delta t_{\text{sample}}, C_\tau\right) = -\log\left\{10^{-8} + \sum_{j=1}^{n_c}\left[\sum_{k=1}^{n_s}\int_{\tau=0}^{\tau=t_j}\frac{\left|X_{jk}^{VODE}(\tau) - X_{jk}^{TSS}(\tau)\right|}{X_{jk}^{VODE}(\tau)}d\tau + \right.\right. \tag{2.36}$$
$$\left.\left. + \int_{\tau=0}^{\tau=t_j}\frac{\left|T_j^{VODE}(\tau) - T_j^{TSS}(\tau)\right|}{T_j^{VODE}(\tau)}d\tau\right]\right\}.$$

According to this formulation, the total integration time t_j is considered for the point-by-point accuracy evaluation of the TSS solver, at each of the n_c cases considered in the simulation matrix. Thus, the merit function produces a value which isn't averaged, but considers the instantaneous behaviour of the solver. Furthermore, both species concentrations and system temperature are included, so that merit is evaluated with respect to both the thermal and the reactive characteristics of the mechanism, as low temperature chemistry is of fundamental importance for the correct prediction of ignition within internal combustion engines.

Then, the merit function has been evaluated over a matrix of 28 solver conditions, spanning the ranges defined in terms of $\Delta t_{sample} = \left\{10^{-5}; 10^{-6}; 10^{-7}; 10^{-8}\right\}$ and $C_\tau = \{10^{0}; 10^{-1}; 10^{-2}; 10^{-5}; 10^{-10}; 10^{-15}; 10^{-20}\}$, and merit landscapes have been computed through ordinary kriging. This procedure has been chosen due to its proven reliability in reconstructing complex response surfaces (145; 146; 147). A similar procedure has been applied also to the analysis of the CPU time requirements of the TSS solver: at the same calculations, the speedup due to the adoption of time scale separation has been computed, in comparison to the requirements of the VODE solver, when run with the same Δt_{sample} bounds. The results of this analysis have been reported in Figures 2.14,2.15. A more detailed overview on the solutions as computed by the solvers at the different sampling time intervals is reported in Figures 2.16,2.17.

From the observation of the merit landscapes, it is pretty evident that the accuracy of the solution mainly depends on the sampling timestep value, and that a lower baseline interval leads to a more accurate solution. Furthermore, it appears that choosing a lower threshold value – thus increasing the residence time of the reactions near equilibrium – only partially affects the accuracy of the solution, and leads to sensible improvements only at very low C_τ values, below 10^{-15}. However, it appears that a correct choice of the equilibrium threshold significantly varies the overall CPU time needed for the integration. In particular, for the IE

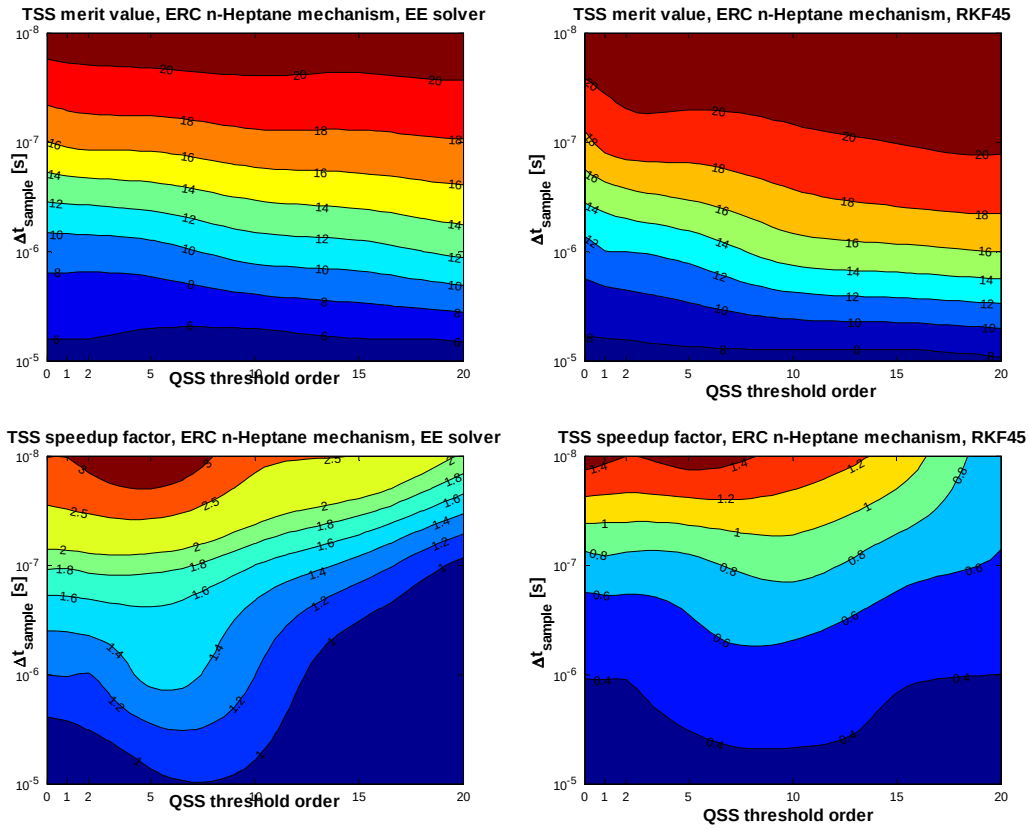

Figure 2.14: Merit and speedup landscapes for the ERC n-heptane mechanism. Left: improved Euler solver; right: RKF-45 solver.

solver, a considerable speedup with respect to VODE is observed for threshold values greater than 10^{-5}. This is particularly true for the ERC n-heptane mechanism, where the choice of that threshold value is mandatory in order to have a benefit at the larger sampling time intervals. Furthermore, it can be observed that the improvement in CPU times is much more significant for the larger, Ethanol mechanism, being in the range of 15 – 40 times, while the improvement measured at the ERC mechanism ranges from unity up to about three times. The fact that the speedup increases as smaller the sampling interval, is of particular relevance to engine simulations. In the KIVA code, for instance, the baseline timestep is chosen as the lowest one, ruled by phenomena such as fluid flow, combustion (heat release), spray development, evaporation, etc. The capability of the TSS solver to have better performance

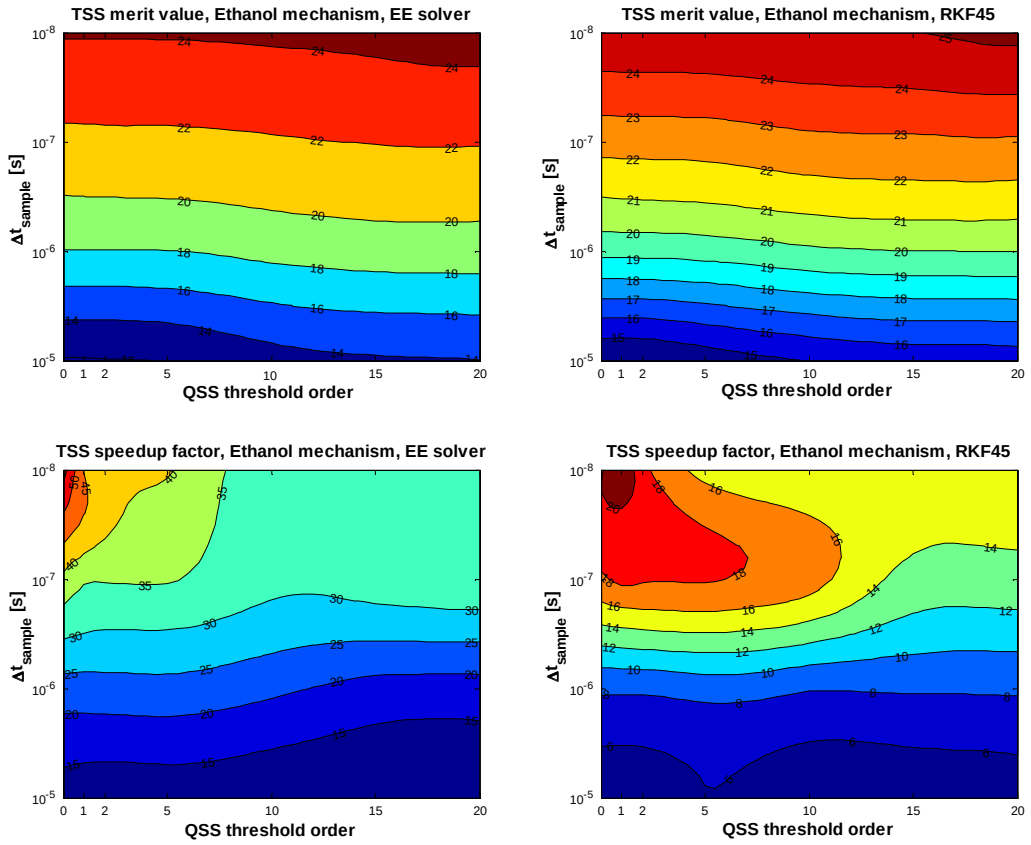

Figure 2.15: Merit and speedup landscapes for the Ethanol mechanism. Left: improved Euler solver; right: RKF-45 solver.

at low timestep values can thus improve the CFD code performance also when the computation implies a baseline integration timestep smaller than one microsecond.

As far as the RKF45 solution is concerned, the landscapes show that the higher accuracy order leads to more accurate results than the explicit Euler solver, if compared at the same sampling interval value. However, the major drawback of this better behavior is a significantly lower speedup factor. In particular, maximum speedups ranged up to 20 for the Ethanol mechanism, and up to 1.4 times for the ERC mechanism. The average speedups were thus between two and three times lower than the corresponding values obtained using the explicit Euler solver. Furthermore, it can be observed that the RKF45 solver isn't competitive with respect to the VODE at the larger timesteps, and it shows to be slower than it

at a broad area of the landscape for the ERC mechanism. For all of these reasons it has been chosen to couple the KIVA-4 code with the TSS explicit Euler solver, which granted greater speedup factors than the RKF45 at similar accuracy values. Lastly, it is worthwhile to point out that the landscapes don't indicate a unique value of C_τ to be the best choice for the integration with the TSS solver. However, both the speedup and merit behaviors of the solution appeared to be pretty consistent across the two mechanisms considered. In particular, their values at C_τ around 10^{-5} appeared to be the best trade-off between speed and accuracy, even if the landscapes themselves suggest that no threshold should be adopted at sampling timesteps lower than 10^{-7} seconds.

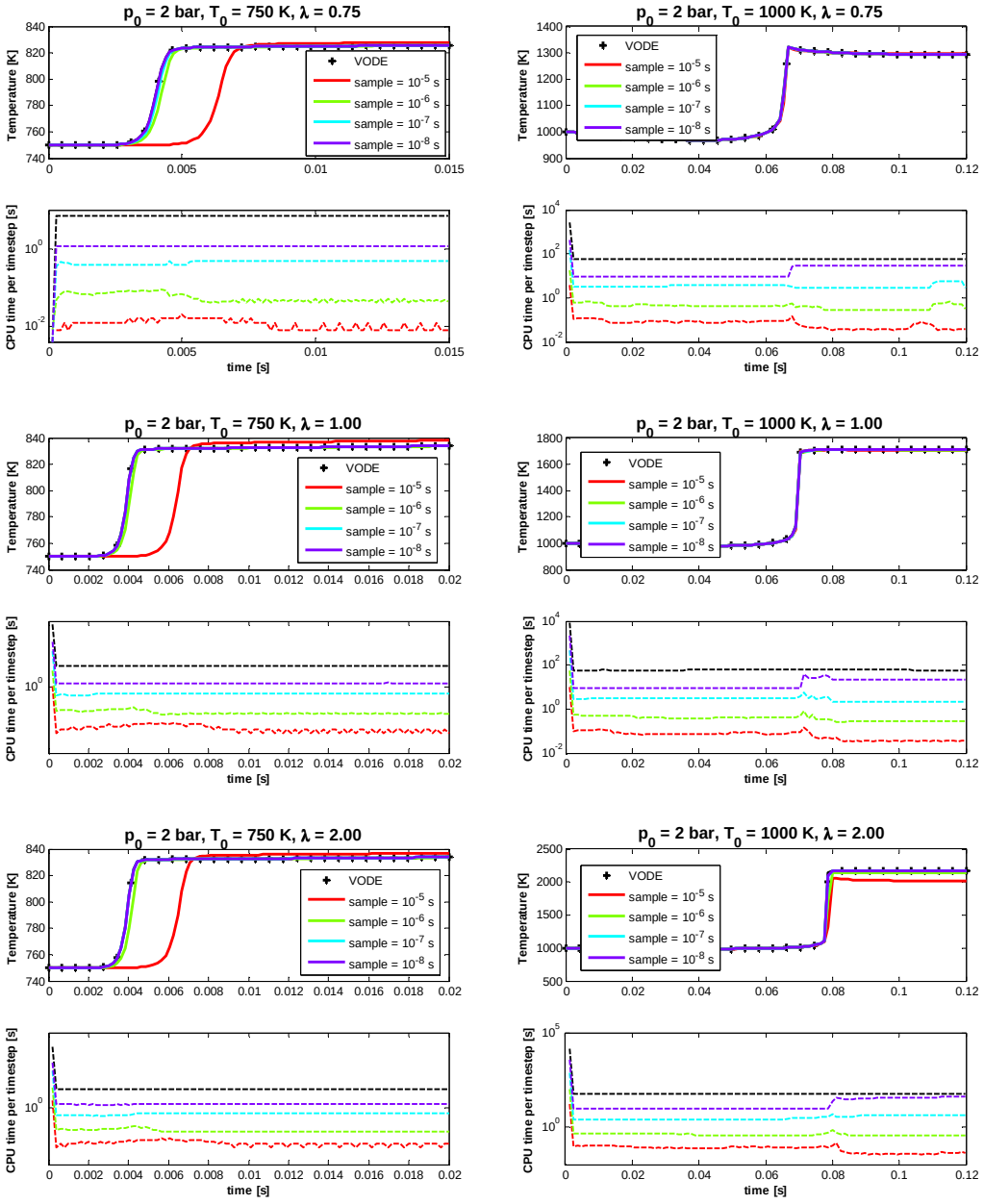

Figure 2.16: Accuracy and time behaviour of the TSS solver in comparison with VODE: ERC n-heptane mechanism.

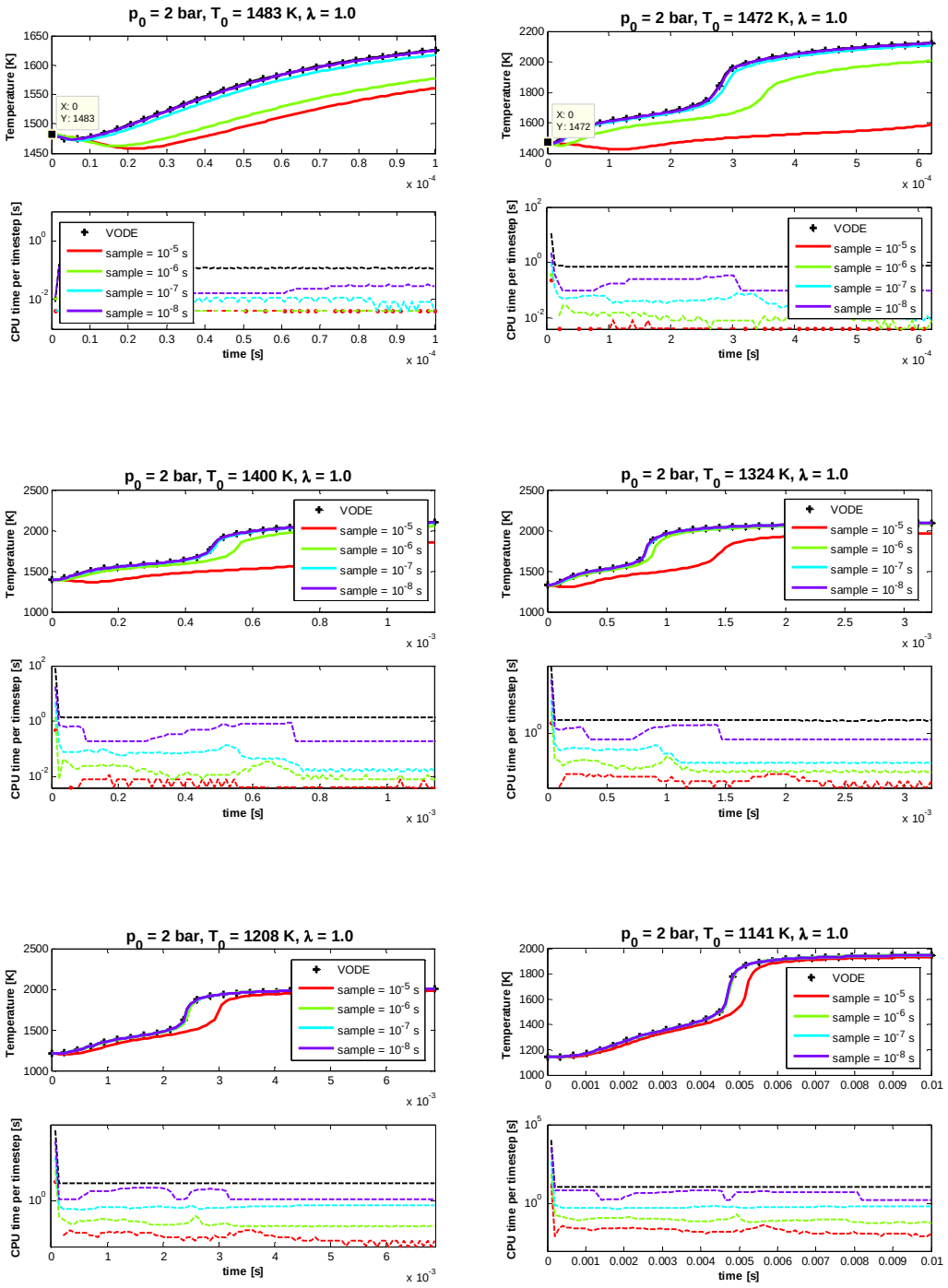

Figure 2.17: Accuracy and time behaviour of the TSS solver in comparison with VODE: Ethanol mechanism.

2.5 Multidimensional modelling through a revised KIVA-4

KIVA-4 (109) is the latest development of the family of KIVA codes (107; 148; 149), coded since the 1980's for the CFD simulation of internal combustion engines. Major improvements have been introduced in the current version of the KIVA code mainly in terms of numerical aspects, while most of the physical submodels coupled to the CFD approach have been inherited from the previous releases. From the point of view of physical modelling, the most important improvement available in the KIVA-4 code is the implementation of multicomponent spray management, which allows spray properties to be evaluated as a function of the composition of the liquid fuel which is injected into the combustion chamber, or simulating internal combustion engines fueled by various fuel blends (150; 151). From the numerical point of view, much effort has been devoted to modifying the code's structure into a more flexible FORTRAN 90 implementation relying on modules which should make further attempts easier for code parallelisation. Furthermore, the code is now capable to manage unstructured grids, this enabling full internal combustion engine simulations to be carried out with greater flexibility, and allowing to achieve better grid quality. There is growing literature about these last issues related to the code; please, refer to (152; 153; 154) for partitioning strategies and parallel implementations, and (155) is a most recent example showing the effectiveness of the code, when adopted for a full-cycle long simulation of a direct injected diesel engine of current production.

For these reasons, it's clear that the KIVA-4 code appeared to be the most interesting choice for the purpose of developing an efficient tool for multidimensional engine simulations: it provided a robust background in terms of both numerical algorithms and physical models, it is an open source code, and it is currently undergoing many research efforts.

2.5.1 Governing equations

As most CFD codes, KIVA-4 solves a set of conservation equations over a 3D domain, subdivided into a finite number of volumes (cells). The following conservation equations are solved in integral form over each cell in the domain:

- Mass conservation for species i:

$$\frac{D}{Dt}\int_V \rho_i dV = \int_S \left[\rho D \nabla\left(\frac{\rho}{\rho_i}\right)\right] d\boldsymbol{A} + \int_V \dot{\rho}_i^{chem} dV + \int_V \dot{\rho}_i^{spray} dV \qquad (2.37)$$

where ρ_i denotes the density of species i, $\dot{\rho}_i^{spray}$ and $\dot{\rho}_i^{chem}$ the source terms due to spray evaporation and chemical reactions, $\boldsymbol{A}$ the cell face area vector. When all the chemical species are solved, the following global mass conservation equation is automatically satisfied:

$$\frac{D}{Dt}\int_V \rho\, dV = \int_V \dot{\rho}^{spray}\, dV.$$

- Momentum conservation:

$$\frac{D}{Dt}\int_V \rho \boldsymbol{u}\, dV = -\int_S \left[\frac{p}{a^2} + \frac{2}{3}A_0\rho k\right] d\boldsymbol{A} + \int_S \boldsymbol{\sigma}\cdot d\boldsymbol{A} + \int_V \boldsymbol{F}^{spray}\, dV + \int_V \rho \boldsymbol{g}\, dV; \tag{2.38}$$

where a represent the pressure gradient scaling parameter, normally equal to 1, $A_0 \in \{0,1\}$ a switch to turn on/off turbulence modeling, k the turbulent kinetic energy per mass unit, $\boldsymbol{\sigma}$ the viscous stress tensor, and $\boldsymbol{F}^{spray}$ the spray momentum transfer term.

- Energy conservation:

$$\frac{D}{Dt}\int_V \rho I\, dV = -\int_V p\nabla\cdot\boldsymbol{u}\, dV + \int_V (1-A_0)\,\boldsymbol{\sigma}:\nabla\boldsymbol{u}\, dV + \int_S \left[K\nabla T + \rho D\sum_m h_m \nabla\left(\frac{\rho_m}{\rho}\right)\right] d\boldsymbol{A} + \int_V A_0\rho\epsilon\, dV + \int_V \dot{Q}^{spray}\, dV + \int_V \dot{Q}^{chem}\, dV; \tag{2.39}$$

where K represents the thermal conductivity coefficient, D Fick's law gas mass diffusion coefficient, h_m the specific enthalpy of species m, ϵ the turbulent dissipation rate, and $\dot{Q}^{spray}$ and $\dot{Q}^{chem}$ the heat source terms due to spray evaporation and chemical reactions.

As well as the turbulent flow representation in KIVA-4 is concerned, a canonical RNG $k-\epsilon$ model is implemented which accounts for turbulence over the RANS approach:

$$\frac{D}{Dt}\int_V \rho k\, dV = -\int_V \frac{2}{3}\rho k\nabla\cdot\boldsymbol{u}\, dV + \int_V \boldsymbol{\sigma}:\nabla\boldsymbol{u}\, dV + \int_S \left[\left(\frac{\mu}{Pr_k}\right)\nabla k\right] d\boldsymbol{A} - \int_V \rho\epsilon\, dV + \int_V \dot{W}^{spray}\, dV; \tag{2.40}$$

$$\frac{D}{Dt}\int_V \rho\epsilon\, dV = -\int_V \left(\frac{2}{3}c_{\epsilon_1} - c_{\epsilon_3}\right)\rho\epsilon\nabla\cdot\boldsymbol{u}\, dV + \int_S \left[\left(\frac{\mu}{Pr_\epsilon}\right)\nabla\epsilon\right] d\boldsymbol{A} + \int_V \frac{\epsilon}{k}\left[c_{\epsilon_1}\boldsymbol{\sigma}:\nabla\boldsymbol{u} - c_{\epsilon_2}\rho\epsilon + c_s\dot{W}^{spray}\right] dV. \tag{2.41}$$

2.5.2 Integration of the chemistry code into KIVA4

Most of the approaches for coupling KIVA to detailed chemistry (see, for example, (156)) only interface the chemistry solver to the CFD code at few points: chemistry is seen by the code only as a thermal source term, which models the enthalpy released during the reactions within each cell of the computational grid, plus the main reactive species are updated into the code (usually, not more than a dozen). All the pieces of information due to chemistry are instead stored separately, and can be accessed only by the chemistry solver. This approach isn't able to manage complex interactions between chemistry and physics, especially when dealing with multi-component fuels. For this reason, the approach developed aims at fully coupling the detailed chemistry solver with KIVA-4, in terms of the following properties:

1. **species management**: both KIVA-4 and the chemistry solver need to manage the same set of species. A unique indexing array for the species allows easy transfer of information between the CFD and the chemistry solver; furthermore, any error introduced by missing conservation of mass, arising from the need to update the condentrations of some of the species, can be avoided. This approach also allows management of multi-component fuel spray modelling not to be affected by chemistry;

2. **thermophysical properties**: a unique framework for the computation of the species' thermophysical properties is enough for the modelling of the gaseous mixture within each cell. Thus, the KIVA `datahk` database, which contains 51 enthalpy values for each of the species, in the range $[100K, 5100K]$, needs to be created for each simulation, fitting the enthalpy values as computed through information from the NASA polynomials;

3. **chemistry solution**: chemistry within each cell of the computational grid is solved independently, i.e. each cell is treated as a closed thermodynamic system when computing its evolution. In particular, every cell is modeled as a closed, adiabatic, constant volume reactor. The change in species densities due to chemistry is accordingly modified prior to the computation of momentum balances due to fluid dynamics.

Figure 2.18 summarizes the procedure which is followed in the current code implementation, prior to launching a KIVA-4 simulation. The two files which define the reaction mechanism and the thermodynamic database are needed for creating the input files needed

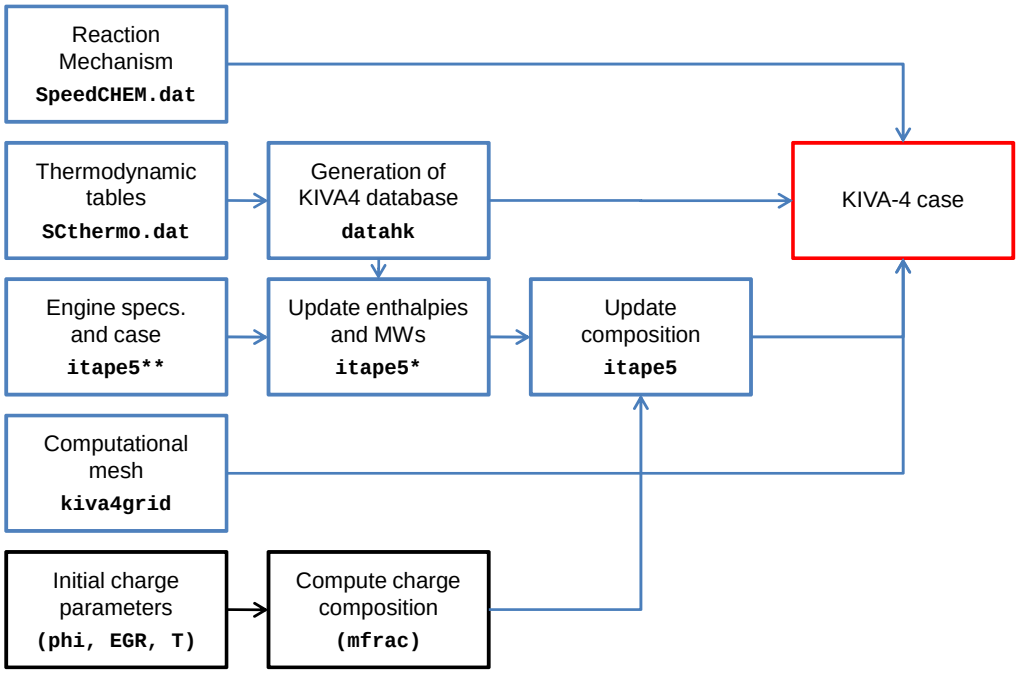

Figure 2.18: Steps for creating a KIVA-4 case with detailed chemistry

by the KIVA calculation: the `datahk` database only depends on the set of species which takes part in the reacting system; the same observation can be made for the pieces of information regarding the species which need to be defined into the `itape5` input file. In this regard, it is worth to mention that the structure of the KIVA-4 code needs the species set to follow a fixed order: the first `nspl` species define the liquid fuel components, and species ranging from index `nspl+1` to `nsp` are gaseous only. So, a prior pre-processing effort is needed when dealing with liquid fuels: the species in the reaction mechanism need to be previously sorted according to this order. Furthermore, KIVA needs species in the liquid species set to be also present in the database of thermophysical properties of liquids, contained in the `fuelib.f` file.

2.5.3 Code validation.

In order to provide evidence of the effectiveness of the new code, two relevant engine cases have been chosen. A first one consists of an HCCI-operated engine: in this case, combustion is kinetically-controlled (157), and the accuracy of the results is mainly due to the reaction mechanism adopted for the simulation. A second one consists of a direct-injected

diesel combustion case, dealing with an engine of current production, manufactured by VM Motori. This case is more complex, as chemical kinetics interact with spray dynamics, breakup and evaporation, as well as turbulent mixing. In this case, direct integration of the combustion chemistry within each cell, treated as a well-stirred reactor, simplifies the physical description of the model, as the turbulence-chemistry interaction is neglected at the subgrid-scale; for this reason, models have been developed which account for the interaction also within the reactor itself; among them, the partially-stirred reactor considers a segregation factor which introduces the effect of mixing onto the combustion development within the cell (158). However, direct integration of the reacting system has been demonstrated to produce equally accurate results (159).

2.5.3.1 2D HCCI engine modelling

In order to test and validate the accuracy of the KIVA-4 code with detailed chemistry solver, simulations were run on the same HCCI operated CFR engine cases already considered when testing the zero-dimensional engine model. A two-dimensional computational mesh was developed, consisting of 1350 cells at BDC. The simulations of the closed-valve part of the engine cycle featured the use of the common RNG k-ε turbulence model; crevice volumes weren't modeled and turbulent mixing effects were neglected. Temperatures of the cylinder liner, of the piston surface and of the head were set uniform and constant at 450K. The results of the simulations are reported in figure 2.20, in comparison with experimental data, featuring three different compression ratio engine settings: even if the predicted average in-cylinder curves slightly overestimate the experimental pressure value especially around TDC, this is usually accepted as no crevice volumes, neither blow-by to the crankcase are modeled. As far as the ignition timings are concerned, an excellent agreement is noticed. Figure 2.19 shows the in-cylinder temperature plots for the $CR = 11.0$ case around TDC.

2.5.3.2 Modeling of a DI diesel engine

In order to provide evidence of the reliability and of the computational efficiency of the code, its performances have been tested through modelling of a 2.8l, direct injected diesel engine of current production, manufactured by VM Motori. The main engine specifications are listed in Table 2.3. Computations were carried out adopting a 60 degrees sector

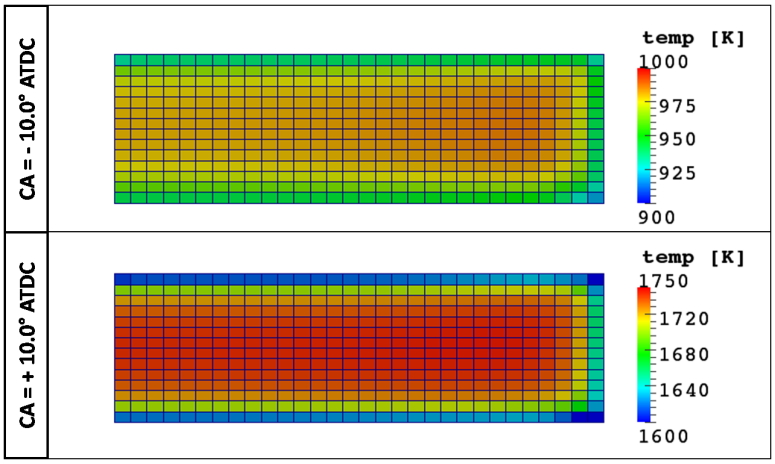

Figure 2.19: Predicted temperature plots for the CFR engine considered, $CR = 11.0$, $n = 900rpm$, $\phi = 0.25$. The mesh is a 2-dimensional sector with 0.5 degrees angle of revolution; cylinder symmetry axis on the left side.

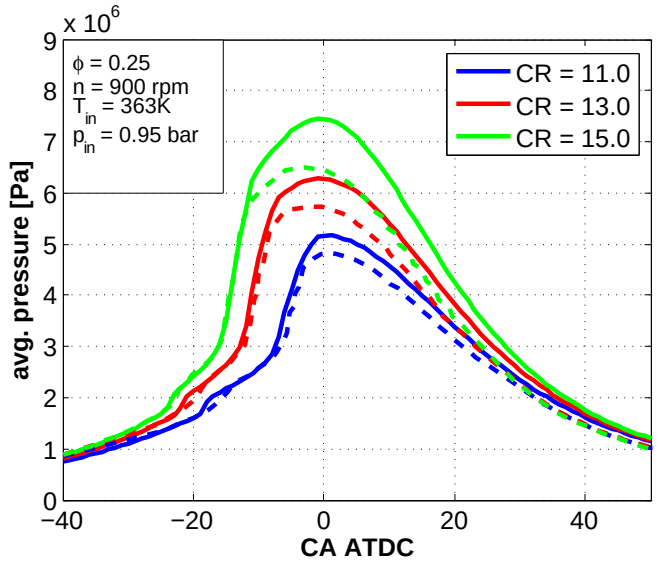

Figure 2.20: Experimental and numerical in-cylinder pressure curves for an HCCI CFR engine (6), at compression ratio values $CR = 11.0, 13.0, 15.0$, equivalence ratio $\phi = 0.25$, engine speed $n = 900rpm$. Experimental vs. KIVA-4 calculation comparison; LLNL n-Heptane combustion mechanism.

Engine model	VM Motori	CFR
Engine operation	4-S DI	HCCI
Number of cylinders	4	1
Total displacement (cm^3)	2776	612.0
Bore (mm)	94.0	82.54
Stroke (mm)	100.0	254.0
Compression ratio	17.5:1	var.
Valves per cylinder	4	2
Injection system	common-rail	-
Max. injection pressure (MPa)	160	-
Injector hole diameter (mm)	0.153	-
Number of injector holes	6	-

Table 2.3: Engine specifications for the two validation cases.

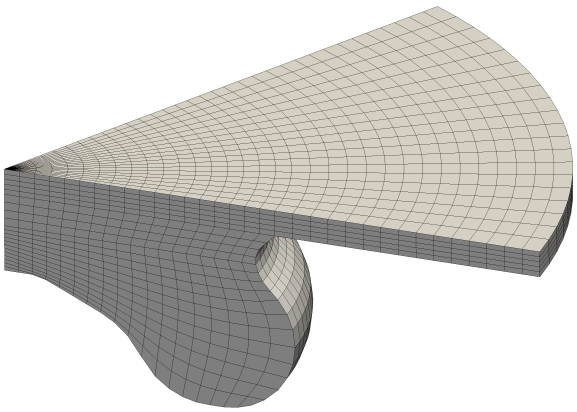

Figure 2.21: Computational mesh adopted for the 2.8l VM Motori engine, at top dead centre. Total number of cells: 28860; total number of vertexes: 31048.

mesh, consisting of 28860 cells; a representation of the mesh appearance at TDC is given in Figure 2.21. Validation was carried out against experimental in-cylinder average pressure traces at a total of six operating conditions, at both full and 50% load. At these conditions, injection strategies featured both single and multiple (two or three pulses) injections, depending on the engine speed and load; for the sake of reference, the injection profiles are reported together with the pressure traces. Estimates of the rates of heat release, which have been reconstructed from pressure data exploiting the well established Rassweiler and Withrow technique (160), have been included. Diesel combustion has been modeled adopting a widely adoptely and previously validated mechanism, developed at the ERC, for n-heptane combustion, consisting of 29 species and 52 reactions (144), while the thermophysical properties of European diesel #2 have been adopted for representing the fuel as a single component. Actual intake mixtures featured recirculated gas fractions ranging from 6% up to 25%; for this reason, an iterative procedure was developed for estimating the intake charge composition for each operating condition. In particular, the intake charge is considered a mixture of recirculated combustion products, and fresh charge, assumed to be standard air. At each of the iterations of the procedure, the reacting mixture composition is computed summing the in-cylinder charge with an amount of fuel vapour equal to the total injected fuel mass; then, its adiabatic flame temperature is estimated according to the algorithm proposed by Warnatz (113); finally, the combustion products composition is computed assuming species equilibrium at the adiabatic flame temperature value. Computation of species mass fractions at equilibrium is carried out through an implementation of the algorithm proposed by Pope (161). This final mixture composition is used as recirculated fraction to mix to the fresh charge into the intake mixture; then, the procedure is iterated until convergence of the species mass fractions.
The effects of this procedure are illustrated in Figure 2.22: the initial estimation of the species mass fractions has been observed to vary up to an order of magnitude prior to reaching convergence. Complete details on the algorithmic procedure have been reported in Appendix B.

The results of the simulations are illustrated in Figure 2.23, showing a good agreement between experimental and simulated in-cylinder pressure traces. In particular, matching of the predicted and measured pressures is particularly good especially at full load, while some discrepancies have been observed at partial load operating conditions, where a higher EGR fraction is present.

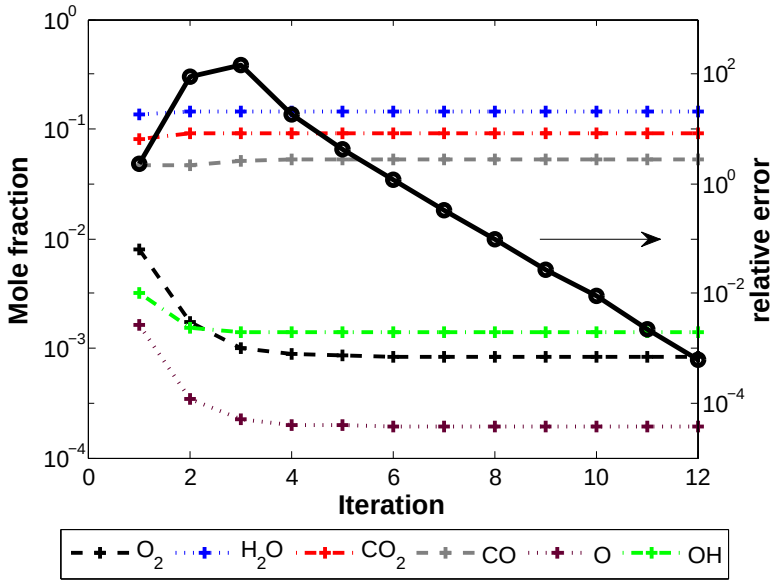

Figure 2.22: Evolution of species mass fractions estimation during the iterative procedure for computing intake mixture composition with recirculated combustion products.

2.5.4 Shared-memory code parallelisation

The addition of detailed chemistry significantly affects the code's computational requirements, as each cell of the physical domain has to be solved as an independent reactor. This leads to most of the CPU time being solved onto the solution of the detailed chemistry mechanism in each cell during CFD engine simulations. Apart from any other attempt to reduce the computational needs due to chemistry solution – included the object of the present work –, modern computers offer the opportunity of multithreaded computations, even on low-end machines. To this regard, the OpenMP shared-memory paradigm OpenMP paradigm (162; 163) is an interesting tool for the parallelisation of combustion chemistry in CFD codes such as KIVA-4. As a matter of fact, the chemistry solution phase within the code doesn't consider any interaction between the cells, as each of them is treated as an independent, closed, adiabatic reactor, and only the heat release and the change in mixture compositions due to chemistry are seen by the CFD code, as arises from Equations 2.39,2.37. Moreover, the efficiency of chemistry parallelisation within a shared-memory framework can be aided by the fact that the same mechanism is solved within each cell, and thus the same amount of information, about both species thermodynamic properties and the reac-

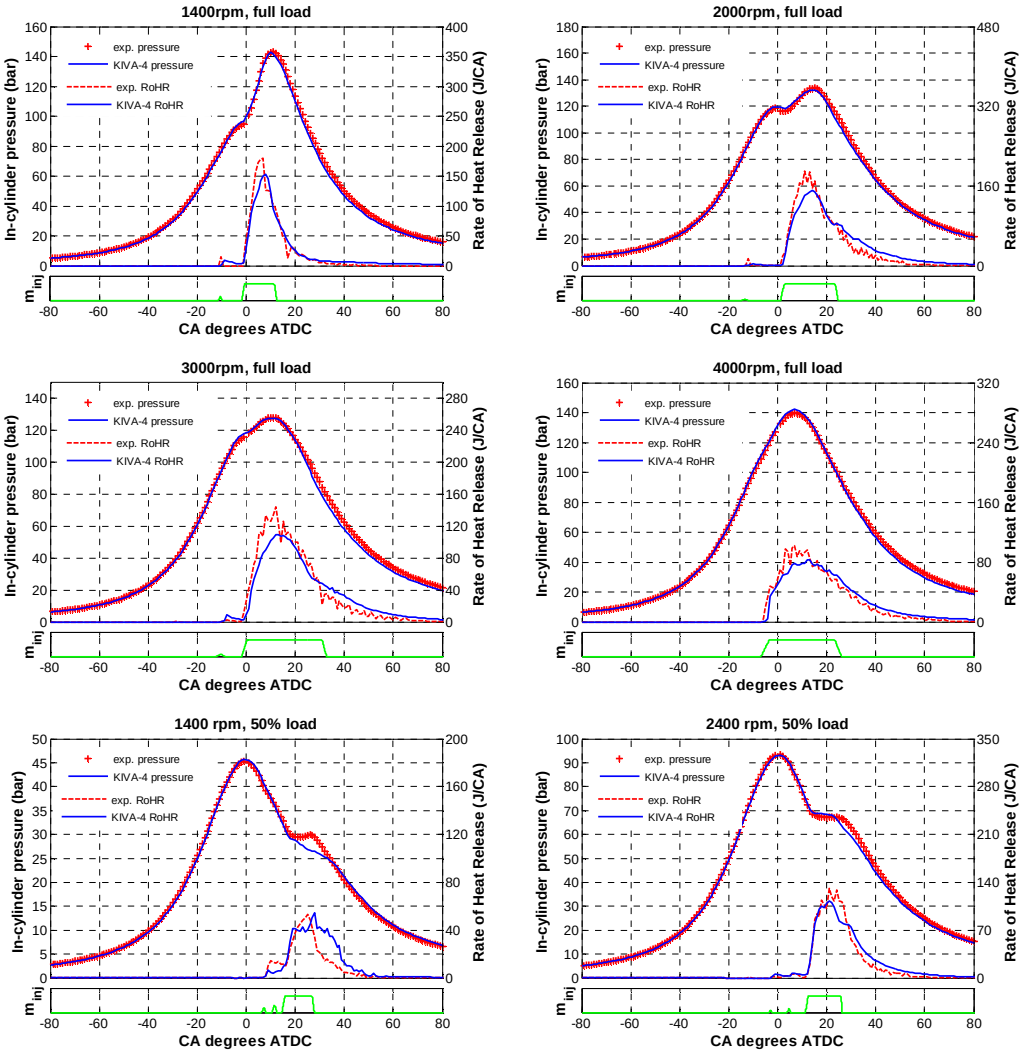

Figure 2.23: KIVA-4 modelling of 2.8l, direct injected diesel engine manufactured by VM Motori; engine specifications in Table 2.3. In-cylinder pressure experimental vs. numerical comparison: operating points are 1400, 2000, 3000 and 4000 rpm at full load; 1400 and 2400 rpm at 50% load.

tion database, is common to all cells in the computational mesh.
In comparison with the MPI approach, which relies on the communication among nodes (164), OpenMP is able to avoid the message passing bottleneck exploiting computers which have a multi-threaded architecture – such as most modern machines –, so that each of the threads is able to access the same memory with a uniform access time. Furthermore, most common pieces of information stored in memory do not need to be duplicated. This is particularly true in the present case: each cell owns its features in terms of species concentrations, temperature, pressure, etc., so, even if those pieces of information need to be updated during the calculation, they are stored in different places in memory, so that even separate threads can access and overwrite them without needing to duplicate any arrays.
A few variables need anyway to be duplicated, for example the working arrays of the DVODE solver, thus leading to some computational overhead when passing from a single thread to a multi-threaded computation.
The second, major advantage obtainable by adopting the OpenMP paradigm is the possibility to enable dynamic scheduling for the loops. In traditional MPI implementations, the computational domain needs to be subdivided *a priori* (see, for example, the METIS algorithm (165)); this usually leads to unbalanced loads over the CPUs, because the stiffness of the chemistry ODE systems can be very different across the regions of the domain (99); on the other hand, OpenMP offers the possibility to automatically distribute the computational burden across the threads, through analyzing the computational times needed by each of the packages sent to the CPUs. The user only needs to determine an appropriate size for the packages into which the main loop has to be subdivided, thus maximising the parallelisation efficiency. Finally, the loop-based syntax of the OpenMP paradigm allows the code chemistry parallelisation to be carried out without affecting the code structure, and can easily be extended to the other most time-consuming parts of the code.

Overall, even being the code parallelisation limited to the solution of the chemistry ODE sistem, it showed a computational time speedup by an average 2.8 times, when using four threads, on a two dimensional HCCI case. A more accurate analysis of the parallel performance of the code has been carried out concerning the full multidimensional case of diesel combustion described later.

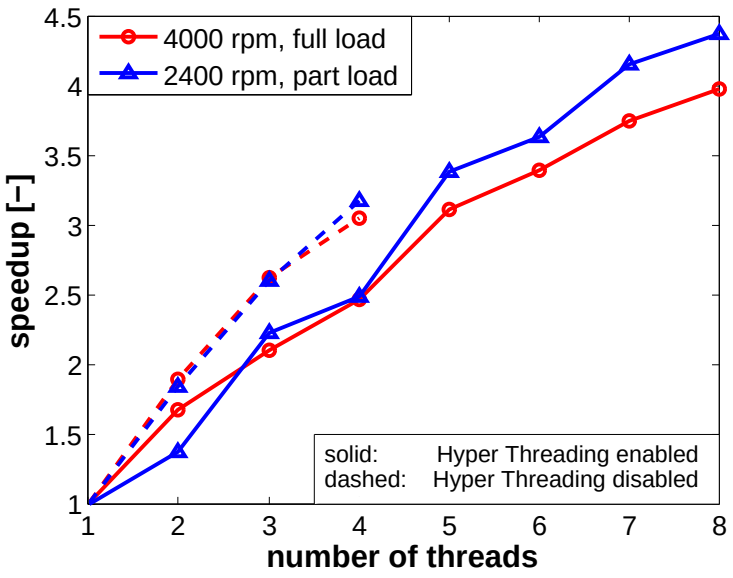

Figure 2.24: Parallelisation speedup for DI diesel engine modelling: comparison between a full-load and a partial-load operating conditions. Intel i7 920 processor (4 real CPU cores) running in either disabled (4 possible concurrent threads) or enabled (8 possible concurrent threads) Hyper Threading mode.

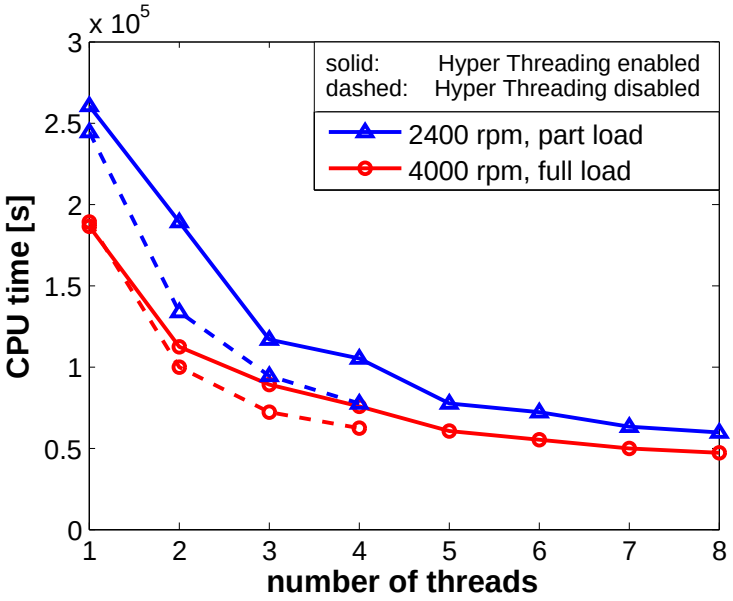

Figure 2.25: Parallelisation CPU times for DI diesel engine modelling: comparison between a full-load and a partial-load operating conditions.

2.5.5 Engine simulations with the TSS solver.

In order to assess the validity and the computational speedup allowed by the TSS solver on engine cases, the code has been coupled with the previously validated version of the parallel KIVA4-CHEM code. The solution of the chemistry ODE system using the DVODE solver within KIVA-4 has been substituted with the TSS solver for comparison. Two different engine cases have been setup: a first one about kinetics-driven combustion, considering a 2D HCCI case, featuring a research engine of Sandia Labs, running on ethanol. The details on the engine specifications and on the operative conditions related to the experimental in-cylinder pressure measurements are reported in ref. (9); the reaction mechanism developed in the current Thesis work, consisting of 33 species and 155 reactions, has been adopted; it is reported in appendix A.1. As a second case, the same set of simulations about direct injected diesel combustion as described in paragraph 2.5.3.2 have been considered for the comparison.

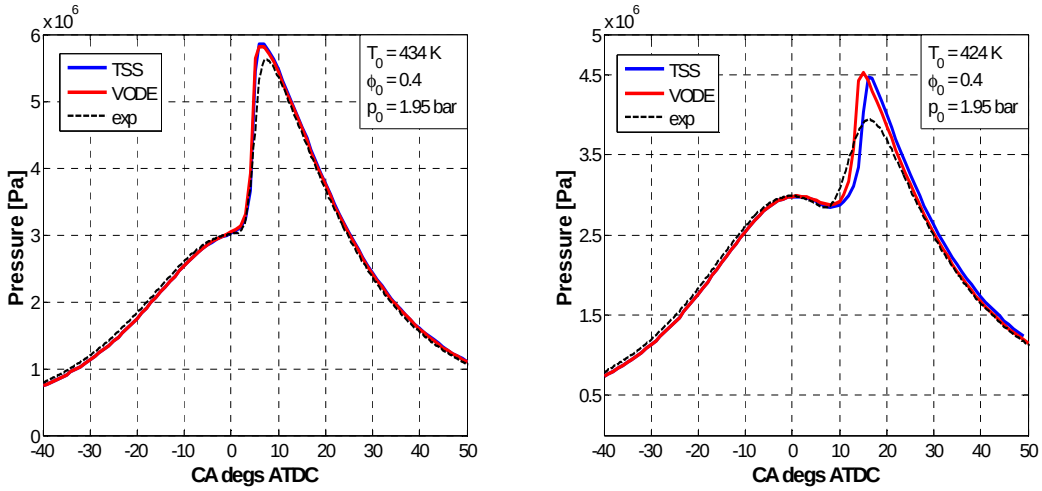

Figure 2.26: In-cylinder pressure comparisons for HCCI cases based on the Ethanol mechanism.

As far as the 2D HCCI cases are concerned, the comparison between experimental and predicted average in-cylinder pressures, for the two engine operating conditions for which experimental data were available, are reported in Figure 2.26. From the plots, it's clear that

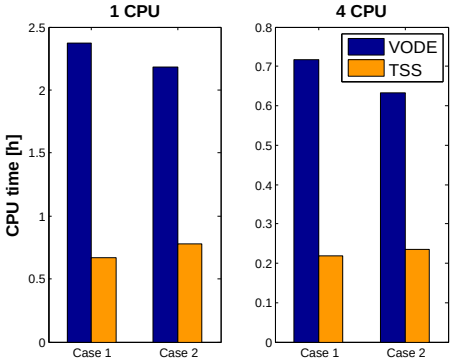

Figure 2.27: CPU times requirements for the Ethanol HCCI simulations: serial (1 CPU) and parallel (4 CPU) computation.

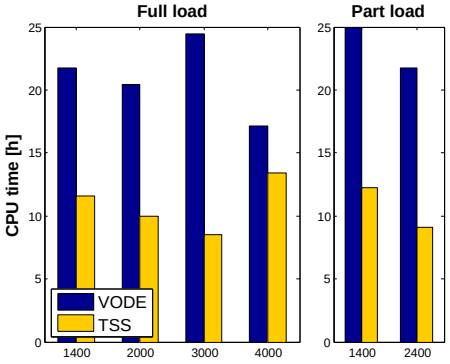

Figure 2.28: CPU times requirements for the DI Diesel simulations in parallel (4 CPU) computation.

– apart from the very good agreement allowed by the reaction mechanism at both operating conditions, excellent agreement was shown by the TSS solver in comparison with the DVODE. The detailed computational times required by the simulations, when either run in serial mode or in parallel onto 4 CPU cores, are instead reported in Figure 2.27. A strong reduction in CPU times was achieved through the TSS solver, which added up to 71% for the first case, and 64% for the second case. Once that the reliability and the computational efficiency of the solver were observed at the simplest, 2D case, more complex direct-injected diesel cases were run in order to assess the validity of this method also when the interaction among physical and chemical phenomena is strong. Thus, the same simulations as those run for the validation of the KIVA4-CHEM code were run adopting the TSS solver for chemistry. It has to be pointed out that the ERC mechanism for diesel combustion has about 2/3 less reactions than the ethanol mechanism, and, as observed in the speedup landscapes at Figures 2.14,2.15, the speedup was expected to be less significant. Moreover, in order to assure the accuracy of the solver at all the possible reactive conditions during the simulation, while still mantaining good computational efficiency, a threshold value $C_\tau = 10^{-5}$ and a sampling timestep $\Delta t_{\text{sample}} = 10^{-6} s$ have been chosen. The results of the simulations have been reported in Figure 2.29, where it is possible to notice the really good agreement between simulated and experimental in-cylinder pressure measurements at all engine cases. Again, the analysis of the computational speedup, reported in Figure 2.28, showed that the TSS solver was computationally efficient beyond the expectations, leading to overall reduc-

tions in total CPU time in the order of 47% up to 64%.

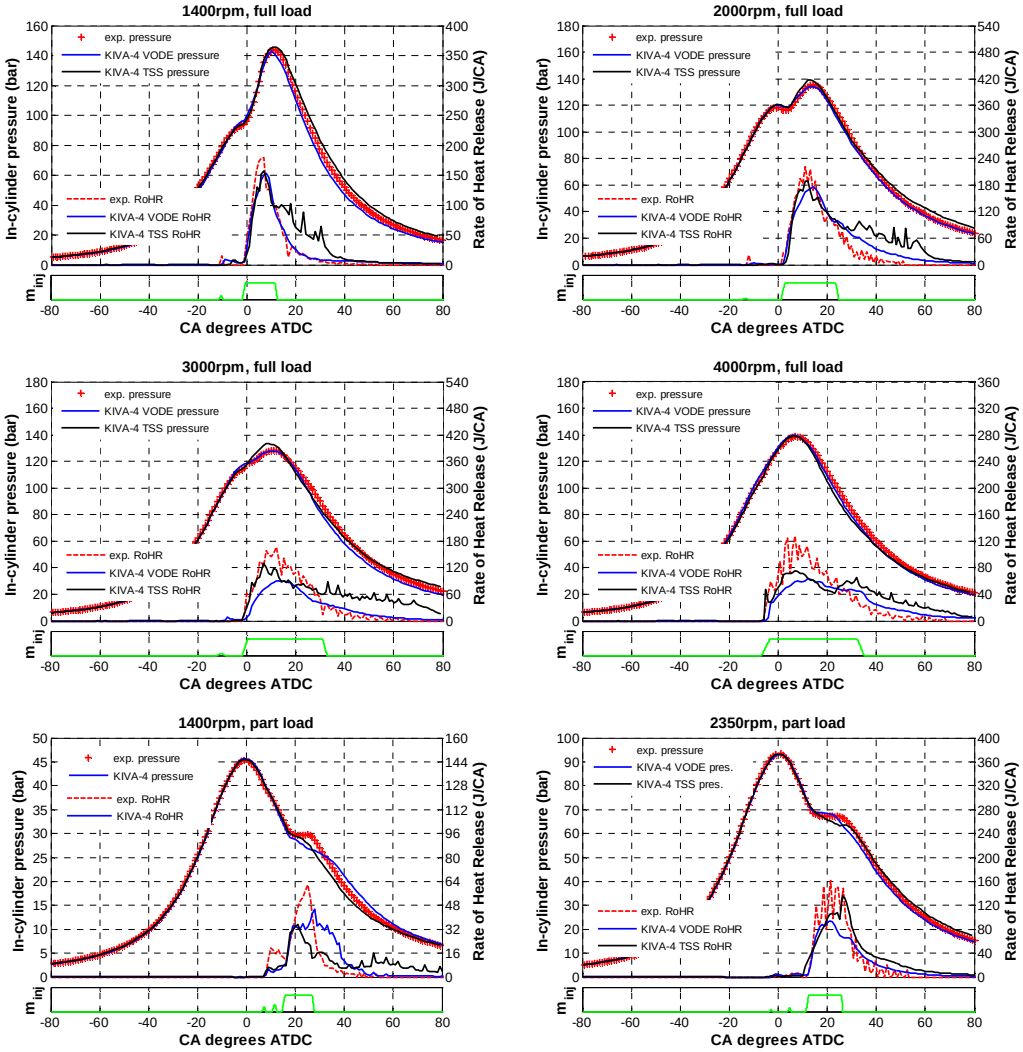

Figure 2.29: In-cylinder pressure comparisons for modeling of the 2.8l VM Motori engine.

3

Mechanism reduction and optimization

The need for complete understanding of the physics and chemistry of combustion phenomena, together with constant progress in computer technology, is currently driving research into adopting full or detailed reaction mechanisms in CFD computations (18; 39). A wide variety of mechanisms has been developed in recent years for hydrocarbon fuels consisting of tens to hundreds of species and hundreds to thousands of reactions (4; 5; 32; 43; 166; 167; 168; 169; 170). However, mechanism reduction is still mandatory for most practical computations, and research is very active in identifying techniques for obtaining accurate estimates of reaction kinetics with limited computational needs. In particular, a number of techniques have been developed for analyzing detailed combustion mechanisms, and then identifying sets of species and reactions which may be unimportant at certain reacting conditions. These methodologies have been exploited for both the generation of skeletal, reduced mechanisms (62; 65; 73; 74; 171; 172), and for accelerating the computation of chemical kinetics during CFD simulations (75; 76; 173; 174). A first class of methods involves the selection of a subset of species and reactions from the detailed mechanism. Among them are sensitivity analysis (175; 176), Directed Relation Graph (DRG) (77), even with error propagation control (DRGEP) (80), principal component analysis (PCA) (52; 177), computational singular perturbation (CSP) (57; 58), element flux analysis (EF) (71; 73; 76), single- and multi-objective optimization (62; 64; 65; 66; 67; 68; 69; 70; 171). A second cathegory involves instead techniques aiming at identifying and separating the different timescales acting at the same time. This allowes one to solve part of the reacting system in terms of algebraic equations, or eventually to reduce its stiffness. Besides the classical quasi steady-state (QSS) and partial equilibrium approximations (PE) (83; 84), other methodologies have been recently developed, such as intrinsic and trajectory-generated low-dimensional manifolds (ILDM, TGLDM) (93; 135), rate-controlled constrained equilibrium (RCCE) (85; 86), and the

invariant constrained equilibrium edge preimage curve method (ICE-PIC) (178). The reduction and optimization method proposed in the present paper aims at the generation of reduced reaction mechanisms for hydrocarbon combustion which are able to capture ignition delay times over broad validity ranges, defined by engine-relevant conditions. In this case, the optimization procedure is not meant to reduce the number of species, but to optimize the reaction rate constants for selected reactions, ranging within the degree of uncertainty retrieved in literature data of the elementary reactions involved, especially for high order hydrocarbons. In particular, the most noticeable example of an optimized reaction mechanism is the GRI-mech for methane and hydrogen combustion (179; 180). An automated optimization methodology for the reaction rate parameters has been proposed and applied by Elliot and coworkers to a reaction mechanism for an aviation fuel (63; 64; 65). Two possible issues arise during reduced mechanism preparation: on the one hand, the need for reducing as much as possible the dimensions of the mechanism may lead to unacceptable errors in the prediction of combustion profiles, especially as far as low temperature chemistry is concerned, thus leading to unaccurate predictions of ignition delay periods. On the other hand, mechanism optimization for a huge number of reaction rate parameters may require long computational times for reaching the optimum mechanism configuration.
In this work a novel approach has been developed. The reduction and optimization procedure is set up as an iterative algorithm, featuring a progressive reduction in the number of species from the full mechanism, and the optimization of the relative reaction rate parameters at each iteration. It is shown that this procedure allows GA-based optimizations to be performed under a pretty limited number of merit function evaluations with fairly good results. The iterative procedure stops as soon as the reduced and optimized mechanism isn't able to fit the requested error tolerances. In the following paragraphs, the reduction and optimization methodology is presented, together with its implementation in the iterative algorithm. Details are given on the development of a single-objective, GA-based optimizer for the calibration of the reaction rate parameters, and on the adoption of a suitable merit function formulation. Then, the aspects of the application of this procedure to the generation of reduced mechanisms for the oxidation of biofuels are presented and discussed, showing that the applicability of the reduced mechanisms to both ignition delay predictions and engine simulations.

3.1 Problem definition

The core of the present approach relies in setting the development of a skeletal mechanism as a constrained optimization problem. As a matter of fact, the target of the algorithmic procedure is to generate a reduced combustion mechanism of the smallest size, complying with specific constraints on its accuracy when compared to both performances shown by the full mechanism and experimental data such as ignition delay measurements or laminar flames.

It is acknowledged that the dimension reduction for a reaction mechanism (39) leads to the removal of reaction pathways which are present in the full, detailed mechanism and which are relevant especially for describing low-temperature chemistry. This feature leads to the possibility that a strong reduction in the overall number of species and reactions can strongly reduce the validity range of the skeletal mechanism. In order to overcome this problem, the idea included in this work is that to compensate for the lack of accuracy due to the deletion of a number of less important reaction pathways within the surviving reactions, by tuning the Arrhenius constants of the reactions themselves. The compensation is thus set up as an optimization problem, in which the independent variables are the constants which define the reaction rates, and the optimization procedure needs to fit the issues arising from considering a huge number of variables (which can add up to thousands when starting from detailed mechanisms involving large hydrocarbons) and from the fact that the strongly non-linear behaviour of combustion chemistry can lead many analytical optimization methods to reach local optima instead than global optima if the initial search space is not chosen to be close enough to the optimum solution. These issues thus drive the choice of the optimization strategy to evolutionary methods, which couple the need for simulating a limited number of candidate solutions if compared to the whole dimension of the search space, to the ability to find global optima even when the number of independent variables is huge (181).

The reliability of the optimization is strongly dependent on the accurate choice of an error function which needs to define how 'good' is a candidate solution when compared to either a reference case – such as the performances predicted by the detailed mechanism – or even experimental data, for strengthening the physical soundness and validity of the optimum solution. For these reasons, the idea of nesting a progressive reduction in the number of species according to a specific reduction methodology, and the successive calibration of the

reaction rate constants through an optimization problem into a robus algorithmic procedure has been developed. The problem of the mechanism reduction and optimization is hence formulated as follows:

- Find a detailed reaction mechanism which suits an appropriate validity range;
- Define a suitable error function which quantifies the accuracy of a skeletal mechanism with respect to the detailed one;
- Define a suitable error function which quantifies the accuracy of a mechanism with respect to a set of experimental measurements;
- Analyse the species reduction methods and find out the most suitable one for the generation of skeletal mechanisms;
- Find an error function constraint to define if a reduced mechanism needs reaction rate constants calibration;
- Define a robust algorithmic procedure which nests the progressive reduction in the number of species, the evaluation of accuracy constraints and which eventually establishes the optimization of reaction rate parameters, comparing the reduced mechanism to both the detailed one and experimental data;
- Verify the accuracy of optimally reduced mechanisms for biofuels to practical data of industrial interest.

3.1.1 Reaction rate constants optimization.

Forward reaction rates in common reaction mechanisms are mostly computed according to the Arrhenius formulation, which features three parameters needed for defining the behaviour of each reaction (113):

$$k_{f,i} = A_i \, T^{b_i} \exp\left(\frac{E_i}{R\,T}\right), \qquad i \in \{1, ..., n_r\}. \tag{3.1}$$

In case the mechanism features more complex reactions, such as pressure-dependent ones, more complex formulations are usually adopted; for example, in the CHEMKIN library (101) the Troe and SRI forms are allowed (182; 183), in which two Arrhenius-like reaction rates are defined at the low and high pressure limits, plus a number of parameters are needed

for computing the pressure-dependent behaviour. Lastly, in practical combustion mechanisms, reverse reaction rate calculation through the equilibrium theory is sometimes overrided by a further explicit Arrhenius-like formulation, which adds three parameters to the reaction definition.

In this work, the optimization problem is approached defining a fixed number of independent variables, twice the number of reactions to be optimized. In particular, only the collision frequency value A_i and the activation energy E_i are optimized. The choice not to include the temperature exponent b_i is motivated by the fact that most temperature exponents in the reactions are zero (39).

Not all of the reactions in the combustion mechanism need to be tuned: as a matter of fact, reaction rates for most of the reactions involving low-order schemes, such as the elementary oxygen - hydrogen system are well established. For this reason, the optimization problem is set not to address the reaction rate coefficients of reactions involving only species within the following set:

$$N_{basic} = \{H, H_2, O, O_2, OH, H_2O, HO_2, H_2O_2, N_2, CO, CO_2\}. \tag{3.2}$$

The reaction rates of all reactions which involve at least one species not in the set N_{basic} are thus optimized. Two reaction rate parameters, A_i and E_i thus need to be identified not only for elementary reactions with an Arrhenius formulation, but also for reactions with an explicit reverse reaction rate espression, as well as pressure dependent reactions. In the first case, assuming an explicit reverse rate expression leads to an 'effective' equilibrium constant which is different from the value computed through minimization of the reaction free energy. In our approach, no actions are taken in order to change this assumption, and, in case such a formulation is found in a detailed mechanism, the independent variables still remain the two forward reaction rate parameters; the explicit reverse reaction rate constants are accordingly modified, in order to mantain the modified equilibrium constant as arising from the original mechanism:

$$A'_{r,i} = A^0_{r,i}\, A'_{f,i} / A^0_{f,i}; \tag{3.3}$$

$$E'_{r,i} = E^0_{r,i} + \left(E'_{f,i} - E^0_{f,i}\right). \tag{3.4}$$

In the second case, two Arrhenius-like formulations describe the reaction rates at the high and low pressure limits. The reaction rate parameters at the high pressure limit are considered as independent variables for the optimization.

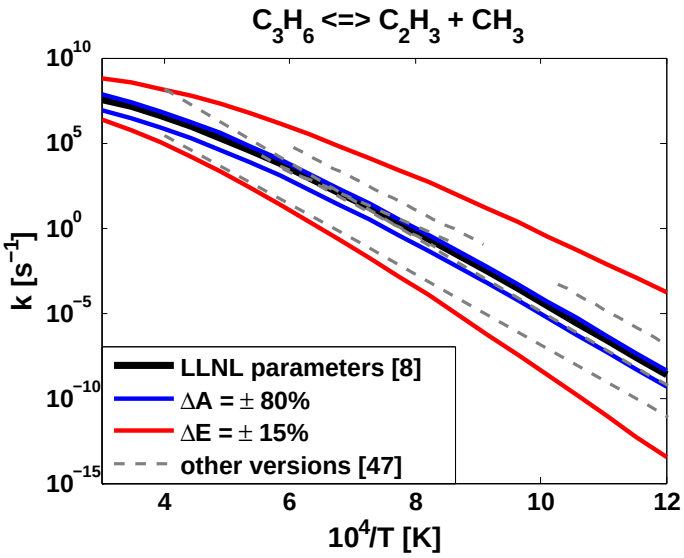

Figure 3.1: Comparison among different forward reaction rate constant sets for reaction $C_3H_6 <=> CH_3 + C_2H_3$. Reaction data from LLNL ethanol combustion mechanism (4) and NIST kinetics database (7).

Once that a unique definition of the set of independent variables is obtained, the allowed validity ranges of the variables need to be defined. In our approach, a fixed validity interval is set for each of the variables, centered on the previous value from the original mechanism, and with fixed width: $A_i \in \left[A_i^0 - \Delta A_i; A_i^0 + \Delta A_i\right]$; $E_i \in \left[E_i^0 - \Delta E_i; E_i^0 + \Delta E_i\right]$. The two range bounds adopted during the optimizations were $\epsilon_A = \Delta A_i / A_i = 80\%$ and $\epsilon_E = \Delta E_i / E_i = 15\%$. These two values were found to fit average uncertainties noticed when comparing reaction rate data involving C1-C3 hydrocarbons. These data were available from the NIST chemical kinetics database (7). As an example, Figure 3.1 shows the comparison among different values of the reaction rate parameters for the decomposition of propene into methyl and vinyl radicals. Here, range bounds defined by the aforementioned delta are applied to the values present in the ethanol combustion mechanism from Marinov (4). The two bands are able to correctly cover all the values reached by the other formulations for the same reaction. It is clear that the choice of assuming average validity intervals with fixed percentage allowance may not fit the data uncertainty for each of the reactions. However, this procedure is particularly suitable for implementation in an iterative algorithm, while detailed estimation of these bounds for each of the reactions in the full mechanism would need a

large pre-processing effort, which is beyond the scope of the approach.

In order to complete the definition of the optimization problem, once the function to be evaluated and the independent variables and their validity ranges have been identified, the solver for the GA-based optimization needs to be set up as described in the following paragraph.

3.2 Evolutionary optimization

3.2.1 Genetic algorithms and chemical kinetics.

The adoption of genetic algorithms for efficient single- and multiple-objective optimization is appealing, due to its effectiveness in getting the solution of the optimization problem, and the relatively small number of function evaluations required (181). There is evidence in the literature concerning the use of genetic algorithms for the development of combustion mechanisms. GA has been used for the generation of reduced combustion mechanisms setting an optimization problem to be the choice of species and reactions (72; 171): Banerjee and Ierapetritou (62) for example show the effectiveness of the genetic algorithm in choosing a reduced set of species and reactions from a detailed mechanism, exploiting the binary representation of chromosomes in the evolutionary algorithm, which allows the presence or absence of an item of the original set to be represented throughout the two possible instances – namely 0, or 1 – of its corresponding allele. Reduced mechanisms achieved through this approach can reach very small dimensions, even if their validity range is limited, and thus a set of reduced mechanisms may be needed for covering the range of operating conditions in practical combustion systems. The method has been used for the development of a unique reduced mechanism, for example when applied to HCCI engine multidimensional simulations. Montgomery et al. (184) have shown that the integration of GA-based optimization into the selection of quasi-steady-state (QSS) species can dramatically improve the procedure. Furthermore, application of the GA technique in terms of reduction in the number of reactions for the development of reduced mechanisms for engine-relevant conditions has been shown to be viable for reductions in the dimension of the original mechanism (185).

A second possible application of GA-based optimization is in the search for optimal values of reaction rates. Among the first examples of this second approach, Hamosfakidis and Reitz adopted a genetic algorithm for calibrating a simplified ignition model for a diesel fuel surrogate (186). In this work, the optimization featured a total of 26 independent variables, and an impressive improvement in the ignition model performance was achieved over a broad range of operating conditions. As far as full combustion mechanisms are concerned, an extensive review on this approach is given by Elliott et al. (67). They showed that the adoption of genetic algorithms can be very efficient in tuning the reaction rate constants, as the large number of variables involved makes this implementation more suitable than

analytical optimization methods. Since most reaction rates for high-order reactions, such those involving large hydrocarbons still are not well established, Elliot et al. (63) suggested that the validity ranges for the independent variables should be chosen to fit the degree of experimental uncertainty given by the data available for the reaction. The most complete collection of reaction rates was provided by the NIST kinetics database (7).
This methodology may require prohibitive CPU times for optimization of mechanisms for large hydrocarbons, and the same authors have more recently developed a novel approach, based on a two-step genetic optimization (64; 65). In the first step, the optimization aims at reducing the number of species. The chromosome is a binary string with a number of alleles equal to the number of species in the full mechanism. The total number of active species is kept fixed and equal to the number of species chosen for the reduced mechanism and the merit function is based on the performance of the reduced mechanism, in comparison with the full one. Once the reduced set of species is gathered, a second optimization step is carried out in order to tune the Arrhenius reaction rate parameters, A_i, b_i and E_i, $i = 1, ..., n_s$.
In the present work, GA-based optimization is nested into the iterative procedure. The reduction in the number of species is treated through the element flux analysis, while the GA is run only for the calibration of the reaction rate parameters. As the number of species is progressively reduced at each iteration, an optimization on the reaction rate parameters of the reduced mechanism is carried out, when the error function of the reduced mechanism exceeds a desired tolerance value. This choice is motivated by two reasons: the need for reducing the total computational time, and the fact that our reduction and optimization approach is ruled by a constraint on the performance of the reduced mechanism, aiming to get as few species as possible.

3.2.2 Development of an efficient GA-based optimizer.

In order to carry out the optimization problem described above, a code for the optimization of reaction rate constants has been developed, based on an evolutionary algorithm (187). The optimizer features a single-objective, binary-coded genetic algorithm, where an initial population of individuals is generated, and then let to evolve for a number of generations following the principles of natural selection operators, such as reproduction, mutation, and crossover. Each individual is represented by a set of binary strings, namely chromosomes,

which stand for the values of the independent variables to be optimized. The binary representation implies thus that the validity ranges of the variables have to be discretized into a finite number of divisions. If the range is defined by the continuous interval $[v_{min}, v_{max}]$, this is spanned through chromosome instances ranging from $v_{min} = 00...0$ to $v_{max} = 11...1$, and the total number of divisions, 2^{n_g}, is set by the number of digits – or genes –, n_g, of the chromosome itself. As a matter of fact, the variable value v matching a generic n-bit chromosome can computed as follows:

$$v(n-bitchr.) = v_{min} + bin2dec\{n-bitchr.\} \cdot \frac{v_{max} - v_{min}}{2^n - 1}, \tag{3.5}$$

where the $bin2dec$ operator is a function that converts into a base-10 number the value represented by the base-2 n-bit binary chromosome (which range spans the integer $\{0, 1, 2, ..., 2n-1\}$ set) (186). The total number of possible solutions (each of the variables has the same chromosome length) is thus given by $2^{n_g \cdot n_v}$, where n_v is the total number of variables. n_v can add up to thousands. Thus, when optizing reaction rate parameters, a three bit chromosome length $n_g = 3$ has been chosen, fixed for each variable, resulting in eight subdivisions of the validity interval. Each chromosome is assigned a merit value, computed through the evaluation of the fitness function, defined in Eq. 3.9, as a result of a set of constant pressure calculations. Each new generation is evolved from the previous one as the three operators of the genetic algorithm are applied. *Fitness-proportionate selection* of the individuals is the main operator affecting reproduction. Each of the new individuals appearing in the new generation has two parents, which are selected randomly from the previous one. The random process is however biased, as the probability that each individual is selected is proportional to its fitness value (181), as shown in Figure 3.2. A *mutation* operator, occurring after reproduction with a fixed probability, introduces new combinations in the genotype by inverting a randomly chosen gene within the chromosome. *Crossover* is a recombination operator which cuts the chromosomes of the two parents at a random locus, and exchanges the two cut parts between them. A schematic representation of these two genetic operators acting on chromosomes at the moment of reproduction is reported in Figure 3.3. In particular, the iterative procedure adopted in the present GA for simulating the evolution of the population can be schematised as follows:

1. Generation of the first population: N_p individuals, consisting of randomly generated chromosomes.

2. Evaluation of the fitness function for each of the individuals.
3. Fitness-proportionate selection of $f_R \cdot N_p$ couples of individuals for reproduction.
4. Reproduction of the individuals: each chromosome randomly chosen from one of the parents.
5. Possible occurrence of mutation and crossover, with p_M and p_C probabilities.
6. Substitution of the $f_R \cdot N_p$ worse individuals with the newly generated ones. Begin a new generation.
7. Evaluation of the fitness function for each of the new individuals.
8. Go to 3.

The parameters ruling the GA operation are summarized in Table 3.1. Most of the parameters follow the guidelines suggested by Mitchell (181). Usually, the GA is iterated up to 50 to 500 generations; and the population size is made up of 5 to 50 individuals. An exception has ben considered for the mutation probability, which is usually very small ($p_M < 0.01$). In this case, however, it is necessary to introduce a high degree of randomness due to the fact that the population size scarcely allows the whole variable space to be covered, and having a high probability of mutation allows zones which are not present in the first generation to be gradually introduced during the optimization process. The reproduction fraction is chosen at 90% as it is acknowledged that keeping only few, near-optimum individuals from one generation to the next can improve the algorithm convergence; crossover probability is the recommended value.

Parameter	symbol	value
number of individuals	N_p	75
number of generations	N_g	200
chromosome length	n_g	3
reproduction fraction	f_R	0.90
mutation probability	p_M	0.60
crossover probability	p_C	0.35

Table 3.1: Parameters setting the genetic optimizer.

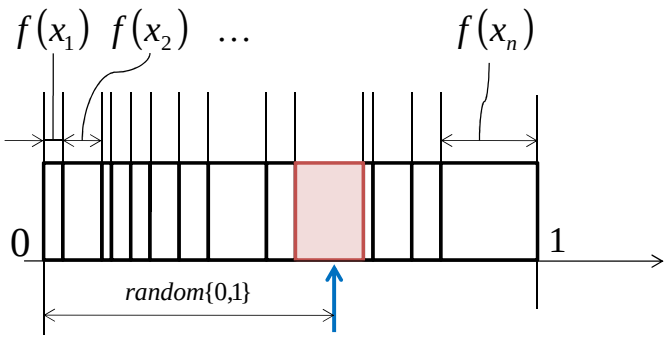

Figure 3.2: Schematic showing fitness-proportionate selection according to the biased 'wheel of fortune' principle.

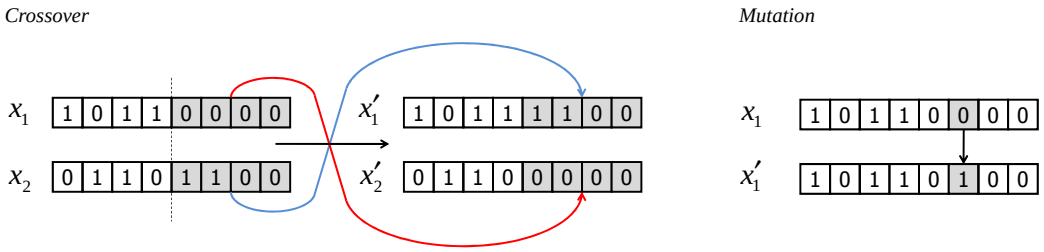

Figure 3.3: Schematic showing how genetic operators act on chromosomes.

3.2.3 Effectiveness of the GA for a case of industrial interest

In order to assess the validity and the effectiveness of the GA optimizer developed, a case of industrial interest was chosen. In particular, the optimization problem was within the framework of the development and optimization of a SI high performance engine, to be used in Formula SAE/Student competitions, at the University of Modena. The base engine was a single cylinder Yamaha 660cc motorcycle unit, rated at about 48 HP at 6000rpm. Modifications were introduced to fit the competition rules (188): besides the reduction of engine capacity to 600cc and the mounting of the required restrictor, mechanical supercharging has been adopted in order to boost performance.
The optimization process involved the engine's complete intake and exhaust systems, simulated by means of the 1D, gas dynamics GT-Power code (189).

Since no specific data were available about combustion, friction losses and the flow through the valves, information has been derived from a database on engines. A lot of care

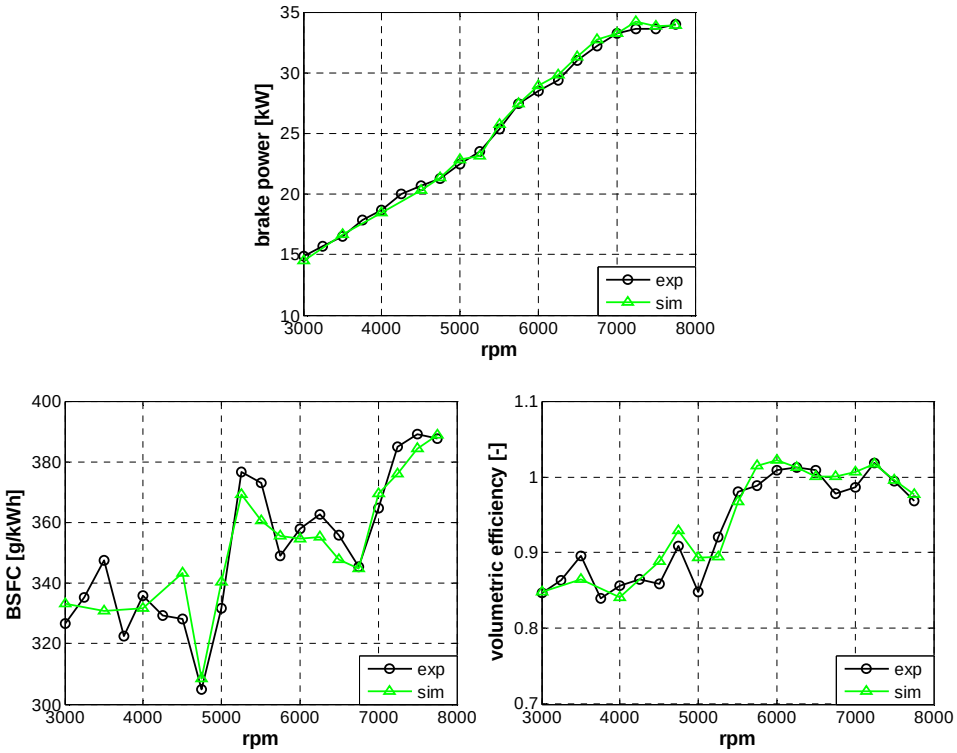

Figure 3.4: Validation of the GT-Power model for the Yamaha XT 660 R engine.

has been devoted to the modeling of the muffler, represented as a net of 21 volumes and 10 series of orifices (tail noise is considered a performance parameter, since it is limited by technical regulations).

The calibration of the model parameters has been carried out by comparison with experiments at the dynamometer on the base engine, in the original configuration. The more relevant measured quantities are: engine torque, speed, fuel rate and Air-Fuel Ratio (by means of a UEGO sensor). After this calibration, the model has been updated to represent the modifications required by the Formula SAE regulations, i.e. with the $20mm$ restrictor and the total displacement reduced to $610cm^3$. Again, a comparison has been made between the results provided by simulation and the values measured at the dynamometer, finding a very satisfactory agreement (this comparison is shown in Figure 3.4). Naturally, the validated GT-Power model of the naturally aspirated Formula SAE engine is the base on which the model of the supercharged engine has been built.

3.2.3.1 Parameter setup

The engine parameters set needed to be defined according to a number of issues to be addressed, thus resulting in a constrained optimization problem. First, maximum boost pressure and top revving speed should be accurately defined, in order to meet performance and reliability and fuel efficiency. It is reminded that in Formula SAE, high speed operations at Wide Open Throttle (WOT) are important only in the acceleration test, while they have a very limited use on the track, both in autocross and in endurance competitions (beside the circuit is very windy, the car must also slalom among cones, therefore the engine runs throttled most of the time). The adopted design strategy has been to keep compressor delivery pressure in a low-medium range (about 1.5 bar, absolute), but let the engine rev up to 7500 rpm. In this way a high power peak may be reached for a few seconds when needed, while under average operating conditions the engine should be safe against knocking. Furthermore, engine top rotational speed is very easy to be electronically controlled (through the advance map in the ECU), while boost pressure would require a specific valve.

Low delivery pressure helps fuel economy too, for two reasons: 1) compressor isentropic and volumetric efficiencies are generally better than at high pressure ratios; 2) as a thumb's rule, the higher is boost pressure, the richer must be the air-fuel mixture, in order to keep in-cylinder temperature under control.

As well known, for a mechanical supercharging system with intercooler, delivery pressure depends on: ratio of compressor capacity to engine capacity, transmission ratio between engine and compressor, ratio of compressor volumetric efficiency to engine volumetric efficiency (referred to intake port pressure) and intercooler outlet temperature. Therefore, once the choice of compressor and target delivery pressure and intercooler outlet temperature is made, on the base of a number of design constraints, the value of transmission ratio is subsequent.

Another critical issue is the trade-off between flow-dynamic tuning and engine transient response. On the one hand, large volumes are suitable to get a proper tuning of the intake system (in particular, a Venturi nozzle is necessary after the restrictor to recover some kinetic energy; furthermore, a large plenum should be placed between the throttle and the engine, in order to damp the pressure and velocity pulses through the restrictor and to provide an open end reflection to the waves traveling along the intake runner). On the other hand, the higher is the volume between the throttle and the engine, the slower is transient

response (and the more difficult is injection parameters calibration). The University team has found a very good trade-off between these issues by adopting an unusual configuration for the plenum. Instead of using a single large volume, two Helmholtz resonators are connected to a short intake runner. Even on a single-cylinder naturally aspirated engine, the influence of these resonators on the intake system dynamics is very complex, since the two pipes (intake duct and air scoop) and the two volumes (cylinder and resonators) form a vibrating system, with two degrees of freedom and two resonant frequencies (160). It may be observed that, when adopting a conventional intake system (made up of an inlet runner, a large plenum and an air scoop), the highest engine speed at which the tuning occurs is almost coincident with the base resonant engine speed, while the lowest speed falls out of the range of interest. Conversely, an intake system with two small Helmholtz resonators yields two tuning peaks, at both low and high engine speed, and presents the further advantage of a faster transient response, due to the reduced volume between throttle and cylinder.

A number of constraints is placed upon the dimensions of pipes and volumes. According to the technical regulations, all parts of the engine air and fuel control systems must lie within the surface defined by the top of the roll bar and the outside edge of the four tires. Furthermore, the exhaust pipe outlet(s) must not extend more than $60cm$ behind the centerline of the rear axle, and shall be no more than $60cm$ above the ground. Many other constraints are given by the specific lay-out of each car, as well as by the need of packaging the whole engine system into an assembly as compact and light as possible, easy to install and access for inspection. Last, but certainly not the least, the cost must be as low as possible (the limit for the cost of the whole car, calculated according to the regulations, is 25,000 USD, thus the use of expensive technologies, beside some exceptions, is not a practical proposition). As a result, on each car the degrees of freedom for the design of the intake and exhaust system are strongly limited.

As far as the intake system is concerned, the part considered for the optimization, visible in figure 3.5, lays between the intercooler outlet (left end) and the engine head inlet (right end). The intake runner and the pipe from the intercooler have the same constant diameter, named DI1, while their length may be different (LI1 and LI4). The two Helmholtz resonators are identical, and they are defined by a set of 4 parameters (DI2, DI3, LI2 and LI3). Finally, the volume of the junction between the resonators and the runner is called VI1.

The exhaust system schematic is presented in figure 6. The twin ducts leaving the cylinder head have a constant diameter, DE1, and a length named LE1. After the junction (whose

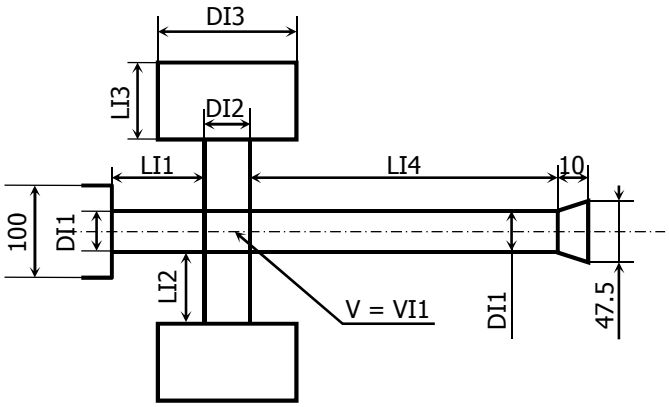

Figure 3.5: Parameters defining the intake system.

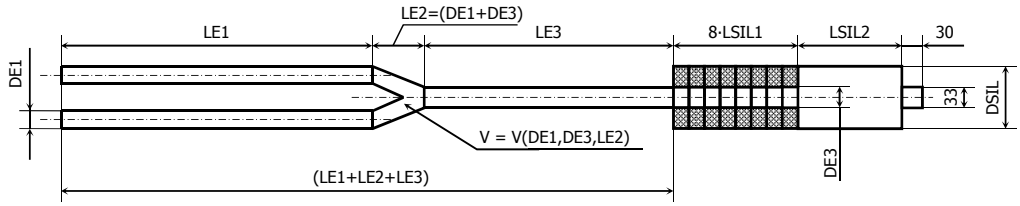

Figure 3.6: Parameters definig the exhaust system.

length is empirically assumed as the sum of the inlet and outlet diameters), the pipe has a diameter DE3 and a length LE3. The silencer is made up of two chambers (the first one stuffed by wool), a perforated duct (diameter is still DE3), and a short duct having a diameter of $33mm$. In the GT-Power model, both the perforated duct and the first chamber are divided into 8 parts, connected by multiple holes and openings through which the flow is free of losses. The length of each component along the silencer axis is called LSIL1, while LSIL2 is the length of the second chamber. Finally, the external diameter of the silencer is DSIL.

It is remarked that the modeling of the muffler is suitable for brake performance analyses, but it is not very accurate for acoustic predictions (according to the technical regulations, the measured Sound Pressure Level at about 6000 rpm must be less than 110 dB). For the last purpose, a higher refinement of the numerical model would be necessary, with unacceptable increase of the computational time. Therefore, empirical criteria have been adopted

Variable	Unit	Min.	Max.
DE1	mm	25	42
DE3	mm	30	70
DI1	mm	38	58
DI2	mm	28	58
DI3	mm	60	200
DSIL	mm	50	200
LE1	mm	300	800
LE3	mm	300	800
LI1	mm	50	300
LI2	mm	30	130
LI3	mm	40	160
LI4	mm	100	500
LSIL1	mm	10	70
LSIL2	mm	40	400
VI1	mm^3	100,000	2,000,000

Table 3.2: List of optimization variables and their validity ranges.

for muffler design, and a further simulation with a more sophisticated model is required to verify the actual noise level. Table 3.2 presents the range of variation allowed for each parameter that must be optimized. Three further constraints are placed upon this set of parameters: the total length of the exhaust pipes (LE1+LE2) must be less than 1.5m; DSIL must be at least 20mm larger than DE3; the total length of the silencer must not exceed 600mm.

3.2.3.2 Optimization and analysis

The influence of the 15 parameters described in the previous section has been explored by means of the code previously described, with the aim of finding the best combination of both the independent and the constrained parameters. Thus, a merit value has to be assigned to define how good each configuration is on an analytical basis. In the present case the 1-D fluid dynamics code itself acts as fitness operator: the values given by chromosomes are inputs for the engine model, and the output fitness value is extracted from the predicted engine performance. For the current optimization, the following fitness function has been

adopted:

$$f(\boldsymbol{x}) = \frac{1}{k}\sum_{i=1}^{k} P_i \; [kW] \tag{3.6}$$

i.e. the average output brake power, upon the simulated engine speeds. A set of $k = 6$ different engine revs has been considered: from 2500 to 7500 rpm, with a 1000 rpm step between each other. The genetic algorithm has been coupled with GT-POWER by means of a Fortran program which integrates the genetic algorithm with 1-D simulations. Since a GT-Power run reads an input file containing model data, all the variables involved in the optimization have been parameterized within the model, so that a string for each of them appears in the input file (tagged as "dat"). Their values are changed by the Fortran program each time a run (i.e. an "individual", in GA lexicon) is started, as a function of values provided by GA. Then, the script is run to get brake power from the output file at each simulated operating condition, and to compute the fitness value of each individual. A schematic view of that procedure is reported in Figure 3.7.

As a term of comparison for the in-house developed GA, a similar optimization has also been run employing one well known commercial GA-based optimization software (modeFRONTIER 4.0 by ES.TEC.O). In this case, even being the objective of the optimization still focused upon the average brake power, a multi-objective genetic algorithm (MOGA) has been applied, and the single output power values at the simulated operating conditions have been chosen to be optimized. Since the same weight was given to each of the power values at the different engine speeds, the fitness value of the same individual resulted to be equal in both the in-house developed and the commercial optimizations. So, adopting a multi-objective GA has proved to be useful not in terms of performance of the optimization, but instead because it allows the user to use a series of analysis tools which investigate the influences of the input variables upon the single brake power values, more than on the average brake power only. Also in this case a procedure similar to the one reported in Figure 3.7 has been used to couple commercial code with GT-POWER.

A base configuration for the supercharged engine has been defined through an empirical optimization process, considering the parameters of Table 3.2 and the following guidelines. First, the length of the intake runner and the volume of the resonators have been set in order to maximize volumetric efficiency at high engine speed. Second, the length of the exhaust pipe has been calculated for a proper breathing from medium to high speed. Third, the transmission ratio between engine and compressor was set in order to get an

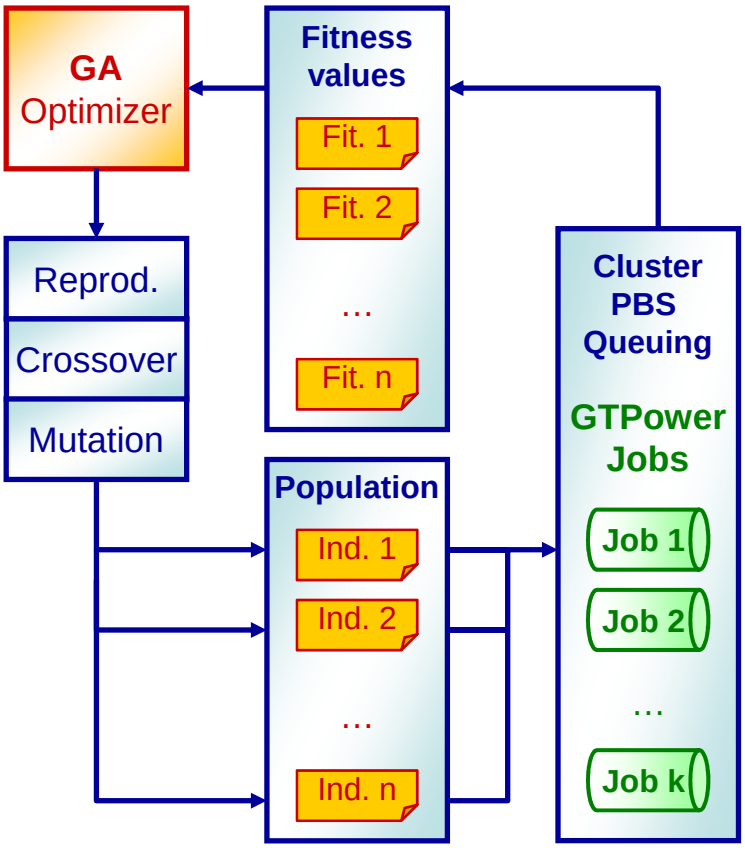

Figure 3.7: Schematic showing the genetic algorithm and GT-Power coupling procedure.

average boost pressure of about $1.6bar$. Modelling of friction losses and combustion and heat transfer has been set as in the naturally aspirated engine, so that any comparison between different configurations is independent on these issues. The authors acknowledge that the increase of intake pressure and temperature affects heat release rates, however the influence on brake performance should be limited, as far as knocking is kept under control. For this purpose, in comparison to the naturally aspirated engine, the cooling system of the supercharged unit has modified, while injection parameters and spark advance have been properly calibrated at the dynamometer bench. Brake power of the base supercharged configuration is reported in Figure 3.8, compared to the performance of the naturally aspirated engine. The fitness of the former, computed according to Eq. 3.6, adds up to $34.483kW$.

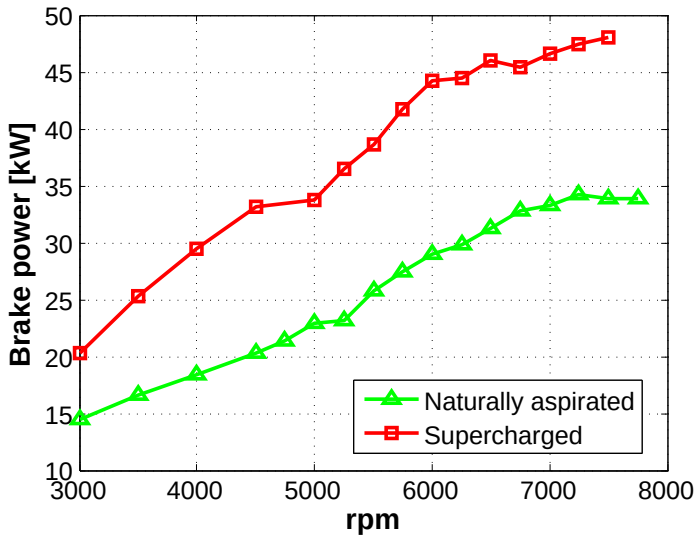

Figure 3.8: Comparison between naturally aspirated and base supercharged brake power output, at full load.

Then, the optimization of the engine model has been performed by using the in-house developed single-objective GA, described in the previous section. A total of 65 generations has been simulated, each one consisting of 150 individuals. Probabilities of crossover and mutation have been set both to $p_M = p_C = 0.4$, while the fraction of the population to be reproduced between one generation and the next has been chosen to be $f_R = 0.35$, resulting in 52 new individuals in each new generation. The definition of these parameters has been decided taking into account the guidelines provided in (181; 190; 191), as well as some other optimizations carried out previously. The variables' allowed ranges have been subdivided into 256 intervals, i.e. 8-bit chromosome strings have been used to genetically represent the variables values. As a result, a total of 9750 individuals have been simulated, and the best individual has been found by the GA after 44 generations, yielding a fitness value of 35.475kW, as shown in figure 3.9. At the same time, the optimization using modeFRONTIER 4.0 has been run considering the same dimension of the population (150 individuals), while different genetic parameters have been chosen. As well known (181), genetic parameters such as mutation, cross-over, and reproduction probabilities, interact among them in a non-linear way, and it is not still clear how such parameters should be properly combined. As a matter of fact, they cannot be optimized one by one, then the values that worked well

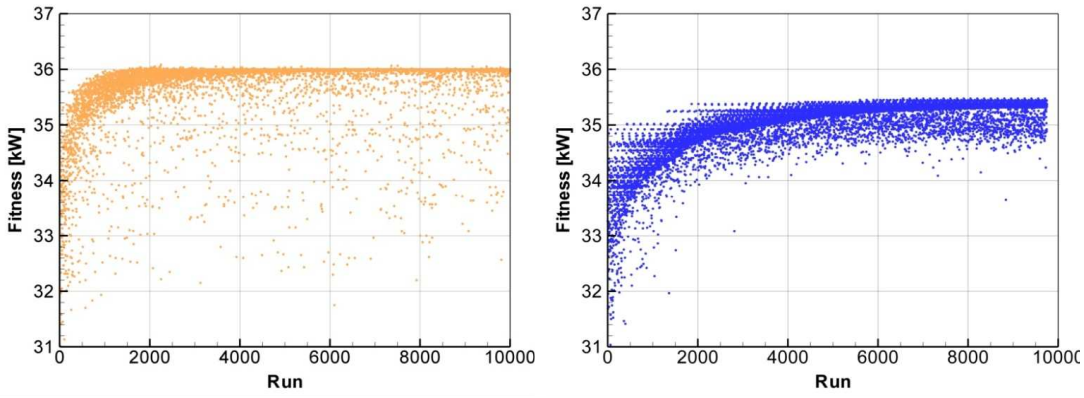

Figure 3.9: Fitness values vs design ID for the commercial code GA optimization. Left: commercial code; right: in-house code.

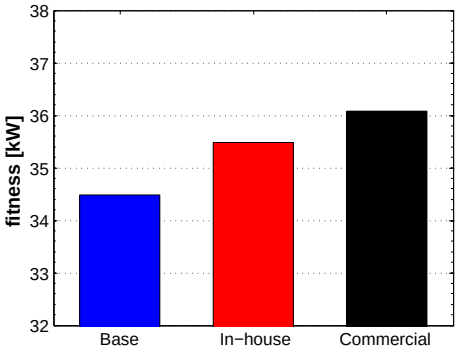

Figure 3.10: Optimal fitness values.

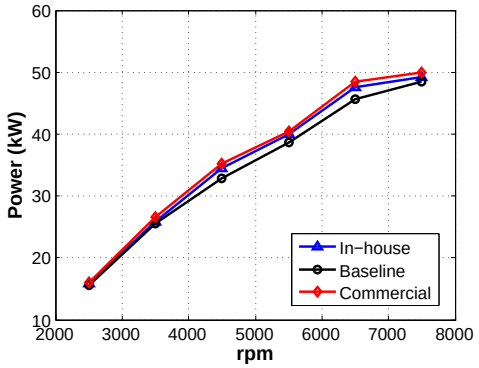

Figure 3.11: Brake Power output.

in previous reported cases are generally adopted. Thus, the parameters set up has been performed using a group of values suggested by developers in the users' guide and refined through a trial and error process. In details, the probabilities of crossover and mutation have been eventually set to 0.5 and 0.1, respectively, while the fraction of the population to be reproduced between generations is 0.95. In the analyzed case, simulations stopped after about 10000 individuals, at the reach of convergence (Figure 3.9). It is mentioned that the best individual, owning a fitness of 36.083 kW, has been found since generation 15. Figure 3.10 shows a graphical comparison among the optimized configurations in terms of fitness, while, in Figure 3.11, the brake power curves are plotted.

In order to further assess the performance of the GA developed by the authors, figure 3.12 shows a comparison between the results of the in-house code with the ones yielded

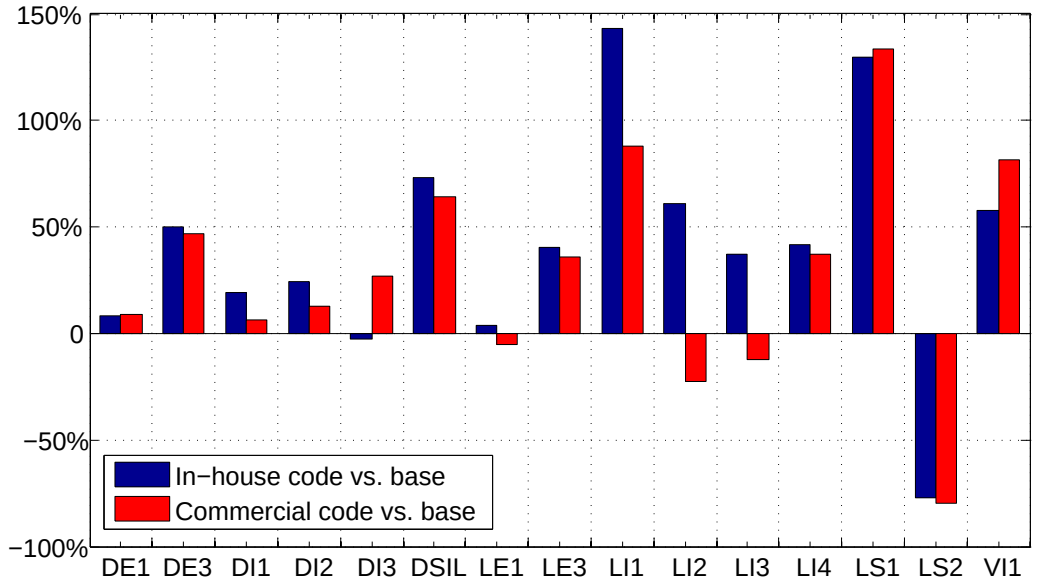

Figure 3.12: Differences between the values of the parameters in the genetic optimisations, and the base configuration.

by the commercial optimizer. The comparison is made in terms of percent variation of the geometric parameters listed in Table 3.2. It may be observed that for almost all the parameters the trend suggested by the in-house code is confirmed by the commercial optimizer, the only significant exceptions being the dimensions of the Helmholtz resonators (LI2, LI3, DI3). However, it is remarkable that the optimum volume of the resonators is almost coincident, while the ratio of neck cross section to length (DI22/LI2) is similar. Since the resonance frequency is given by (192):

$$f = \frac{c}{2\pi}\sqrt{\frac{S}{V\,L}} \tag{3.7}$$

(where c is speed of sound, S is neck cross section, L its length and V is the resonator volume), the two configurations are very close from an acoustic point of view. Figure 3.13 presents a comparison among the three optimized configurations in terms of engine performance. It may be noticed that the geometry of intake and exhaust system affects boost pressure: both the GA optimizers allow lower pumping losses than on the BASE layout, as demonstrated by the PMEP graph, so that the compressor delivery pressure is relieved. The automatic optimizations yield slightly higher airflow rates at low-medium engine speeds, while the improvement of IMEP at high speed is mainly due to the lower pumping losses and

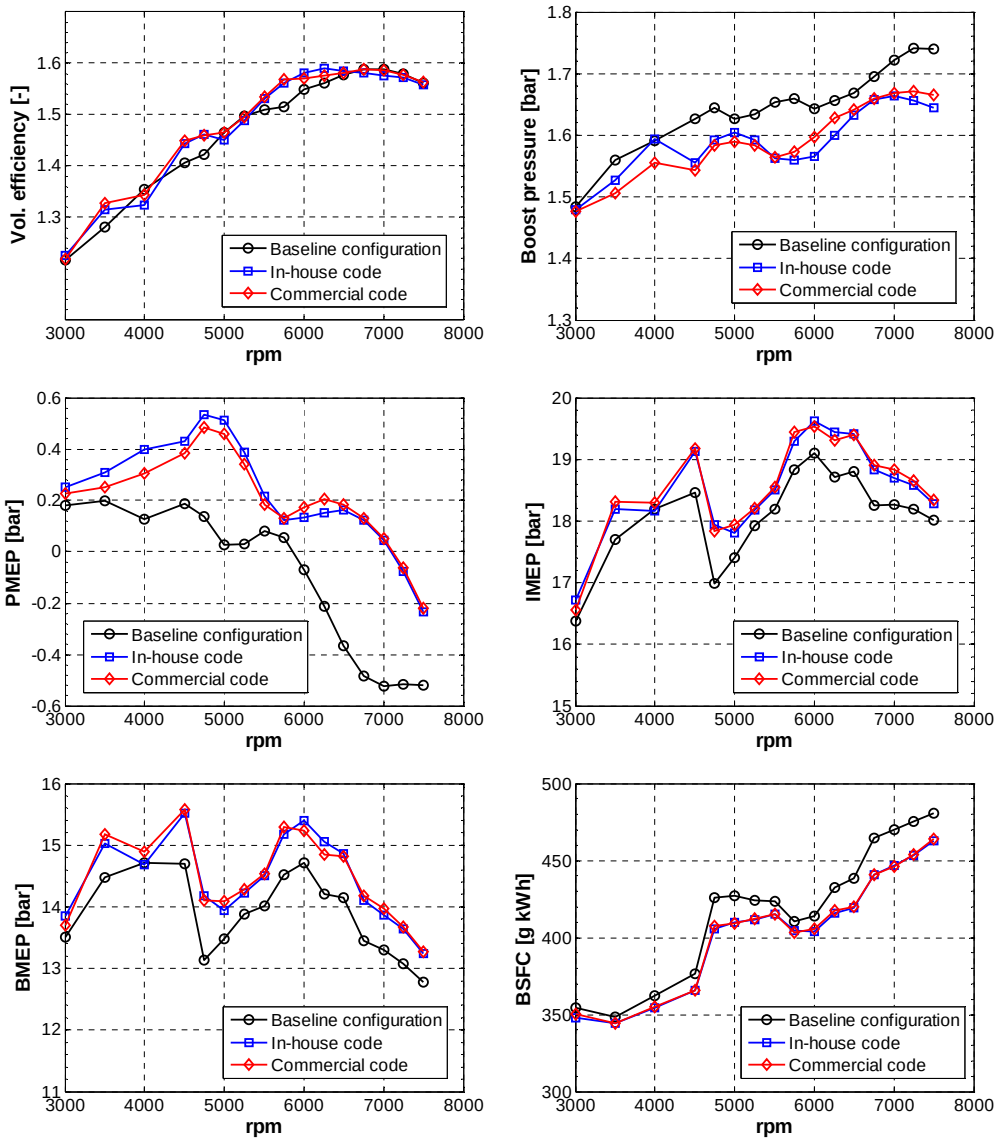

Figure 3.13: Comparison among the three optimized configurations in terms of engine performance

the reduction of power absorbed by the compressor (same airflow rate, lower delivery pressure). Since FMEPs are almost constant for all the configurations (the difference in terms of in-cylinder maximum pressure are small, being the values of boost pressure very close), the enhancement of indicated work also improves mechanical efficiency a little bit. As a result of better pumping and organic efficiency, fuel consumption is slightly lower in the configurations optimized by Genetic Algorithms. Finally, it is observed that the improvement of engine performance yielded by optimization is quite significant, considering the good level of the base configuration and the high number of constraints. However, sophisticated multi-objective genetic algorithms, as the ones employed in the commercial software, not always produce relevant benefits, in comparison to simple single objective algorithms, as the one developed by the authors.

3.3 A robust algorithmic procedure

The methodology herein proposed aims at generating a comprehensive reduced mechanism which is able, while considering the major reaction paths, to predict accurate combustion profiles at a variety of engine-relevant conditions. However, simply reducing the number of species and the reactions involving them usually leads to inaccurate predictions of reduced combustion mechanisms, usually due to the lack of resolution in the representation of low-temperature chemistry (39). Furthermore, sometimes the detailed mechanisms themselves are validated for limited ranges of pressures, temperatures and equivalence ratios, and their predictive capability can be weaker when simulating many practical combustion systems in which broad ranges of operating conditions are observed.

For these reasons, the present approach relies on the generation of a reduced combustion mechanism starting from an already established, detailed one. Then, as the number of species and reactions is reduced, the progressive loss of accuracy due to the elimination of the less important reaction paths needs to be compensated for. This can be accomplished by correcting the collision frequencies and activation energies of the reactions involving such hydrocarbons. This operation is not meant to generate artificial, unphysical reaction rates. Thus, the allowed ranges of variation of the reaction rate parameters were commensurate with the uncertainty associated with them in the literature. The aim is to account for the effects of the reaction paths which have been deleted in the surviving reactions. Hence, after analysis of the data in the NIST kinetics database (7), valid ranges for allowed variations of the Arrhenius parameters during the correction process were limited to ±15% for the activation energy, and ±80% for the collision frequency value.

An iterative procedure was established, ruled by an error function formulation, which quantifies the deviation of the reduced mechanism from the detailed one. This kind of procedure can easily be automated, as all of its steps can be defined through analytical formulas and logical operators. The details of this procedure are represented in the form of a flow chart in Figure 3.14, while the methods defined and adopted for the mechanism reduction and optimization are discussed in the following paragraphs. In particular, a desired error tolerance for the reduced mechanism needs to be set. The iterative procedure then starts from a first reduction in the number of species and reactions, with a high cut-off value for species deletion, so that a high number of species is retained in the reduced mechanism. Next, an error

function is evaluated to check whether the reduced mechanism still behaves within the requested tolerance. In this case, the cutoff value is further reduced, so that a greater number of species – together with the reactions involving them – can be deleted from the mechanism. This progressive reduction of the dimensions of the reduced mechanism is continued until the error function value exceeds the maximum tolerance allowed. In this case, the reduced mechanism is corrected through the optimization of the Arrhenius parameters so that the effects of the reaction paths progressively excluded from it can be accounted for in the selected reactions from the remaining scheme. In case the optimum solution still fits the error tolerance requirements, a further reduction step can be pursued. Otherwise, the procedure restores the latest valid mechanism configuration.
Once these steps are completed, a reduced mechanism is generated, which behaves consistently with the detailed one. Then, the performances of the mechanism are compared to available experimental data, in order to have it fit the desired range of temperature and pressures. For this purpose a secondary optimization is carried out and a different error function formulation is adopted for quantifying the mean squared error, shown in terms of ignition delay predictions, and compared to available sets of experimental ignition delay measurements.

3.3.1 Definition of an error function for the reduced mechanism.

The definition of the error function for estimating the global error introduced in a reaction mechanism due to the elimination of less important species and reactions is mandatory, since the effectiveness of this indicator affects not only the possibility of finding the optimum reduced mechanism, but also the efficiency of the algorithms chosen for the mechanism reduction and optimization. In particular, some observations have been posed that define the requirements for the error formulation:

- The function should cover a broad range of operating conditions, as the reduction and optimization process aims at generating a mechanism which is valid over the broadest range of conditions occurring in practical combustion systems, and in particular in internal combustion engines. Particular relevance needs to be posed on lean conditions and low temperatures, as it is acknowledged that the generation of reduced mechanisms usually affects low-temperature chemistry (39);

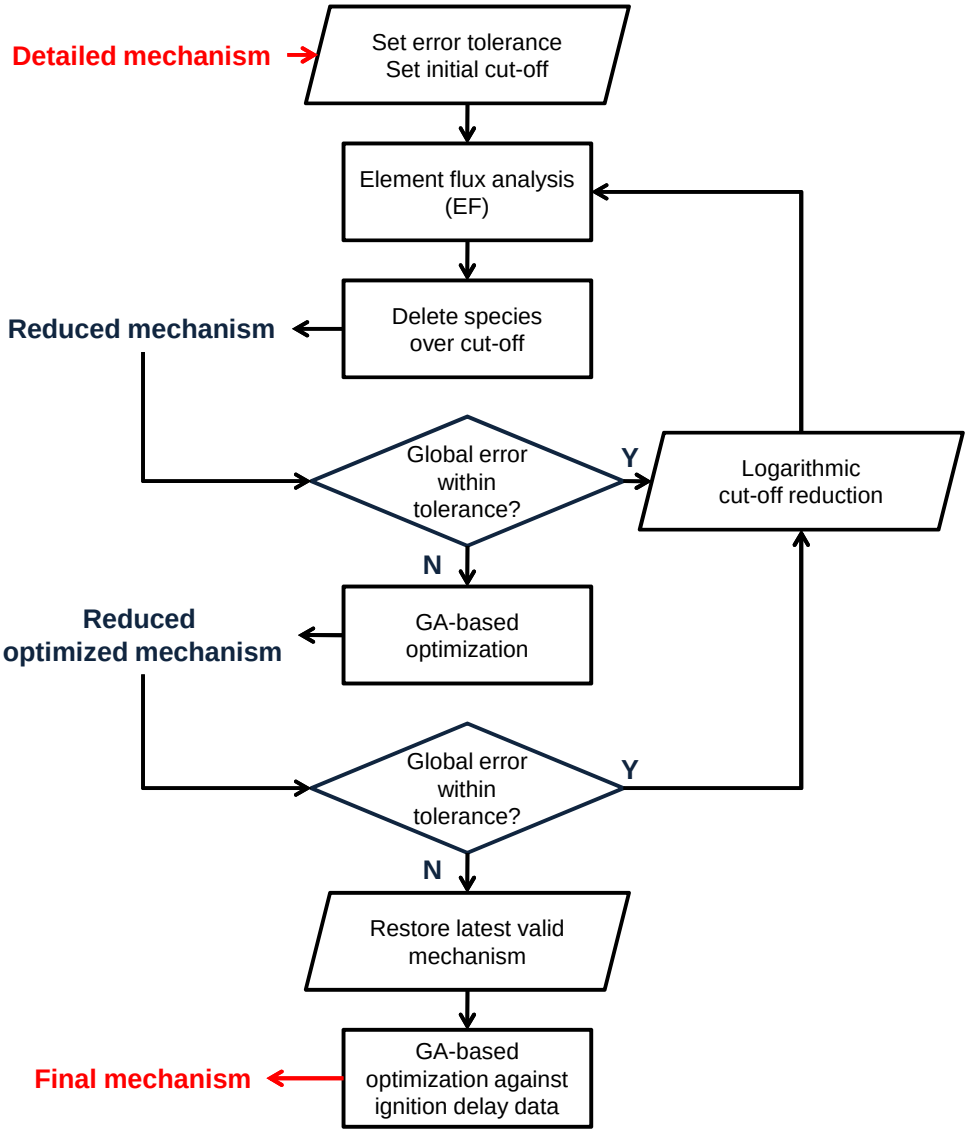

Figure 3.14: Flow chart of the procedure for mechanism reduction and optimization.

- The function should not vary by many orders of magnitude: genetic algorithms based on fitness-proportionate selection rely on the assumption that, when creating a new generation of individuals, the probability an individual has to be selected for reproduction is proportional to its fitness value. Thus, in case the best individual has a fitness value much higher than the others, it is likely that most of the next generation will be made with its chromosomes only, so that most of the genome of the previous generations are lost;

- The formulation of the error function should be valid both during the mechanism reduction procedure, and during the optimization phase. In the first case, the independent variables of the problem are binary, as they can be represented as the presence or absence of any reaction in the reduced mechanism. On the other hand, in the optimization problem all of the Arrhenius parameters can vary within a continuous validity range. Thus, the error function should not explicitly rely on these parameters, but should instead involve the actual physical behaviour of the mechanism.

As a reference for building an error function the formulation proposed by Elliot et al. (67) was chosen:

$$f = \left\{ 10^{-8} + \sum_{j=1}^{n_c} \sum_{k=1}^{n_s} W_k \frac{\left| X_{jk}^{calc} - X_{jk}^{orig} \right|}{X_{jk}^{orig}} \right\}^{-1} . \tag{3.8}$$

In equation 3.8, a merit value for a modified mechanism is expressed through the comparison to the reference one. The merit value is higher as the model error is reduced. In order to estimate the model error, a sum of relative errors is made, which compares the final molar fractions X of all the n_s species in the mechanism after constant volume simulations over a set n_c of initial reactor conditions.
This formulation has proven to be suitable for the optimization of combustion mechanisms of large hydrocarbons (64; 65). Moreover, it is able to account for important or unimportant species through a weighting factor W_k; however, it is not designed to take into account the time evolution of the species, and its value may be misleading in this case, where the optimization focuses not only on the ignition delay time, but on the overall behaviour of the reduced mechanism. For this reason, it has been modified, and improved as follows:

$$f = -\log\left\{10^{-8} + \sum_{j=1}^{n_c}\left[\sum_{k=1}^{n_s}\int_{\tau=0}^{\tau=t_j} W_k \frac{\left|X_{jk}^{full}(\tau) - X_{jk}^{red}(\tau)\right|}{X_{jk}^{full}(\tau)} d\tau + \right.\right. \\ \left.\left. + \int_{\tau=0}^{\tau=t_j} \frac{\left|T_j^{full}(\tau) - T_j^{red}(\tau)\right|}{T_j^{full}(\tau)} d\tau\right]\right\}. \tag{3.9}$$

In particular, a total integration time t_j is defined for each of the reactor operating conditions, and needs to be estimated a priori; it has been chosen to add up to 1.5 times the mixture ignition delay period at the current conditions. Thus, the relative error from the comparison between the full and the reduced mechanisms is numerically integrated over the whole simulated time, for each of the n_c cases. A total of one thousand sampling points for the numerical integration was found to perform well. The weighting factor W_k is used not to give different weights to the species, but instead as a binary selector for the species to either be included or not in the error function computation. Furthermore, an error analysis on temperature profiles T_j has been added similar to the approach proposed by Banerjee and Ierapetritou (62), as global heat release is one of the key quantities for defining the effectiveness of the reaction mechanism. Finally, the logarithm operator is considered, as the error function derived from the integration of the relative errors of the species profiles can vary many orders of magnitude. Applying the logarithm implies that the resulting values of f remain of the order of unity and thus are particularly suitable for GA-based optimization. The choice of the operating conditions to be simulated for defining the reduced model's error function is problem-dependent. However, the whole set is intended to cover the range of operating points that the mechanism is developed for. The choice of a small number of points, or of a narrow space will eventually lead to a mechanism with a limited validity range. More details for the 18 operating points chosen in the present analysis for the ethanol combustion mechanism are given in the following.

Finally, the following set of species to be monitored has been assumed:

$$N_s = \{fuel, O_2, OH, HO_2\}. \tag{3.10}$$

Apart from fuel and oxidizer, OH and HO_2 radicals have been chosen due to their well acknowledged importance in slow hydrocarbon oxidation and ignition delay timing (193; 194).

3.3.2 Species reduction through element flux analysis (EF).

Among the methodologies for the analysis of species activity in reaction mechanisms, Element flux analysis (EF) is based on the assumption that the instantaneous reactivity of the species across all the reactions can be quantified by the fluxes of atoms of selected elements. This method, first introduced by Revel et al. in 1994 (71), has also been proposed by Androulakis et al. (73) as a tool for identifying the the contributions of species in detailed reaction mechanisms over an integrated time interval. More recently, He, Ierapetritou and Androulakis have improved the methodology and shown the potential of this approach as an efficient pointer for quantifying the instantaneous reactivity of the species. In some recent papers, (74; 75; 76) they have adopted element flux analysis to identify reaction pathways, and to develop reduced mechanisms on-the-fly both in batch reactor and in CFD combustion simulations.

The core of the EF analysis is the definition of an instantaneous flux pointer $\dot{A}_{ijk}$, which quantifies the flux of atom A, in the i-th reaction, from the species with index j to the one with index k:

$$\dot{A}_{ijk}(t) = \left(\left|q_{f,i}(t)\right| + \left|q_{b,i}(t)\right|\right) \frac{n_{A,j}\, n_{A,k}}{N_{A,i}}, \tag{3.11}$$

where $n_{A,j}$ represents the number of atoms of element A in species j, and $N_{A,i}$ the total number of atoms of the element involved in the whole reaction i. He et al. have improved the original formulation by Revel et al. by explicitly separating the original term for the reaction progress variable, q_i, into the sum of two absolute values, cumulatively accounting for the forward and backward atom fluxes within the same reaction. This assumption is motivated by the need to prevent the atom fluxes of reactions near equilibrium from being evaluated as negligible.

In our approach, the element flux analysis is the basis for mechanism reduction, as it is meant to provide an index of the importance the species play across the whole ranges of validity the mechanism is intended for. Thus, the concept of flux time-integration introduced by Androulakis et al. (73) has been modified into:

$$A_{jk} = \sum_{c=1}^{n_c} \left\{ \int_{\tau=0}^{\tau=t_c} \left[\sum_{i=1}^{n_r} \dot{A}_{ijk,c}(\tau) \right] d\tau \right\}; \tag{3.12}$$

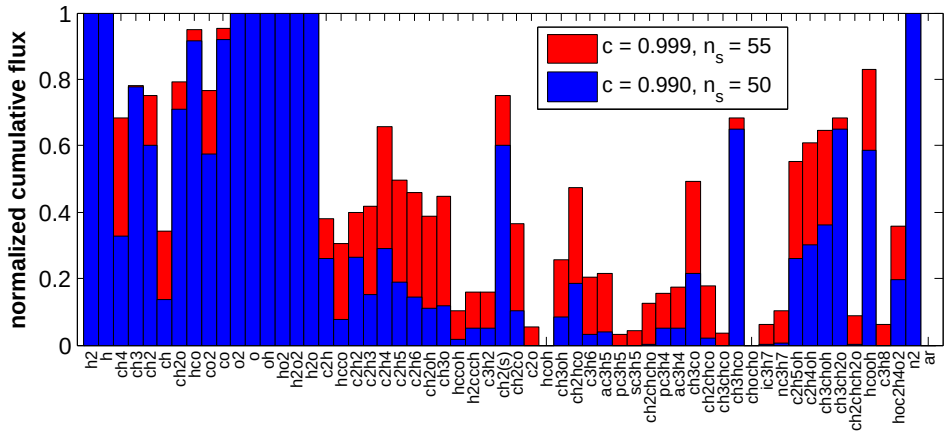

Figure 3.15: Species selection through EF analysis for an ethanol combustion mechanism (4): normalized cumulative fluxes for carbon and oxygen atoms over 18 operating conditions. Cut-off values: $c = 0.999$ and $c = 0.990$.

the overall flux indicator A_{jk}, for the species source-sink pair (j,k), is thus numerically integrated over the simulated time, and summed over the whole set of mechanism operating points n_c chosen for defining its desired validity range. The total flux of element A exchanged during the whole set of simulations is evaluated taking into account all the possible source-sink pairs, represented by the cartesian product of the species array with itself:

$$A_t = \sum_{j,k \in N_s \times N_s} A_{jk}. \tag{3.13}$$

The species selection is then made upon the analysis of the contribution of the element fluxes A_{jk} to the total flux A_t. The element fluxes are first sorted in decreasing order, and a cut-off value $c \in [0.0, 1.0]$ represents the fraction of total element flux chosen to be accounted for in the reduced mechanism. Only the species involved in the fluxes at the first n positions of the sorted flux array, n defined as the minimum number of positions for which the cumulative sum of their values reaches the total flux threshold, is retained in the reduced mechanism.

As an example to clarify this assumption, in Figure 3.15 the results of the EF analysis performed on an ethanol combustion mechanism (4) – used as a test in the present study – are presented. The sum of the element fluxes for carbon and oxygen atoms are plotted for each of the species contributing to the cutoff value. The values are normalised against the sum of the total exchanged element fluxes, as in Eq. 3.13. The figure shows that the species

which participate less to the total element fluxes are more likely to be deleted, as the cutoff value is decreased. For example, in the figure two different cutoffs – 99.9% and 99.0% of the total amount, respectively – are compared. The resulting selected numbers of species, having positive normalized contribution to the element flux, adds up to $n_s = 55$ and $n_s = 50$. A fixed contribution, equal to 1.0, is set to the whole set of species of the O-H system, which is assumed to always be present in every reduced combustion mechanism.

In the present mechanism reduction procedure, as illustrated in Figure 3.14, the EF analysis is called at each iterative step with a different cutoff value, in order to achieve the progressive deletion of the less important species. The initial cutoff value is set at $c = 99.9\%$, and at each following step it is decreased following a power law: $c(n+1) = c(n)^{1.1}$. This choice is motivated by the fact that, during the first optimization steps, the reduced mechanism still consists of a huge number of reactions: the number of variables to be optimized is high, thus either requiring unacceptably high computational times to carry on the optimization, or leading to a non negligible probability that the GA-based optimizer won't find the optimum solution in case a limited numbers of evolutionary steps and a narrow population size is considered.

4

Results and analysis

4.1 Ethanol

The methodology was tested through the development of a reduced mechanism for ethanol oxidation. As a starting mechanism for the reduction and optimization procedure, the mechanism developed by Marinov (4) was chosen. This mechanism consists of 58 species and 383 reactions, and has been validated against experimental data for high temperature oxidation (T > 1000K). In order to test the reliability of the reduction approach, a broader set of temperatures and equivalence ratios was chosen to define the validity range of the new mechanism. In particular, cases of interest to internal combustion engine simulations were chosen, resulting in a total of 18 different initial conditions with pressure values $p_0 \in \{2.0; 20.0\}\, bar$; mixture equivalence ratios $\phi_0 \in \{0.5; 1.0; 2.0\}$; temperatures $T_0 \in \{750; 1000; 1500\}\, K$. This set of operating conditions was kept fixed during the whole reduction and optimization procedure. Integration times for the constant pressure reactors were found for each of the cases after proper analysis, and set equal to 1.5 times the ignition delay period, where the ignition delay is defined as the time needed by the system to reach a 200K increase in temperature. Each of the integration intervals was then subdivided into a set of one thousand equally-spaced observation points for the following evaluation of the accuracy of the reduced mechanisms.

The reduction and optimization algorithm was then run setting an error tolerance in terms of a merit function value. The condition for carrying out a further reduction without the need for optimizing the Arrhenius parameters was set at $f > 3$, corresponding to a cumulative relative error – summed over the 18 cases (hence, 18000 observation points) – to be less than $5.0e-2$. The second part of the optimization, aimed at the calibration of the reduced mechanism against experimental ignition delay measurements, was run instead

Acronym	n_s	n_r	details
LLNL	58	383	Marinov, 1999 (4)
R	33	155	EF-analysis reduced only
RO	33	155	Reduced and optimized against LLNL
ROO	33	155	RO optimized against Curran, 1992 data (8)

Table 4.1: Description of the starting ethanol oxidation mechanism, and of the three reduced ones.

considering a different set of initial conditions, also spanning the range of available data. The measurements by Curran et al. (8) were used for dilute ethanol oxidation at stoichiometric equivalence ratio ($C_2H_5OH = 2.5\%, O_2 = 7.5\%$), at three different pressure values $p_0 = \{2.0, 3.0, 4.5\}\, bar$. For each pressure level, 20 different initial temperature conditions were considered, logarithmically spanning the range between 1100K and 1500K. Furthermore, the merit function was defined using the reciprocal of the global error, computed as the cumulative sum of the least squares comparisons between the simulated and experimental data over the three pressure levels considered.

The final reduced and optimized mechanism consisted of 33 species and 155 reactions. The computations lasted 9 hours on a personal computer running on a Core i7 860 CPU. The complete reaction scheme achieved is reported in the Appendix A.1. During the run, the algorithm performed a total of 9 mechanism reductions through element flux analysis, two genetic optimizations for calibration on the original LLNL mechanism, and one GA-based optimization for mechanism calibration against experimental ignition delay measurements. The following analysis of the results compares the behaviour of four different mechanisms: the full LLNL mechanism by Marinov, and three different reduced mechanisms with the same reactions, but with different reaction rate parameters. The first mechanism is the direct reduction of the LLNL mechanism through element flux analysis, and thus has its same Arrhenius parameters; the second reduced one is optimized to give the detailed mechanism's behaviour; the third one is further optimized against the experimental ignition delay measurements from Curran et al. (8). The acronyms adopted and the differences among them are summarized in Table 4.1.

Figure 4.1 shows the full comparison among mechanisms LLNL, R and RO at the eighteen initial conditions considered. For the sake of simplicity only the temperature traces

have been plotted, since they well represent the overall behaviour of the mechanism. In particular, it is observed that the simple reduction in the number of species through EF analysis cannot fit the broad range of operating conditions. As a matter of fact, the behaviour of mechanism R is never similar to that of the original mechanism, and it is closer to it only at low initial temperatures and low pressures. The optimized mechanism RO provides similar behaviour to that of the Livermore mechanism, where an excellent agreement is found especially at low initial temperatures. Furthermore, the predictiveness of the mechanism seems not to be affected by the change in pressure.
Figure 4.2 shows the history of the optimization ended in the generation of the RO mechanism: the optimum individual has an overall merit value $f = 18.532$, while the R mechanism, from which the GA-based optimization started, had $f = 2.678$; the maximum in merit value having been found by the genetic optimizer at generation 197. Values for the Arrhenius parameters of collision frequencies and activation energies are in the optimum mechanism different for each reaction, except for the set of reactions involving the basic species set as previously defined. In order to compare the values of the optimized RO mechanism with those of the reduced one, R, Figure 4.3 plots the relative variations of collision frequencies and activation energies in terms of relative differencies, $\varepsilon_r(A_i) = \left(A_i^{RO} - A_i^R\right)/A_i^R$ and $\varepsilon_r(E_i) = \left(E_i^{RO} - E_i^R\right)/E_i^R$. In particular, the variation in Arrhenius parameters reached the bounds of the collision frequency for 27.7% of the reactions, and of the activation energy for 10.2% of the reactions, showing that the optimum values led to a new mechanism whose parameters were close to those of the original. The average variation in the collision frequency was $\overline{\Delta A} = 22.86\%$, and $\overline{\Delta E} = 4.29\%$ the average variation in activation energies.

The results of the second optimization process are summarized in Figure 4.4. The comparison between LLNL and RO mechanisms shows that both mechanisms suffer a slight overestimation of the ignition delays especially at the lowest initial temperature values. The generation of the ROO mechanism, optimized with the available set of experimental data, plotted in Figure 4.4 b), shows that this overestimation is completely solved after the optimization procedure.

4.1.1 Application to HCCI engine simulations

As evidence of the predictive capability of the reduced mechanism, it was applied for modeling the combustion of an ethanol-air mixture in a HCCI-operated internal combustion en-

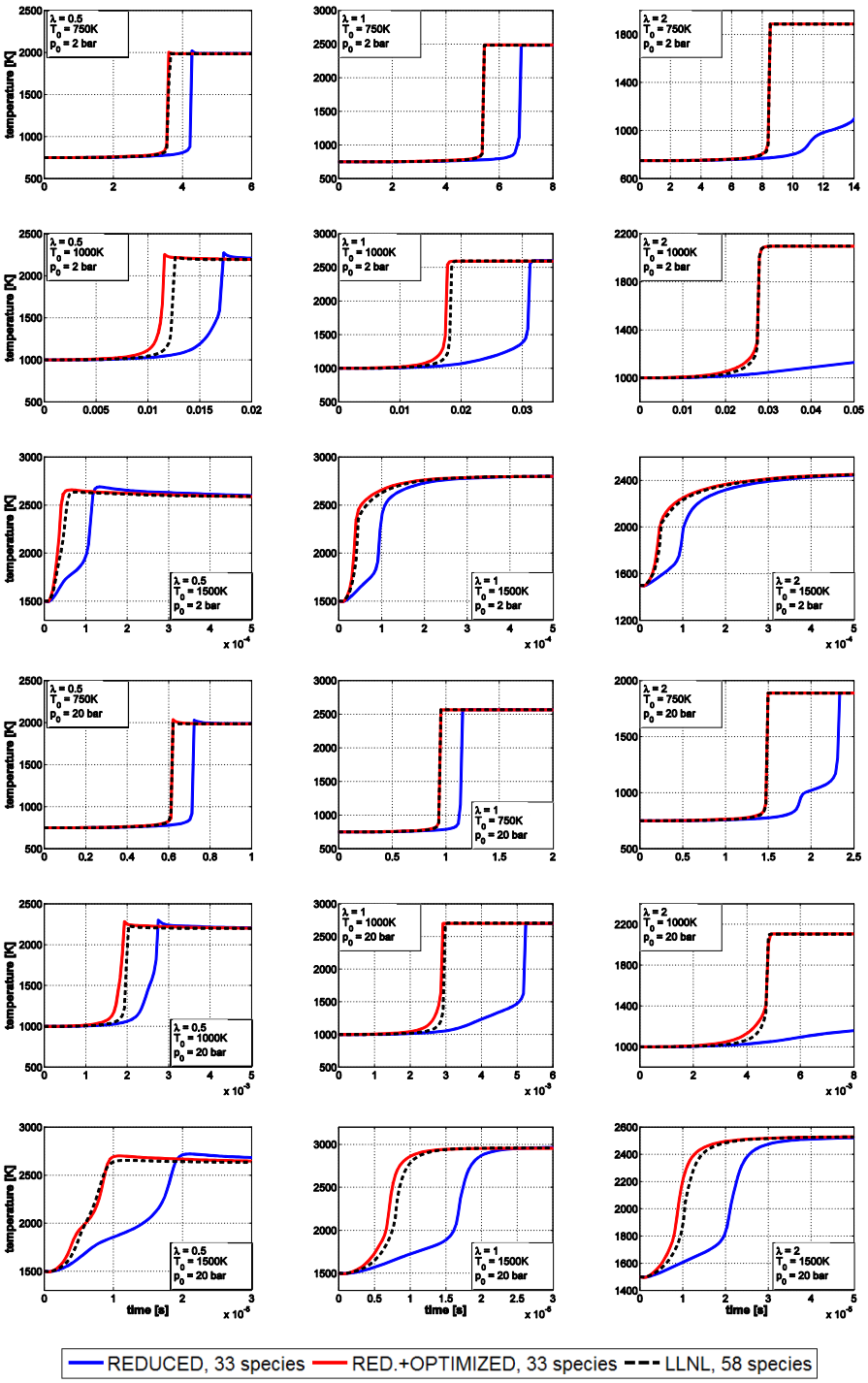

Figure 4.1: Temperature profiles simulated at the 18 operating conditions chosen for ethanol mechanism reduction. Comparison among LLNL, R and RO mechanisms.

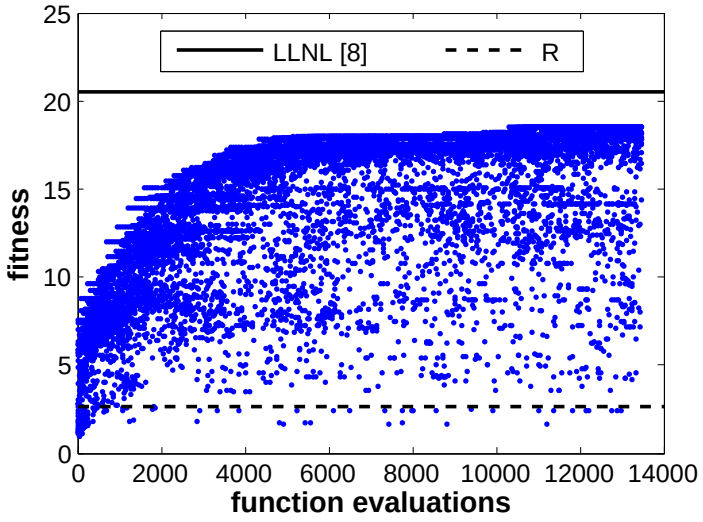

Figure 4.2: Evolution of the individuals' merit value during GA-based optimization over the 33 species, 155 reactions reduced mechanism.

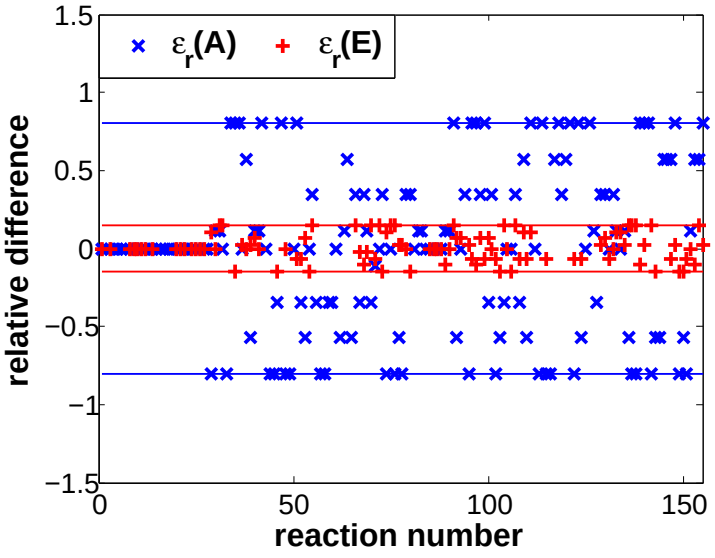

Figure 4.3: Relative differences of the optimized Arrhenius parameters in mechanism RO, in comparison with constants in the original LLNL mechanism (4).

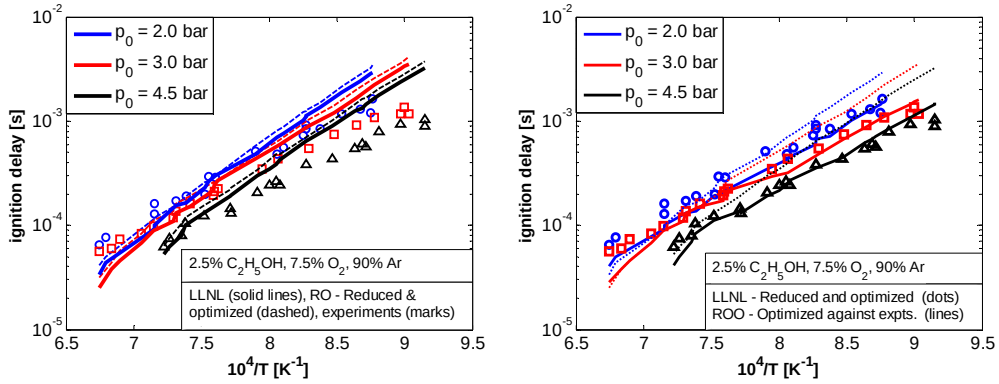

Figure 4.4: Comparison among predicted and experimental (8) ignition delays for dilute stoichiometric ethanol-oxygen mixtures. a) Left: comparison between LLNL and RO mechanisms; b) Right: comparison between LLNL and ROO mechanisms.

gine. The simulation model is a zero-dimensional, adiabatic, single-cylinder HCCI research engine, with 14:1 compression ratio, running at 1200 rpm. Detailed specifications of the slider-crank mechanism can be found in (9). Two baseline cases were considered, both at initial mixture equivalence ratio $\phi = 0.4$, and with different initial temperatures, $T_0 = 437K$ and $T_0 = 424K$. These reference conditions correspond to the Sandia experiments. Figures 4.5 and 4.6 show the comparison among the 4 mechanisms – namely, full Livermore (LLNL), EF-reduced (R), reduced and optimized (RO), optimized against experimental ignition delays (ROO) – in terms of pressure history, plus histories of the most important species. Figure 4.5 shows good agreement between the full Livermore's mechanism and the reduced and optimized one, while the simple reduction based on EF analysis fails to predict mixture ignition at these conditions. Concerning the ROO mechanism, it shows slightly earlier mixture ignition, in agreement with the results of the final optimization where the ignition delay predictions tended to earlier ignition especially when starting from the lowest temperature values. Similar behaviour is observed in the $T_0 = 424K$ case, as in Figure 4.6. The only difference is that the LLNL mechanism failed to predict mixture ignition. The two reduced and optimized mechanisms showed less dependence on the initial mixture temperature, as the ignition delays predicted were consistent with those observed in Figure 4.5.

Figure 4.7 displays the behaviour of the mechanisms when doubling the in-cylinder pressure at intake valve closure. The same two initial temperature values as in the baseline cases

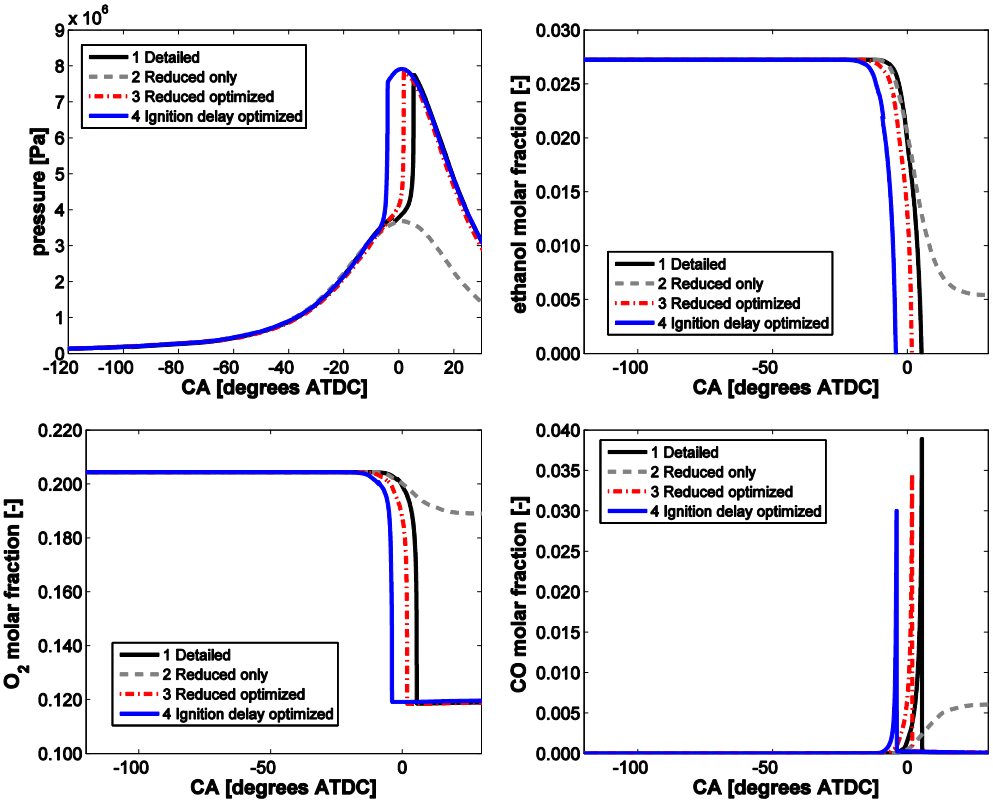

Figure 4.5: Simulation of baseline case 1 for the HCCI Sandia engine (9): $\phi_0 = 0.40$, $T_0 = 437K$.

were considered. Here, all the mechanisms show consistent behaviour. The LLNL mechanism is able to predict ignition even at the lower initial temperature, thus showing the mechanism's sensitivity to pressure; the R mechanism still is not able to predict ignition at both temperatures. In Figure 4.8, the first baseline case ($T_0 = 437K$) is operated with equivalence ratios leaner – $\phi_0 = 0.25$ – and richer – $\phi_0 = 0.70$ – than the original case. The same behaviour seen in the two baseline cases is observed, proving that the mechanisms show less dependence on mixture composition than on temperature and pressure. Finally, Figure 4.9 shows the results of multidimensional simulations carried out using the KIVA-4 code (109) coupled with detailed chemistry: the ROO mechanism agrees well with the experiments at both cases.

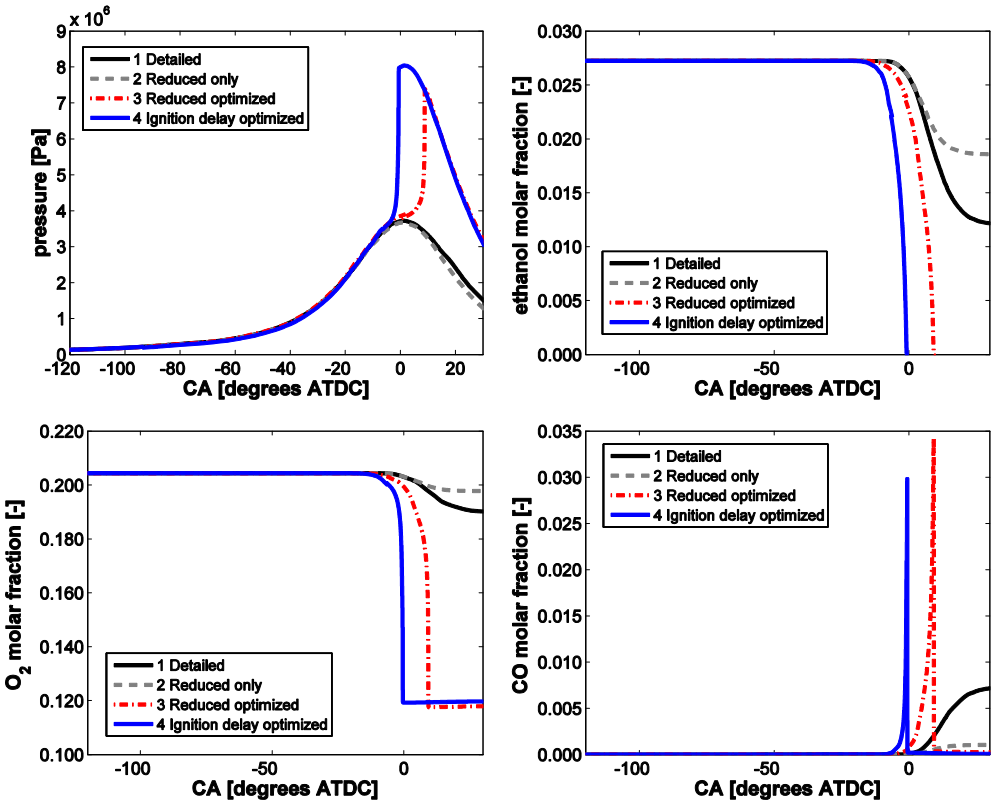

Figure 4.6: Simulation of baseline case 2 for the HCCI Sandia engine (9): $\phi_0 = 0.40$, $T_0 = 424K$.

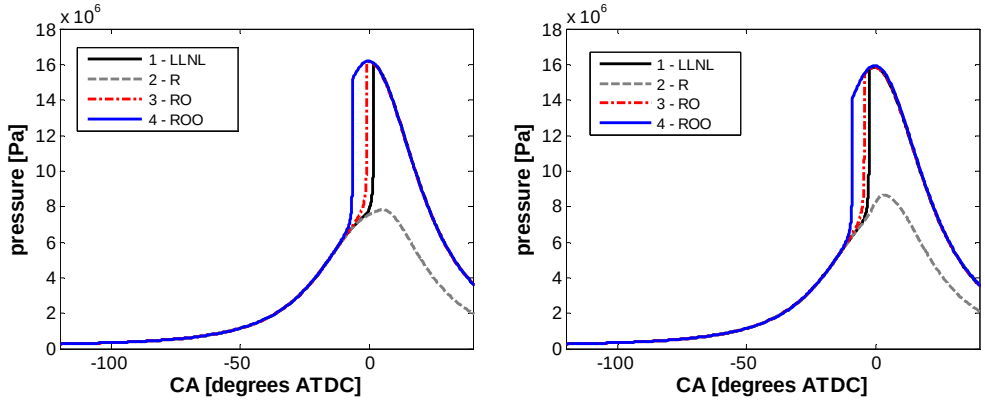

Figure 4.7: Simulation of the HCCI cases with doubled IVC pressure; initial temperatures: 437K (left), 424K (right).

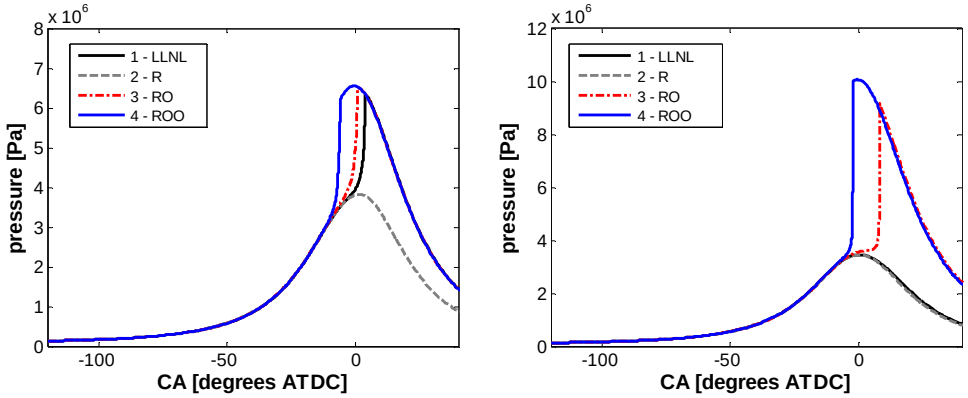

Figure 4.8: Simulation of the baseline HCCI case 1 with modified mixture equivalence ratios: $\phi = 0.25$ (left) and $\phi = 0.70$ (right).

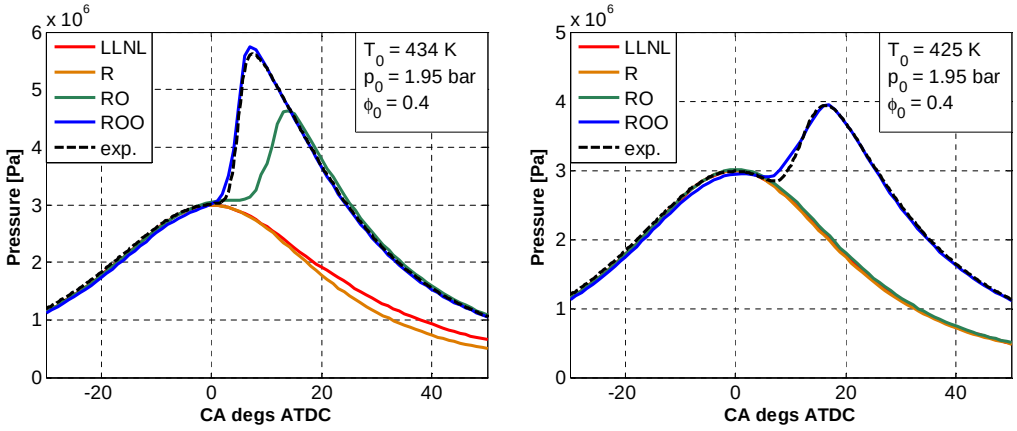

Figure 4.9: Comparison between multidimensional simulations and experimental data about the two baseline cases considered.

4.2 Biodiesel

4.2.1 Methyl butanoate (MB)

As a second test bench for the mechanism reduction procedure, kinetic modelling of biodiesel compounds has been chosen. In particular, two different detailed reaction mechanisms, developed at LLNL, and concerning methyl-butanoate (MB) and methyl-decanoate (MD) combustion have been chosen as the reference ones for biodiesel. The two mechanisms (10; 31) respectively consist of 264 species and 1219 reactions (MB), and 2878 species and 8555 reactions (MD). The dimension of these mechanisms is greater of at least one order of magnitude than the ethanol reaction mechanism over which the reduction and optimization methodology has been firstly tested. For these reasons, the genetic optimization code has been modified in order to accomplish for parallel computations of the individuals, thus allowing reduced CPU time needs on a computing cluster with quad-core nodes. The first optimization procedure was run on the MB mechanism, and stopped after 8 reduction + optimization iterations, yielding a reduced mechanism made of 58 species and 245 reactions. A schematic of the statistics of the iterative procedure is shown in Figure 4.10: on the left size, it is possible to observe that the logaritm-based law for decreasing the element flux cutoff value resulted in an almost logarithm-shaped decrease in the number of reactions and species, as the iterations proceeded; furthermore, a proportional increase in the number and in the size of the populations to be considered during the genetic optimization was set, in order to accomplish for the increasing distance of the starting reduced mechanism from the full one. While all of the optimizations from iteration 4 to iteration 7 were able to strongly improve the reduced mechanism performance, improving their fitness values by more than one order of magnitude, the last optimization, at 42 species and 146 reaction values, wasn't able to introduce a suitable optimized mechanism. Since the size of the latest valid mechanism was judged as too big for practical usefulness, a second algorithmic procedure was established, starting from that mechanism, but still considering the solution of the full mechanism as the reference for the evaluation of the fitness function. During this second algorithmic procedure, whose results have been shown in Figure 4.10 b), 5 more iterations were carried out, achieving a final reduced and optimized mechanism made of 45 species and 179 reactions. This final mechanism was characterized by a merit value of 21.1447, similar to the value of the first reduced mechanism made of 134 species and 710 reactions.

Fuel	Ref.	n_s	n_r	p_i [bar]	ϕ_i [-]	T_i [K]
MB	(10)	264	1219	2.0; 20.0	0.75; 1.0; 2.0	750; 1000; 1500
MD	(31)	2878	8555	2.0; 20.0	0.75; 1.0; 2.0	750; 1000; 1500

Table 4.2: Reaction conditions considered for the mechanism reduction and optimization of biodiesel compounds.

In the detail of the temperature histories of Figure 4.11, the 'reduced only' mechanism is the mechanism which consists of a subset of species and reactions of the optimal one achieved during the first of the two algorithmic procedures carried out. It is encouraging to notice that simply reducing the number of species and reactions tends to shorten the ignition delay times, while after the effects of the optimization the ignition delays are much more similar to the values predicted by the full mechanism. Thus, the methodology appears able to supply for the lack of resolution in low-temperature chemistry. As a matter of fact, this effect is almost not needed at the lowest initial temperature values ($T = 750K$), while it becomes significant at the highest temperature levels. Furthermore, the optimized mechanism appears to well correct the prediction errors which arise, after the reduction only, especially at the leaner mixture compositions, which need wider simulation times.

A full comparison with the experimental ignition delay measurements by Dooley et al. (10) is presented in Figure 4.12. The measurements have been conducted on dilute methyl butanoate – oxygen mixtures in Argon, at different equivalence ratios and behind reflected shock wave pressures of 1 atm and 4 atm. In particular, in Figure 4.12 a) it is possible to notice that the original MB mechanism from LLNL does provide accurate ignition delay estimations. The observated predictions are quite deteriorated for the reduced and optimized mechanism. The final mechanism, which arises from the optimization against these data, shows instead excellent agreement with the experimental points at all the compositions and at both pressure levels. The predictions seem even better than the original MB mechanism especially for the lean mixture cases. These results confirm the reliability of the procedure as already observed for the Ethanol mechanism, and prove its ability to correctly generate reduced and optimized reaction mechanisms also per huge starting mechanism dimensions.

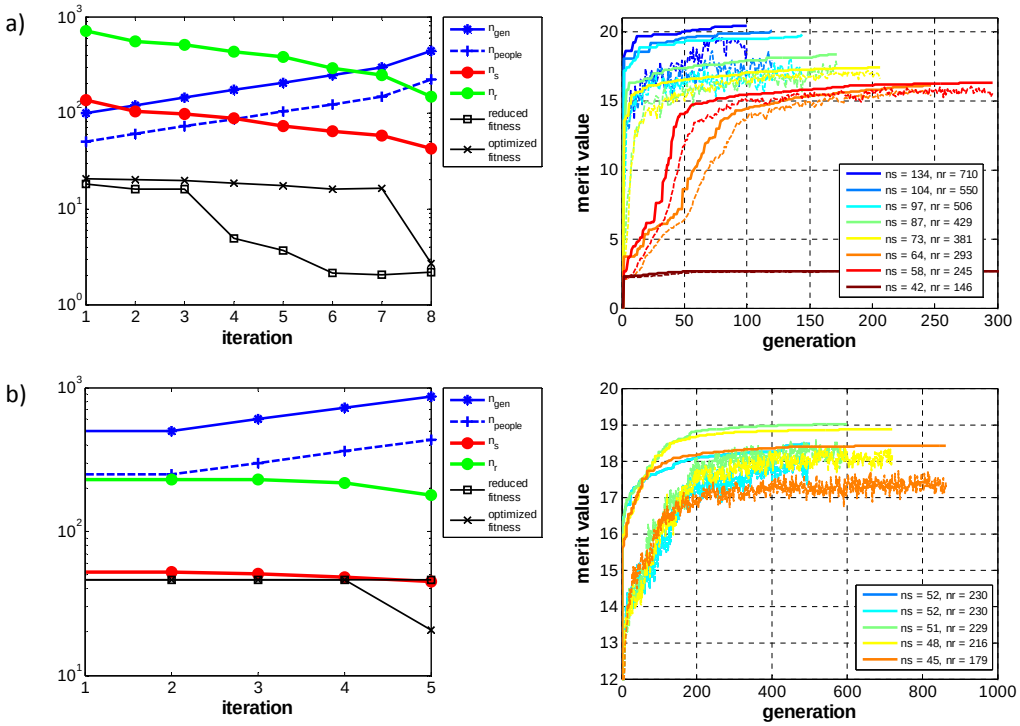

Figure 4.10: MB mechanism reduction and optimization history. Left: mechanism features per iteration. Right: Optimization maximum (solid lines) and average (dashed lines) population fitness values.

4.2.2 Methyl Decanoate (MD)

A similar procedure has been applied to a detailed mechanism for methyl decanoate combustion, originally developed at LLNL (31), and consisting of 2878 species and 8555 reactions. Due to the huge dimensions of the mechanism, the algorithmic implementation has been slightly modified in order to account for the huge computational needs that even the evaluation a single reactor condition requires. For this reason, a first mechanism reduction only, not followed by a corresponding optimization for calibrating reaction rate parameters, has been applied to the original mechanism in order to achieve a reduced set of species and reactions of practical usefulness. In particular, a first cutoff value of 90% the total element flux amount has been applied, resulting in a reduced set of 186 species and 357 reactions, this generating a mechanism of medium size (more or less similar to the original size of Marinov's ethanol one). Then, the standard mechanism reduction and optimization proce-

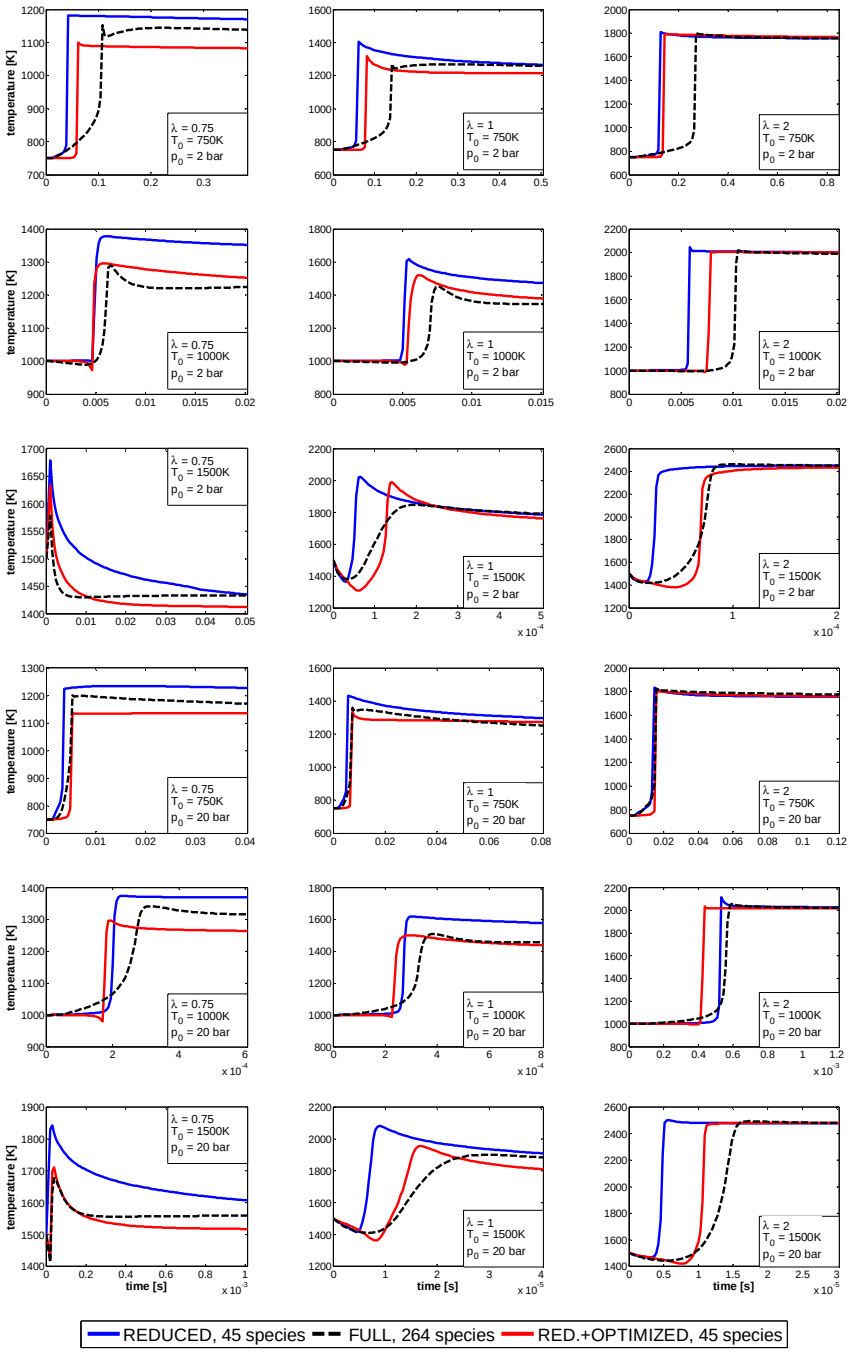

Figure 4.11: Temperature profiles simulated at the 18 operating conditions chosen for MB mechanism reduction. Comparison among full, reduced and reduced+optimized mechanisms.

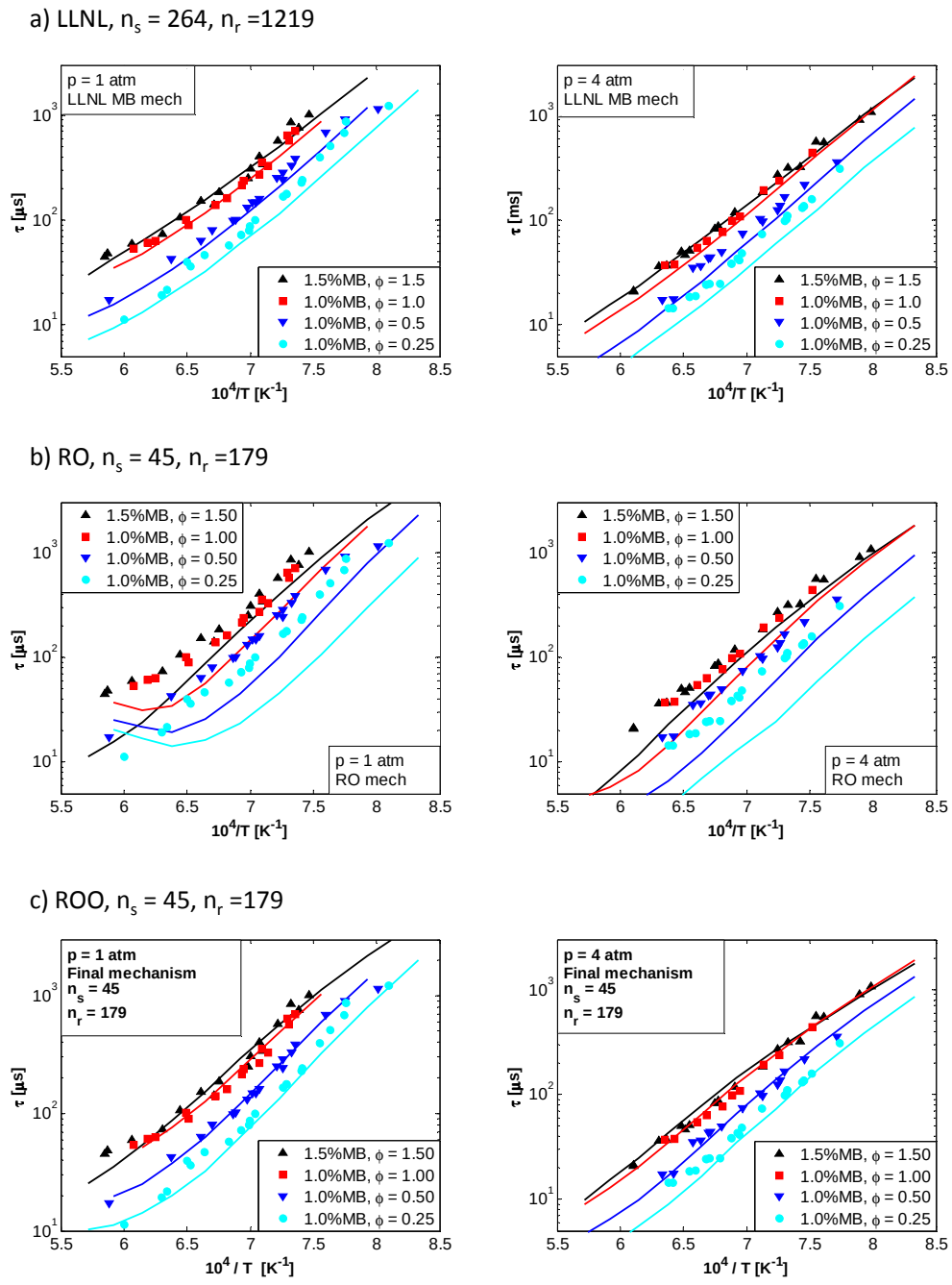

Figure 4.12: Comparison among predicted and experimental (10) ignition delay measurements, at reactor pressures p = 1 atm and p = 4 atm. a) full LLNL mechanism; b) reduced and optimized mechanism; c) mechanism further optimized against experimental data.

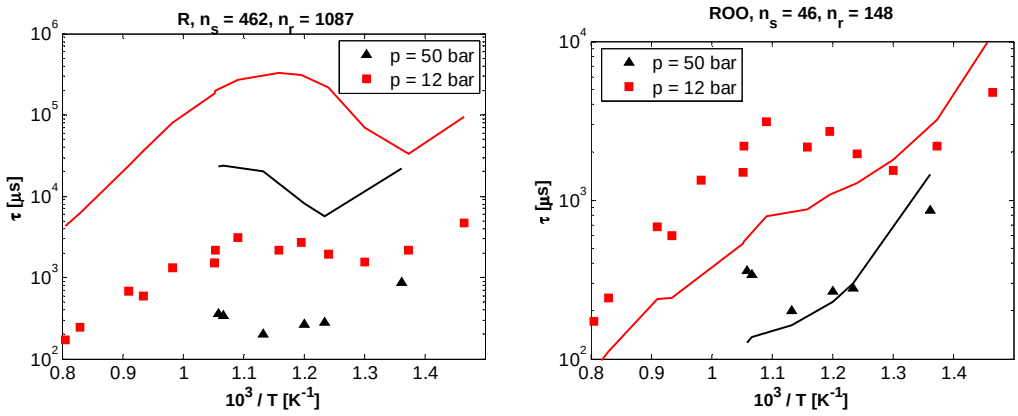

Figure 4.13: Comparison among predicted and experimental (11) ignition delay measurements, at reactor pressures p = 12 bar and p = 50 bar. left) medium-size, reduced LLNL mechanism; right) reduced mechanism optimized against experimental data.

dure has been started, though increasing the average optimization parameters in order to comply with the fact that the first huge reduction hadn't been followed by gradual optimization steps.

After the end of the reduction and optimization procedure, a final skeletal mechanism has been obtained, consisting of 64 species and 148 reactions. Experimental data in terms of ignition delay measurements of dilute methyl-decanoate – oxygen mixture weren't available, due to the fact that research in this field is very recent, and the only public efforts in this direction are currently in progress through specific facilities for low-vapor-pressure fuels at Stanford University (195). For this reason, as usual in literature (196), the mechanism performance has been evaluated in comparison with experimental data of stoichiometric n-decane – air mixtures at elevated pressures (11).

The optimization has been carried out considering the operating conditions corresponding to the experimental ignition delay measurement points in Reference (11). Figure 4.13 shows the comparison among a mid-size, reduced MD mechanism and the newly generated optimized mechanism. The first one corresponds to the shrinking of the original LLNL mechanism, where the reduction has been carried out through EF analysis at a cut-off value $c = 0.90$. This choice has been motivated by the excessive computational requirements that the full mechanism would have implied over the whole set of simulations. This anyway big mechanism showed to fail average ignition delay measurements by almost two orders of magnitude in time. The tiny, reduced mechanism consisting of 46 species and 148 reac-

tions however proved to yield results in the same order of magnitude, where pretty good agreement was observed especially at the highest reflected wave pressure value, while at low pressure the mechanism tended to underpredict ignition, as it can be inferred that the limited reaction set isn't able to fully reproduce slow timescale chemistry. Overall, also in this case the methodology showed to provide a useful tool for mechanism reduction, where an impressive degree of reduction was achieved, of about two orders of magnitude in both number of mechanism species and reactions.

5

Conclusions and Outlook

5.1 Summary

The research activity carried out during this Ph.D. has focused on the development of novel methodologies devoted to the efficient simulation of practical combustion systems, such as internal combustion engines, especially tailored for reacting environment involving large hydrocarbons and FAME. In this respect, particular attention has been paid to the simulation of combustion of mixtures with biofuels surrogates, as the need for cleaner engines is now facing the need to gradually substitute petroleum-derived fuels.

In this context, the first research effort has been spent to the development of an efficient solution environment for reaction chemistry. In particular, a vectorized code for the simulation and the analysis of combustion systems has been developed. The code features a framework for the evaluation of thermodynamic properties of pure species and of gaseous mixtures; and packages for the simulation of zero-dimensional batch reactors at constant pressure or constant volume, as well as internal combustion engine models. The code has been implemented in both Matlab and FORTRAN languages, and validated against sets of experimental data available in the open literature, concerning shock-tube ignition delay times, as well as internal combustion engine simulations. Finally, the routines have been coupled to a standard version of KIVA-4, providing detailed chemistry capabilities to the code; the chemistry solution has been parallelised adopting a shared memory paradigm.

The following major achievements obtained in comparison to the literature have been observed:

- The choice of a matrix-based code allowed efficient computations to be carried out: in particular, as far as the FORTRAN implementation is concerned, an increased computational efficiency was achieved by the adoption of libraries for full and sparse matrix based algebra; moreover, for maximum computational efficiency, the code can be linked to the architecture-tailored versions available on the internet (122; 123), or even can be tailored for GPU computation;

- The Matlab implementation showed overall computing times of the same order of magnitude as the compiled FORTRAN simulations; furthermore, the fully vectorized structure of the Matlab code can make it particularly suitable for the analysis, optimization and reduction of combustion mechanisms;

- Among the tested solvers, DVODE showed to have the best overall performance in terms of computing times;

- The performance of the solvers was consistent across the three different combustion mechanism tested, thus showing the efficiency of the vectorized implementation of the code; the time requirements were observed to increase linearly with the number of reactions;

- Coupling of the code with KIVA-4 provided an accurate and efficient tool for the multidimensional simulation of internal combustion engines; evidence of the reliability of the results has been provided by both an HCCI combustion case, where chemistry rules over combustion, and thus an accurate library for the estimation of finite-rate kinetics is mandatory;

- Modelling of a direct injected diesel engine of current production through the parallel KIVA4-CHEM code showed to yield pretty accurate results in terms of average in-cylinder pressure traces, even with limited computational resources;

- The OpenMP paradigm allowed the chemistry routine of the KIVA-4 code to be easily made multithreaded, with a significant reduction in computing times; in the opinion of the authors, this choice is particularly suitable for tailoring the code to engine optimization: even if the shared memory implementation doesn't allow the code to run on more than one machine, the time needed for exchanging information among the threads is minimised, as no ethernet bottleneck is present; thus, optimizations which

feature one multithreaded simulation per machine of the computing cluster can maximise the overall computational efficiency.

The new idea of reducing reaction mechanisms and gradually optimizing their reaction rate parameters requires huge computational efforts. For this reason, further efforts have been spent for the development of an extremely efficient ODE solver, tailored for chemical kinetics. In particular, a solver relying on the time scale separation assumption (TSSA) has been developed and tested. The idea behind this is to enable explicit integration to be carried out even at highly stiff systems, such as those characterizing combustion chemistry. This is even more true when considering reduced reaction mechanisms, where the stiffness of the system is usually extreme, as few reactions need to take into account the whole set of system timescales. Thus, the explicit integration can be allowed by assuming a peculiar integration timestep per each system variable, estimated in terms of residence time through a simple linearization analysis of the system at the current time. The species with lowest characteristic timescales are thus integrated with a small timestep, and early extincted, so that the stiffness of the ODE system is more reduced as the integration proceeds. This procedure has been developed and tested onto two reduced reaction mechanisms of average dimensions, in order to assess its efficiency at the most usual conditions during practical computations of reactive systems. After the analysis, the following conclusions have been drawn:

- The solver showed good accuracy in comparison with the commonly adopted VODE solver, also showing that it was consistent over a range of sampling intervals;
- Significant speedup factors were achieved especially at the lowest time sampling intervals, less than $10^{-6}s$, as usually occurs during practical internal combustion engine simulations; the speedup were higher at the larger mechanism, thus enabling more complete reaction mechanisms to be considered in practical computations, avoiding CPU time blowups;
- The TSSA solver was coupled with the KIVA-4 code, and tested over both HCCI and DI diesel combustion simulations. In both cases, high degrees of accuracy were seen in comparison with the previously validated solutions of DVODE; the HCCI case required about 70% less computational time, and similar speedups were observed at the DI diesel simulations, which allowed – with respect to the DVODE – larger timesteps

during the crank angle degrees of maximum heat release, without the risk of the solver to fail convergence.

Once that all the set of tools allowed reaction chemistry computations with maximum efficiency, focus has been posed onto the true object of the present Ph.D., i.e. the development of a new methodology for the development of reduced reaction mechanisms from detailed ones, with extended validity ranges and with maximum computational efficiency at all the reactive conditions which are usually experienced during the simulation of practical combustion systems. As a matter of fact, the new methodology relies on an iterative procedure, which features the progressive reduction in the mechanism dimensions, through selecting subsets of species and reactions identified through the element flux analysis (EF) method. At each mechanism reduction step, the accuracy of the mechanism is assessed by comparison with the detailed one over a huge set of reactor conditions, at low and high pressure values. If the reduced mechanism doesn't fit an imposed accuracy constraint, many of its reaction rate parameters are calibrated by means of a genetic algorithm, in order to account for the deleted reaction pathways into the surviving reactions. The physical soundness of the mechanism is mantained by the fact that the ranges over which the reaction rate constants are calibrated have been defined after the analysis of the actual uncertainty observed in experimental and numerically-derived reaction rates for large hydrocarbons available in the literature.
The methodology was applied to three detailed reaction mechanisms, of – respectively – medium, large and huge sizes, accounting for about 400 up to about 10 000 reactions. The three mechanisms, developed at Lawrence Livermore National Laboratories, describe the combustion of ethanol and of two fatty acid methyl esters, important surrogates for biodiesel: methyl-butanoate (MB, $C_5H_10O_2$), methyl ester of butyric acid, and methyl-decanoate (MD, $C_11H_22O_2$). After the reduction, three novel mechanisms of about 150-300 reactions were developed. Among the most important achievements obtained through the newly developed methodology, the following have been summed up:

- Genetic-algorithm-based optimization proved to be really suitable for this kind of problem, where the optimization space is huge and characterized by thousands of variables. In this context, the developed tool, relying on binary-coded chromosomes, allowed small computational times, which added up to about 1-2 days per optimization step;

- The advantage of the iterative procedure is that the optimization is likely to reach the optimum value even with a limited number of merit function evaluations, when compared to the approach of including all possible values of the variables to be optimized;
- The element-flux analysis allowed the subset of species and reactions to be evaluated not instantly, but averaging a wide horizon of reactive conditions, experienced over the whole set of 18 reactor conditions simulated per mechanism;
- The algorithm implementation requested analytical definitions of the reduced mechanism accuracy and of the error tolerance constraint. This made the procedure rigorous and robust, with almost no action from the user. This is the exact opposite of common manual, systematic reduction methodologies which require huge efforts from the scientist to analyse reaction pathways and sensitivity analysis data.
- An innovative feature, which has been introduced for strengthening the physical soundness of the developed models, has been the optimization in comparison to experimental data available in the literature. The reduced mechanisms showed to have similar behaviour in comparison with the detailed ones, and sometimes showed better accuracy in the prediction of the ignition delays at the experimental shock tube conditions.
- The mechanisms obtained in the end proved to have a high degree of accuracy also when considered into internal combustion engine simulations, enabling accurate solutions with detailed chemistry to be achieved in limited computational times.

5.2 Recommendations for future work

No research effort can be considered as concluded, and also in this case the study has highlighted many points to go into in more depth. First of all the last step of the optimization procedure showed that is is much beneficial to the reduced mechanism to be compared with experimental measurements. However, only ignition delay times have been considered. A further research effort would be needed including cases where not only chemical kinetics are present, but also transport effects are non negligible, such as in case of laminar flame computations. Then, the application of the methodology could be studied for the generation of multi-component reaction mechanisms: one may think of generating a set of skeletal mechanisms for species groups, and then combine them into a unique mechanism, finally optimizing the whole one in comparison with experimental data concerning the different sets of species. This procedure would allow reliable mechanisms to be generates, and reactivity-controlled combustion systems to be simulated, thus accelerating research in this field. Also for the code numerics, a lot of research still needs to be done for identifying different reactive conditions, for choosing each time the most appropriate solver, and for better managing matrices and matrix storage.

Il tombe enfin!... et se relève roi!

V. Hugo

Appendices

A

Reaction mechanisms

A.1 Ethanol ignition

No.	Reaction	A	b	E
1.	$H_2 + OH <=> H + H_2O$	+2.140e+008	1.52	+3.449e+003
2.	$O + OH <=> H + O_2$	+2.020e+014	-0.40	+0.000e+000
3.	$H_2 + O <=> H + OH$	+5.060e+004	2.67	+6.290e+003
4.	$H + O_2(+M) <=> HO_2(+M)$	+4.520e+013	0.00	+0.000e+000
	LOW / +1.05e+019 -1.26 +0.00e+000 /			
	Enhanced third-body efficiencies:			
	H_2/0.00/ CH_4/10.00/ CO_2/3.80/ CO/1.90/ H_2O/0.00/ N_2/0.00/			
5.	$H + O_2(+N_2) <=> HO_2(+N_2)$	+4.520e+013	0.00	+0.000e+000
	LOW / +2.03e+020 -1.59 +0.00e+000 /			
6.	$H + O_2(+H_2) <=> HO_2(+H_2)$	+4.520e+013	0.00	+0.000e+000
	LOW / +1.52e+019 -1.13 +0.00e+000 /			
7.	$H + O_2(+H_2O) <=> HO_2(+H_2O)$	+4.520e+013	0.00	+0.000e+000
	LOW / +2.10e+023 -2.44 +0.00e+000 /			
8.	$OH + HO_2 <=> O_2 + H_2O$	+2.130e+028	-4.83	+3.500e+003
	(Duplicate reaction)			
9.	$OH + HO_2 <=> O_2 + H_2O$	+9.100e+014	0.00	+1.096e+004
	(Duplicate reaction)			
10.	$H + HO_2 <=> 2OH$	+1.500e+014	0.00	+1.000e+003
11.	$H + HO_2 <=> H_2 + O_2$	+6.630e+013	0.00	+2.126e+003
12.	$H + HO_2 <=> O + H_2O$	+3.010e+013	0.00	+1.721e+003
13.	$O + HO_2 <=> O_2 + OH$	+3.250e+013	0.00	+0.000e+000
14.	$2OH <=> O + H_2O$	+3.570e+004	2.40	-2.112e+003
15.	$2H <=> H_2$	+1.000e+018	-1.00	+0.000e+000
16.	$H_2 + 2H <=> 2H_2$	+9.200e+016	-0.60	+0.000e+000
17.	$2H + H_2O <=> H_2 + H_2O$	+6.000e+019	-1.25	+0.000e+000
18.	$H + OH <=> H_2O$	+2.210e+022	-2.00	+0.000e+000
19.	$H + O <=> OH$	+4.710e+018	-1.00	+0.000e+000

20.	$2O <=> O_2$	+1.890e+013	0.00	-1.788e+003
21.	$2HO_2 <=> O_2 + H_2O_2$	+4.200e+014	0.00	+1.198e+004
	(Duplicate reaction)			
22.	$2HO_2 <=> O_2 + H_2O_2$	+1.300e+011	0.00	-1.629e+003
	(Duplicate reaction)			
23.	$2OH(+M) <=> H_2O_2(+M)$	+1.240e+014	-0.37	+0.000e+000
	LOW / +3.04e+030 -4.63 +2.05e+003 /			
	TROE / +4.70e-001 +1.00e+002 +2.00e+003 +1.00e+015 /			
24.	$H + H_2O_2 <=> H_2 + HO_2$	+1.980e+006	2.00	+2.435e+003
25.	$H + H_2O_2 <=> OH + H_2O$	+3.070e+013	0.00	+4.217e+003
26.	$O + H_2O_2 <=> OH + HO_2$	+9.550e+006	2.00	+3.970e+003
27.	$OH + H_2O_2 <=> HO_2 + H_2O$	+2.400e+000	4.04	-2.162e+003
28.	$H + CH_3(+M) <=> CH_4(+M)$	+2.140e+015	-0.40	+4.286e+000
	LOW / +3.31e+030 -4.00 +2.11e+003 /			
	TROE / +0.00e+000 +1.00e-015 +1.00e-015 +4.00e+001 /			
	Enhanced third-body efficiencies:			
	H_2/2.00/ CO_2/3.00/ CO/2.00/ H_2O/5.00/			
29.	$H + CH_4 <=> H_2 + CH_3$	+6.914e+003	3.00	+9.875e+003
30.	$CH_4 + OH <=> CH_3 + H_2O$	+5.148e+006	2.00	+2.547e+003
31.	$CH_4 + O <=> CH_3 + OH$	+8.502e+008	1.56	+9.940e+003
32.	$CH_4 + HO_2 <=> CH_3 + H_2O_2$	+1.120e+013	0.00	+2.886e+004
33.	$CH_3 + HO_2 <=> CH_4 + O_2$	+9.429e+011	0.00	+4.286e+000
34.	$CH_3 + O <=> H + CH_2O$	+1.531e+014	0.00	+0.000e+000
35.	$CH_3 + O_2 <=> CH_2O + OH$	+4.805e+011	0.00	+1.276e+004
36.	$H + CH_2OH <=> CH_3 + OH$	+1.914e+013	0.00	+1.429e+000
37.	$CH_3 + OH <=> H_2O + CH_2(S)$	+2.000e+013	0.00	+5.736e+002
38.	$CH_3 + OH <=> CH_2 + H_2O$	+5.057e+006	2.00	+2.500e+003
39.	$H + CH_3 <=> H_2 + CH_2$	+4.886e+013	0.00	+1.575e+004
40.	$CH_3 <=> H + CH_2$	+2.334e+016	0.00	+9.925e+004
41.	$H + CH_2O(+M) <=> CH_2OH(+M)$	+6.634e+011	0.45	+3.600e+003
	LOW / +9.10e+031 -4.82 +6.53e+003 /			
	TROE / +7.19e-001 +1.03e+002 +1.29e+003 +4.16e+003 /			
	Enhanced third-body efficiencies:			
	H_2O/5.00/			
42.	$H + CH_2OH <=> H_2 + CH_2O$	+3.829e+013	0.00	+1.429e+000
43.	$OH + CH_2OH <=> CH_2O + H_2O$	+1.000e+013	0.00	+7.143e+000
44.	$O + CH_2OH <=> CH_2O + OH$	+3.143e+012	0.00	+4.286e+000
45.	$O_2 + CH_2OH <=> CH_2O + HO_2$	+4.934e+014	-1.00	+2.857e+000
	(Duplicate reaction)			
46.	$O_2 + CH_2OH <=> CH_2O + HO_2$	+5.577e+013	0.00	+3.117e+003
	(Duplicate reaction)			
47.	$CH_2 + OH <=> H + CH_2O$	+4.786e+013	0.00	+1.429e+000
48.	$CH_2 + CO_2 <=> CH_2O + CO$	+3.457e+010	0.00	+1.000e+003

49.	$CH_2 + O <=> 2H + CO$	+1.571e+013	0.00	+1.429e+000
50.	$CH_2 + O <=> H_2 + CO$	+3.000e+013	0.00	+7.143e+000
51.	$CH_2 + O_2 <=> CH_2O + O$	+6.298e+021	-3.30	+2.745e+003
52.	$CH_2 + O_2 <=> 2H + CO_2$	+2.538e+021	-3.30	+2.745e+003
53.	$CH_2 + O_2 <=> H_2 + CO_2$	+5.483e+020	-3.30	+1.637e+003
54.	$CH_2 + O_2 <=> CO + H_2O$	+7.280e+019	-2.54	+1.576e+003
55.	$CH_2 + O_2 <=> HCO + OH$	+1.880e+020	-3.30	+3.327e+002
56.	$CH_3 + CH_2 <=> H + C_2H_4$	+3.086e+013	0.00	+2.857e+000
57.	$2CH_2 <=> 2H + C_2H_2$	+1.257e+013	0.00	+0.000e+000
58.	$CH_2(S) <=> CH_2$	+3.143e+012	0.00	+5.714e+000
59.	$CH_4 + CH_2(S) <=> 2CH_3$	+3.086e+013	0.00	+1.000e+001
60.	$O_2 + CH_2(S) <=> H + CO + OH$	+5.400e+013	0.00	+5.714e+000
61.	$H_2 + CH_2(S) <=> H + CH_3$	+7.000e+013	0.00	+0.000e+000
62.	$O + CH_2(S) <=> 2H + CO$	+1.629e+013	0.00	+1.000e+001
63.	$OH + CH_2(S) <=> H + CH_2O$	+3.686e+013	0.00	+1.000e+001
64.	$CO_2 + CH_2(S) <=> CH_2O + CO$	+5.057e+012	0.00	+4.286e+000
65.	$CH_3 + CH_2(S) <=> H + C_2H_4$	+1.086e+013	0.00	+1.000e+001
66.	$HCOOH <=> CO + H_2O$	+3.045e+014	0.00	+4.733e+004
67.	$HCOOH <=> H_2 + CO_2$	+1.041e+015	0.00	+6.060e+004
68.	$OH + HCOOH <=> H + CO_2 + H_2O$	+3.818e+006	2.06	+8.375e+002
69.	$OH + HCOOH <=> CO + OH + H_2O$	+2.273e+007	1.50	-9.620e+002
70.	$H + HCOOH <=> H_2 + H + CO_2$	+3.271e+006	2.10	+5.703e+003
71.	$H + HCOOH <=> H_2 + CO + OH$	+6.060e+013	-0.35	+2.860e+003
72.	$CH_3 + HCOOH <=> CH_4 + CO + OH$	+3.900e-007	5.80	+2.577e+003
73.	$HO_2 + HCOOH <=> CO + OH + H_2O_2$	+3.497e+019	-2.20	+1.223e+004
74.	$O + HCOOH <=> CO + 2OH$	+5.563e+017	-1.90	+3.357e+003
75.	$CH_2O + OH <=> HCO + H_2O$	+3.430e+009	1.18	-5.236e+002
76.	$H + CH_2O <=> H_2 + HCO$	+6.883e+007	1.77	+3.514e+003
77.	$CH_2O <=> H + HCO$	+1.797e+016	0.00	+8.447e+004
78.	$CH_2O + O <=> HCO + OH$	+5.657e+012	0.00	+3.212e+003
79.	$HCO + O_2 <=> CO + HO_2$	+1.105e+013	0.00	+4.100e+002
80.	$HCO <=> H + CO$	+2.710e+017	-1.00	+1.481e+004
81.	$HCO + OH <=> CO + H_2O$	+1.000e+014	0.00	+2.857e+000
82.	$H + HCO <=> H_2 + CO$	+1.462e+013	0.25	+5.714e+000
83.	$HCO + O <=> CO + OH$	+3.686e+013	0.00	+1.429e+000
84.	$HCO + O <=> H + CO_2$	+3.000e+013	0.00	+2.857e+000
85.	$CO + OH <=> H + CO_2$	+9.420e+003	2.25	-2.351e+003
86.	$CO + O <=> CO_2$	+6.170e+014	0.00	+3.000e+003
87.	$CO + O_2 <=> CO_2 + O$	+2.530e+012	0.00	+4.769e+004
88.	$CO + HO_2 <=> CO_2 + OH$	+5.800e+013	0.00	+2.293e+004
89.	$C_2H_5OH(+M) <=> CH_3 + CH_2OH(+M)$	+7.298e+023	-1.68	+8.335e+004
	LOW / +2.88e+085 -18.90 +1.10e+005 /			
	TROE / +5.00e-001 +2.00e+002 +8.90e+002 +4.60e+003 /			

	Enhanced third-body efficiencies:			
	H_2/2.00/ CO_2/3.00/ CO/2.00/ H_2O/5.00/			
90.	$C_2H_5OH(+M) <=> OH + C_2H_5(+M)$	+1.536e+023	-1.54	+9.601e+004
	LOW / +3.25e+085 -18.81 +1.15e+005 /			
	TROE / +5.00e-001 +3.00e+002 +9.00e+002 +5.00e+003 /			
	Enhanced third-body efficiencies:			
	H_2/2.00/ CO_2/3.00/ CO/2.00/ H_2O/5.00/			
91.	$C_2H_5OH(+M) <=> H_2O + C_2H_4(+M)$	+5.341e+013	0.09	+7.747e+004
	LOW / +2.57e+083 -18.85 +8.65e+004 /			
	TROE / +7.00e-001 +3.50e+002 +8.00e+002 +3.80e+003 /			
	Enhanced third-body efficiencies:			
	H_2O/5.00/			
92.	$C_2H_5OH(+M) <=> H_2 + CH_3HCO(+M)$	+3.930e+011	0.10	+9.881e+004
	LOW / +4.46e+087 -19.42 +1.16e+005 /			
	TROE / +9.00e-001 +9.00e+002 +1.10e+003 +3.50e+003 /			
	Enhanced third-body efficiencies:			
	H_2O/5.00/			
93.	$OH + C_2H_5OH <=> H_2O + C_2H_4OH$	+1.740e+011	0.27	+6.514e+002
94.	$OH + C_2H_5OH <=> H_2O + CH_3CHOH$	+6.761e+011	0.15	+2.857e+000
95.	$OH + C_2H_5OH <=> H_2O + CH_3CH_2O$	+2.345e+011	0.30	+1.704e+003
96.	$H + C_2H_5OH <=> H_2 + C_2H_4OH$	+2.355e+007	1.80	+4.880e+003
97.	$H + C_2H_5OH <=> H_2 + CH_3CHOH$	+4.939e+007	1.65	+2.585e+003
98.	$H + C_2H_5OH <=> H_2 + CH_3CH_2O$	+2.186e+007	1.60	+3.298e+003
99.	$O + C_2H_5OH <=> OH + C_2H_4OH$	+1.801e+008	1.70	+5.225e+003
100.	$O + C_2H_5OH <=> OH + CH_3CHOH$	+1.450e+007	1.85	+1.980e+003
101.	$O + C_2H_5OH <=> OH + CH_3CH_2O$	+2.302e+007	2.00	+4.448e+003
102.	$CH_3 + C_2H_5OH <=> CH_4 + C_2H_4OH$	+6.883e+001	3.18	+9.210e+003
103.	$CH_3 + C_2H_5OH <=> CH_4 + CH_3CHOH$	+3.952e+002	2.99	+6.926e+003
104.	$CH_3 + C_2H_5OH <=> CH_4 + CH_3CH_2O$	+1.119e+002	2.99	+8.960e+003
105.	$HO_2 + C_2H_5OH <=> H_2O_2 + CH_3CHOH$	+8.200e+003	2.55	+1.075e+004
106.	$HO_2 + C_2H_5OH <=> H_2O_2 + C_2H_4OH$	+1.230e+004	2.55	+1.373e+004
107.	$HO_2 + C_2H_5OH <=> H_2O_2 + CH_3CH_2O$	+3.643e+012	0.00	+2.811e+004
108.	$CH_3CH_2O <=> H + CH_3HCO$	+8.949e+034	-5.89	+2.419e+004
109.	$CH_3CH_2O <=> CH_3 + CH_2O$	+2.276e+038	-6.96	+2.686e+004
110.	$O_2 + CH_3CH_2O <=> HO_2 + CH_3HCO$	+2.171e+010	0.00	+1.053e+003
111.	$CO + CH_3CH_2O <=> CO_2 + C_2H_5$	+8.959e+002	3.16	+6.072e+003
112.	$H + CH_3CH_2O <=> CH_3 + CH_2OH$	+3.000e+013	0.00	+8.571e+000
113.	$H + CH_3CH_2O <=> H_2O + C_2H_4$	+9.429e+012	0.00	+8.571e+000
114.	$OH + CH_3CH_2O <=> H_2O + CH_3HCO$	+1.914e+013	0.00	+2.857e+000
115.	$O_2 + CH_3CHOH <=> HO_2 + CH_3HCO$	+1.515e+014	0.00	+4.802e+003
	(Duplicate reaction)			
116.	$O_2 + CH_3CHOH <=> HO_2 + CH_3HCO$	+2.649e+015	-1.20	+2.857e+000
	(Duplicate reaction)			

117.	$O + CH_3CHOH <=> OH + CH_3HCO$	+1.686e+014	0.00	+0.000e+000
118.	$H + CH_3CHOH <=> H_2O + C_2H_4$	+5.743e+013	0.00	+4.286e+000
119.	$H + CH_3CHOH <=> CH_3 + CH_2OH$	+4.371e+013	0.00	+1.429e+000
120.	$HO_2 + CH_3CHOH <=> 2OH + CH_3HCO$	+6.743e+013	0.00	+8.571e+000
121.	$OH + CH_3CHOH <=> H_2O + CH_3HCO$	+9.571e+012	0.00	+0.000e+000
122.	$CH_3CHOH <=> H + CH_3HCO$	+3.143e+013	0.00	+2.393e+004
123.	$OH + CH_3HCO <=> CH_3 + HCOOH$	+5.743e+015	-1.08	+1.429e+000
124.	$H + C_2H_5 <=> H_2 + C_2H_4$	+6.786e+013	0.00	+7.657e+003
125.	$H + C_2H_5 <=> 2CH_3$	+3.000e+013	0.00	+8.571e+000
126.	$OH + C_2H_5 <=> H_2O + C_2H_4$	+7.657e+013	0.00	+5.714e+000
127.	$O + C_2H_5 <=> CH_3 + CH_2O$	+1.229e+014	0.00	+7.143e+000
128.	$HO_2 + C_2H_5 <=> OH + CH_3CH_2O$	+2.314e+013	0.00	+1.000e+001
129.	$O_2 + C_2H_5 <=> HO_2 + C_2H_4$	+4.211e+028	-5.40	+7.910e+003
130.	$O_2 + C_2H_5 <=> OH + CH_3HCO$	+7.140e+011	-0.48	+9.073e+003
131.	$OH + C_2H_4 <=> C_2H_4OH$	+1.290e+012	0.00	-7.820e+002
132.	$O_2 + C_2H_4OH <=> HOC_2H_4O_2$	+1.457e+012	0.00	-1.100e+003
133.	$HOC_2H_4O_2 <=> 2CH_2O + OH$	+7.371e+010	0.00	+2.765e+004
134.	$OH + C_2H_4 <=> H_2O + C_2H_3$	+2.020e+013	0.00	+6.699e+003
135.	$O + C_2H_4 <=> CH_3 + HCO$	+1.253e+007	1.88	+1.867e+002
136.	$CH_3 + C_2H_4 <=> CH_4 + C_2H_3$	+3.594e+000	3.70	+1.113e+004
137.	$H + C_2H_4 <=> H_2 + C_2H_3$	+1.056e-007	6.00	+1.982e+003
138.	$H + C_2H_4(+M) <=> C_2H_5(+M)$	+3.394e+011	0.45	+2.134e+003
	LOW / +1.11e+034 -5.00 +4.45e+003 /			
	TROE / +1.00e+000 +1.00e-015 +9.50e+001 +2.00e+002 /			
	Enhanced third-body efficiencies:			
	H_2/2.00/ CO_2/3.00/ CO/2.00/ H_2O/5.00/			
139.	$C_2H_4(+M) <=> H_2 + C_2H_2(+M)$	+3.446e+014	0.00	+7.954e+004
	LOW / +1.50e+015 0.00 +5.54e+004 /			
140.	$H + C_2H_3(+M) <=> C_2H_4(+M)$	+1.168e+013	0.27	+2.920e+002
	LOW / +9.80e+029 -3.86 +3.32e+003 /			
	TROE / +7.82e-001 +2.08e+002 +2.66e+003 +6.10e+003 /			
	Enhanced third-body efficiencies:			
	H_2O/5.00/			
141.	$H + C_2H_3 <=> H_2 + C_2H_2$	+1.723e+014	0.00	+5.714e+000
142.	$O_2 + C_2H_3 <=> CH_2O + HCO$	+5.343e+028	-5.31	+7.614e+003
143.	$O_2 + C_2H_3 <=> HO_2 + C_2H_2$	+1.151e-006	6.00	+8.265e+003
144.	$OH + C_2H_3 <=> H_2O + C_2H_2$	+1.086e+013	0.00	+5.714e+000
145.	$C_2H + C_2H_3 <=> 2C_2H_2$	+5.057e+013	0.00	+1.000e+001
146.	$CH_3 + C_2H_3 <=> CH_4 + C_2H_2$	+3.371e+013	0.00	+1.429e+000
147.	$OH + C_2H_2 <=> H_2O + C_2H$	+5.681e+007	2.00	+1.340e+004
148.	$OH + C_2H_2 <=> CH_3 + CO$	+9.246e-004	4.00	-2.086e+003
149.	$O + C_2H_2 <=> CH_2 + CO$	+1.923e+006	2.00	+1.656e+003
150.	$O + C_2H_2 <=> OH + C_2H$	+1.715e+015	-0.60	+1.307e+004

151.	$CH_3 + C_2H_2 <=> CH_4 + C_2H$	+5.689e+010	0.00	+1.655e+004
152.	$C_2H_2 <=> H + C_2H$	+5.160e+016	0.00	+1.070e+005
153.	$H + C_2H_2(+M) <=> C_2H_3(+M)$	+5.243e+011	0.58	+2.367e+003
	LOW / +2.25e+040 -7.27 +6.58e+003 /			
	TROE / +1.00e+000 +1.00e-015 +6.75e+002 +1.00e+015 /			
	Enhanced third-body efficiencies:			
	H_2/2.00/ CO_2/3.00/ CO/2.00/ H_2O/5.00/			
154.	$H_2 + C_2H <=> H + C_2H_2$	+6.895e+005	2.39	+1.012e+003
155.	$O_2 + C_2H <=> H + 2CO$	+1.731e+013	0.00	-4.766e+002

Table A.1: 155 reactions and 33 species reduced and optimized reaction mechanism for ethanol ignition. Rate constants $k = AT^b exp(-E/R_uT)$; units are cm, mol, s, cal, K.

A.2 Biodiesel

A.2.1 Methyl-butanoate (MB)

No.	Reaction	A	b	E
1.	$MB_3.J + H <=> MB$	+3.266e+013	0.00	+6.193e+000
2.	$MB_2.J + H <=> MB$	+7.015e+014	0.00	+8.750e+000
3.	$MP_3.J + CH_3 <=> MB$	+3.550e+013	0.00	+3.224e+000
4.	$BAO.J + CH_3 <=> MB$	+7.056e+013	0.00	+1.537e+000
5.	$ME_2.J + C_2H_5 <=> MB$	+2.232e+013	0.00	+1.309e+000
6.	$CH_3OCO + NC_3H_7 <=> MB$	+3.284e+013	0.00	+3.921e+000
7.	$CH_3O + NC_3H_7CO <=> MB$	+9.429e+012	0.00	+2.857e+000
8.	$MB + C_2H_3 <=> MB_3.J + C_2H_4$	+7.161e+011	0.00	+1.668e+004
9.	$MB + C_2H_5 <=> MB_3.J + C_2H_6$	+4.336e+010	0.00	+1.266e+004
10.	$MB + H <=> MB_3.J + H_2$	+1.329e+007	2.40	+2.705e+003
11.	$MB + HO_2 <=> MB_3.J + H_2O_2$	+1.567e+013	0.00	+1.120e+004
12.	$MB + O <=> MB_3.J + OH$	+4.182e+004	2.71	+2.784e+003
13.	$MB + O_2 <=> MB_3.J + HO_2$	+1.603e+013	0.00	+5.532e+004
14.	$MB + OH <=> MB_3.J + H_2O$	+1.165e+008	1.61	-2.860e+001
15.	$MB + MB_2OO <=> MB_2OOH + MB_3.J$	+1.748e+011	0.00	+1.825e+004
16.	$MB + C_2H_3 <=> MB_2.J + C_2H_4$	+1.987e+011	0.00	+1.366e+004
17.	$MB + C_2H_5 <=> MB_2.J + C_2H_6$	+3.371e+011	0.00	+9.101e+003
18.	$MB + H <=> MB_2.J + H_2$	+3.058e+013	0.00	+1.045e+004
19.	$MB + HO_2 <=> MB_2.J + H_2O_2$	+1.668e+012	0.00	+1.542e+004
20.	$MB + O <=> MB_2.J + OH$	+2.038e+012	0.00	+4.925e+003
21.	$MB + O_2 <=> MB_2.J + HO_2$	+4.165e+014	0.00	+3.762e+004
22.	$MB + OH <=> MB_2.J + H_2O$	+2.167e+010	0.51	+8.064e+001
23.	$MB + MB_2OO <=> MB_2.J + MB_2OOH$	+4.135e+012	0.00	+1.295e+004

24.	$CO_2 + NC_3H_7 <=> BAO.J$	+4.641e+010	0.00	+5.236e+004
25.	$CH_3OCO + C_3H_6 <=> MB_3.J$	+9.092e+011	0.00	+5.582e+003
26.	$CH_3O + CH_2CO <=> ME_2.J$	+2.649e+011	0.00	-6.957e+002
27.	$CO + CH_3O <=> CH_3OCO$	+8.927e+010	0.00	+3.676e+003
28.	$CO_2 + CH_3 <=> CH_3OCO$	+1.373e+011	0.00	+3.743e+004
29.	$CH_3OCO + C_2H_4 <=> MP_3.J$	+3.600e+010	0.00	+7.337e+003
30.	$C_2H_5 + CH_2CO <=> NC_3H_7CO$	+5.298e+010	0.00	+9.991e+003
31.	$MB_3.J <=> MB_2.J$	+1.397e+009	0.86	+4.425e+004
32.	$MB_2.J + O_2 <=> MB_2OO$	+9.954e+012	0.00	+3.501e+000
33.	$MB_2.J + MB_2OO <=> 2MB_2O$	+2.200e+012	0.00	-7.088e+002
34.	$MB_2OO + CH_3 <=> MB_2O + CH_3O$	+5.334e+011	0.00	-7.891e+002
35.	$MB_2OO + C_2H_5 <=> MB_2O + C_2H_5O$	+7.099e+012	0.00	-7.088e+002
36.	$MB_2.J + CH_3O_2 <=> MB_2O + CH_3O$	+6.914e+011	0.00	-1.008e+003
37.	$MB_2.J + HO_2 <=> MB_2O + OH$	+2.286e+012	0.00	-1.047e+003
38.	$MB_2OO + HO_2 <=> MB_2OOH + O_2$	+4.243e+009	0.00	-2.371e+003
39.	$MB_2OO + H_2O_2 => MB_2OOH + HO_2$	+1.220e+011	0.00	+1.265e+004
40.	$MB_2OOH + HO_2 => MB_2OO + H_2O_2$	+2.196e+012	0.00	+9.076e+003
41.	$MB_2OO + CH_3O_2 => MB_2O + O_2 + CH_3O$	+2.186e+015	-1.61	+2.166e+003
42.	$2MB_2OO => 2MB_2O + O_2$	+2.482e+015	-1.61	+1.938e+003
43.	$MB_2OOH <=> MB_2O + OH$	+3.437e+016	0.00	+3.861e+004
44.	$OH + HCO <=> H_2O + CO$	+4.796e+014	0.00	+1.352e+000
	REV / +2.8960e+015 0.00 +1.05e+005 /			
45.	$OH + CO <=> H + CO_2$	+1.400e+005	1.95	-1.347e+003
	REV / +1.5680e+007 1.95 +2.10e+004 /			
46.	$H + O_2 <=> O + OH$	+1.970e+014	0.00	+1.654e+004
	REV / +1.5550e+013 0.00 +4.25e+002 /			
47.	$H_2 + O <=> H + OH$	+5.080e+004	2.67	+6.292e+003
	REV / +2.2310e+004 2.67 +4.20e+003 /			
48.	$O + H_2O <=> 2OH$	+2.970e+006	2.02	+1.340e+004
	REV / +3.0130e+005 2.02 -3.85e+003 /			
49.	$H_2 + OH <=> H + H_2O$	+2.160e+008	1.51	+3.430e+003
	REV / +9.3520e+008 1.51 +1.86e+004 /			
50.	$HCO <=> H + CO$	+2.142e+017	-1.00	+1.289e+004
	REV / +6.4670e+013 0.00 -4.42e+002 /			
51.	$OH + H_2O_2 <=> H_2O + HO_2$	+1.000e+012	0.00	+0.000e+000
	(Duplicate reaction)			
	REV / +1.6850e+011 0.33 +3.15e+004 /			
52.	$O + C_2H_4 <=> HCO + CH_3$	+9.667e+006	1.88	+1.978e+002
	REV / +2.8510e+008 1.05 +3.18e+004 /			
53.	$H + C_2H_4(+M) <=> C_2H_5(+M)$	+1.596e+012	0.45	+1.502e+003
	LOW / +1.11e+034 -5.00 +4.45e+003 /			
	TROE / +1.00e+000 +1.00e-015 +9.50e+001 +2.00e+002 /			
	Enhanced third-body efficiencies:			

	H_2/2.00/ H_2O/5.00/ CO/2.00/ CO_2/3.00/			
54.	$H + C_2H_6 <=> H_2 + C_2H_5$	+8.502e+002	3.50	+3.419e+003
	REV / +1.3550e-001 4.06 +8.86e+003 /			
55.	$O_2 + C_2H_5 <=> HO_2 + C_2H_4$	+3.074e+029	-5.76	+8.985e+003
	REV / +1.2590e+030 -5.63 +2.23e+004 /			
56.	$OH + C_2H_6 <=> H_2O + C_2H_5$	+5.762e+006	2.06	+9.070e+002
	REV / +1.0100e+007 2.06 +2.30e+004 /			
57.	$O + C_2H_6 <=> OH + C_2H_5$	+3.551e+013	0.00	+7.327e+003
	REV / +2.0800e+013 0.00 +1.27e+004 /			
58.	$CH_3 + HO_2 <=> OH + CH_3O$	+5.235e+012	0.00	+2.929e+000
	REV / +4.7800e+014 -0.35 +2.46e+004 /			
59.	$CO + HO_2 <=> OH + CO_2$	+3.010e+013	0.00	+2.300e+004
	REV / +6.4350e+015 -0.33 +8.46e+004 /			
60.	$2CH_3(+M) <=> C_2H_6(+M)$	+4.220e+016	-1.17	+7.434e+002
	LOW / +1.14e+036 -5.25 +1.71e+003 /			
	TROE / +4.05e-001 +1.12e+003 +6.96e+001 +1.00e+015 /			
	Enhanced third-body efficiencies:			
	H_2/2.00/ H_2O/5.00/ CO/2.00/ CO_2/3.00/			
61.	$H_2O <=> H + OH$	+1.837e+027	-3.00	+1.226e+005
	REV / +2.2500e+022 -2.00 +0.00e+000 /			
62.	$H + O_2(+M) <=> HO_2(+M)$	+1.475e+012	0.60	+0.000e+000
	LOW / +3.50e+016 -0.41 -1.12e+003 /			
	TROE / +5.00e-001 +1.00e-030 +1.00e+030 +1.00e+100 /			
	Enhanced third-body efficiencies:			
	H_2/2.50/ H_2O/12.00/ CO/1.90/ CO_2/3.80/			
63.	$O + CO(+M) <=> CO_2(+M)$	+1.800e+010	0.00	+2.384e+003
	LOW / +1.35e+024 -2.79 +4.19e+003 /			
	Enhanced third-body efficiencies:			
	H_2/2.50/ H_2O/12.00/ CO/1.90/ CO_2/3.80/			
64.	$O_2 + CO <=> O + CO_2$	+1.068e-015	7.13	+1.332e+004
	REV / +9.4440e-015 7.13 +1.95e+004 /			
65.	$H + HCO <=> H_2 + CO$	+2.762e+013	0.00	+5.460e+000
	REV / +4.8130e+014 0.00 +9.00e+004 /			
66.	$O + HCO <=> OH + CO$	+8.900e+012	0.00	+7.423e+000
	REV / +8.6970e+013 0.00 +8.79e+004 /			
67.	$CH_2O <=> H + HCO$	+2.804e+029	-3.57	+1.007e+005
	REV / +2.6600e+024 -2.57 +4.27e+002 /			
68.	$OH + CH_2O <=> H_2O + HCO$	+7.519e+009	1.18	-3.692e+002
	REV / +1.1860e+009 1.18 +2.94e+004 /			
69.	$H + CH_2O <=> H_2 + HCO$	+1.554e+008	1.50	+3.303e+003
	REV / +7.4530e+007 1.50 +1.77e+004 /			
70.	$O + CH_2O <=> OH + HCO$	+2.477e+011	0.57	+4.141e+003
	REV / +1.4590e+010 0.57 +1.53e+004 /			

71.	$OH + CH_3 <=> H_2 + CH_2O$	+2.282e+013	0.00	+4.985e+003
	REV / +6.7560e+014 0.00 +7.60e+004 /			
72.	$O + CH_3 <=> H + CH_2O$	+4.017e+013	0.00	+9.571e+000
	REV / +1.0550e+015 0.00 +6.96e+004 /			
73.	$O_2 + CH_3 <=> O + CH_3O$	+4.293e+018	-1.57	+3.110e+004
	REV / +3.5850e+018 -1.59 -1.63e+003 /			
74.	$CH_3O(+M) <=> H + CH_2O(+M)$	+8.048e+013	0.00	+1.126e+004
	LOW / +2.34e+025 -2.70 +3.06e+004 /			
75.	$C_2H_4(+M) <=> H_2 + C_2H_2(+M)$	+2.660e+013	0.00	+7.191e+004
	LOW / +1.50e+015 0.00 +5.54e+004 /			
76.	$O + HO_2 <=> O_2 + OH$	+3.250e+013	0.00	+0.000e+000
	REV / +7.8570e+014 -0.33 +5.54e+004 /			
77.	$HCO + HO_2 <=> O_2 + CH_2O$	+5.013e+010	0.33	-2.636e+003
	REV / +2.0500e+013 0.00 +3.90e+004 /			
78.	$O_2 + CH_3O <=> HO_2 + CH_2O$	+1.638e+010	0.00	+2.272e+003
	REV / +1.3180e+009 0.35 +3.14e+004 /			
79.	$O_2 + HCO <=> CO + HO_2$	+7.487e+011	0.00	+5.222e+002
	REV / +9.0290e+011 0.33 +3.29e+004 /			
80.	$H + HO_2 <=> 2OH$	+7.080e+013	0.00	+3.000e+002
	REV / +1.3520e+014 -0.33 +3.96e+004 /			
81.	$H + HO_2 <=> H_2 + O_2$	+1.660e+013	0.00	+8.200e+002
	REV / +9.1380e+014 -0.33 +5.83e+004 /			
82.	$OH + HO_2 <=> O_2 + H_2O$	+2.890e+013	0.00	-5.000e+002
	REV / +6.8880e+015 -0.33 +7.21e+004 /			
83.	$O_2 + H_2O_2 <=> 2HO_2$	+5.942e+017	-0.66	+5.315e+004
	(Duplicate reaction)			
	REV / +4.2000e+014 0.00 +1.20e+004 /			
84.	$2OH(+M) <=> H_2O_2(+M)$	+1.236e+014	-0.37	+0.000e+000
	LOW / +3.04e+030 -4.63 +2.05e+003 /			
	TROE / +4.70e-001 +1.00e+002 +2.00e+003 +1.00e+015 /			
	Enhanced third-body efficiencies:			
	H_2/2.50/ H_2O/12.00/ CO/1.90/ CO_2/3.80/			
85.	$H + H_2O_2 <=> OH + H_2O$	+2.410e+013	0.00	+3.970e+003
	REV / +7.7500e+012 0.00 +7.47e+004 /			
86.	$HO_2 + CH_2O <=> HCO + H_2O_2$	+2.620e-002	4.53	+6.132e+003
	REV / +1.1940e-002 4.20 +4.92e+003 /			
87.	$OH <=> H + O$	+3.909e+022	-2.00	+1.053e+005
	REV / +4.7200e+018 -1.00 +0.00e+000 /			
88.	$O_2 <=> 2O$	+6.473e+020	-1.50	+1.215e+005
	REV / +6.1700e+015 -0.50 +0.00e+000 /			
89.	$H_2 <=> 2H$	+4.570e+019	-1.40	+1.044e+005
	REV / +2.4230e+015 -0.40 -3.04e+003 /			
90.	$H + C_2H_3(+M) <=> C_2H_4(+M)$	+1.041e+012	0.27	+3.814e+002

	LOW / +9.80e+029 -3.86 +3.32e+003 /			
	TROE / +7.82e-001 +2.08e+002 +2.66e+003 +6.10e+003 /			
91.	$C_2H_5 + C_2H_3 <=> 2C_2H_4$	+2.002e+012	0.00	+8.714e+000
	REV / +4.8200e+014 0.00 +7.15e+004 /			
92.	$H + C_2H_2(+M) <=> C_2H_3(+M)$	+3.973e+011	0.58	+2.252e+003
	LOW / +2.25e+040 -7.27 +6.58e+003 /			
	TROE / +1.00e+000 +1.00e-015 +6.75e+002 +1.00e+015 /			
	Enhanced third-body efficiencies:			
	H_2/2.00/ H_2O/5.00/ CO/2.00/ CO_2/3.00/			
93.	$H + C_2H_4 <=> H_2 + C_2H_3$	+7.014e-003	4.62	+2.721e+003
	REV / +5.7230e-001 3.79 +3.23e+003 /			
94.	$OH + C_2H_4 <=> H_2O + C_2H_3$	+8.210e+013	0.00	+5.180e+003
	REV / +1.0150e+013 0.00 +2.02e+004 /			
95.	$O_2 + C_2H_3 <=> HO_2 + C_2H_2$	+4.935e-015	-1.26	+4.592e+003
	(Duplicate reaction)			
	REV / +2.7270e-016 -0.93 +1.14e+004 /			
96.	$C_2H_2 <=> H + C_2H$	+1.018e+016	0.00	+1.303e+005
	REV / +7.1300e+007 2.08 -2.89e+004 /			
97.	$O_2 + CH_2 <=> H_2O + CO$	+1.303e+020	-2.54	+2.202e+003
	REV / +8.5080e+020 -2.54 +1.80e+005 /			
98.	$OH + C_2H_2 <=> H_2O + C_2H$	+1.799e+008	2.00	+1.055e+004
	REV / +4.6710e+003 3.08 +6.85e+002 /			
99.	$O + C_2H_2 <=> OH + C_2H$	+7.962e+014	-0.60	+1.675e+004
	REV / +4.4430e+010 0.48 -1.56e+004 /			
100.	$O + C_2H_2 <=> CO + CH_2$	+1.542e+006	2.00	+2.175e+003
	REV / +1.1520e+006 2.00 +5.26e+004 /			
101.	$O_2 + C_2H <=> CO + HCO$	+1.886e+012	0.00	+3.235e+000
	REV / +1.3280e+016 -1.08 +1.54e+005 /			
102.	$O_2 + CH_2 <=> OH + HCO$	+2.862e+019	-3.30	+2.461e+002
	REV / +5.3100e+019 -3.30 +7.32e+004 /			
103.	$O + CH_2 <=> 2H + CO$	+7.488e+013	0.00	+5.714e+000
	REV / +0.0000e+000 0.00 +0.00e+000 /			
104.	$O_2 + CH_2 <=> 2H + CO_2$	+4.200e+021	-3.30	+3.318e+003
	REV / +0.0000e+000 0.00 +0.00e+000 /			
105.	$O_2 + C_2H_3 <=> HO_2 + C_2H_2$	+1.310e-005	6.00	+8.154e+003
	(Duplicate reaction)			
	REV / +1.1140e-007 6.33 +1.76e+004 /			
106.	$O + H_2O_2 <=> OH + HO_2$	+9.550e+006	2.00	+3.970e+003
	REV / +2.5410e+007 1.68 +1.99e+004 /			
107.	$OH + C_2H_2 <=> H + CH_2CO$	+3.236e-004	4.50	-8.108e+002
	REV / +2.1610e-003 4.50 +1.97e+004 /			
108.	$H + CH_2CO <=> CO + CH_3$	+7.716e+013	0.00	+2.963e+003
	REV / +2.4000e+012 0.00 +4.02e+004 /			

109.	$O + CH_2CO <=> CO_2 + CH_2$	+4.243e+011	0.00	+1.319e+003
	REV / +3.7390e+012 0.00 +5.37e+004 /			
110.	$O_2 + CH_2 <=> O + CH_2O$	+1.851e+021	-3.30	+4.293e+003
	REV / +3.8620e+022 -3.30 +6.32e+004 /			
111.	$CH_2CO(+M) <=> CO + CH_2(+M)$	+3.641e+013	0.00	+7.958e+004
	LOW / +3.60e+015 0.00 +5.93e+004 /			
112.	$O_2 + C_2H_6 <=> HO_2 + C_2H_5$	+3.088e+013	0.00	+5.289e+004
	REV / +3.0000e+011 0.00 +0.00e+000 /			
113.	$HO_2 + C_2H_6 <=> H_2O_2 + C_2H_5$	+3.163e+013	0.00	+2.268e+004
	REV / +1.0690e+011 0.24 +7.84e+003 /			
114.	$O_2 + CH_2 <=> H_2 + CO_2$	+3.900e+020	-3.30	+1.629e+003
	REV / +3.0540e+023 -3.30 +1.87e+005 /			
115.	$H + C_2H_3 <=> H_2 + C_2H_2$	+4.201e+013	0.00	+2.792e+003
	REV / +1.3310e+013 0.00 +6.81e+004 /			
116.	$H + C_2H_5 <=> 2CH_3$	+4.158e+013	0.00	+9.982e+000
	REV / +5.4460e+016 -1.03 +1.70e+004 /			
117.	$O_2 + C_2H_3 <=> HCO + CH_2O$	+7.994e+029	-5.31	+5.148e+003
	REV / +1.6570e+029 -5.31 +9.31e+004 /			
118.	$C_2H_6 <=> H + C_2H_5$	+5.764e+021	-1.56	+1.381e+005
	REV / +3.6100e+013 0.00 +0.00e+000 /			
119.	$CH_3CO(+M) <=> CO + CH_3(+M)$	+1.177e+013	0.00	+1.389e+004
	LOW / +1.20e+015 0.00 +1.25e+004 /			
120.	$CH_3CHO <=> HCO + CH_3$	+6.421e+015	0.15	+8.927e+004
	REV / +2.0000e+013 0.00 +0.00e+000 /			
121.	$O_2 + CH_3CHO <=> HO_2 + CH_3CO$	+2.937e+011	0.00	+3.850e+004
	REV / +8.5520e+010 0.32 -1.94e+003 /			
122.	$OH + CH_3CHO <=> H_2O + CH_3CO$	+2.953e+006	1.80	+1.230e+003
	REV / +1.3540e+006 1.79 +3.29e+004 /			
123.	$H + CH_3CHO <=> H_2 + CH_3CO$	+3.738e+013	0.00	+3.697e+003
	REV / +2.0960e+012 -0.01 +1.97e+004 /			
124.	$O + CH_3CHO <=> OH + CH_3CO$	+2.152e+012	0.00	+2.191e+003
	REV / +4.0800e+011 -0.01 +1.62e+004 /			
125.	$HO_2 + CH_3CHO <=> H_2O_2 + CH_3CO$	+4.931e+012	0.00	+9.545e+003
	REV / +1.2100e+013 -0.34 +1.20e+004 /			
126.	$CH_3 + C_2H_2 <=> H + C_3H_4 - P$	+5.694e+017	-1.20	+1.640e+004
	REV / +1.0000e+014 0.00 +4.00e+003 /			
127.	$C_3H_5 - A <=> CH_3 + C_2H_2$	+4.705e+048	-9.90	+1.126e+005
	REV / +2.6100e+046 -9.82 +3.70e+004 /			
128.	$C_3H_6 <=> CH_3 + C_2H_3$	+8.045e+061	-13.28	+1.078e+005
	REV / +4.7120e+059 -13.19 +2.95e+004 /			
129.	$CH_3 + C_2H_2 <=> H + C_3H_4 - A$	+3.128e+019	-2.08	+3.957e+004
	REV / +1.1490e+016 -0.70 +1.58e+004 /			
130.	$C_3H_6 <=> H + C_3H_5 - A$	+1.551e+061	-13.26	+1.992e+005

	REV / +4.8870e+056 -12.25 +2.81e+004 /			
131.	$O + C_3H_6 <=> H + CH_3 + CH_2CO$	+4.379e+007	1.76	+6.339e+001
	REV / +1.0000e+000 0.00 +0.00e+000 /			
132.	$O + C_3H_6 <=> HCO + C_2H_5$	+5.415e+007	1.76	-9.596e+002
	REV / +1.4020e+005 1.88 +2.65e+004 /			
133.	$HO_2 + C_3H_6 <=> H_2O_2 + C_3H_5 - A$	+1.458e+011	0.00	+2.117e+004
	REV / +5.8670e+005 1.33 +9.76e+003 /			
134.	$OH + C_3H_6 <=> H_2O + C_3H_5 - A$	+1.827e+007	2.00	-3.025e+002
	REV / +6.1940e+006 2.01 +3.19e+004 /			
135.	$O_2 + C_2H_4 <=> HO_2 + C_2H_3$	+8.284e+013	0.00	+5.687e+004
	REV / +4.9390e+013 -0.50 +1.37e+003 /			
136.	$CH_2O <=> H_2 + CO$	+1.731e+032	-4.42	+1.008e+005
	REV / +5.0700e+027 -3.42 +8.44e+004 /			
137.	$NC_3H_7 <=> CH_3 + C_2H_4$	+5.755e+013	-0.55	+2.475e+004
	REV / +4.1000e+011 0.00 +7.20e+003 /			
138.	$NC_3H_7 <=> H + C_3H_6$	+1.736e+015	-0.64	+2.885e+004
	REV / +1.0000e+013 0.00 +2.50e+003 /			
139.	$O_2 + NC_3H_7 <=> HO_2 + C_3H_6$	+1.609e+010	0.00	+3.471e+003
	REV / +2.0000e+011 0.00 +1.75e+004 /			
140.	$O + C_3H_6 <=> OH + C_3H_5 - A$	+1.128e+012	0.70	+6.115e+003
	REV / +1.0550e+011 0.71 +2.08e+004 /			
141.	$H + C_3H_6 <=> H_2 + C_3H_5 - A$	+1.776e+004	2.50	+2.669e+003
	REV / +7.9330e+004 2.51 +1.95e+004 /			
142.	$H + C_3H_6 <=> CH_3 + C_2H_4$	+9.133e+032	-5.81	+1.794e+004
	REV / +2.3130e+033 -5.90 +3.16e+004 /			
143.	$_IC_3H_7 <=> H + C_3H_6$	+2.422e+019	-1.57	+3.457e+004
	REV / +1.3000e+013 0.00 +1.56e+003 /			
144.	$H +_I C_3H_7 <=> H_2 + C_3H_6$	+9.404e+013	0.00	+7.054e+000
	REV / +4.8220e+009 0.69 +1.21e+004 /			
145.	$O_2 +_I C_3H_7 <=> HO_2 + C_3H_6$	+5.461e+010	0.00	+5.881e+003
	REV / +2.0000e+011 0.00 +1.75e+004 /			
146.	$C_2H_5CO <=> CO + C_2H_5$	+5.122e+014	-0.73	+1.169e+004
	REV / +1.5100e+011 0.00 +4.81e+003 /			
147.	$H + H_2O_2 <=> H_2 + HO_2$	+4.820e+013	0.00	+7.950e+003
	REV / +1.8750e+012 0.33 +2.43e+004 /			
148.	$O + HCO <=> H + CO_2$	+2.118e+013	0.00	+5.938e+000
	REV / +9.6770e+015 0.00 +1.10e+005 /			
149.	$CH_3 <=> H + CH_2$	+2.624e+016	0.00	+8.635e+004
	REV / +2.1070e+011 1.00 -1.96e+004 /			
150.	$H + CH_3 <=> H_2 + CH_2$	+1.363e+014	0.00	+1.485e+004
	REV / +1.8180e+013 0.00 +1.04e+004 /			
151.	$OH + CH_3 <=> H_2O + CH_2$	+1.226e+006	2.00	+2.147e+003
	REV / +2.6230e+006 2.00 +1.30e+004 /			

152.	$H + CH_3CO <=> H_2 + CH_2CO$	+6.286e+012	0.00	+1.026e-010
	REV / +7.2700e+009 0.00 +8.30e+004 /			
153.	$O + CH_3CO <=> OH + CH_2CO$	+1.185e+014	0.00	+1.549e-010
	REV / +7.2700e+009 0.00 +8.30e+004 /			
154.	$O + C_2H_5 <=> H + CH_3CHO$	+1.790e+013	0.00	+1.225e+001
	REV / +9.0000e+013 0.00 +7.27e+004 /			
155.	$C_2H_5O <=> CH_3 + CH_2O$	+1.724e+038	-6.96	+2.473e+004
	REV / +6.4420e+036 -6.99 +1.69e+004 /			
156.	$O_2 + C_2H_5O <=> HO_2 + CH_3CHO$	+1.038e+010	0.00	+1.330e+003
	REV / +3.8720e+008 0.44 +3.19e+004 /			
157.	$O_2 + H_2O_2 <=> 2HO_2$	+1.839e+014	-0.66	+3.955e+004
	(Duplicate reaction)			
	REV / +1.3000e+011 0.00 -1.63e+003 /			
158.	$CH_3O_2 <=> O_2 + CH_3$	+6.413e+027	-3.42	+3.125e+004
	REV / +5.4400e+025 -3.30 +0.00e+000 /			
159.	$HO_2 + C_2H_5 <=> OH + C_2H_5O$	+1.173e+014	0.00	+9.771e+000
	REV / +3.0750e+015 -0.32 +2.75e+004 /			
160.	$CH_3 + CH_3O_2 <=> 2CH_3O$	+1.241e+012	0.00	-1.019e+003
	REV / +2.9710e+016 -0.93 +2.83e+004 /			
161.	$C_2H_5 + CH_3O_2 <=> CH_3O + C_2H_5O$	+1.226e+013	0.00	-8.108e+002
	REV / +6.5690e+016 -0.90 +3.13e+004 /			
162.	$OH + H_2O_2 <=> H_2O + HO_2$	+5.800e+014	0.00	+9.560e+003
	(Duplicate reaction)			
	REV / +9.7710e+013 0.33 +4.10e+004 /			
163.	$2CH_3O_2 <=> O_2 + 2CH_3O$	+5.078e+016	-1.61	+2.345e+003
	REV / +0.0000e+000 0.00 +0.00e+000 /			
164.	$C_2H_5O <=> H + CH_3CHO$	+5.312e+034	-5.89	+2.979e+004
	REV / +3.0630e+030 -4.78 +6.10e+003 /			
165.	$OH + CH_3 <=> H_2O + CH_2(S)$	+1.459e+013	0.00	+1.729e+003
	REV / +3.2360e+010 0.89 +1.21e+003 /			
166.	$HO_2 + C_3H_4 - A <=> OH + CO + C_2H_4$	+1.665e+011	0.00	+1.220e+004
	REV / +1.0000e+000 0.00 +0.00e+000 /			
167.	$HO_2 + C_3H_4 - A <=> H_2O_2 + C_3H_3$	+7.633e+013	0.00	+1.390e+004
	REV / +1.5510e+016 -1.38 +4.40e+004 /			
168.	$O_2 + C_3H_6 <=> HO_2 + C_3H_5 - A$	+2.895e+012	0.00	+4.087e+004
	REV / +3.3320e+010 0.34 -5.56e+002 /			
169.	$C_2H_5 + C_3H_6 <=> C_2H_6 + C_3H_5 - A$	+2.278e+011	0.00	+1.022e+004
	REV / +5.3690e+005 1.33 +1.64e+004 /			
170.	$HO_2 + C_3H_5 - A <=> OH + CH_2O + C_2H_3$	+1.138e-019	0.00	+4.278e+000
	REV / +1.0000e-030 0.00 +0.00e+000 /			
171.	$H + C_3H_5 - A <=> H_2 + C_3H_4 - A$	+3.422e+012	0.00	+4.375e+000
	REV / +1.2300e+013 0.12 +4.72e+004 /			
172.	$C_2H_5 + C_3H_5 - A <=> C_2H_6 + C_3H_4 - A$	+9.407e+011	0.00	+1.490e+000

	REV / +1.8020e+012 0.05 +4.03e+004 /			
173.	$C_2H_5 + C_3H_5 - A <=> C_2H_4 + C_3H_6$	+5.265e+010	0.00	+1.333e+000
	REV / +6.9370e+016 -1.33 +5.28e+004 /			
174.	$C_2H_3 + C_3H_5 - A <=> C_2H_4 + C_3H_4 - A$	+6.673e+011	0.00	+1.086e+001
	REV / +1.6240e+013 0.05 +4.82e+004 /			
175.	$C_3H_4 - A + C_3H_6 <=> 2C_3H_5 - A$	+4.555e+017	-1.29	+4.263e+004
	REV / +1.0000e+012 0.00 +0.00e+000 /			
176.	$C_3H_4 - A <=> H + C_3H_3$	+2.842e+016	0.00	+8.064e+004
	REV / +1.7980e+015 -0.38 +1.06e+004 /			
177.	$C_3H_4 - A <=> C_3H_4 - P$	+6.418e+015	0.00	+8.037e+004
	REV / +3.2220e+018 -0.99 +9.66e+004 /			
178.	$O_2 + C_3H_4 - A <=> HO_2 + C_3H_3$	+2.676e+013	0.00	+4.340e+004
	REV / +1.1750e+011 0.30 +3.80e+001 /			
179.	$HO_2 + C_3H_4 - A <=> OH + CH_2 + CH_2CO$	+1.306e+012	0.00	+1.621e+004
	REV / +1.0000e+000 0.00 +0.00e+000 /			
180.	$OH + C_3H_4 - A <=> H_2O + C_3H_3$	+3.664e+007	2.00	+1.272e+003
	REV / +7.0030e+006 1.97 +3.45e+004 /			
181.	$O + C_3H_4 - A <=> CO + C_2H_4$	+3.012e+012	0.00	+1.948e+003
	REV / +8.2800e+013 -0.21 +1.25e+005 /			
182.	$C_3H_5 - A <=> H + C_3H_4 - A$	+4.009e+015	-0.43	+6.461e+004
	REV / +2.4000e+011 0.69 +3.01e+003 /			
183.	$H + C_3H_4 - A <=> H_2 + C_3H_3$	+2.329e+007	2.00	+4.359e+003
	REV / +3.2350e+006 1.97 +2.34e+004 /			
184.	$C_3H_4 - A + C_3H_5 - A <=> C_3H_6 + C_3H_3$	+3.580e+011	0.00	+6.752e+003
	REV / +2.6440e+019 -2.71 +4.21e+004 /			
185.	$C_2H + C_3H_4 - A <=> C_2H_2 + C_3H_3$	+4.641e+012	0.00	+9.143e+000
	REV / +1.4200e+016 -1.38 +5.38e+004 /			
186.	$C_3H_4 - P <=> H + C_3H_3$	+2.396e+016	0.00	+9.912e+004
	REV / +6.7080e+011 0.61 +6.42e+003 /			
187.	$C_3H_4 - P <=> CH_3 + C_2H$	+2.225e+016	0.00	+1.490e+005
	REV / +1.0180e+012 0.61 -1.60e+003 /			
188.	$O_2 + C_3H_4 - P <=> HO_2 + C_3H_3$	+6.496e+013	0.00	+4.710e+004
	REV / +2.3540e+011 0.14 +7.80e+001 /			
189.	$HO_2 + C_3H_4 - P <=> OH + CO + C_2H_4$	+6.213e+012	0.00	+1.794e+004
	REV / +1.0000e+000 0.00 +0.00e+000 /			
190.	$OH + C_3H_4 - P <=> H_2O + C_3H_3$	+5.340e+007	2.00	+9.927e+002
	REV / +2.8050e+007 1.81 +3.21e+004 /			
191.	$O + C_3H_4 - P <=> OH + C_3H_3$	+2.137e+008	1.50	+6.531e+003
	REV / +2.1770e+008 1.31 +2.25e+004 /			
192.	$O + C_3H_4 - P <=> HCO + C_2H_3$	+9.093e+012	0.00	+2.369e+003
	REV / +2.5480e+012 -0.39 +3.24e+004 /			
193.	$H + C_3H_4 - P <=> H_2 + C_3H_3$	+1.816e+007	2.00	+5.126e+003
	REV / +1.2960e+007 1.81 +2.10e+004 /			

194.	$C_2H + C_3H_4 - P <=> C_2H_2 + C_3H_3$	+2.199e+012	0.00	+9.535e+000
	REV / +5.2970e+011 -0.39 +4.96e+004 /			
195.	$C_2H_3 + C_3H_4 - P <=> C_2H_4 + C_3H_3$	+4.886e+012	0.00	+8.002e+003
	REV / +9.5410e+011 -0.39 +5.25e+004 /			
196.	$C_3H_4 - P + C_3H_5 - A <=> C_3H_6 + C_3H_3$	+5.440e+012	0.00	+8.954e+003
	REV / +4.9310e+016 -1.73 +3.80e+004 /			
197.	$O + C_3H_3 <=> CH_2O + C_2H$	+1.124e+013	0.00	+6.120e+000
	REV / +5.4460e+014 0.00 +3.16e+004 /			
198.	$O_2 + C_3H_3 <=> HCO + CH_2CO$	+1.859e+011	0.00	+2.772e+003
	REV / +4.8810e+011 0.00 +5.95e+004 /			
199.	$CH_3 + C_3H_3 <=> C_2H_5 + C_2H$	+8.170e+017	-1.10	+5.960e+004
	REV / +1.8100e+013 0.00 +0.00e+000 /			
200.	$C_2H_3O_{1,2} <=> CH_3CO$	+1.760e+015	0.00	+1.340e+004
	REV / +1.1360e+010 2.11 +3.35e+004 /			
201.	$O_2 + C_3H_5 - A <=> HO_2 + C_3H_4 - A$	+1.786e+021	-2.85	+3.310e+004
	REV / +2.6900e+019 -2.40 +2.05e+004 /			
202.	$O_2 + C_3H_5 - A <=> OH + CH_2O + C_2H_2$	+1.249e+029	-5.71	+2.096e+004
	REV / +0.0000e+000 0.00 +0.00e+000 /			
203.	$O_2 + CH_3 <=> OH + CH_2O$	+1.835e+012	0.00	+1.547e+004
	REV / +7.7780e+011 0.00 +6.78e+004 /			
204.	$H_2 + C_2H_4 <=> 2CH_3$	+2.980e+012	0.83	+1.031e+005
	REV / +1.0000e+014 0.00 +3.20e+004 /			
205.	$OH +_I C_3H_7 <=> H_2O + C_3H_6$	+4.314e+013	0.00	+7.469e+000
	REV / +2.9850e+012 0.57 +8.38e+004 /			
206.	$O +_I C_3H_7 <=> CH_3 + CH_3CHO$	+6.654e+013	0.00	+5.691e+000
	REV / +1.2790e+011 0.80 +8.65e+004 /			
207.	$NC_3H_7CO <=> CO + NC_3H_7$	+2.740e+015	-0.86	+1.510e+004
	REV / +1.5000e+011 0.00 +4.80e+003 /			
208.	$CH_2(S) <=> CH_2$	+5.373e+012	0.00	+7.149e+000
	REV / +7.1610e+015 -0.89 +1.14e+004 /			
209.	$C_2H_6 + CH_2(S) <=> CH_3 + C_2H_5$	+3.829e+012	0.00	+1.245e+000
	REV / +1.0410e+014 -0.33 +1.98e+004 /			
210.	$O_2 + CH_2(S) <=> H + OH + CO$	+3.709e+013	0.00	+7.967e+000
	REV / +0.0000e+000 0.00 +0.00e+000 /			
211.	$H_2 + CH_2(S) <=> H + CH_3$	+3.603e+013	0.00	+6.120e+000
	REV / +2.4820e+017 -0.89 +1.61e+004 /			
212.	$O + CH_2(S) <=> 2H + CO$	+4.543e+013	0.00	+5.052e+000
	REV / +0.0000e+000 0.00 +0.00e+000 /			
213.	$OH + CH_2(S) <=> H + CH_2O$	+1.763e+012	0.00	+3.575e+000
	REV / +3.1940e+018 -0.89 +8.79e+004 /			
214.	$CO_2 + CH_2(S) <=> CO + CH_2O$	+5.443e+012	0.00	+1.521e+000
	REV / +2.8520e+015 -0.89 +6.55e+004 /			
215.	$CH_3 + CH_2(S) <=> H + C_2H_4$	+2.601e+013	0.00	+1.271e+000

	REV / +2.6710e+015 -0.06 +6.88e+004 /			
216.	$CH_2CO + CH_2(S) <=> CO + C_2H_4$	+6.700e+013	0.00	+1.354e+000
	REV / +4.5960e+015 -0.06 +1.06e+005 /			

Table A.2: 216 reactions and 48 species reduced and optimized reaction mechanism for ignition of methyl-butanoate. Rate constants $k = AT^b exp(-E/R_uT)$; units are cm, mol, s, cal, K.

A.2.2 Methyl-decanoate (MD)

No.	Reaction	A	b	E
1.	$H + O_2 <=> O + OH$	+3.547e+015	-0.41	+1.660e+004
	REV / +1.0150e+013 -0.01 -1.33e+002 /			
2.	$O + H_2 <=> H + OH$	+5.080e+004	2.67	+6.292e+003
	REV / +2.6670e+004 2.65 +4.88e+003 /			
3.	$OH + H_2 <=> H + H_2O$	+2.160e+008	1.51	+3.430e+003
	REV / +2.2980e+009 1.40 +1.83e+004 /			
4.	$O + H_2O <=> 2OH$	+2.970e+006	2.02	+1.340e+004
	REV / +1.4650e+005 2.11 -2.90e+003 /			
5.	$H_2 <=> 2H$	+4.577e+019	-1.40	+1.044e+005
	REV / +1.1460e+020 -1.68 +8.20e+002 /			
6.	$O_2 <=> 2O$	+4.515e+017	-0.64	+1.189e+005
	REV / +6.1650e+015 -0.50 +0.00e+000 /			
7.	$OH <=> H + O$	+9.880e+017	-0.74	+1.021e+005
	REV / +4.7140e+018 -1.00 +0.00e+000 /			
8.	$H_2O <=> H + OH$	+1.912e+023	-1.83	+1.185e+005
	REV / +4.5000e+022 -2.00 +0.00e+000 /			
9.	$H + O_2(+M) <=> HO_2(+M)$	+1.475e+012	0.60	+0.000e+000
	TROE / +5.00e-001 +1.00e-030 +1.00e+030 +1.00e+000 /			
	Enhanced third-body efficiencies:			
	H_2/1.30/ H_2O/14.00/ CO/1.90/ CO_2/3.80/			
10.	$H + HO_2 <=> H_2 + O_2$	+1.660e+013	0.00	+8.230e+002
	REV / +3.1640e+012 0.35 +5.55e+004 /			
11.	$H + HO_2 <=> 2OH$	+7.079e+013	0.00	+2.950e+002
	REV / +2.0270e+010 0.72 +3.68e+004 /			
12.	$O + HO_2 <=> OH + O_2$	+3.250e+013	0.00	+0.000e+000
	REV / +3.2520e+012 0.33 +5.33e+004 /			
13.	$OH + HO_2 <=> O_2 + H_2O$	+2.890e+013	0.00	-4.970e+002
	REV / +5.8610e+013 0.24 +6.91e+004 /			
14.	$O_2 + H_2O_2 <=> 2HO_2$	+4.634e+016	-0.35	+5.067e+004
	(Duplicate reaction)			
	REV / +4.2000e+014 0.00 +1.20e+004 /			

15.	$O_2 + H_2O_2 <=> 2HO_2$	+1.434e+013	-0.35	+3.706e+004
	(Duplicate reaction)			
	REV / +1.3000e+011 0.00 -1.63e+003 /			
16.	$H_2O_2(+M) <=> 2OH(+M)$	+2.951e+014	0.00	+4.843e+004
	TROE / +5.00e-001 +1.00e-030 +1.00e+030 +1.00e+000 /			
	Enhanced third-body efficiencies:			
	H_2/2.50/ H_2O/12.00/ CO/1.90/ CO_2/3.80/			
17.	$H + H_2O_2 <=> OH + H_2O$	+2.410e+013	0.00	+3.970e+003
	REV / +1.2690e+008 1.31 +7.14e+004 /			
18.	$H + H_2O_2 <=> HO_2 + H_2$	+6.025e+013	0.00	+7.950e+003
	REV / +1.0410e+011 0.70 +2.40e+004 /			
19.	$O + H_2O_2 <=> OH + HO_2$	+9.550e+006	2.00	+3.970e+003
	REV / +8.6600e+003 2.68 +1.86e+004 /			
20.	$OH + H_2O_2 <=> HO_2 + H_2O$	+1.000e+012	0.00	+0.000e+000
	(Duplicate reaction)			
	REV / +1.8380e+010 0.59 +3.09e+004 /			
21.	$OH + H_2O_2 <=> HO_2 + H_2O$	+5.800e+014	0.00	+9.557e+003
	(Duplicate reaction)			
	REV / +1.0660e+013 0.59 +4.05e+004 /			
22.	$O + CO + M <=> CO_2 + M$	+1.800e+010	0.00	+2.384e+003
	Enhanced third-body efficiencies:			
	H_2/2.00/ O_2/6.00/ H_2O/6.00/ CO/1.50/ CO_2/3.50/			
23.	$O_2 + CO <=> O + CO_2$	+1.050e+012	0.00	+4.254e+004
	REV / +7.9500e+015 -0.80 +5.12e+004 /			
24.	$OH + CO <=> H + CO_2$	+1.750e+005	1.95	-4.348e+002
	REV / +4.6290e+011 0.76 +2.50e+004 /			
25.	$HO_2 + CO <=> OH + CO_2$	+1.570e+005	2.18	+1.794e+004
	REV / +1.1890e+008 1.71 +7.99e+004 /			
26.	$HCO <=> H + CO$	+1.474e+018	-1.00	+1.281e+004
	REV / +1.4030e+016 -0.62 +1.67e+003 /			
27.	$HCO + O_2 <=> HO_2 + CO$	+2.677e+009	0.68	-3.555e+002
	REV / +4.2830e+009 0.99 +3.31e+004 /			
28.	$H + HCO <=> H_2 + CO$	+3.482e+013	0.00	+1.278e+001
	REV / +2.2110e+012 0.66 +8.82e+004 /			
29.	$O + HCO <=> OH + CO$	+1.437e+013	0.00	+1.617e+000
	REV / +4.7750e+011 0.64 +8.68e+004 /			
30.	$O + HCO <=> H + CO_2$	+1.189e+014	0.00	+5.889e+000
	REV / +1.2550e+018 -0.55 +1.12e+005 /			
31.	$OH + HCO <=> H_2O + CO$	+2.473e+013	0.00	+1.039e+001
	REV / +3.2690e+013 0.55 +1.03e+005 /			
32.	$HO_2 + HCO <=> O_2 + CH_2O$	+4.041e+013	-0.06	+1.559e+004
	REV / +8.0700e+015 0.00 +5.34e+004 /			
33.	$HO_2 + HCO <=> H + OH + CO_2$	+4.433e+013	0.00	+8.714e+000

	REV / +0.0000e+000 0.00 +0.00e+000 /			
34.	$CO + CH_2O <=> 2HCO$	+8.204e+013	0.37	+1.010e+005
	REV / +1.8000e+013 0.00 +0.00e+000 /			
35.	$2HCO <=> H_2 + 2CO$	+1.288e+012	0.00	+7.370e+000
	REV / +0.0000e+000 0.00 +0.00e+000 /			
36.	$H + HCO(+M) <=> CH_2O(+M)$	+3.289e+012	0.48	-2.764e+002
	TROE / +7.82e-001 +2.71e+002 +2.76e+003 +6.57e+003 /			
	Enhanced third-body efficiencies:			
	H_2/2.00/ H_2O/6.00/ CO/1.50/ CO_2/2.00/			
37.	$H_2 + CO(+M) <=> CH_2O(+M)$	+2.659e+007	1.50	+7.902e+004
	TROE / +9.32e-001 +1.97e+002 +1.54e+003 +1.03e+004 /			
	Enhanced third-body efficiencies:			
	H_2/2.00/ H_2O/6.00/ CO/1.50/ CO_2/2.00/			
38.	$OH + CH_2O <=> HCO + H_2O$	+1.683e+008	1.63	-1.494e+003
	REV / +4.9110e+006 1.81 +2.90e+004 /			
39.	$H + CH_2O <=> HCO + H_2$	+1.875e+007	1.90	+3.778e+003
	REV / +3.3880e+005 2.19 +1.79e+004 /			
40.	$O + CH_2O <=> OH + HCO$	+1.055e+008	1.15	+3.393e+003
	REV / +1.9400e+007 1.42 +1.60e+004 /			
41.	$HO_2 + CH_2O <=> HCO + H_2O_2$	+5.836e-003	4.52	+5.488e+003
	REV / +2.4260e-002 4.11 +5.77e+003 /			
42.	$CH_3O(+M) <=> H + CH_2O(+M)$	+2.008e+014	0.00	+1.987e+004
	TROE / +9.00e-001 +2.50e+003 +1.30e+003 +1.00e+099 /			
	Enhanced third-body efficiencies:			
	H_2/2.00/ H_2O/6.00/ CO/1.50/ CO_2/2.00/			
43.	$CH_3O + O_2 <=> HO_2 + CH_2O$	+1.006e-019	9.50	-6.106e+003
	REV / +1.4160e-020 9.82 +2.11e+004 /			
44.	$H + CH_3O <=> H_2 + CH_2O$	+9.531e+013	0.00	+5.001e+000
	REV / +1.2320e+011 0.66 +8.13e+004 /			
45.	$HO_2 + CH_3O <=> H_2O_2 + CH_2O$	+5.012e+010	0.00	+1.138e+000
	REV / +1.0740e+012 -0.03 +6.53e+004 /			
46.	$CH_3 + OH <=> H_2 + CH_2O$	+7.252e+008	0.00	+4.588e+003
	REV / +4.2490e+011 -0.18 +7.50e+004 /			
47.	$CH_3 + OH <=> CH_2(S) + H_2O$	+5.722e+017	-1.34	+1.718e+003
	REV / +2.3710e+016 -0.86 +1.04e+003 /			
48.	$CH_3 + OH <=> H + CH_3O$	+3.718e+011	0.00	+5.880e+003
	REV / +1.5620e+016 -0.84 -5.82e+003 /			
49.	$CH_3 + OH <=> CH_2 + H_2O$	+9.440e+007	1.60	+4.842e+003
	REV / +1.4760e+009 1.19 +1.65e+004 /			
50.	$CH_3 + HO_2 <=> OH + CH_3O$	+7.781e+012	0.27	-6.417e+002
	REV / +6.1900e+012 0.15 +2.46e+004 /			
51.	$CH_3 + O <=> H + CH_2O$	+3.702e+014	0.05	-1.603e+002
	REV / +3.8730e+015 -0.15 +6.84e+004 /			

52.	$CH_3 + O_2 <=> O + CH_3O$	+1.465e+013	0.00	+2.058e+004
	REV / +4.6680e+014 -0.45 +2.88e+002 /			
53.	$CH_3 + O_2 <=> OH + CH_2O$	+8.469e+010	0.00	+1.347e+004
	REV / +1.1750e+011 0.19 +6.57e+004 /			
54.	$CH_3 + O_2(+M) <=> CH_3O_2(+M)$	+2.591e+007	1.63	+1.009e+001
	TROE / +4.50e-002 +8.80e+002 +2.50e+009 +1.79e+009 /			
55.	$CH_3 + CH_3O_2 <=> 2CH_3O$	+9.258e+012	0.00	-1.081e+003
	REV / +3.4840e+012 0.18 +2.83e+004 /			
56.	$2CH_3O_2 <=> 2CH_3O + O_2$	+1.035e+016	-1.61	+1.684e+003
	REV / +0.0000e+000 0.00 +0.00e+000 /			
57.	$H + CH_3O_2 <=> OH + CH_3O$	+1.884e+014	0.00	+1.681e+000
	REV / +1.7190e+009 1.02 +4.08e+004 /			
58.	$O + CH_3O_2 <=> CH_3O + O_2$	+7.161e+013	0.00	+3.881e+000
	REV / +2.2530e+011 0.63 +5.75e+004 /			
59.	$CH_2(S) <=> CH_2$	+4.448e+012	0.00	+6.120e+000
	REV / +7.1610e+015 -0.89 +1.14e+004 /			
60.	$CH_2(S) + O_2 <=> H + OH + CO$	+4.669e+013	0.00	+4.187e+000
	REV / +0.0000e+000 0.00 +0.00e+000 /			
61.	$CH_2(S) + H_2 <=> H + CH_3$	+2.809e+013	0.00	+1.396e+000
	REV / +2.0230e+016 -0.59 +1.53e+004 /			
62.	$H + CH_2(S) <=> H + CH_2$	+1.242e+014	0.00	+4.367e+000
	REV / +2.1480e+016 -0.89 +1.14e+004 /			
63.	$CH_2(S) + O <=> 2H + CO$	+1.226e+013	0.00	+6.787e+000
	REV / +0.0000e+000 0.00 +0.00e+000 /			
64.	$CH_2(S) + OH <=> H + CH_2O$	+8.696e+013	0.00	+1.117e+001
	REV / +1.1550e+018 -0.77 +8.52e+004 /			
65.	$CH_2(S) + CO_2 <=> CO + CH_2O$	+8.696e+012	0.00	+5.959e+000
	REV / +4.3660e+010 0.42 +5.98e+004 /			
66.	$H + CH_2(+M) <=> CH_3(+M)$	+4.907e+016	-0.80	+3.639e+000
	TROE / +6.80e-001 +7.80e+001 +2.00e+003 +5.59e+003 /			
	Enhanced third-body efficiencies:			
	H_2/2.00/ H_2O/6.00/ CO/1.50/ CO_2/2.00/			
67.	$CH_2 + O_2 <=> 2H + CO_2$	+4.292e+011	0.00	+9.771e+002
	REV / +0.0000e+000 0.00 +0.00e+000 /			
68.	$CH_2 + O <=> 2H + CO$	+9.302e+013	0.00	+9.126e+000
	REV / +0.0000e+000 0.00 +0.00e+000 /			
69.	$H + C_2H_4(+M) <=> C_2H_5(+M)$	+2.224e+012	0.45	+1.578e+003
	TROE / +9.75e-001 +2.10e+002 +9.84e+002 +4.37e+003 /			
	Enhanced third-body efficiencies:			
	H_2/2.00/ H_2O/6.00/ CO/1.50/ CO_2/2.00/			
70.	$H + C_2H_5 <=> 2CH_3$	+1.120e+018	-0.93	+3.190e+002
	REV / +6.8400e+012 0.10 +1.06e+004 /			
71.	$H + C_2H_5 <=> H_2 + C_2H_4$	+2.553e+012	0.00	+1.032e+001

	REV / +4.4380e+011 0.40 +6.81e+004 /			
72.	$C_2H_5O_2 <=> C_2H_5 + O_2$	+1.052e+062	-14.78	+5.768e+004
	REV / +2.8760e+056 -13.82 +1.46e+004 /			
73.	$C_2H_5 + O_2 <=> HO_2 + C_2H_4$	+3.282e+014	-1.01	+5.740e+003
	(Duplicate reaction)			
	REV / +8.8020e+014 -0.96 +1.81e+004 /			
74.	$C_2H_5 + O_2 <=> HO_2 + C_2H_4$	+1.223e+000	3.88	+1.408e+004
	(Duplicate reaction)			
	REV / +4.6560e-001 3.93 +2.70e+004 /			
75.	$C_2H_5O_2 <=> HO_2 + C_2H_4$	+7.878e+037	-8.45	+4.430e+004
	REV / +4.6320e+032 -7.44 +1.67e+004 /			
76.	$CH_3CO + M <=> CH_3 + CO + M$	+7.558e+011	0.00	+1.935e+004
77.	$H + CH_3CO <=> CH_2CO + H_2$	+6.286e+012	0.00	+5.083e+000
	REV / +3.8410e+015 -0.55 +6.07e+004 /			
78.	$O + CH_3CO <=> OH + CH_2CO$	+8.174e+012	0.00	+5.083e+000
	REV / +2.0160e+015 -0.57 +5.93e+004 /			
79.	$CH_2 + CO(+M) <=> CH_2CO(+M)$	+1.095e+012	0.00	+5.044e+000
	TROE / +5.91e-001 +2.75e+002 +1.23e+003 +5.19e+003 /			
	Enhanced third-body efficiencies:			
	H_2/2.00/ H_2O/6.00/ CO/1.50/ CO_2/2.00/			
80.	$H + CH_2CO <=> CH_3 + CO$	+2.106e+013	0.00	+2.709e+003
	REV / +2.4000e+012 0.00 +4.02e+004 /			
81.	$O + CH_2CO <=> CH_2 + CO_2$	+7.334e+011	0.00	+1.029e+003
	REV / +1.2410e+010 0.68 +5.17e+004 /			
82.	$CH_2(S) + CH_2CO <=> C_2H_4 + CO$	+7.757e+013	0.00	+9.038e+000
	REV / +1.0110e+012 0.96 +1.03e+005 /			
83.	$O + C_2H_4 <=> CH_3 + HCO$	+1.000e+007	1.88	+1.787e+002
	REV / +3.3330e+002 2.60 +2.61e+004 /			
84.	$CH_2(S) + CH_3 <=> H + C_2H_4$	+4.458e+013	0.00	+8.309e+000
	REV / +6.1310e+019 -1.22 +7.31e+004 /			
85.	$CH_3OCO <=> CH_3 + CO_2$	+1.512e+013	0.33	+1.225e+004
	REV / +4.7600e+007 1.54 +3.47e+004 /			
86.	$CH_3OCO <=> CH_3O + CO$	+1.684e+013	0.46	+3.313e+004
	REV / +1.5500e+006 2.02 +5.73e+003 /			
87.	$_IC_3H_7 <=> H + C_3H_6$	+2.490e+013	-0.01	+3.695e+004
	REV / +2.6400e+013 0.00 +2.16e+003 /			
88.	$H +_I C_3H_7 <=> CH_3 + C_2H_5$	+9.182e+012	0.00	+7.469e+000
	REV / +5.5140e+007 1.16 +8.36e+003 /			
89.	$_IC_3H_7 + O_2 <=> HO_2 + C_3H_6$	+2.680e-019	0.00	+6.088e+003
	REV / +2.0000e-019 0.00 +1.75e+004 /			
90.	$_IC_3H_7 + OH <=> C_3H_6 + H_2O$	+3.897e+012	0.00	+7.143e+000
	REV / +2.9850e+012 0.57 +8.38e+004 /			
91.	$NC_3H_7 <=> CH_3 + C_2H_4$	+4.745e+040	-8.60	+3.584e+004

	REV / +2.4220e+034 -7.01 +1.69e+004 /			
92.	$NC_3H_7 <=> H + C_3H_6$	+6.945e+039	-8.10	+5.894e+004
	REV / +2.0700e+037 -7.39 +1.20e+004 /			
93.	$NC_3H_7 + O_2 <=> HO_2 + C_3H_6$	+1.150e-019	0.00	+2.185e+003
	REV / +2.0000e-019 0.00 +1.75e+004 /			
94.	$O + C_3H_6 <=> C_2H_5 + HCO$	+1.299e+007	1.76	-1.290e+003
	REV / +9.2720e+001 2.72 +2.31e+004 /			
95.	$O + C_3H_6 <=> H + CH_3 + CH_2CO$	+1.953e+006	1.76	+5.503e+001
	REV / +0.0000e+000 0.00 +0.00e+000 /			
96.	$H + C_3H_6 <=> CH_3 + C_2H_4$	+2.432e+034	-5.81	+1.721e+004
	REV / +4.5720e+028 -4.54 +2.72e+004 /			
97.	$NC_3H_7O_2 <=> NC_3H_7 + O_2$	+9.604e+020	-1.64	+3.197e+004
	REV / +4.5200e+012 0.00 +0.00e+000 /			
98.	$_IC_3H_7O_2 <=> _IC_3H_7 + O_2$	+6.801e+022	-2.19	+3.311e+004
	REV / +7.5400e+012 0.00 +0.00e+000 /			
99.	$_IC_3H_7O_2 <=> HO_2 + C_3H_6$	+5.711e+042	-9.41	+3.861e+004
	REV / +1.9570e+033 -7.29 +1.67e+004 /			
100.	$NC_3H_7O_2 <=> HO_2 + C_3H_6$	+1.057e+038	-8.11	+4.126e+004
	REV / +1.2000e+030 -6.23 +2.04e+004 /			
101.	$PC_4H_9 <=> C_2H_5 + C_2H_4$	+1.066e+012	0.46	+2.559e+004
	REV / +1.3200e+004 2.48 +6.13e+003 /			
102.	$H + MD_2.J <=> MD$	+1.351e+014	0.00	+1.138e+000
103.	$H + MD_3.J <=> MD$	+3.659e+013	0.00	+6.193e+000
104.	$H + MD_4.J <=> MD$	+8.982e+013	0.00	+1.002e+001
105.	$H + MD_5.J <=> MD$	+1.870e+013	0.00	+8.123e+000
106.	$H + MD_6.J <=> MD$	+1.026e+013	0.00	+1.808e+000
107.	$H + MD_7.J <=> MD$	+2.644e+014	0.00	+1.298e+000
108.	$H + MD_8.J <=> MD$	+3.266e+013	0.00	+3.921e+000
109.	$H + MD_9.J <=> MD$	+3.659e+013	0.00	+1.000e+001
110.	$CH_3 + MN_9.J <=> MD$	+2.644e+013	0.00	+1.095e+001
111.	$C_2H_5 + MO_8.J <=> MD$	+3.089e+012	0.00	+5.644e+000
112.	$NC_3H_7 + MS_7.J <=> MD$	+1.991e+013	0.00	+5.666e+000
113.	$PC_4H_9 + MH_6.J <=> MD$	+7.775e+012	0.00	+4.629e+000
114.	$C_5H_{11} - .1 + MF_5.J <=> MD$	+1.022e+013	0.00	+9.610e+000
115.	$C_6H_{13} - .1 + MB_4.J <=> MD$	+1.349e+013	0.00	+9.161e+000
116.	$C_7H_{15} - .1 + MP_3.J <=> MD$	+5.913e+012	0.00	+6.519e+000
117.	$C_8H_{17} - .1 + ME_2.J <=> MD$	+1.881e+013	0.00	+6.407e+000
118.	$C_9H_{19} - .1 + CH_3OCO <=> MD$	+8.051e+012	0.00	+3.453e+000
119.	$H + MD <=> MD_2.J + H_2$	+1.310e+006	2.54	+7.519e+003
120.	$HO_2 + MD <=> MD_2.J + H_2O_2$	+1.386e+004	2.55	+8.638e+003
121.	$OH + MD <=> MD_2.J + H_2O$	+1.176e+010	0.51	+7.258e+001
122.	$O_2 + MD <=> HO_2 + MD_2.J$	+2.795e+014	0.00	+2.736e+004
123.	$O + MD <=> OH + MD_2.J$	+5.868e+004	2.40	+1.640e+003

124.	$H + MD <=> MD_3.J + H_2$	+6.688e+005	2.40	+4.556e+003
125.	$HO_2 + MD <=> MD_3.J + H_2O_2$	+2.359e+004	2.50	+1.730e+004
126.	$OH + MD <=> MD_3.J + H_2O$	+4.372e+006	1.61	-4.825e+001
127.	$O_2 + MD <=> HO_2 + MD_3.J$	+2.471e+014	0.00	+4.949e+004
128.	$O + MD <=> OH + MD_3.J$	+3.628e+005	2.44	+3.338e+003
129.	$H + MD <=> MD_4.J + H_2$	+2.191e+004	2.40	+7.803e+003
130.	$HO_2 + MD <=> MD_4.J + H_2O_2$	+1.620e+004	2.50	+1.701e+004
131.	$OH + MD <=> MD_4.J + H_2O$	+3.558e+006	1.61	-3.280e+001
132.	$O_2 + MD <=> HO_2 + MD_4.J$	+6.660e+012	0.00	+4.912e+004
133.	$O + MD <=> OH + MD_4.J$	+3.188e+004	2.44	+2.423e+003
134.	$H + MD <=> MD_5.J + H_2$	+6.692e+005	2.40	+6.458e+003
135.	$HO_2 + MD <=> MD_5.J + H_2O_2$	+6.953e+005	2.50	+9.834e+003
136.	$OH + MD <=> MD_5.J + H_2O$	+5.962e+007	1.61	-5.885e+001
137.	$O_2 + MD <=> HO_2 + MD_5.J$	+2.382e+013	0.00	+3.809e+004
138.	$O + MD <=> OH + MD_5.J$	+3.628e+005	2.44	+3.095e+003
139.	$H + MD <=> MD_6.J + H_2$	+8.670e+005	2.40	+4.798e+003
140.	$HO_2 + MD <=> MD_6.J + H_2O_2$	+5.293e+005	2.50	+8.991e+003
141.	$OH + MD <=> MD_6.J + H_2O$	+4.204e+008	1.61	-3.311e+001
142.	$O_2 + MD <=> HO_2 + MD_6.J$	+7.766e+013	0.00	+4.924e+004
143.	$O + MD <=> OH + MD_6.J$	+1.216e+005	2.44	+3.222e+003
144.	$H + MD <=> MD_7.J + H_2$	+4.515e+006	2.40	+4.962e+003
145.	$HO_2 + MD <=> MD_7.J + H_2O_2$	+1.142e+005	2.50	+1.235e+004
146.	$OH + MD <=> MD_7.J + H_2O$	+1.781e+006	1.61	-2.544e+001
147.	$O_2 + MD <=> HO_2 + MD_7.J$	+1.586e+014	0.00	+3.989e+004
148.	$O + MD <=> OH + MD_7.J$	+8.558e+004	2.44	+3.440e+003
149.	$H + MD <=> MD_8.J + H_2$	+5.377e+004	2.40	+4.819e+003
150.	$HO_2 + MD <=> MD_8.J + H_2O_2$	+4.539e+004	2.50	+2.312e+004
151.	$OH + MD <=> MD_8.J + H_2O$	+2.504e+006	1.61	-3.879e+001
152.	$O_2 + MD <=> HO_2 + MD_8.J$	+7.957e+013	0.00	+4.348e+004
153.	$O + MD <=> OH + MD_8.J$	+1.442e+005	2.44	+2.559e+003
154.	$H + MD <=> MD_9.J + H_2$	+5.020e+005	2.40	+6.203e+003
155.	$HO_2 + MD <=> MD_9.J + H_2O_2$	+2.015e+005	2.50	+1.032e+004
156.	$OH + MD <=> MD_9.J + H_2O$	+1.343e+007	1.61	-3.170e+001
157.	$O_2 + MD <=> HO_2 + MD_9.J$	+2.058e+013	0.00	+3.809e+004
158.	$O + MD <=> OH + MD_9.J$	+2.101e+005	2.44	+2.481e+003
159.	$MS_7.J + C_3H_6 <=> MD_9.J$	+5.084e+004	2.48	+5.989e+003
160.	$MF_5.J + C_5H_{10} - .1 <=> MD_7.J$	+7.715e+003	2.48	+5.984e+003
161.	$MB_4.J + C_6H_{12} - .1 <=> MD_6.J$	+1.245e+004	2.48	+5.476e+003
162.	$C_7H_{15} - .1 + MP_2D <=> MD_2.J$	+8.767e+010	0.00	+8.784e+003
163.	$MS_7.J + C_2H_4 <=> MN_9.J$	+2.162e+004	2.48	+8.799e+003
164.	$MH_6.J + C_2H_4 <=> MO_8.J$	+2.951e+004	2.48	+5.989e+003
165.	$MF_5.J + C_2H_4 <=> MS_7.J$	+1.068e+003	2.48	+7.691e+003
166.	$MB_4.J + C_2H_4 <=> MH_6.J$	+2.488e+004	2.48	+7.489e+003

167.	$MP_3.J + C_2H_4 <=> MF_5.J$	+5.436e+004	2.48	+6.018e+003
168.	$ME_2.J + C_2H_4 <=> MB_4.J$	+1.072e+010	0.00	+6.093e+003
169.	$CH_3OCO + C_2H_4 <=> MP_3.J$	+5.633e+011	0.00	+7.489e+003
170.	$H + MP_2D <=> MP_3.J$	+3.627e+013	0.00	+2.514e+003
171.	$CH_3O + CH_2CO <=> ME_2.J$	+1.322e+012	0.00	-1.261e+003
172.	$C_7H_{15}-.1 + C_2H_4 <=> C_9H_{19}-.1$	+4.030e+003	2.48	+4.646e+003
173.	$C_6H_{13}-.1 + C_2H_4 <=> C_8H_{17}-.1$	+4.792e+003	2.48	+4.646e+003
174.	$C_5H_{11}-.1 + C_2H_4 <=> C_7H_{15}-.1$	+6.287e+002	2.48	+8.051e+003
175.	$PC_4H_9 + C_2H_4 <=> C_6H_{13}-.1$	+8.150e+002	2.48	+6.867e+003
176.	$H + C_6H_{12}-.1 <=> C_6H_{13}-.1$	+1.508e+012	0.51	+3.468e+003
177.	$NC_3H_7 + C_2H_4 <=> C_5H_{11}-.1$	+3.489e+004	2.48	+5.530e+003
178.	$H + C_5H_{10}-.1 <=> C_5H_{11}-.1$	+2.956e+012	0.51	+1.808e+003
179.	$CH_3OCO + C_6H_{12}-.1 <=> MS_3.J$	+3.404e+011	0.00	+5.540e+003
180.	$H + MP_2D <=> MP_2.J$	+3.058e+013	0.00	+4.321e+003
181.	$CH_3CO + CH_2O <=> MEM.J$	+1.235e+012	0.00	+1.455e+004
182.	$NC_3H_7 + C_5H_{10}-.1 <=> C_8H_{17}-.4$	+1.144e+004	2.48	+6.596e+003
183.	$C_2H_5 + C_6H_{12}-.1 <=> C_8H_{17}-.4$	+1.637e+004	2.48	+6.553e+003
184.	$CH_3 + C_6H_{12}-.1 <=> C_7H_{15}-.3$	+3.962e+004	2.48	+5.231e+003
185.	$C_5H_{11}-.1 + O_2 <=> HO_2 + C_5H_{10}-.1$	+2.587e+011	0.00	+4.572e+003
186.	$C_6H_{13}-.1 + O_2 <=> HO_2 + C_6H_{12}-.1$	+1.170e+012	0.00	+4.954e+003
187.	$MP_3.J + O_2 <=> HO_2 + MP_2D$	+2.106e+011	0.00	+7.412e+003
188.	$C_8H_{17}-.1 <=> C_8H_{17}-.4$ (Duplicate reaction)	+3.993e+012	-0.12	+2.637e+004
189.	$C_8H_{17}-.1 <=> C_8H_{17}-.4$ (Duplicate reaction)	+1.117e+002	2.55	+1.032e+004
190.	$C_7H_{15}-.1 <=> C_7H_{15}-.3$ (Duplicate reaction)	+5.067e+010	0.67	+3.611e+004
191.	$C_7H_{15}-.1 <=> C_7H_{15}-.3$ (Duplicate reaction)	+5.200e+002	2.55	+1.371e+004
192.	$NC_3H_7 <=>_I C_3H_7$	+2.981e+010	0.88	+3.785e+004
193.	$MD_9.J <=> MD_8.J$	+5.928e+009	0.88	+4.602e+004
194.	$MD_9.J <=> MD_7.J$	+5.754e+010	0.67	+3.918e+004
195.	$MD_9.J <=> MD_6.J$	+1.189e+012	-0.12	+2.204e+004
196.	$MD_9.J <=> MD_5.J$	+5.632e+012	-0.60	+1.364e+004
197.	$MD_8.J <=> MD_7.J$	+1.428e+010	0.88	+3.681e+004
198.	$MD_8.J <=> MD_6.J$	+6.803e+010	0.67	+5.718e+004
199.	$MD_8.J <=> MD_5.J$	+8.455e+011	-0.12	+2.399e+004
200.	$MD_8.J <=> MD_4.J$	+1.417e+012	-0.60	+9.728e+003
201.	$MD_7.J <=> MD_6.J$	+5.584e+010	0.88	+4.380e+004
202.	$MD_7.J <=> MD_5.J$	+1.228e+010	0.67	+3.642e+004
203.	$MD_7.J <=> MD_4.J$	+7.349e+010	-0.12	+3.101e+004
204.	$MD_7.J <=> MD_3.J$	+3.183e+012	-0.60	+1.404e+004
205.	$MD_6.J <=> MD_5.J$	+2.926e+010	0.88	+5.379e+004

206.	$MD_6.J <=> MD_4.J$	+5.135e+010	0.67	+3.813e+004
207.	$MD_6.J <=> MD_3.J$	+6.293e+011	-0.12	+2.823e+004
208.	$MD_6.J <=> MD_2.J$	+6.939e+011	-0.60	+1.794e+004
209.	$MD_5.J <=> MD_4.J$	+5.688e+010	0.88	+4.010e+004
210.	$MD_5.J <=> MD_3.J$	+7.201e+010	0.67	+3.284e+004
211.	$MD_5.J <=> MD_2.J$	+4.039e+011	-0.12	+2.383e+004
212.	$MD_4.J <=> MD_3.J$	+3.068e+011	0.88	+3.681e+004
213.	$MD_4.J <=> MD_2.J$	+6.657e+010	0.67	+3.231e+004
214.	$MD_3.J <=> MD_2.J$	+1.832e+010	0.88	+3.354e+004
215.	$MS_7.J <=> MS_3.J$	+5.905e+002	2.55	+6.631e+003
216.	$MP_3.J <=> MP_2.J$	+4.103e+010	0.88	+2.762e+004
217.	$MPM.J <=> MP_3.J$	+1.413e+002	2.55	+9.521e+003
218.	$MPM.J <=> MP_2.J$	+4.209e+010	-0.12	+1.800e+004
219.	$MEM.J <=> ME_2.J$	+2.847e+012	-0.12	+1.723e+004
220.	$C_6H_{12} - .1 <=> 2C_3H_6$	+6.679e+012	0.00	+4.985e+004
221.	$C_5H_{10} - .1 <=> C_2H_4 + C_3H_6$	+9.246e+011	0.00	+5.966e+004
222.	$C_8H_{17} - .1 + O_2 <=> C_8H_{17}O_2 - .1$	+2.365e+011	0.00	+1.673e+000
223.	$C_7H_{15} - .1 + O_2 <=> C_7H_{15}O_2 - .1$	+5.711e+012	0.00	+3.086e+000
224.	$C_7H_{15} - .3 + O_2 <=> C_7H_{15}O_2 - .3$	+5.745e+011	0.00	+1.178e+000
225.	$MD_9.J + O_2 <=> MD_9O_2$	+5.513e+012	0.00	+7.917e+000
226.	$MD_8.J + O_2 <=> MD_8O_2$	+9.924e+011	0.00	+1.970e+000
227.	$MD_7.J + O_2 <=> MD_7O_2$	+1.580e+012	0.00	+1.071e+001
228.	$MD_6.J + O_2 <=> MD_6O_2$	+4.151e+012	0.00	+3.363e+000
229.	$MD_5.J + O_2 <=> MD_5O_2$	+2.403e+012	0.00	+4.835e+000
230.	$MD_4.J + O_2 <=> MD_4O_2$	+5.099e+012	0.00	+6.981e+000
231.	$MD_3.J + O_2 <=> MD_3O_2$	+2.227e+013	0.00	+3.501e+000
232.	$MD_2.J + O_2 <=> MD_2O_2$	+1.464e+013	0.00	+5.666e+000
233.	$MS_7.J + O_2 <=> MS_7O_2$	+6.844e+012	0.00	+4.937e+000
234.	$MS_3.J + O_2 <=> MS_3O_2$	+1.465e+013	0.00	+4.163e+000
235.	$MB_4.J + O_2 <=> MB_4O_2$	+2.154e+013	0.00	+8.086e+000
236.	$MP_3.J + O_2 <=> MP_3O_2$	+2.257e+013	0.00	+6.204e+000
237.	$MP_2.J + O_2 <=> MP_2O_2$	+4.242e+012	0.00	+8.465e+000
238.	$ME_2.J + O_2 <=> ME_2O_2$	+2.011e+012	0.00	+6.407e+000
239.	$MEM.J + O_2 <=> MEMO_2$	+1.050e+012	0.00	+6.994e+000
240.	$MEMO_2 <=> MEMOOH_2.J$	+3.717e+010	0.00	+1.924e+004
241.	$MB_4O_2 <=> MB_4OOH_3.J$	+2.427e+010	0.00	+3.872e+004
242.	$MB_4O_2 <=> MB_4OOH_2.J$	+1.022e+010	0.00	+2.325e+004
243.	$MS_7O_2 <=> MS_7OOH_5.J$	+6.521e+010	0.00	+2.336e+004
244.	$MS_7O_2 <=> MS_7OOH_4.J$	+1.254e+009	0.00	+1.657e+004
245.	$MD_2O_2 <=> MD_2OOH_4.J$	+6.110e+010	0.00	+1.380e+004
246.	$MD_3O_2 <=> MD_3OOH_2.J$	+2.028e+011	0.00	+2.419e+004
247.	$MD_3O_2 <=> MD_3OOH_4.J$	+5.579e+011	0.00	+3.108e+004
248.	$MD_3O_2 <=> MD_3OOH_5.J$	+1.956e+010	0.00	+2.244e+004

249.	$MD_3O_2 <=> MD_3OOH_6.J$	+9.228e+009	0.00	+2.034e+004
250.	$MD_4O_2 <=> MD_4OOH_3.J$	+2.028e+011	0.00	+3.566e+004
251.	$MD_4O_2 <=> MD_4OOH_2.J$	+1.999e+010	0.00	+1.802e+004
252.	$MD_4O_2 <=> MD_4OOH_5.J$	+2.249e+011	0.00	+3.140e+004
253.	$MD_4O_2 <=> MD_4OOH_6.J$	+8.951e+009	0.00	+3.352e+004
254.	$MD_5O_2 <=> MD_5OOH_4.J$	+1.386e+011	0.00	+4.316e+004
255.	$MD_5O_2 <=> MD_5OOH_3.J$	+4.042e+009	0.00	+2.739e+004
256.	$MD_5O_2 <=> MD_5OOH_2.J$	+4.014e+008	0.00	+1.985e+004
257.	$MD_5O_2 <=> MD_5OOH_6.J$	+9.159e+010	0.00	+3.289e+004
258.	$MD_5O_2 <=> MD_5OOH_7.J$	+4.973e+010	0.00	+2.093e+004
259.	$MD_6O_2 <=> MD_6OOH_5.J$	+9.531e+011	0.00	+3.854e+004
260.	$MD_6O_2 <=> MD_6OOH_4.J$	+3.786e+010	0.00	+1.590e+004
261.	$MD_6O_2 <=> MD_6OOH_3.J$	+1.758e+009	0.00	+2.288e+004
262.	$MD_6O_2 <=> MD_6OOH_8.J$	+1.048e+010	0.00	+2.220e+004
263.	$MD_6O_2 <=> MD_6OOH_9.J$	+1.035e+009	0.00	+1.865e+004
264.	$MD_7O_2 <=> MD_7OOH_6.J$	+2.248e+011	0.00	+3.280e+004
265.	$MD_7O_2 <=> MD_7OOH_5.J$	+2.192e+010	0.00	+1.590e+004
266.	$MD_7O_2 <=> MD_7OOH_4.J$	+1.471e+009	0.00	+2.409e+004
267.	$MD_7O_2 <=> MD_7OOH_8.J$	+8.129e+011	0.00	+4.178e+004
268.	$MD_7O_2 <=> MD_7OOH_9.J$	+4.973e+010	0.00	+2.993e+004
269.	$MD_8O_2 <=> MD_8OOH_7.J$	+9.404e+011	0.00	+3.385e+004
270.	$MD_8O_2 <=> MD_8OOH_6.J$	+1.930e+010	0.00	+2.528e+004
271.	$MD_8O_2 <=> MD_8OOH_5.J$	+9.545e+008	0.00	+2.423e+004
272.	$MD_8O_2 <=> MD_8OOH_9.J$	+1.896e+011	0.00	+3.689e+004
273.	$MD_9O_2 <=> MD_9OOH_7.J$	+6.438e+009	0.00	+2.520e+004
274.	$MD_9O_2 <=> MD_9OOH_6.J$	+5.526e+008	0.00	+2.726e+004
275.	$CH_3O_2 + MS_3O_2 <=> CH_3O + MS_3O + O_2$	+1.843e+015	-1.61	+1.545e+003
276.	$C_2H_5 + MF_5OXO <=> MS_5O$	+1.276e+010	0.00	+1.033e+004
277.	$ME_2.J + C_4H_9CHO <=> MS_3O$	+1.067e+011	0.00	+9.240e+003
278.	$MB_4OOH_2.J <=> OH + MP_2D + CH_2O$	+2.820e+014	-0.14	+2.673e+004
	REV / +0.0000e+000 0.00 +0.00e+000 /			
279.	$MD_5OOH_7.J <=> OH + C_5H_{10} - .1 + MF_5OXO$	+1.218e+019	-1.67	+1.632e+004
	REV / +0.0000e+000 0.00 +0.00e+000 /			
280.	$MD_2OOH_4.J + O_2 <=> MD_2OOH_4O_2$	+1.429e+013	0.00	+1.465e+000
281.	$MD_3OOH_2.J + O_2 <=> MD_3OOH_2O_2$	+5.573e+012	0.00	+2.388e+000
282.	$MD_3OOH_4.J + O_2 <=> MD_3OOH_4O_2$	+1.755e+013	0.00	+1.035e+001
283.	$MD_3OOH_5.J + O_2 <=> MD_3OOH_5O_2$	+8.973e+012	0.00	+1.399e+000
284.	$MD_3OOH_6.J + O_2 <=> MD_3OOH_6O_2$	+1.041e+013	0.00	+9.161e+000
285.	$MD_4OOH_3.J + O_2 <=> MD_4OOH_3O_2$	+4.718e+012	0.00	+8.407e+000
286.	$MD_4OOH_2.J + O_2 <=> MD_4OOH_2O_2$	+2.103e+013	0.00	+6.725e+000
287.	$MD_4OOH_5.J + O_2 <=> MD_4OOH_5O_2$	+1.942e+012	0.00	+1.970e+000
288.	$MD_4OOH_6.J + O_2 <=> MD_4OOH_6O_2$	+5.039e+013	0.00	+9.076e+000
289.	$MD_5OOH_4.J + O_2 <=> MD_5OOH_4O_2$	+3.025e+012	0.00	+1.817e+000

290.	$MD_5OOH_3.J + O_2 <=> MD_5OOH_3O_2$	+1.005e+013	0.00	+9.771e+000
291.	$MD_5OOH_2.J + O_2 <=> MD_5OOH_2O_2$	+1.829e+012	0.00	+1.182e+001
292.	$MD_5OOH_6.J + O_2 <=> MD_5OOH_6O_2$	+3.453e+012	0.00	+2.724e+000
293.	$MD_5OOH_7.J + O_2 <=> MD_5OOH_7O_2$	+4.601e+012	0.00	+5.715e+000
294.	$MD_6OOH_5.J + O_2 <=> MD_6OOH_5O_2$	+2.403e+012	0.00	+1.537e+000
295.	$MD_6OOH_4.J + O_2 <=> MD_6OOH_4O_2$	+3.499e+012	0.00	+1.602e+000
296.	$MD_6OOH_3.J + O_2 <=> MD_6OOH_3O_2$	+8.973e+012	0.00	+9.085e+000
297.	$MD_6OOH_8.J + O_2 <=> MD_6OOH_8O_2$	+2.306e+013	0.00	+8.750e+000
298.	$MD_6OOH_9.J + O_2 <=> MD_6OOH_9O_2$	+2.246e+012	0.00	+9.771e+000
299.	$MD_7OOH_6.J + O_2 <=> MD_7OOH_6O_2$	+1.041e+013	0.00	+6.829e+000
300.	$MD_7OOH_5.J + O_2 <=> MD_7OOH_5O_2$	+5.867e+013	0.00	+8.508e+000
301.	$MD_7OOH_4.J + O_2 <=> MD_7OOH_4O_2$	+1.664e+013	0.00	+1.137e+001
302.	$MD_7OOH_8.J + O_2 <=> MD_7OOH_8O_2$	+3.082e+012	0.00	+4.261e+000
303.	$MD_7OOH_9.J + O_2 <=> MD_7OOH_9O_2$	+1.019e+013	0.00	+5.406e+000
304.	$MD_8OOH_7.J + O_2 <=> MD_8OOH_7O_2$	+1.448e+013	0.00	+5.224e+000
305.	$MD_8OOH_6.J + O_2 <=> MD_8OOH_6O_2$	+1.622e+013	0.00	+9.306e+000
306.	$MD_8OOH_5.J + O_2 <=> MD_8OOH_5O_2$	+2.169e+012	0.00	+8.009e+000
307.	$MD_8OOH_9.J + O_2 <=> MD_8OOH_9O_2$	+2.275e+013	0.00	+1.530e+000
308.	$MD_9OOH_7.J + O_2 <=> MD_9OOH_7O_2$	+1.580e+012	0.00	+3.086e+000
309.	$MD_9OOH_6.J + O_2 <=> MD_9OOH_6O_2$	+2.333e+013	0.00	+1.134e+001
310.	$MEMOOH_2.J + O_2 <=> MEMOOH_2O_2$	+3.057e+012	0.00	+2.948e+000
311.	$MB_4OOH_3.J + O_2 <=> MB_4OOH_3O_2$	+1.271e+013	0.00	+9.875e+000
312.	$MB_4OOH_2.J + O_2 <=> MB_4OOH_2O_2$	+1.271e+013	0.00	+6.204e+000
313.	$MF_5OOH_3.J + O_2 <=> MF_5OOH_3O_2$	+2.131e+013	0.00	+3.203e+000
314.	$MF_5OOH_2.J + O_2 <=> MF_5OOH_2O_2$	+5.964e+012	0.00	+6.132e+000
315.	$MS_7OOH_5.J + O_2 <=> MS_7OOH_5O_2$	+3.499e+012	0.00	+5.125e+000
316.	$MS_7OOH_4.J + O_2 <=> MS_7OOH_4O_2$	+1.102e+013	0.00	+1.039e+001
317.	$MD_2OOH_4O_2 <=> OH + MDKET_{24}$	+1.928e+010	0.00	+1.412e+004
318.	$MD_6OOH_4O_2 <=> OH + MDKET_{64}$	+8.136e+009	0.00	+1.792e+004
319.	$C_5H_{11} - .1 + CH_2CO <=> C_5H_{11}COCH_2$	+1.822e+004	2.48	+6.890e+003
320.	$C_6H_{13} - .1 + CH_2CO <=> C_6H_{13}COCH_2$	+1.894e+004	2.48	+4.675e+003
321.	$C_5H_{11}COCH_2 + CO <=> C_5H_{11}COCH_2CO$	+1.173e+004	2.48	+8.465e+003
322.	$C_6H_{13}COCH_2 + CO <=> C_6H_{13}COCH_2CO$	+4.845e+003	2.48	+5.721e+003

Table A.3: 322 reactions and 163 species reduced and optimized reaction mechanism for ignition of methyl-decanoate. Rate constants $k = AT^b exp(-E/R_uT)$; units are cm, mol, s, cal, K.

B

Algorithms

B.1 Computation of forward and reaction rate productories.

Since the computation of the productories $P_{f,k} = \prod_{i=1}^{n_s} C_i^{\nu'_{k,i}}$ and $P_{b,k} = \prod_{i=1}^{n_s} C_i^{\nu''_{k,i}}$ is usually the most computationally demanding task, when evaluating reaction rates, a procedure has been developed for reducing the computational cost exploiting vectorized operations. In particular, attention has been focused on the exponents and on the productories. First of all, it has been noticed that, even if the exponents $\nu'_{k,i}$,$\nu''_{k,i}$ to the concentration values C_i, which represent the stoichiometric coefficients of the product and that of the reactant, concerning specie i in reaction k, can eventually be any real number, although the majority of the reactions in reaction mechanisms are elementary reaction steps, which involve two molecules, eventually of the same specie. For this reason, most values in ν' are integer numbers, either 0, 1 or 2. Thus, in order to reduce the computational time devoted to the evaluation of powers, 6 pointers have been considered for addressing indexes in the ν' and ν'' matrices having the respective values, 1, 2, or arbitrary.

In order to evaluate the two productories in a vectorized fashion, two matrices, namely $\mathbf{C}'_2$ and $\mathbf{C}''_2$ are created, having dimensions the number of reactions versus the maximum number of reactants/products ($n_r \times n_{maxr}$), and initialised at each timestep filled with ones. Then, the values of the concentrations having exponent 1 – given by the pointer computed at the first timestep only – are stored, while those having exponent 2 are multiplied by themselves and then stored, too. Finally, the power operator is applied to the concentrations which have exponent other than 1 or 2, whose results are stored in $\mathbf{C}'_2$ and $\mathbf{C}''_2$ too. The productories are then evaluated as products on the second dimension of $\mathbf{C}'_2$ and $\mathbf{C}''_2$. A pseudocode illustrating this whole procedure is reported in the following.

if $istep == 1$ **then**

$n_{maxr} \leftarrow$ get max number of reactants

$n_{maxp} \leftarrow$ get max number of products

inur1 $\leftarrow find\left(\nu' == 1\right)$

inur2 $\leftarrow find\left(\nu' == 2\right)$

inuro $\leftarrow find\left(\nu' \notin \{0;1;2\}\right)$

inup1 $\leftarrow find\left(\nu'' == 1\right)$

inup2 $\leftarrow find\left(\nu'' == 2\right)$

inupo $\leftarrow find\left(\nu'' \notin \{0;1;2\}\right)$

for $i = 1$ to n_r **do**

$ireacs(i,:) \leftarrow find\left(\nu'(i,:) \neq 0\right)$

$iprods(i,:) \leftarrow find\left(\nu''(i,:) \neq 0\right)$

end for

end if

initialise $C_2' \leftarrow ones(n_r \times n_{maxr})$

initialise $C_2'' \leftarrow ones\left(n_r \times n_{maxp}\right)$

C_2' (**inur1**) $\leftarrow C$ (**ireacs** == **inur1**)

C_2' (**inur2**) $\leftarrow C$ (**ireacs** == **inur2**) $\circ\, C$ (**ireacs** == **inur2**)

C_2' (**inuro**) $\leftarrow C$ (**ireacs** == **inuro**)

C_2' (**inuro**) $\leftarrow C_2'$ (**inuro**)$^{\nu'(\textbf{inuro})}$

$C_2''\left(\textbf{inup1}\right) \leftarrow C\left(\textbf{iprods} == \textbf{inup1}\right)$

$C_2''\left(\textbf{inup2}\right) \leftarrow C\left(\textbf{iprods} == \textbf{inup2}\right) \circ C\left(\textbf{iprods} == \textbf{inup2}\right)$

$C_2''\left(\textbf{inupo}\right) \leftarrow C\left(\textbf{iprods} == \textbf{inupo}\right)$

$C_2''\left(\textbf{inupo}\right) \leftarrow C_2'\left(\textbf{inupo}\right)^{\nu'(\textbf{inupo})}$

$P_f \leftarrow prod\left(C_2', 2\right)$

$P_b \leftarrow prod\left(C_2'', 2\right)$

B.2 Estimation of in-cylinder charge composition with EGR.

An iterative algorithm has been developed for the estimation of in-cylinder charge when an EGR fraction is present. First of all, the in-cylinder composition is initialised as standard air. Then, a number of iterations is started following the scheme:

1. estimate the mixture equivalence ratio assuming complete evaporation of the injected fuel mass;
2. compute the in-cylinder mass assuming perfect gas mixture;
3. estimate mixture's adiabatic flame temperature for the mixture (see in the following);
4. compute composition of combustion products assuming equilibrium at the adiabatic flame temperature value;
5. mix charge composition from the previous iteration with combustion products at EGR fraction;
6. estimate relative error
7. go to 1.

The cycle is stopped when differences in charge composition between two successive iterations are less than the desired error tolerance (usually $1.0e-4$).

The estimation of mixture's adiabatic flame temperature relies on the assumption that the complete combustion of the reactive mixture occurs within a closed thermodynamic environment, at constant pressure. Starting from the first law of thermodynamics:

$$dU = \delta Q - \delta W \tag{B.1}$$

and recalling the definition of enthalpy:

$$H = U + pV \qquad \rightarrow \qquad dH = dU + pdV + Vdp \tag{B.2}$$

we have, in case the only work is due to compression or expansion ($\delta W = pdV$) of the gas mixture:

$$dU = \delta Q - pdV \qquad \rightarrow \qquad dH = \delta Q + Vdp \tag{B.3}$$

in the case of an adiabatic system ($\delta Q = 0$) at constant pressure ($dp = 0$),

$$dH = 0. \tag{B.4}$$

Starting from this assumption, it descends that the specific enthalpy of the unburnt mixture has to be equal to the enthalpy of the burnt mixture, which is in equilibrium conditions at the adiabatic flame temperature value:

$$\bar{h}_u = \boldsymbol{H}(T_u)^T \boldsymbol{Y_u} = \boldsymbol{H}(T_b)^T \boldsymbol{Y_b} = \bar{h}_b \tag{B.5}$$

Being the enthalpy of the unburnt mixture known, an iterative procedure can be setup for finding the temperature value at which the composition of the gaseous mixture, computed at equilibrium conditions, owns the same enthalpy value. First of all, two tentative temperatures are set, estimating $T_1 < T_b$ and $T_2 > T_b$; then, at each step the temperature interval is restricted through by subdividing it into two parts: $T_m = 0.5 \cdot (T_1 + T_2)$. The lowest part $[T_1, T_m]$ is retained in case $\bar{h}_u < \bar{h}_m$; the highest part $[T_m, T_2]$ in case $\bar{h}_m < \bar{h}_u$. The iterative procedure is then stopped after an adequate accuracy constraint. For more details about the development of this procedure, and about adiabatic flame temperature values and composition for flames involving some important hydrocarbons, please refer to (113).
Each step in the procedure requires the estimation of the equilibrium composition of the mixture at the desired temperature value: most algorithms rely on the minimization of the Gibbs function, and they are not always able to get to convergence, if the problem initialisation is too far from the actual solution. For this reason, the algorithm proposed by Pope (197) has been implemented. This approach has many interesting aspects; among them, a full vectorized definition which allows computationally efficient computations to be performed; furthermore, the Gibbs function continuation method guarantees the solution to be obtained. For details on the derivation and the implementation of this method, please refer to the documentation proposed by Pope (161).

References

[1] **Alternative Fuels and Advanced Vehicles Data Center**, January 2011. xxix, 6, 7

[2] **Biomass Energy Data Book**, January 2011. xxix, 8

[3] G.P. Smith, D.M. Golden, M. Frenklach, N.W. Moriarty, B. Eiteneer, and M. Goldenberg. **GRI-mech. 3.0**. xxix, xxx, 37, 38, 41, 42

[4] Nick M. Marinov. **A detailed chemical kinetic model for high temperature ethanol oxidation**. *International Journal of Chemical Kinetics*, **31**(3):183 – 220, 1999. xxix, xxx, xxxi, xxxii, 6, 13, 37, 39, 41, 43, 57, 79, 84, 109, 111, 112, 115

[5] H.J. Curran, P. Gaffuri, W.J. Pitz, and C.K. Westbrook. **A Comprehensive Modeling Study of n-Heptane Oxidation**. *Combustion and Flame*, **114**(1-2):149 – 177, 1998. xxix, xxx, 37, 40, 43, 79

[6] Hongsheng Guo, W. Stuart Neill, Wally Chippior, Hailin Li, and Joshua D. Taylor. **An Experimental and Modeling Study of HCCI Combustion Using n-Heptane**. *Journal of Engineering for Gas Turbines and Power*, **132**(2):022801, 2010. xxx, 44, 69

[7] W.G. Mallard, F. Westley, J.T. Herron, R.F. Hampson, and D. Frizzell. **NIST Chemical Kinetics Database on the Web**, 2000. Standard Reference Database 17, Version 7.0 (Web Version), Release 1.5. xxxi, 84, 87, 103

[8] Henry J. Curran, Mary P. Dunphy, John M. Simmie, Charles K. Westbrook, and William J. Pitz. **Shock tube ignition of ethanol, isobutene and MTBE: Experiments and modeling**. *Symposium (International) on Combustion*, **24**(1):769 – 776, 1992. Twenty-Fourth Symposium on Combustion. xxxii, 112, 116

[9] Magnus Sjöberg and John E. Dec. **Influence of EGR Quality and Unmixedness on the High-Load Limits of HCCI Engines**. *SAE International Journal of Engines*, **2**(1):492–510, 2009. xxxii, 76, 116, 117, 118

[10] S. Dooley, H.J. Curran, and J.M. Simmie. **Autoignition measurements and a validated kinetic model for the biodiesel surrogate, methyl butanoate**. *Combustion and Flame*, **153**(1-2):2 – 32, 2008. xxxiii, 7, 13, 120, 121, 124

[11] Charles K. Westbrook, William J. Pitz, Olivier Herbinet, Henry J. Curran, and Emma J. Silke. **A comprehensive detailed chemical kinetic reaction mechanism for combustion of n-alkane hydrocarbons from n-octane to n-hexadecane**. *Combustion and Flame*, **156**(1):181 – 199, 2009. xxxiii, 125

[12] Martin I. Hoffert, Ken Caldeira, Gregory Benford, David R. Criswell, Christopher Green, Howard Herzog, Atul K. Jain, Haroon S. Kheshgi, Klaus S. Lackner, John S. Lewis, H. Douglas Lightfoot, Wallace Manheimer, John C. Mankins, Michael E. Mauel, L. John Perkins, Michael E. Schlesinger, Tyler Volk, and Tom M. L. Wigley. **Advanced Technology Paths to Global Climate Stability: Energy for a Greenhouse Planet**. *Science*, **298**(5595):981–987, 2002. 4

[13] S. Pacala and R. Socolow. **Stabilization Wedges: Solving the Climate Problem for the Next 50 Years with Current Technologies**. *Science*, **305**(5686):968–972, 2004. 4

[14] Arthur J. Ragauskas, Charlotte K. Williams, Brian H. Davison, George Britovsek, John Cairney, Charles A. Eckert, William J. Frederick, Jason P. Hallett, David J. Leak, Charles L. Liotta, Jonathan R. Mielenz, Richard Murphy, Richard Templer, and Timothy Tschaplinski. **The Path Forward for Biofuels and Biomaterials**. *Science*, **311**(5760):484–489, 2006. 4

[15] % bf DIRECTIVE 2003/30/EC OF THE EUROPEAN PARLIAMENT AND OF THE COUNCIL of 8 May 2003, on the promotion of the use of biofuels or other renewable fuels for transport. *Official Journal of the European Union*, **L 123**:42 – 46, 2003. 4

[16] Jason Hill, Erik Nelson, David Tilman, Stephen Polasky, and Douglas Tiffany. **Environmental, economic, and energetic costs and benefits of biodiesel and ethanol biofuels**. *Proceedings of the National Academy of Sciences*, **103**(30):11206–11210, 2006. 4

[17] Katharina Kohse-Höinghaus, Patrick Osswald, Terrill A. Cool, Tina Kasper, Nils Hansen, Fei Qi, Charles K. Westbrook, and Phillip R. Westmoreland. **Biofuel Combustion Chemistry: From Ethanol to Biodiesel**. *Angewandte Chemie International Edition*, **49**(21):3572–3597, 2010. 5

[18] Chung K. Law. **Combustion at a crossroads: Status and prospects**. *Proceedings of the Combustion Institute*, **31**(1):1 – 29, 2007. 5, 22, 79

[19] Katharina Kohse-Höinghaus, Robert S. Barlow, Marcus Aldã‚l'n, and Jã‚ijrgen Wolfrum. **Combustion at the focus: laser diagnostics and control**. *Proceedings of the Combustion Institute*, **30**(1):89 – 123, 2005. 5

[20] James A. Miller, Michael J. Pilling, and Jã‚ijrgen Troe. **Unravelling combustion mechanisms through a quantitative understanding of elementary reactions**. *Proceedings of the Combustion Institute*, **30**(1):43 – 88, 2005. 5

[21] Charles K. Westbrook, Yasuhiro Mizobuchi, Thierry J. Poinsot, Phillip J. Smith, and Jã‚ijrgen Warnatz. **Computational combustion**. *Proceedings of the Combustion Institute*, **30**(1):125 – 157, 2005. 5

[22] J. Buckmaster, P. Clavin, A. Liã‚śã‚n, M. Matalon, N. Peters, G. Sivashinsky, and F.A. Williams. **Combustion theory and modeling**. *Proceedings of the Combustion Institute*, **30**(1):1 – 19, 2005. 5

[23] Avinash Kumar Agarwal. **Biofuels (alcohols and biodiesel) applications as fuels for internal combustion engines**. *Progress in Energy and Combustion Science*, **33**(3):233 – 271, 2007. 6, 7, 8, 9

[24] **DIRECTIVE 2009/28/EC OF THE EUROPEAN PARLIAMENT AND OF THE COUNCIL of 23 April 2009 on the promotion of the use of energy from renewable sources and amending and subsequently repealing Directives 2001/77/EC and 2003/30/EC**. *Official Journal of the European Union*, **L 140**:16 – 62, 2009. 6

[25] Alan C. Hansen, Qin Zhang, and Peter W. L. Lyne. **Ethanol-diesel fuel blends – a review**. *Bioresource Technology*, **96**(3):277 – 285, 2005. 6

[26] F.N. Egolfopoulos, D.X. Du, and C.K. Law. **A study on ethanol oxidation kinetics in laminar premixed flames, flow reactors, and shock tubes**. *Symposium (International) on Combustion*, **24**(1):833 – 841, 1992. Twenty-Fourth Symposium on Combustion. 6

[27] Mary P. Dunphy and John M. Simmie. **High-temperature oxidation of ethanol. Part 1.-Ignition delays in shock waves**. *Journal of the Chemical Society, Faraday Transactions*, **87**(11):1691 – 1696, 1991. 6

[28] T. S. Norton and F. L. Dryer. **An experimental and modeling study of ethanol oxidation kinetics in an atmospheric pressure flow reactor**. *Int. J. Chem. Kinet.*, **24**(4):319–344, 1992. 6

REFERENCES

[29] Priyank Saxena and Forman A. Williams. **Numerical and experimental studies of ethanol flames**. *Proceedings of the Combustion Institute*, **31**(1):1149 – 1156, 2007. 6, 13

[30] N. Leplat, P. Dagaut, C. TogbÃĽ, and J. Vandooren. **Numerical and experimental study of ethanol combustion and oxidation in laminar premixed flames and in jet-stirred reactor**. *Combustion and Flame*, **In Press, Corrected Proof**:–, 2011. 6

[31] Olivier Herbinet, William J. Pitz, and Charles K. Westbrook. **Detailed chemical kinetic oxidation mechanism for a biodiesel surrogate**. *Combustion and Flame*, **154**(3):507 – 528, 2008. 7, 13, 120, 121, 122

[32] Olivier Herbinet, William J. Pitz, and Charles K. Westbrook. **Detailed chemical kinetic mechanism for the oxidation of biodiesel fuels blend surrogate**. *Combustion and Flame*, **157**(5):893 – 908, 2010. 7, 13, 79

[33] S. Gaïl, S.M. Sarathy, M.J. Thomson, P. DiÃĽvart, and P. Dagaut. **Experimental and chemical kinetic modeling study of small methyl esters oxidation: Methyl (E)-2-butenoate and methyl butanoate**. *Combustion and Flame*, **155**(4):635 – 650, 2008. 7

[34] S. Gaïl, M.J. Thomson, S.M. Sarathy, S.A. Syed, P. Dagaut, P. DiÃĽvart, A.J. Marchese, and F.L. Dryer. **A wide-ranging kinetic modeling study of methyl butanoate combustion**. *Proceedings of the Combustion Institute*, **31**(1):305 – 311, 2007. 7

[35] S.M. Sarathy, S. GaÃŕl, S.A. Syed, M.J. Thomson, and P. Dagaut. **A comparison of saturated and unsaturated C4 fatty acid methyl esters in an opposed flow diffusion flame and a jet stirred reactor**. *Proceedings of the Combustion Institute*, **31**(1):1015 – 1022, 2007. 7

[36] C.J. Hayes and D.R. Burgess Jr. **Exploring the oxidative decompositions of methyl esters: Methyl butanoate and methyl pentanoate as model compounds for biodiesel**. *Proceedings of the Combustion Institute*, **32**(1):263 – 270, 2009. 7

[37] Lam K. Huynh, Kuang C. Lin, and Angela Violi. **Kinetic Modeling of Methyl Butanoate in Shock Tube**. *The Journal of Physical Chemistry A*, **112**(51):13470–13480, 2008. 7

[38] K. HadjAli, M. Crochet, G. Vanhove, M. Ribaucour, and R. Minetti. **A study of the low temperature autoignition of methyl esters**. *Proceedings of the Combustion Institute*, **32**(1):239 – 246, 2009. 8

[39] Tianfeng Lu and Chung K. Law. **Toward accommodating realistic fuel chemistry in large-scale computations**. *Progress in Energy and Combustion Science*, **35**(2):192 – 215, 2009. 11, 45, 47, 79, 81, 83, 103, 104

[40] W.J. Pitz, C.V. Naik, T. NÃŋ Mhaoldÿin, C.K. Westbrook, H.J. Curran, J.P. Orme, and J.M. Simmie. **Modeling and experimental investigation of methylcyclohexane ignition in a rapid compression machine**. *Proceedings of the Combustion Institute*, **31**(1):267 – 275, 2007. 13

[41] E.M. Fisher, W.J. Pitz, H.J. Curran, and C.K. Westbrook. **Detailed chemical kinetic mechanisms for combustion of oxygenated fuels**. *Proceedings of the Combustion Institute*, **28**(2):1579 – 1586, 2000. 13

[42] Pierre A. Glaude, William J. Pitz, and Murray J. Thomson. **Chemical kinetic modeling of dimethyl carbonate in an opposed-flow diffusion flame**. *Proceedings of the Combustion Institute*, **30**(1):1111 – 1118, 2005. 13

[43] S. L. Fischer, F. L. Dryer, and H. J. Curran. **The reaction kinetics of dimethyl ether. I: High-temperature pyrolysis and oxidation in flow reactors**. *International Journal of Chemical Kinetics*, **32**(12):713 – 740, 2000. 13, 79

[44] A.A. Konnov. **Implementation of the NCN pathway of prompt-NO formation in the detailed reaction mechanism**. *Combustion and Flame*, **156**(11):2093 – 2105, 2009. 13

[45] Valeri I. Golovitchev and Junfeng Yang. **Construction of combustion models for rapeseed methyl ester bio-diesel fuel for internal combustion engine applications**. *Biotechnology Advances*, **27**(5):641 – 655, 2009. Bioenergy Research & Development in China - ICBT 2008. 13

[46] K. Yasunaga, J.M. Simmie, H.J. Curran, T. Koike, O. Takahashi, Y. Kuraguchi, and Y. Hidaka. **Detailed chemical kinetic mechanisms of ethyl methyl, methyl tert-butyl and ethyl tert-butyl ethers: The importance of uni-molecular elimination reactions**. *Combustion and Flame*, **In Press, Corrected Proof**:–, 2010. 13

[47] C.V. Naik, C.K. Westbrook, O. Herbinet, W.J. Pitz, and M. Mehl. **Detailed chemical kinetic reaction mechanism for biodiesel components methyl stearate and methyl oleate**. *Proceedings of the Combustion Institute*, **33**(1):383 – 389, 2011. 13

[48] Alison S. Tomlin, Michael J. Pilling, John H. Merkin, John Brindley, Neill Burgess, and Arthur Gough. **Reduced Mechanisms for Propane Pyrolysis**. *Industrial & Engineering Chemistry Research*, **34**(11):3749–3760, 1995. 11

[49] Alison S. Tomlin, Michael J. Pilling, TamÃąs TurÃąnyi, John H. Merkin, and John Brindley. **Mechanism reduction for the oscillatory oxidation of hydrogen: Sensitivity and quasi-steady-state analyses**. *Combustion and Flame*, **91**(2):107 – 130, 1992. 11

[50] L. E. Whitehouse, A. S. Tomlin, and M. J. Pilling. **Systematic reduction of complex tropospheric chemical mechanisms, Part I: sensitivity and time-scale analyses**. *Atmospheric Chemistry and Physics*, **4**(7):2025–2056, 2004. 11

[51] Nancy J. Brown, Guoping Li, and Michael L. Koszykowski. **Mechanism reduction via principal component analysis**. *Int. J. Chem. Kinet.*, **29**(6):393–414, 1997. 12

[52] P. Gokulakrishnan, A.D. Lawrence, P.J. McLellan, and E.W. Grandmaison. **A functional-PCA approach for analyzing and reducing complex chemical mechanisms**. *Computers & Chemical Engineering*, **30**(6-7):1093 – 1101, 2006. 12, 79

[53] Christos E. Frouzakis and Konstantinos Boulouchos. **Analysis and Reduction of the CH₄-Air Mechanism at Lean Conditions**. *Combustion Science and Technology*, **159**(1):281–303, 2000. 12

[54] S. Vajda and T. Turanyi. **Principal component analysis for reducing the Edelson-Field-Noyes model of the Belousov-Zhabotinskii reaction**. *The Journal of Physical Chemistry*, **90**(8):1664–1670, 1986. 12

[55] S. Vajda, P. Valko, and T. TurÃČÂąnyi. **Principal component analysis of kinetic models**. *Int. J. Chem. Kinet.*, **17**(1):55–81, 1985. 12

[56] S.H. Lam and D.A. Coussis. **The CSP method for simplifying kinetics**. *International Journal of Chemical Kinetics*, **26**:461 – 486, 1994. 13, 50

[57] S.H. Lam and D.A. Coussis. **Understanding complex chemical kinetics with computational singular perturbation**. *Symposium (International) on Combustion*, **22**(1):931 – 941, 1989. 13, 50, 79

[58] Tianfeng Lu, Yiguang Ju, and Chung K. Law. **Complex CSP for chemistry reduction and analysis**. *Combustion and Flame*, **126**(1-2):1445 – 1455, 2001. 13, 79

[59] A. Massias, D. Diamantis, E. Mastorakos, and D.A. Goussis. **An algorithm for the construction of global reduced mechanisms with CSP data**. *Combustion and Flame*, **117**(4):685 – 708, 1999. 13

[60] Mauro Valorani, Francesco Creta, Filippo Donato, Habib N. Najm, and Dimitris A. Goussis. **Skeletal mechanism generation and analysis for n-heptane with CSP**. *Proceedings of the Combustion Institute*, **31**(1):483 – 490, 2007. 13

[61] Mauro Valorani, Francesco Creta, Dimitris A. Goussis, Jeremiah C. Lee, and Habib N. Najm. **An automatic procedure for the simplification of chemical kinetic mechanisms based on CSP**. *Combustion and Flame*, **146**(1-2):29 – 51, 2006. 13

[62] Ipsita Banerjee and Marianthi G. Ierapetritou. **An adaptive reduction scheme to model reactive flow**. *Combustion and Flame*, **144**(3):619 – 633, 2006. 13, 79, 86, 107

[63] L. Elliott, D.B. Ingham, A.G. Kyne, N.S. Mera, M. Pourkashanian, and C.W. Wilson. **Incorporation of physical bounds on rate parameters for reaction mechanism optimization using genetic algorithms**. *Combustion Science and Technology*, **175**(4):619 – 648, 2003. 13, 80, 87

[64] Lionel Elliott, Derek B. Ingham, Adrian G. Kyne, Nicolae S. Mera, Mohamed Pourkashanian, and Sean Whittaker. **Reaction mechanism reduction and optimisation for modelling aviation fuel oxidation using standard and hybrid genetic algorithms**. *Computers & Chemical Engineering*, **30**(5):889 – 900, 2006. 13, 79, 80, 87, 106

[65] L. Elliott, D. B. Ingham, A. G. Kyne, N. S. Mera, M. Pourkashanian, and C. W. Wilson. **A Novel Approach to Mechanism Reduction Optimization for an Aviation Fuel/Air Reaction Mechanism Using a Genetic Algorithm**. *Journal of Engineering for Gas Turbines and Power*, **128**(2):255–263, 2006. 13, 79, 80, 87, 106

[66] Lionel Elliott, Derek B. Ingham, Adrian G. Kyne, Nicolae S. Mera, Mohamed Pourkashanian, and Christopher W. Wilson. **Reaction Mechanism Reduction and Optimization Using Genetic Algorithms**. *Industrial & Engineering Chemistry Research*, **44**(4):658–667, 2005. 13, 79

[67] L. Elliott, D. B. Ingham, A. G. Kyne, N. S. Mera, M. Pourkashanian, and C. W. Wilson. **Genetic algorithms for optimisation of chemical kinetics reaction mechanisms**. *Progress in Energy and Combustion Science*, **30**(3):297 – 328, 2004. 13, 79, 86, 106

[68] Binita Bhattacharjee, Douglas A. Schwer, Paul I. Barton, and William H. Green. **Optimally-reduced kinetic models: reaction elimination in large-scale kinetic mechanisms**. *Combustion and Flame*, **135**(3):191 – 208, 2003. 13, 79

[69] O. O. Oluwole, P. I. Barton, and W. H. Green. **Obtaining accurate solutions using reduced chemical kinetic models: a new model reduction method for models rigorously validated over ranges**. *Combustion Theory and Modelling*, **11**(1):127–146, 2007. 13, 79

[70] Oluwayemisi O. Oluwole, Binita Bhattacharjee, John E. Tolsma, Paul I. Barton, and William H. Green. **Rigorous valid ranges for optimally reduced kinetic models**. *Combustion and Flame*, **146**(1-2):348 – 365, 2006. 13, 79

[71] J. Revel, J. C. Boettner, M. Cathonnet, and J. S. Bachman. **Derivation of a global chemical kinetic mechanism for methane ignition and combustion**. *Journal de chimie physique*, **91**(4):365 – 382, 1994. 14, 25, 79, 108

[72] Ioannis P. Androulakis. **Kinetic mechanism reduction based on an integer programming approach**. *AIChE Journal*, **46**(2):361 – 371, 2000. 14, 86

[73] Ioannis P. Androulakis, Jeffrey M. Grenda, and Joseph W. Bozzelli. **Time-integrated pointers for enabling the analysis of detailed reaction mechanisms**. *AIChE Journal*, **50**(11):2956 – 2970, 2004. 14, 79, 108

[74] Kaiyuan He, Marianthi G. Ierapetritou, and Ioannis P. Androulakis. **A graph-based approach to developing adaptive representations of complex reaction mechanisms**. *Combustion and Flame*, **155**(4):585 – 604, 2008. 14, 52, 79, 108

[75] Kaiyuan He, Marianthi G. Ierapetritou, and Ioannis P. Androulakis. **Integration of on-the-fly kinetic reduction with multidimensional CFD**. *AIChE Journal*, **56**(5):1305 – 1314, 2010. 14, 79, 108

[76] Kaiyuan He, Ioannis P. Androulakis, and Marianthi G. Ierapetritou. **On-the-fly reduction of kinetic mechanisms using element flux analysis**. *Chemical Engineering Science*, **65**(3):1173 – 1184, 2010. 14, 79, 108

[77] Tianfeng Lu and Chung K. Law. **A directed relation graph method for mechanism reduction**. *Proceedings of the Combustion Institute*, **30**(1):1333 – 1341, 2005. 14, 79

[78] Tianfeng Lu and Chung K. Law. **On the applicability of directed relation graphs to the reduction of reaction mechanisms**. *Combustion and Flame*, **146**(3):472 – 483, 2006. 14

[79] Tianfeng Lu and Chung K. Law. **Linear time reduction of large kinetic mechanisms with directed relation graph: n-Heptane and iso-octane**. *Combustion and Flame*, **144**(1-2):24 – 36, 2006. 14

[80] P. Pepiot-Desjardins and H. Pitsch. **An efficient error-propagation-based reduction method for large chemical kinetic mechanisms**. *Combustion and Flame*, **154**(1-2):67 – 81, 2008. 14, 79

[81] Ramanan Sankaran, Evatt R. Hawkes, Jacqueline H. Chen, Tianfeng Lu, and Chung K. Law. **Structure of a spatially developing turbulent lean methane-air Bunsen flame**. *Proceedings of the Combustion Institute*, **31**(1):1291 – 1298, 2007. 14

[82] X.L. Zheng, T.F. Lu, and C.K. Law. **Experimental counterflow ignition temperatures and reaction mechanisms of 1,3-butadiene**. *Proceedings of the Combustion Institute*, **31**(1):367 – 375, 2007. 14

[83] M. Bodenstein. **Eine Theorie der photochemischen Reaktionsgeschwindigkeiten**. *Z. Phys. Chem*, **85**:329 – 397, 1913. 15, 79

[84] L.K. Underhill and D.L. Chapman. **The interaction of chlorine and hydrogen. The influence of mass**. *J. Chem. Soc. Trans.*, **103**:496 – 508, 1913. 15, 79

[85] James C. Keck. **Rate-controlled constrained-equilibrium theory of chemical reactions in complex systems**. *Progress in Energy and Combustion Science*, **16**(2):125 – 154, 1990. 15, 79

[86] James C. Keck and David Gillespie. **Rate-controlled partial-equilibrium method for treating reacting gas mixtures**. *Combustion and Flame*, **17**(2):237 – 241, 1971. 15, 79

[87] Vreg Yousefian. **A Rate-Controlled Constrained-Equilibrium Thermochemistry Algorithm for Complex Reacting Systems**. *Combustion and Flame*, **115**(1-2):66 – 80, 1998. 15

[88] Qing Tang and Stephen B. Pope. **Implementation of combustion chemistry by in situ adaptive tabulation of rate-controlled constrained equilibrium manifolds**. *Proceedings of the Combustion Institute*, **29**(1):1411 – 1417, 2002. 15

[89] Qing Tang and Stephen B. Pope. **A more accurate projection in the rate-controlled constrained-equilibrium method for dimension reduction of combustion chemistry**. *Combustion Theory and Modelling*, **8**(2):255–279, 2004. 15

[90] STELIOS RIGOPOULOS. **The Rate-Controlled Constrained Equilibrium (RCCE) Method for Reducing Chemical Kinetics in Systems with Time-Scale Separation**. *International Journal for Multiscale Computation Engineering*, **5**(1):11–18, 2007. 15

[91] W.P. JONES AND STELIOS RIGOPOULOS. **Rate-controlled constrained equilibrium: Formulation and application to nonpremixed laminar flames**. *Combustion and Flame*, **142**(3):223 – 234, 2005. 15

[92] W. P. JONES AND STELIOS RIGOPOULOS. **Reduced chemistry for hydrogen and methanol premixed flames via RCCE**. *Combustion Theory and Modelling*, **11**(5):755–780, 2007. 15

[93] U. MAAS AND S.B. POPE. **Simplifying chemical kinetics: Intrinsic low-dimensional manifolds in composition space**. *Combustion and Flame*, **88**(3-4):239 – 264, 1992. 15, 50, 79

[94] H. BONGERS, J.A. VAN OIJEN, AND L.P.H. DE GOEY. **Intrinsic low-dimensional manifold method extended with diffusion**. *Proceedings of the Combustion Institute*, **29**(1):1371 – 1378, 2002. 15

[95] J. NAFE AND U. MAAS. **A general algorithm for improving ILDMs**. *Combustion Theory and Modelling*, **6**(4):697–709, 2002. 15

[96] ZHUYIN REN AND STEPHEN B. POPE. **Transport-chemistry coupling in the reduced description of reactive flows**. *Combustion Theory and Modelling*, **11**(5):715–739, 2007. 15

[97] XIAOLONG GOU, WENTING SUN, ZHENG CHEN, AND YIGUANG JU. **A dynamic multi-timescale method for combustion modeling with detailed and reduced chemical kinetic mechanisms**. *Combustion and Flame*, **157**(6):1111 – 1121, 2010. 19, 23, 49, 50, 53

[98] D. TAMAGNA, Y. RA, AND R.D. REITZ. **Multidimensional Simulation of PCCI Combustion Using Gasoline and Dual-Fuel Direct Injection with Detailed Chemical Kinetics**. In SAE INTERNATIONAL, editor, *SAE technical paper 2007-01-0190*, 2007. 22, 45

[99] Y. SHI, S. KOKJOHN, H.-W. GE, AND R.D. REITZ. **Efficient Multidimensional Simulation of HCCI and DI Engine Combustion with Detailed Chemistry.** In SAE INTERNATIONAL, editor, *technical paper 2009-01-0701*, 2009. 22, 74

[100] SAGE L. KOKJOHN AND ROLF D. REITZ. **A Computational Investigation of Two-Stage Combustion in a Light-Duty Engine**. *SAE International Journal of Engines*, **1**(1):1083–1104, April 2009. 22, 45

[101] ROBERT J. KEE, FRAN M. RUPLEY, ELLEN MEEKS, AND JAMES A. MILLER. **CHEMKIN-III: a FORTRAN chemical kinetics package for the analysis of gasphase chemical and plasma kinetics**. Technical report, Sandia National Laboratories, 1996. SAND96-8216. 22, 82

[102] SONG-CHARNG KONG AND ROLF D. REITZ. **Application of detailed chemistry and CFD for predicting direct injection HCCI engine combustion and emissions**. *Proceedings of the Combustion Institute*, **29**(1):663 – 669, 2002. 22

[103] Z. WANG, J.-X. WANG, S.-J. SHUAI, AND F. ZHANG. **Numerical Simulation of HCCI Engine With Multi-Stage Gasoline Direct Injection Using 3D-CFD With Detailed Chemistry**. In SAE INTERNATIONAL, editor, *technical paper 2004-01-0563*, 2004. 22

[104] R. OGINK AND V. GOLOVITCHEV. **Gasoline Hcci Modeling: Computer Program Combining Detailed Chemistry and Gas Exchange Processes**. In *technical paper 2001-01-3614*, 2001. 22

[105] D.G. GOODWIN. **Cantera: Object-oriented software for reacting flows.** Technical report, California Institute of Technology, 2002. 22

[106] YU SHI, LONG LIANG, HAI-WEN GE, AND ROLF D. REITZ. **Acceleration of the chemistry solver for modeling DI engine combustion using dynamic adaptive chemistry (DAC) schemes**. *Combustion Theory and Modelling*, **14**(1):69–89, 2010. 22

[107] A.A. AMSDEN, P.J. O'ROURKE, AND T.D. BUTLER. **KIVA-2: A computer program for chemically reactive flows with sprays**. *NASA STI/Recon Technical Report N*, **89**:27975–+, May 1989. 23, 64

[108] PETER N. BROWN, GEORGE D. BYRNE, AND ALAN C. HINDMARSH. **VODE: A Variable-Coefficient ODE Solver**. *SIAM Journal on Scientific and Statistical Computing*, **10**(5):1038–1051, 1989. 24, 36

[109] DAVID J. TORRES AND MARIO F. TRUJILLO. **KIVA-4: An unstructured ALE code for compressible gas flow with sprays**. *Journal of Computational Physics*, **219**(2):943 – 975, 2006. 24, 29, 64, 117

[110] D.A. MCQUARRIE. *Statistical Mechanics*. University Science Books, 2000. 30

[111] R.J. KEE, F.M. RUPLEY, AND J.A. MILLER. **The Chemkin Thermodynamic Data Base**. Technical Report SAND-87-8215B, Sandia National Labs., Livermore, CA (USA), Mar 1990. 30

[112] B.J. MCBRIDE, M.J. ZEHE, AND S. GORDON. **NASA Glenn Coefficients for Calculating Thermodynamic Properties of Individual Species**. Technical paper NASA/TP-2002-211556, NASA, 2002. 30

[113] J. WARNATZ, U. MAAS, AND R. W. DIBBLE. *Combustion: Physical and Chemical Fundamentals, Modeling and Simulation, Experiments, Pollutant Formation*. Springer, 2006. 31, 32, 71, 82, 166

[114] F. A. LINDEMANN, SVANTE ARRHENIUS, IRVING LANGMUIR, N. R. DHAR, J. PERRIN, AND W. C. MCC. LEWIS. **Discussion on "the radiation theory of chemical action"**. *Trans. Faraday Soc.*, **17**:598–606, 1922. 32

[115] J. TROE. **Theory of thermal unimolecular reactions at high pressures**. *The Journal of Chemical Physics*, **75**(1):226–237, 1981. 32

[116] R.E. MITCHELL AND R.J. KEE. **SHOCK: General-purpose computer code for predicting chemical-kinetic behavior behind incident and reflected shocks**. Technical Report SAND-82-8205, Sandia National Labs., Livermore, CA (USA), March 1982. 34

[117] A.E. LUTZ, R.J. KEE, AND J.A. MILLER. **SENKIN: A Fortran program for predicting homogeneous gas phase chemical kinetics with sensitivity analysis**. Technical report SAND-87-8248, Sandia National Labs., Livermore, CA (USA), 1988. 34, 37

[118] **Matlab. The language of technical computing.** 36

[119] S.J. CHAPMAN. *Fortran 90/95 for Scientists and Engineers*. WCB/McGraw-Hill, 1998. 36

[120] P. GETREUER. **Writing Fast Matlab Code**, 2010 2010. 36

[121] KALYANMOY DEB, SAMIR AGRAWAL, AMRIT PRATAP, AND T. MEYARIVAN. **A Fast Elitist Non-dominated Sorting Genetic Algorithm for Multi-objective Optimization: NSGA-II**. In MARC SCHOENAUER, KALYANMOY DEB, GUNTHER RUDOLPH, XIN YAO, EVELYNE LUTTON, JUAN MERELO, AND HANS-PAUL SCHWEFEL, editors, *Parallel Problem Solving from Nature PPSN VI*, **1917** of *Lecture Notes in Computer Science*, pages 849–858. Springer Berlin / Heidelberg, 2000. 36

[122] **Intel Math Kernel Library 10.3**. 36, 128

[123] **AMD Core Math Library**. 36, 128

[124] L.S. BLACKFORD, J. DEMMEL, J. DONGARRA, I. DUFF, S. HAMMARLING, G. HENRY, M. HEROUX, L. KAUFMAN, A. LUMSDAINE, A. PETITET, R. POZO, K. REMINGTON, AND C. WHALEY. **An updated set of basic linear algebra subprograms (BLAS)**. *ACM Trans. Math. Softw.*, **28**:135–151, June 2002. 36

[125] IAIN S. DUFF, MICHELE MARRONE, GIUSEPPE RADICATI, AND CARLO VITTOLI. **Level 3 basic linear algebra subprograms for sparse matrices: a user-level interface**. *ACM Trans. Math. Softw.*, **23**:379–401, September 1997. 36

[126] LAWRENCE F. SHAMPINE AND MARK W. REICHELT. **The MATLAB ODE Suite**. *SIAM Journal on Scientific Computing*, **18**(1):1–22, 1997. 36

[127] KRISHNAN RADHAKRISHNAN AND ALAN C. HINDMARSH. **Description and Use of LSODE, the Livermore Solver for Ordinary Differential Equations**. Technical report, NASA, 1993. 36

[128] E. HAIRER AND G. WANNER. *Solving Ordinary Differential Equations II: Stiff and Differential-Algebraic Problems*. Springer Series in Computational Mathematics. Springer, 2010. 36

[129] R. WEINER, B. A. SCHMITT, AND H. PODHAISKY. **ROWMAP–a ROW-code with Krylov techniques for large stiff ODEs**. *Applied Numerical Mathematics*, **25**(2-3):303 – 319, 1997. Special Issue on Time Integration. 36

[130] C.M. COATS AND ALAN WILLIAMS. **Investigation of the ignition and combustion of n-heptane-oxygen mixtures**. *Symposium (International) on Combustion*, **17**(1):611 – 621, 1979. Seventeenth Symposium (International) on Combustion. 41

[131] S.C. KONG, R.D. REITZ, M. CHRISTENSEN, AND B. JOHANSSON. **Modeling the Effects of Geometry Generated Turbulence on HCCI Engine Combustion**. In SAE INTERNATIONAL, editor, *technical paper 2003-01-1088*, 2003. 44

[132] DOUGLAS A. SCHWER, JOHN E. TOLSMA, WILLIAM H. GREEN, AND PAUL I. BARTON. **On upgrading the numerics in combustion chemistry codes**. *Combustion and Flame*, **128**(3):270 – 291, 2002. 47

[133] Y. JU, X. GOU, W. SUN, AND Z. CHEN. **An On-Grid Dynamic Multi-Timescale Method with Path-Flux Analysis for Multi-Physics Detailed Modeling of Combustion**. *Journal of the Combustion Society of Japan*, **51**:200 – 208, 2009. 49

[134] WENTING SUN, ZHENG CHEN, XIAOLONG GOU, AND YIGUANG JU. **A path flux analysis method for the reduction of detailed chemical kinetic mechanisms**. *Combustion and Flame*, **157**(7):1298 – 1307, 2010. 49

[135] S.B. POPE AND U. MAAS. **Simplifying chemical kinetics: trajectory-generated low-dimensional manifolds**. Technical report, Cornell University, 1993. 50, 79

[136] MAURO VALORANI AND DIMITRIOS A. GOUSSIS. **Explicit Time-Scale Splitting Algorithm for Stiff Problems: Auto-ignition of Gaseous Mixtures behind a Steady Shock**. *Journal of Computational Physics*, **169**(1):44 – 79, 2001. 50, 53

[137] D. A. KNOLL, L. CHACON, L. G. MARGOLIN, AND V. A. MOUSSEAU. **On balanced approximations for time integration of multiple time scale systems**. *Journal of Computational Physics*, **185**(2):583 – 611, 2003. 51

[138] L. LIANG, S.-C. KONG, C. JUNG, AND R.D. REITZ. **Development of a Semi-Implicit Solver for Detailed Chemistry in Internal Combustion Engine Simulations**. *Journal of Engineering for Gas Turbines and Power*, **129**:271 – 278, 2007. 53

[139] E.S. ORAN AND J.P. BORIS. *Numerical Simulation of Reactive Flow*. Elsevier, 1987. 53

[140] O.T. HANNA. **New explicit and implicit 'Improved Euler' methods for the integration of ordinary differential equations**. *Computers & Chemical Engineering*, **12**:1083–1086, 1988. 54

[141] E. FEHLBERG. **Low-order classical Runge-Kutta formulas with stepsize control and their application to some heat transfer problems**. Technical Report TR R-315, NASA, 1969. 54

[142] L. SHAMPINE. **Error Estimation and Control for ODEs**. *Journal of Scientific Computing*, **25**:3–16, 2005. 10.1007/s10915-004-4629-3. 56

[143] A. SANDU, J. G. VERWER, J. G. BLOM, B. J. SPEE, G. R. CARMICHAEL, AND F. A. POTRA. **Benchmarking Stiff ODE Solvers for Atmospheric Chemistry Problems II: Rosenbrock Solvers**. Technical Report Report on Computational Mathematics 90/1996, also CWI Report NM-R9614/1996, Department of Mathematics, The University of Iowa / Department of Numerical Mathematics, CWI Amsterdam, January 1997. 56

[144] AMAR PATEL, S.-C. KONG, AND R.D. REITZ. **Development and Validation of a Reduced Reaction Mechanism for HCCI Engine Simulations**. In SAE INTERNATIONAL, editor, *technical paper 2004-01-0558*, 2004. 57, 71

[145] J.-C. JOUHAUD, P. SAGAUT, AND B. LABEYRIE. **A Kriging Approach for CFD/Wind-Tunnel Data Comparison**. *Journal of Fluids Engineering*, **128**(4):847–855, 2006. 58

[146] J.-C. JOUHAUD, P. SAGAUT, B. ENAUX, AND J. LAURENCEAU. **Sensitivity Analysis and Multiobjective Optimization for LES Numerical Parameters**. *Journal of Fluids Engineering*, **130**(2):021401, 2008. 58

[147] J. LAURENCEAU AND P. SAGAUT. **Building Efficient Response Surfaces of Aerodynamic Functions with Kriging and Cokriging**. *AIAA Journal*, **46**(2):10, 2008. Anglais. 58

[148] A.A. AMSDEN, J.D. RAMSHAW, P.J. O'ROURKE, AND J.K. DUKOWICZ. **KIVA: a computer program for two- and three-dimensional fluid flows with chemical reactions and fuel sprays**. Technical report LA-10245-MS, Los Alamos National Lab., NM (USA), 1985. 64

[149] A.A. AMSDEN. **KIVA-3: A KIVA program with block-structured mesh for complex geometries**. Technical Report LA–12503-MS, Los Alamos National Lab., NM (United States), March 1993. 64

[150] D. J. TORRES, P. J. O'ROURKE, AND A. A. AMSDEN. **A discrete multicomponent fuel model**. *Atomization and Sprays*, **13**(2-3):131–172, June 2003. 64

[151] D. J. TORRES, P. J. O'ROURKE, AND A. A. AMSDEN. **Efficient multicomponent fuel algorithm**. *Combustion Theory and Modelling*, **7**(1):66–86, 2003. 64

[152] Y. LI, Q. XUE, S.-C. KONG, Z. XU, J. YI, AND D. J. TORRES. **Parallel Computing of KIVA-4 Using Adaptive Mesh Refinement**. In SAE INTERNATIONAL, editor, *technical paper 2009-01-0723*, 2009. 64

[153] YUANHONG LI AND SONG-CHARNG KONG. **Integration of parallel computation and dynamic mesh refinement for transient spray simulation**. *Computer Methods in Applied Mechanics and Engineering*, **198**(17-20):1596 – 1608, 2009. 64

[154] DAVID J. TORRES, YUANHONG H. LI, AND SONG-CHARNG KONG. **Partitioning strategies for parallel KIVA-4 engine simulations**. *Computers & Fluids*, **39**(2):301 – 309, 2010. 64

[155] A. IMREN, V. GOLOVITCHEV, C. SORUSBAY, AND G. VALENTINO. **The Full Cycle HD Diesel Engine Simulations Using KIVA-4 Code**. In SAE INTERNATIONAL, editor, *technical paper 2010-01-2234*, 2010. 64

[156] H. A. MAZI. *Coupling of chemical kinetics with computational fluid dynamics in a three-dimensional engine model*. PhD thesis, University of Illinois at Urbana-Champaign, 2009. 66

[157] MINGFA YAO, ZHAOLEI ZHENG, AND HAIFENG LIU. **Progress and recent trends in homogeneous charge compression ignition (HCCI) engines**. *Progress in Energy and Combustion Science*, **35**(5):398 – 437, 2009. 67

[158] N. NORDIN. *Complex Chemistry Modeling of Diesel Spray Combustion*. PhD thesis, Chalmers University of Technology, 2001. 68

[159] Y. SHI. *Optimization of a compression-ignition engine fueled with diesel and gasoline-like fuels*. Mechanical engineering, University of Wisconsin-Madison, 2009. 68

[160] J.B. HEYWOOD. *Internal combustion engine fundamentals*. McGraw-Hill series in mechanical engineering. McGraw-Hill, 1988. 71, 93

[161] S. B. POPE. **The Computation of Constrained and Unconstrained Equilibrium Compositions of Ideal Gas Mixtures using Gibbs Function Continuation**. Technical Report FDA 03-02, Cornell University, 2003. 71, 166

[162] L. DAGUM AND R. MENON. **OpenMP: an industry standard API for shared-memory programming**. *Computational Science & Engineering, IEEE*, **5**:46–55, 1998. 72

[163] BARBARA CHAPMAN, GABRIELE. JOST, AND RUUD VAN DER. PAS. % em Using OpenMP : portable shared memory parallel programming. MIT Press, Cambridge, Mass., 2008. 72

[164] WILLIAM GROPP, EWING LUSK, NATHAN DOSS, AND ANTHONY SKJELLUM. **A high-performance, portable implementation of the MPI message passing interface standard**. *Parallel Computing*, **22**(6):789 – 828, 1996. 74

[165] GEORGE KARYPIS AND VIPIN KUMAR. **METIS - Unstructured Graph Partitioning and Sparse Matrix Ordering System, Version 2.0**. Technical report, 1995. 74

[166] JOHN M. SIMMIE. **Detailed chemical kinetic models for the combustion of hydrocarbon fuels**. *Progress in Energy and Combustion Science*, **29**(6):599 – 634, 2003. 79

[167] J. WARNATZ. **The structure of laminar alkane-, alkene-, and acetylene flames**. *Symposium (International) on Combustion*, **18**(1):369–384, 1981. cited By (since 1996) 38. 79

[168] CHARLES K. WESTBROOK, JÃIJRGEN WARNATZ, AND WILLIAM J. PITZ. **A detailed chemical kinetic reaction mechanism for the oxidation of iso-octane and n-heptane over an extended temperature range and its application to analysis of engine knock**. *Symposium (International) on Combustion*, **22**(1):893 – 901, 1989. 79

[169] R. P. LINDSTEDT AND L. Q. MAURICE. **Detailed kinetic modelling of n-heptane combustion**. *Combustion Science and Technology*, **107**(4):317 – 353, 1995. 79

[170] H. J. CURRAN, P. GAFFURI, W. J. PITZ, AND C. K. WESTBROOK. **A comprehensive modeling study of iso-octane oxidation**. *Combustion and Flame*, **129**(3):253 – 280, 2002. 79

[171] KEITH EDWARDS, T. F. EDGAR, AND V. I. MANOUSIOUTHAKIS. **Kinetic model reduction using genetic algorithms**. *Computers & Chemical Engineering*, **22**(1-2):239 – 246, 1998. 79, 86

[172] MOHAMMAD JANBOZORGI, SERGIO UGARTE, HAMEED METGHALCHI, AND JAMES. C. KECK. **Combustion modeling of mono-carbon fuels using the rate-controlled constrained-equilibrium method**. *Combustion and Flame*, **156**(10):1871 – 1885, 2009. 79

[173] LONG LIANG, JOHN G. STEVENS, AND JOHN T. FARRELL. **A dynamic adaptive chemistry scheme for reactive flow computations**. *Proceedings of the Combustion Institute*, **32**(1):527 – 534, 2009. 79

[174] YU SHI, HAI-WEN GE, JESSICA L. BRAKORA, AND ROLF D. REITZ. **Automatic Chemistry Mechanism Reduction of Hydrocarbon Fuels for HCCI Engines Based on DRGEP and PCA Methods with Error Control**. *Energy & Fuels*, **24**(3):1646–1654, 2010. 79

[175] H RABITZ, M KRAMER, AND D DACOL. **Sensitivity analysis in chemical kinetics**. *Annual Review of Physical Chemistry*, **34**:419–461, 1983. 79

[176] T. TURANYI. **Reduction of large reaction mechanisms**. *New journal of chemistry*, **14**:795 – 803, 1990. 79

[177] NANCY J. BROWN, GUOPING LI, AND MICHAEL L. KOSZYKOWSKI. **Mechanism reduction via principal component analysis**. *International Journal of Chemical Kinetics*, **29**(6):393 – 414, 1997. 79

[178] ZHUYIN REN, STEPHEN B. POPE, ALEXANDER VLADIMIRSKY, AND JOHN M. GUCKENHEIMER. **The invariant constrained equilibrium edge preimage curve method for the dimension reduction of chemical kinetics**. *The Journal of Chemical Physics*, **124**(11):114111, 2006. 80

[179] CRAIG T. BOWMAN, RONALD K. HANSON, WILLIAM C. GARDINER, V. LISSIANSKI, MICHAEL FRENKLACH, MIKHAIL GOLDENBERG, GREGORY P. SMITH, DAVID R. CROSLEY, AND DAVID M. GOLDEN. **GRI-Mech 2.11–An Optimized Detailed Chemical Reaction Mechanism for Methane Combustion and NO Formation and Reburning.** Technical report, GRI Topical Report 97/0020., 1997. 80

[180] MICHAEL FRENKLACH, H. WANG, M. GOLDENBERG, , GREGORY P. SMITH, DAVID M. GOLDEN, CRAIG T. BOWMAN, RONALD K. HANSON, WILLIAM C. GARDINER, AND V. LISSIANSKI. **GRI-Mech–An Optimized Detailed Chemical Reaction Mechanism for Methane Combustion.** Technical report, GRI Topical Record 95/0058, 1995. 80

[181] M. MITCHELL. *An Introduction to Genetic Algorithms*. MIT Press, Cambridge, MA, 1996. 81, 86, 88, 89, 98

[182] R. G. GILBERT, K. LUTHER, AND J. TROE. **Theory of Thermal Unimolecular Reactions in the Fall-off Range. II. Weak Collision Rate Constants**. *Berichte der Bunsengesellschaft fur physikalische Chemie*, **87**(2):169–177, 1983. 82

[183] P.H. STEWART, C.W. LARSON, AND D.M. GOLDEN. **Pressure and temperature dependence of reactions proceeding via a bound complex. 2. Application to 2CH3 –> C2H5 + H**. *Combustion and Flame*, **75**(1):25 – 31, 1989. 82

[184] CHRISTOPHER J. MONTGOMERY, CHONGGUAN YANG, ALAN R. PARKINSON, AND J.-Y. CHEN. **Selecting the optimum quasi-steady-state species for reduced chemical kinetic mechanisms using a genetic algorithm**. *Combustion and Flame*, **144**(1-2):37 – 52, 2006. 86

[185] JUAN J. HERNÃĄNDEZ, ROSARIO BALLESTEROS, AND JOSEP SANZ-ARGENT. **Reduction of kinetic mechanisms for fuel oxidation through genetic algorithms**. *Mathematical and Computer Modelling*, **52**(7-8):1185 – 1193, 2010. Mathematical Models in Medicine, Business & Engineering 2009. 86

[186] V. HAMOSFAKIDIS AND R. D. REITZ. **Optimization of a hydrocarbon fuel ignition model for two single component surrogates of diesel fuel**. *Combustion and Flame*, **132**(3):433 – 450, 2003. 86, 88

[187] E. MATTARELLI, F. PERINI, AND C. A. RINALDINI. **Optimization of a Supercharged Single Cylinder Engine for a Formula SAE Racing Car**. *SAE International Journal of Engines*, **2**(1):199–210, 2009. 87

[188] **2009 Formula SAEÂő Rules**. 90

[189] **GT Power v.6.2.0 Manual**. 90

[190] T. DONATEO, A. DE RISI, AND D. LAFORGIA. **Optimization of High Pressure Common Rail Electro-injector Using Genetic Algorithms**. In SAE INTERNATIONAL, editor, *technical paper 2001-01-1980*, 2001. 98

[191] H. HIROYASU, H. MIAO, T. HIROYASU, M. MIKI, J. KAMIURA, AND S. WATANABE. **Genetic Algorithms Optimization of Diesel Engine Emissions and Fuel Efficiency with Air Swirl, EGR,Injection Timing and Multiple Injections**. In SAE INTERNATIONAL, editor, *technical paper 2003-01-1853*, 2003. 98

[192] H. HELMHOLTZ. *On the Sensations of Tone*. Dover Classics of Science and Mathematics Series. Dover Publications, 1954. 100

[193] V.N. KONDRATIEV AND V.V. AZATYAN. **HO2 radicals in combustion reactions**. *Symposium (International) on Combustion*, **14**(1):37 – 44, 1973. Fourteenth Symposium (International) on Combustion. 107

[194] R.W. WALKER. **Reactions of HO2 radicals in combustion chemistry**. *Symposium (International) on Combustion*, **22**(1):883 – 892, 1989. 107

[195] R.K. HANSON AND D.F. DAVIDSON. **Energy Frontier Research Center for Combustion Science - Stanford University Contribution: Butanol and Methyl Ester Studies**. Presentation, 2010. 125

[196] W.J. PITZ, C.K. WESTBROOK, AND O. HERBINET. **Chemical Kinetic Modeling of Advanced Transportation Fuels**. LLNL Technical Report LLNL-TR-410103, Lawrence Livermore National Laboratory, 2009. 125

[197] STEPHEN B. POPE. **Gibbs function continuation for the stable computation of chemical equilibrium**. *Combustion and Flame*, **139**(3):222 – 226, 2004. 166